

# Organic Monolayers and Fluoropolymer Brushes

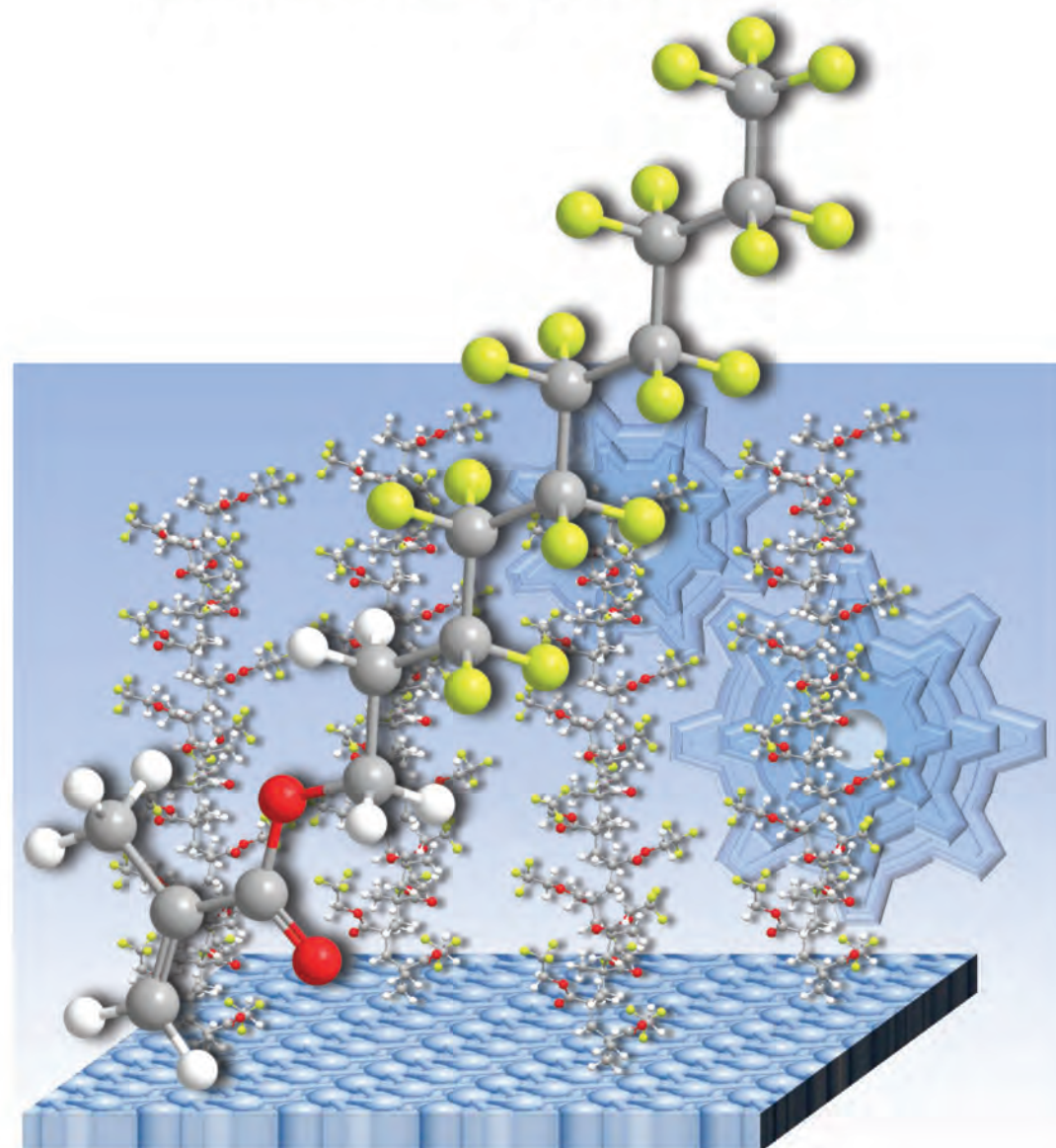
Functionalization, Stability and Tribology

2014

Nagendra S. Bhairamadgi

Organic Monolayers and Fluoropolymer Brushes

**Nagendra Somaling Bhairamadgi**



# **Organic Monolayers and Fluoropolymer Brushes**

## **Functionalization, Stability and Tribology**

Nagendra Somaling Bhairamadgi

## **Thesis committee**

### **Promotors**

Prof. Dr. H. Zuilhof  
Professor of Organic Chemistry  
Wageningen University

Prof. Dr. C.J.M. van Rijn  
Professor of Microsystem and Nano Technology for Agro, Food and Health  
Wageningen University

### **Other members**

Prof. Dr. H van Amerongen, Wageningen University  
Dr. A. Zdravkov, ASML Netherlands B.V.  
Dr. C.H. Venner, University of Twente  
Dr. L.C.P.M. de Smet, Delft University of Technology

This research was conducted under the auspices of the Graduate School VLAG (Advanced studies in Food Technology, Agrobiotechnology, Nutrition and Health Sciences).

# **Organic Monolayers and Fluoropolymer Brushes**

## **Functionalization, Stability and Tribology**

Nagendra Somaling Bhairamadgi

### **Thesis**

submitted in fulfillment of the requirements for the degree of doctor  
at Wageningen University

by the authority of the Rector Magnificus

Prof. Dr. M.J. Kropff,

in the presence of the

Thesis Committee appointed by the Academic Board

to be defended in public

on Tuesday 17 June 2014

at 1:30 p.m. in the Aula.

Nagendra Somaling Bhairamadgi

Organic Monolayers and Fluoropolymer Brushes: Functionalization, Stability and Tribology

186 pages.

PhD thesis, Wageningen University, Wageningen, NL (2014)

With references, with summaries in English and Dutch.

ISBN: 978-94-6173-963-6

*Dedicated to my Family and Friends*



# Table of Contents

<b>Chapter 1</b>	General Introduction	1
<b>Chapter 2</b>	Efficient Functionalization of Oxide-free Silicon(111) Surfaces: Thiol-yne versus Thiol-ene Click Chemistry	19
<b>Chapter 3</b>	Hydrolytic and Thermal Stability of Organic Monolayers on Various Inorganic Substrates	37
<b>Chapter 4</b>	Adhesion and Friction Properties of Polymer Brushes: Fluoro versus Non-fluoro Polymer Brushes at Varying Thickness	61
<b>Chapter 5</b>	Adhesion and Friction Properties of Fluoropolymer Brushes: On the Tribological Inertness of Fluorine	83
<b>Chapter 6</b>	General Discussion	103
<b>Appendix A</b>	Supporting Information: Chapter 2	113
<b>Appendix B</b>	Supporting Information: Chapter 3	129
<b>Appendix C</b>	Supporting Information: Chapter 4	143
<b>Appendix D</b>	Supporting Information: Chapter 5	153
<b>Summary</b>		155
<b>Samenvatting</b>		161
<b>Overview of Completed Training Activities</b>		167
<b>Acknowledgment</b>		169
<b>List of Publications</b>		173
<b>About the Author</b>		175





# Chapter 1

---

## General Introduction

### Abstract

This thesis deals with the adhesion and friction properties of densely grafted and covalently bound fluoropolymer brushes on silicon surfaces with varying thickness and fluorine content. A novel surface-functionalizing method is described using the thiol-yne click (TYC) reaction. The TYC reaction is highly useful for the attachment of functional (bio-)molecules and immobilization of radical initiators onto a surface with high density. Next, the hydrolytic and thermal stability of 24 different types of monolayers on Si(111), Si(100), SiC, SiN, SiO<sub>2</sub>, CrN, ITO, PAO, Au and stainless steel surfaces was evaluated. Subsequently, based on this outcome, highly stable fluorinated polymers are described as obtained using surface-initiated atom transfer radical polymerization (SI-ATRP) reactions. The effects of thickness and fluorine content on tribological properties of these layers were studied. The adhesion and friction properties were investigated using colloidal probe atomic force microscopy under dry and ambient conditions. The solvent-free lubricating properties of obtained fluoropolymer brushes have been characterized in detail, and demonstrate their potential for e.g., MEMS/NEMS devices.

## Contents

<b>1. General Introduction .....</b>	<b>1</b>
Abstract .....	1
1.1 Introduction .....	3
1.2 Functional Organic Monolayers.....	4
1.3 Thiol-yne Click Reaction .....	5
1.4 Polymer Brushes .....	7
1.5 Tribology.....	9
1.6 Tribological Properties of Polymer Brushes .....	11
1.7 Aim of the Research.....	11
1.8 Outline of the Thesis .....	12
1.9 References .....	14

## 1.1 Introduction

*“There’s Plenty of Room at the Bottom”* a momentous and inspiring talk was given by physicist Richard Feynman at the American Physical Society meeting on December 29<sup>th</sup> 1959. He considered the advent of miniaturization by manipulation of individual atoms some 55 years ago.<sup>1</sup> Today we can see the reality in the form of Micro Electro Mechanical Systems (MEMS) and Nano Electro Mechanical Systems (NEMS). MEMS/NEMS have a major impact on everyday life of human being. The smartphone is a good example having amongst others accelerometers, gyroscopes and recently also a proximity sensor as MEMS components (Figure 1). Other MEMS/NEMS elements are gears, springs, diaphragms, beams, etc. The functions of these components are to measure or induce tiny movements controlled by external electronic circuitries. The scale of MEMS/NEMS elements is rapidly shrinking due to an ongoing fast miniaturization of the devices in which they are used, which implies that they are characterized by an increasing surface-to-volume ratio. Therefore adhesion and friction become increasingly critical, and resulting surface forces, such as capillary action, hydrogen bonding, electrostatic and Van der Waals forces, dominate over body forces at the micro- and nano-scale. Recent studies indicate that these forces dominate and co-determine the efficiency and reliability of MEMS/NEMS devices.<sup>2</sup>

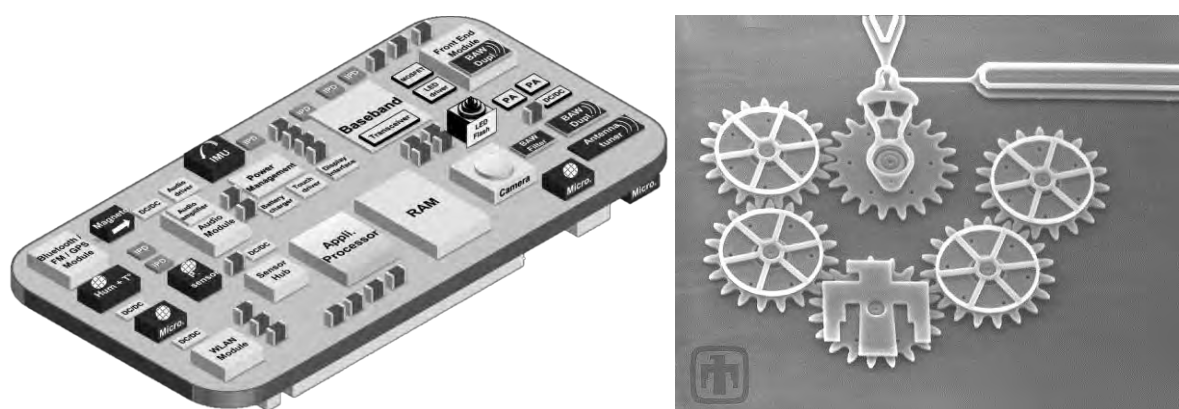


**Figure 1.** Schematic representation of smartphone board with MEMS components (left) (Yole Développement, [www.yole.fr](http://www.yole.fr)) and micro gear fabricated on silicon wafer (Sandia National Laboratories [www.mems.sandia.gov](http://www.mems.sandia.gov)).

Low-surface energy coatings based on fluorocarbons or fluoro-hydrocarbons are generally used in MEMS to prevent unwanted stiction associated with high adhesion forces. Fluoro-based coatings are hydrophobic, which minimizes the stiction forces related to capillary condensation. Normally fluorocarbon or fluoro-hydrocarbon coatings are obtained with vapor deposition or plasma deposition methods.<sup>3</sup> However, reproducibility and reliability are a main concern of these coating methods. An alternative to obtain low friction and wear resistant MEMS device coatings can be provided by self-assembled monolayers (SAMs). Especially fluorinated SAMs are attractive due to their low surface

energy.<sup>4, 5</sup> Of course, their usefulness depends strongly on their stability, and this hinges on the attachment chemistry that is invoked. For example, SAMs derived from thiols on Au surface were found to have appreciable wear due to the weak Au-S bond compared to silane chemistry-based monolayers.<sup>6</sup> Klein et al. have recently studied both the thermal and mechanical stability of silane-based fluorinated and non-fluorinated SAMs in heated, dry, and an oxygen-rich environment. They found that both types of monolayers rapidly degraded. Pujari et al. obtained an ultra-low adhesion, friction and good wear resistance with an increase of the fluorine content in the monolayers on Si(111), SiC and CrN under ambient conditions.<sup>7-9</sup> Alike SAMs, surface-tethered polymer brushes seem also good alternative coatings for MEMS/NEMS. The advantage of polymer brushes over SAMs is that their inherent mechanical properties can be easily tuned with proper design and simply by changing solvent compositions.<sup>10</sup> Therefore, polymer brushes can also be useful in Bio-MEMS. Polymer brushes have not been explored as much for MEMS/NEMS applications as SAMs. This is somewhat surprising, as the lowest coefficient of friction ( $\mu$ ) has been obtained under both solvent (polyelectrolyte brushes,  $\mu = 0.0006$ )<sup>11</sup> and ambient condition (PDMS brushes,  $\mu \approx 0.0024$ )<sup>12</sup> on polymer brushes.

In conclusion, several studies indicate that the mechanical stability of monolayers and/or polymer brushes is worth a detailed study. However, currently a systematic study on monolayers and polymer brushes, which combines probes of the effects of properties like surface-tethering group, thickness, fluorine content, and substrate, is lacking. Therefore, the work in this thesis aims to bridge this gap and provide insight that will help to develop new solutions to stiction and friction issues in MEMS and NEMS.

## 1.2 Functional Organic Monolayers

In this modern era of technology surface science has a major impact on the performance of MEMS/NEMS devices due to the ongoing miniaturization, particularly of their electronic components, such as sensors, energy and data storage elements. Faster and smaller semiconductor materials in the electronics become a key drive. The performance of components relies on adequate passivation and functionalization techniques. Surface chemistry may combine formation of organic passivating layers with the advantage of covalent molecular binding. In spite of well-established surface chemistry available for functionalization of these semiconductor materials, the emerging markets with new devices still require faster, cheaper and better controllable methods to obtain well-defined, functional, easy adaptability in any kind of environment, and responsiveness to external stimuli (such as pH, chemicals and biological agents).<sup>13-15</sup>

Well-developed surface chemistry is now available allowing us to tune semiconductor materials and contribute to emerging technology. Zisman et al. initiated surface modification in 1946 and eventually it became established to assemble monolayers using thiols on gold<sup>16-18</sup> and silanes on oxide surfaces.<sup>19-21</sup> Covalently bound organic monolayers

on semiconductor surfaces were first reported in 1993 by Linford et al.<sup>22</sup> The advantage of having organic monolayers on semiconductor surfaces is that it provides passivation as well as functionality. Recent studies showed that direct linking of Si to C atoms can be achieved on hydrogen-terminated surfaces using UV,<sup>23</sup> visible<sup>24</sup> or thermal activation techniques.<sup>25, 26</sup> Generally, functional monolayers consist of three main domains including (1) the head groups, capable of forming bonds with surfaces, e.g., thiols, carboxylic, phosphonic acids, and silanes (-Cl or O-CH<sub>3</sub>), etc.; (2) the tail- alkyl or aromatic backbone, responsible for ordering/packing of the monolayer, and (3) the end group, dominating the surface properties to the formed monolayer while also providing access to further modification (Figure 2). The main challenge here is obtaining  $\omega$ -functionalized surfaces, especially on H-terminated silicon surfaces, due to their high reactivity towards most of the functional groups (e.g., -OH, -C(O)H, -NH<sub>2</sub>, -Br, -C(O)Cl, -SH).<sup>27</sup> This has been achieved with functionalities like carboxylic acid,<sup>23, 28</sup> acid fluoride<sup>29</sup> and N-hydroxy succinimide groups<sup>30</sup>, which were prepared successfully with negligible upside down attachment. Additionally, the stability of monolayers is dependent on the head/anchoring group, which connects the monolayer to the surface substrate. The stability of this linkage may vary depending on environments in which monolayer surfaces were utilized, e.g., under acidic, neutral or basic conditions, in physiologically relevant media or at elevated temperatures.

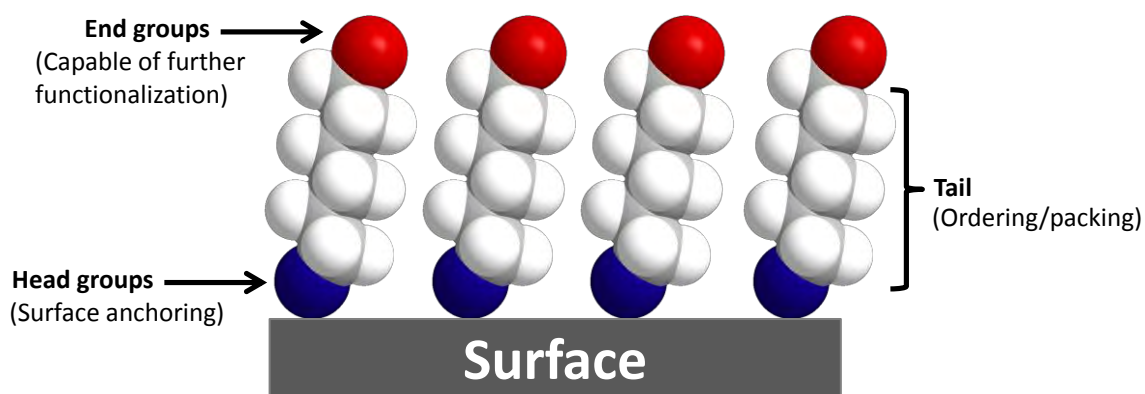


**Figure 2.** Schematic representation of  $\omega$ -functionalized monolayers on solid surfaces.

### 1.3 Thiol-yne Click (TYC) Reaction

After the introduction of the click chemistry concept in 2001 by Sharpless and co-workers,<sup>31</sup> an overwhelming attention of scientists in different fields of chemistry and biochemistry have contributed to its success. Reactions are labelled as click reactions, as they are highly efficient, do only yield inoffensive by-products, use readily available starting materials and reagents, while the reactions can be carried out in the absence of organic solvents, yield a simple-to-purify product, are modular, wide in scope, and stereospecific. About a decade ago, the copper-catalyzed azide-alkyne cycloaddition

(CuAAC) was the only recognized click reaction. However, the drawback of CuAAC is that it uses the potentially toxic metal catalyst (Cu), and consequently this diminished its impact in biological and physiological fields where such toxic metals cannot be used.<sup>32</sup> Therefore, there was a need of developing alternative click reactions that do not require toxic metal catalysts. Recently, metal-free [3+2] cycloaddition reactions,<sup>33-36</sup> Diels-Alder reactions<sup>37-39</sup> and thiol-based click reactions<sup>40-43</sup> were also being termed as click reactions, because they fulfil most of the click reaction requirements. Several of these alternative metal-free click reactions can overcome the issues in the classical CuAAC click reaction and further expand their usefulness in allowing access to biocompatible conjugates under physiological conditions. However, all above click reactions are having advantages as well as disadvantages like the use of toxic metals and need of special conditions i.e. light, radical initiators, etc. The disadvantages can be overcome by choosing proper click reaction depending on the final application and reaction conditions. It will be out of scope to discuss all of them here, but we discuss here the thiol-based click reaction in more detail, which was used in this work.

The reactions between thiols and alkenes were recently recognized as click reactions, termed as thiol-ene click (TEC) reactions, because of their high reaction rate, simplicity, compatibility with a wide range of functional groups and the broad range of available reagents. The TEC reaction can be conducted under ambient conditions by exposing mixtures of thiols and alkenes to either direct UV or sunlight (365 nm).<sup>40, 44</sup> Hawker and co-workers have efficiently utilized the TEC reaction, e.g., to synthesize fourth-generation dendrimers in a robust, efficient, and orthogonal manner.<sup>45</sup> Due to the simplicity and use of mild reaction conditions, TEC reactions are widely explored in variety of materials and polymer synthesis.<sup>46</sup> Buriak and co-workers used TEC reactions to assemble layer-by-layer deposition of dithiols and dienes on semiconductor surfaces. Recently, Caipa Campos et al. have reported the use of TEC reactions for the functionalization of oxide-free Si(111) surfaces with various thiols.<sup>47</sup> These examples provide an interesting platform for surface modification of electrodes for biosensing and tuning of the surface properties of microelectronic devices.

A thiol-based click reaction that attracted attention more recently is between a thiol and an alkyne, and is called as “thiol-yne” click (TYC) reaction. However, this type of reaction is not new, as examples of such reactions were already reported in 1930.<sup>48, 49</sup> The attractiveness of the TYC reaction is that it does not need special reactant materials and can be performed with readily available reactants of both CuAAC and TEC reactions, but under milder conditions. In a TYC reaction, up to two thiols react with one alkyne leading to the formation of dithioether using a chemical radical source, UV or sunlight under ambient conditions. In 2009, Bowman and co-workers have introduced a TYC coupling procedure for the development of a highly cross-linked polymer network.<sup>50</sup> Additionally, they also studied the kinetics of TYC reaction and proposed a novel mechanism (Figure

3).<sup>50</sup> The TYC reaction processes via a radical mechanism; first thiyl radical forms either thermally or photochemically in the presence of an initiator. The thiyl radical then adds to an alkyne forming a carbon-centred radical, which subsequently abstracts a hydrogen from another thiol leading to the formation of vinyl sulphide with the regeneration of a thiyl radical. The vinyl sulphide further undergoes addition of a second thiyl radical yielding dithioether after abstracting hydrogen from a thiol. Therefore the advantage of TYC reaction over TEC is that after completion of TYC reaction each alkyne group is having up to two thiols, yielding a dithioether. In addition, the thiyl radical reacts ~3 times more faster with an intermediate vinyl sulphide than with an alkyne, which stimulates the second thiol addition.<sup>50</sup> The first study of utilizing TYC reaction for surface modification was reported by Ryan et al.<sup>51</sup> They carried out sequential TYCs with two different thiols on propargyl methacrylate polymer brushes on oxidized silicon surfaces in the presence or absence of a photomask. Inspired by this work, Wendeln et al. reported the selective immobilization of thiols on silicon oxide surfaces by micro-contact printing ( $\mu$ CP), an emerging method for patterning surfaces.<sup>52</sup>

We utilized TYC reaction for surface functionalization in this thesis because it gives a high surface coverage by allowing us to immobilize up to two thiols per alkyne group under mild reaction conditions. Thus, this compares favorably to the TEC or CuAAC reactions, which only couples one thiol or azide to unsaturated carbon-carbon bonds.

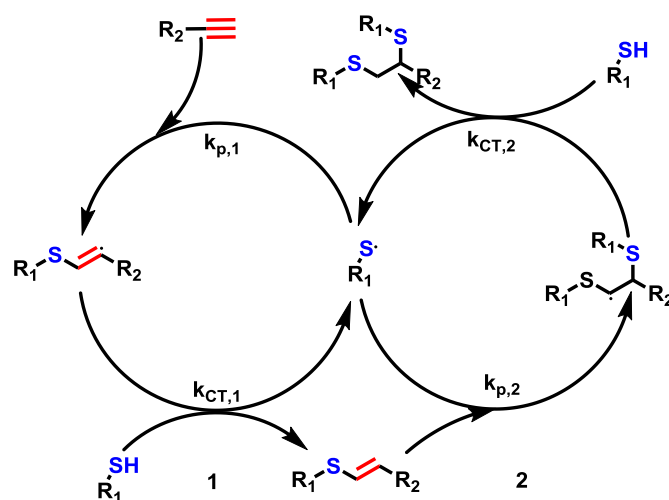


**Figure 3.** The radical mechanism of TYC click reaction, displaying the sequential addition and hydrogen abstraction steps of (1) a primary alkyne and subsequently (2) vinyl sulfide.<sup>50</sup>

## 1.4 Polymer Brushes

Polymer chains tethered by one end to a substrate surface are referred as polymer brushes.<sup>53</sup> These surface-grafted individual polymer chains overlap under high grafting density and are forced to stretch away from the surface to minimize steric repulsions



between the chains. Therefore, the surface-tethered polymers (i.e. polymer brushes) behave differently in many ways from free/bulk polymers and show some unique features such as tuning wettability,<sup>54</sup> antifouling,<sup>55</sup> stimuli responsiveness (pH, heat or light),<sup>56</sup> lubrication,<sup>57</sup> and corrosion resistance.<sup>58</sup> In addition, the attachment of polymer brushes may increase the biocompatibility.<sup>59</sup> Thin polymer films are therefore increasingly used in MEMS/NEMS devices such as computer chips, hard disks and also in biomedical applications.<sup>53, 60</sup>

The polymer brushes can be prepared by either “grafting to” or “grafting from” approaches (Figure 4). In the “grafting to” approach a pre-synthesized polymer will attach onto the surface via physisorption or covalent bond formation. However, this grafting-to approach suffers from certain limitations, e.g., the difficulty to produce thick and very dense polymer brushes, due to the steric repulsion between polymer chains. The reaction between the polymer end groups and the complementary group on the substrate becomes less efficient with increasing polymer molecular weight. In contrast, in the “grafting from” approach, the polymer chains are directly grown from the surface by using a surface-initiated polymerization step. In this approach the main limitation resides in the availability of useful reactants and this may require significant synthetic efforts.<sup>61</sup>

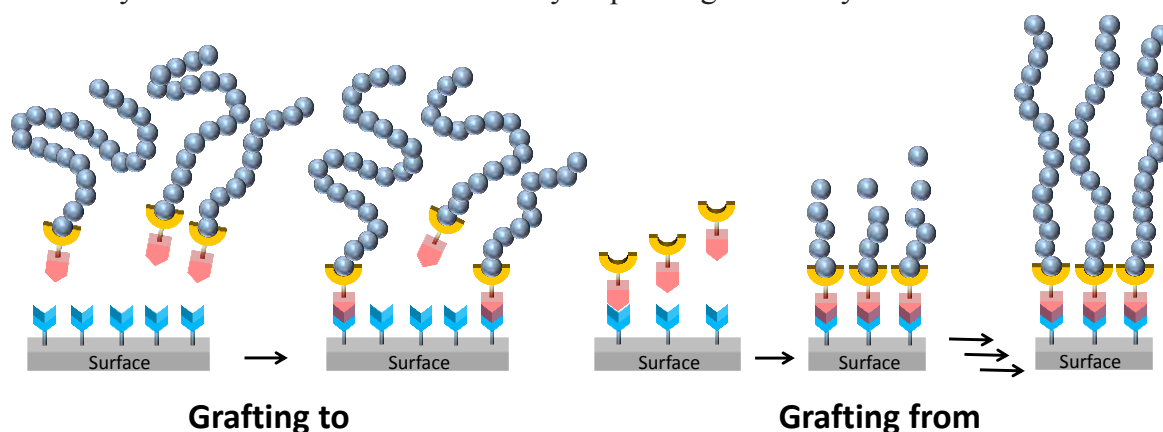


**Figure 4.** Polymer brushes obtained via “grafting to” and “grafting from” approaches on solid surfaces.

Nowadays various controlled radical polymerization (CRP) techniques are available to obtain novel polymers with a controlled molecular weight and molecular weight distribution, such as atom-transfer radical polymerization (ATRP), reversible addition-fragmentation chain transfer (RAFT) and nitroxide-mediated polymerization (NMP).<sup>62</sup> Among controlled radical polymerization techniques, ATRP is one of the most powerful and widely used synthetic techniques in polymer science. It allows the synthesis of polymers with predetermined and controlled molecular weight with desired molecular architecture.<sup>62</sup> Initiation of an ATRP reaction occurs through a reversible one-electron redox process between a transition metal-ligand complex  $Mt^m/L$  and an alkyl halide  $R-X$  to generate  $X-Mt^{m+1}/L$  and a radical  $R^\bullet$ , with a rate constant of activation  $k_{act}$ . The radical can further react with a monomer  $M$  with a rate constant of propagation  $k_p$ , or can be

reversibly deactivated by  $X-Mt^{m+1}/L$  with a rate constant  $k_{\text{deact}}$ , or terminated by coupling or disproportionation with a rate constant  $k_t$  (Figure 5).<sup>63</sup>

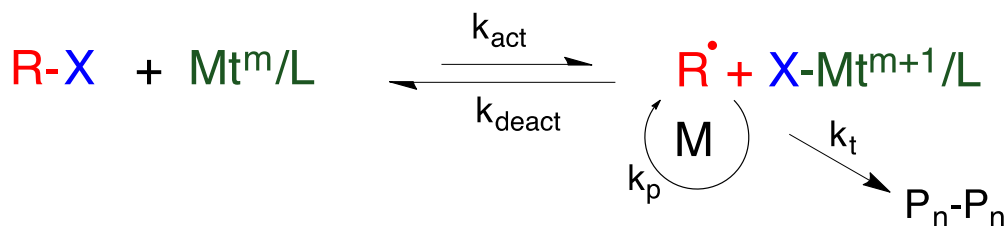


**Figure 5.** Mechanism of the ATRP reaction.<sup>63</sup>

The CRP initiated from the surface is generally termed as surface-initiated (SI) CRP.<sup>62</sup> The SI-ATRP chemistry is versatile and is compatible with a wide range of monomers with different functional groups. Another advantage of SI-ATRP is that it tolerates a trace of oxygen (it can be readily removed by oxidation of the ATRP catalyst). Compared to other CRP methods, ATRP is less laborious because monomers and surface-immobilized initiators can be easily synthesized and most of them are commercially available. Therefore, here we utilized SI-ATRP for preparation of polymer brushes with a range of fluoro and non-fluoro methacrylates on Si(111) surfaces.

## 1.5 Tribology

The term *tribology* means the study of rubbing and deals with interacting surfaces in relative motion and is derived from the Greek word *tribos*. Though the term tribology has only emerged since 1966, the history goes back to about 500,000 B.C., when our ancestors learned about generating fire by rubbing two flint stones together with great force,<sup>64</sup> or started to use animal fat to make chariots run smoothly. An understanding of experimental and theoretical aspects of tribology in terms of design of moving components like bearings, better lubricants and so on was evidently needed.<sup>65</sup> Further developments in the 20<sup>th</sup> century allowed the understanding of tribological behavior at the molecular level.<sup>66</sup> The development of modern tools such as surface force apparatus (SFA) in 1960s and atomic force microscopy (AFM) in 1990s further enhanced tribological research and broadened the field.<sup>65, 67</sup>

This has led to the involvement of tribology in the design of novel and complex architectures at the micrometer scale, and more recently down to the nanometer scale. Therefore, a proper understanding of tribological behavior on such small scales, so-called “nanotribology”, becomes important to further improve the performance and durability of new MEMS/NEMS devices. This was boosted by the development of AFM techniques, which have a major advantage that they allow nanotribological measurements on various materials such as metals, semiconductors, ceramics, minerals, organic monolayers, polymers and biomaterials under controlled atmosphere, in liquids, in ambient and under vacuum environments. The AFM measures the force between the AFM tip mounted on a

flexible cantilever and a sample surface (Figure 6). The forces are measured with the help of the optical deflection of a cantilever.

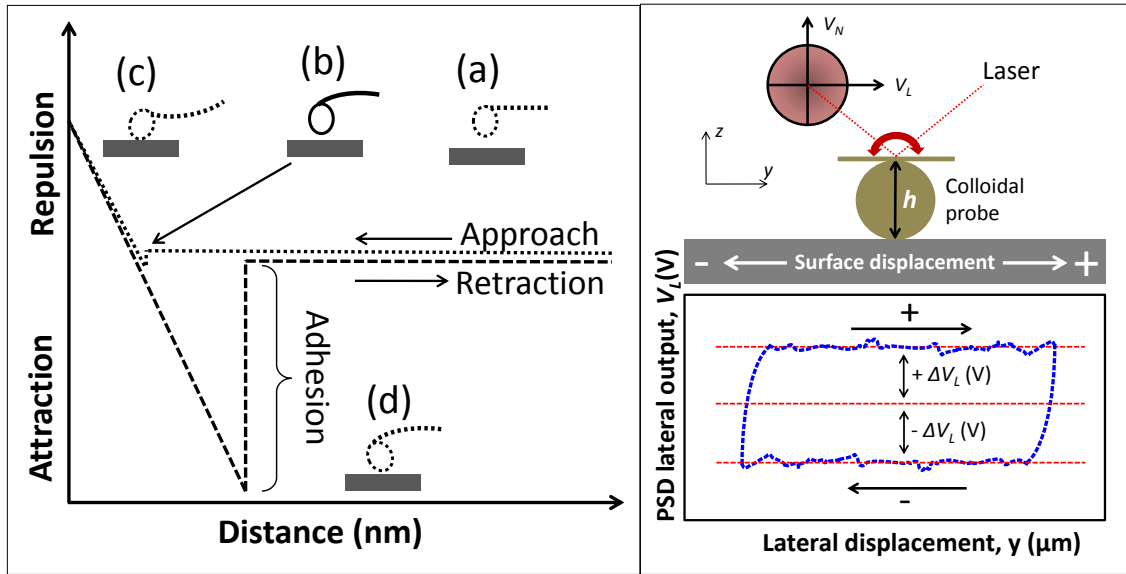


**Figure 6.** A typical force-distance curve depicting the approach and retraction cycle during adhesion measurements (left), and a lateral friction force measurement setup with a characteristic trace-retrace loop obtained during friction measurements (right).

Adhesive forces can be measured by detecting the interaction during approach and retraction of the tip from the sample surface. A typical force-distance curve is shown in Figure 6 (left). Initially the cantilever is away from the sample in an equilibrium position and no force will be detected (a). Upon slowly approaching the sample with the cantilever, the tip experiences an adhesive force and the cantilever bends due to Van der Waals/electrostatic interactions (b). Upon applying a normal load, the cantilever bends in the opposite direction due to the action of repulsive forces on the tip, the so-called repulsive regime (c). During retraction, the tip stays in contact mode until the cantilever overcomes the adhesive forces (d), after which it goes back to initial equilibrium position (a). The force necessary to pull-out the cantilever is called the adhesion force.

The lateral friction force microscope (LFM) measures lateral friction forces. An LFM is a modified version of the AFM. A “colloidal probe” is glued to an AFM tip and is used to measure lateral friction forces instead of the regular up and down motion of a cantilever tip.<sup>68</sup> A schematic representation of an LFM is shown in Figure 6 (right). The cantilever long axis twists upon application of force in the y-direction, the deflection of the laser beam from the cantilever is measured with the help of a quadrant position-sensitive photodetector (PSD), and corresponds to the torsional deflection in the cantilever (axis VL normal to VN). A hysteretic “friction loop” resulted from dissipation of friction energy during sliding, and the half width of it is propositional to the friction force at the interface.<sup>69</sup>

## 1.6 Tribological Properties of Polymer Brushes

Polymer brushes present in a good solvent were predicted to be highly extended chains and that experience repulsive forces. Upon bringing them in close proximity with an object, the repulsive forces between the polymer brushes and the counterface rapidly increases. In this type of measurements, polymer brushes displayed a series of interesting and novel tribological properties, such as a relatively low adhesion, low friction and good lubrication.<sup>70-72</sup> However, understanding tribological phenomena at the molecular level of polymer brushes is still challenging due to the complexity and interplay of adhesion, friction and lubrication forces. Many considerations like the density of the polymer brushes, the swelling behavior in different solvents and the environmental conditions, have to be taken in account.<sup>65</sup> Several research groups have analyzed the tribological properties of polymer brushes under good solvents conditions using LFM, SFM and tribometer.<sup>70, 73-75</sup>

For example, Klein et al. have studied the friction behavior of charged polymers attached to surfaces rubbing across aqueous medium. They have found a friction coefficient as low as  $< 0.0006$  at a pressure of 0.3 MPa. This is attributed to the suppressed interpenetration of opposing charged brushes due to the presence of mobile counterions within the brush layers. Such polymer brushes with ultra-low lubrication can have potential implications as biolubricants and can be implemented into artificial implants.<sup>11</sup> Additionally, friction properties of polyelectrolyte brushes can be tuned by simply exposing polyelectrolyte brushes to different counterions.<sup>76</sup> Not only polyelectrolyte brushes show low-friction properties, but also a few hydrophobic brushes displayed similar properties. Spencer and coworkers have recently obtained low friction for hydrophobic polymer brushes ( $\mu = 0.002$ ) in presence of hexadecane as a lubricating solvent.<sup>75</sup> These studies indicate that good lubrication properties of polymer brushes exhibiting low friction can only be achieved in the presence of good solvents. Limpoco et al. studied the influence of solvent quality (mixture of different solvents) on polystyrene brushes using different solvents including toluene, 2-propanol and *n*-butanol. Low friction was obtained using toluene as a solvent.<sup>70</sup> Their study supports that good solvent conditions are a prerequisite for the polymer brushes to enable low friction. However, only a few reports are available on the tribological properties of polymer brushes in the absence of solvents.<sup>12, 77</sup>

## 1.7 Aim of the Research

A main challenge in miniaturized (MEMS/NEMS) device technology is to find adequate techniques to compensate for the adverse effects of the size reduction. Because of the reduced size, devices are more hampered by unwanted surface forces such as stiction and friction, affecting device performance and durability. One way of solving this tribological issue of MEMS devices is to modify the surface topography by applying

proper coatings that have low adhesion, low friction and high resistance to wear. Therefore, the aim of this research is to develop and characterize new coating materials, which have a strong binding ability to the required surface, have a low surface energy and act as good lubricants under ambient conditions.

## 1.8 Outline of the Thesis

Most of the current MEMS/NEMS devices are based on silicon and silicon-derived materials; we therefore primarily study here detailed modification of these surfaces. To obtain robust coatings, we chemically modify and functionalize oxide-free silicon surfaces with functional organic monolayers. Further we study the hydrolytic and thermal stability of the monolayers on a variety of inorganic substrates, by choosing suitable combinations of substrate and monolayer. Next, we extend our study with the further modification of functional monolayers onto fluoropolymers brushes, and study their adhesion and friction properties and compare them with analogous non-fluoropolymer brushes.

In **Chapter 2** we report on the functionalization of oxide-free Si(111) surfaces with alkyne-terminated monolayers. In order to achieve a high surface coverage these functional monolayers were further modified with various thiols via a TYC reaction. In addition, we compare the efficiency of TYC versus TEC reactions. Each stage of modification is investigated by various surface characterization techniques, including X-ray photoelectron spectroscopy (XPS), contact angle measurements and Fourier transform infrared reflection absorption spectroscopy (FT-IRRAS).

In **Chapter 3** we investigate the hydrolytic and thermal stability of monolayers on a variety of inorganic substrates in order to find proper combinations of monolayer head groups and substrates. For this aim, we choose 24 different monolayer-substrate combinations for study of their hydrolytic stability and 14 of them for thermal stability tests. We used organic monolayers with a fixed alkyl chain length (C18) with a wide range of linker groups depending on the substrate reactivity. The hydrolytic stability of these modified surfaces was investigated by measuring the static water contact angle and by XPS measurements. The analyses were performed after prolonged immersion in water, under acidic (pH 3), neutral (pH 7; deionized water and phosphate-buffered saline) and basic (pH 11) conditions. The thermal stability of modified surfaces is examined using XPS having *in-situ* heating system, and the stability was then measured as a function of the loss in carbon signal upon heating from 25 °C to 600 °C.

In **Chapter 4** we study the adhesion and friction properties of fluoro and non-fluoropolymer brushes with varying thickness. To this aim, we prepared different thicknesses of fluoro and non-fluoropolymer brushes with a high grafting density on oxide-free Si(111). To achieve the high grafting density, we immobilized an ATRP initiator via TYC onto alkyne-terminated monolayers on oxide-free Si(111). Both above-mentioned polymer brushes were prepared using ethyl methacrylate (EMA) and 2,2,2-

trifluoroethyl methacrylate (TFEMA) as monomers and we obtained a varied thickness and a high grafting density via SI-ATRP. The resulting polymer brushes were characterized in detail by ellipsometry, XPS, FT-IRRAS, and static water contact angle measurements. Finally, the adhesion and friction properties were investigated by CP-AFM under ambient (relative humidity  $RH = 44 \pm 2\%$ ) and dry ( $RH < 5\%$ ) conditions. This study helps us to tune adhesion and friction properties by varying the thickness of the polymer brushes.

In **Chapter 5** we explore the adhesion and friction properties of fluoropolymer brushes with increasing fluoroalkyl side chain at a constant polymer brush thickness ( $\sim 80$  nm). The polymer brushes with different fluorine content were obtained via SI-ATRP with methacrylate monomers with a varying number of fluorine atoms in the fluoroalkyl side chain. The adhesion and friction properties of fluoropolymer brushes were again followed by CP-AFM under ambient ( $RH = 44 \pm 2\%$ ) and dry ( $RH < 5\%$ ) conditions without introducing any external lubricant. The dry-lubricating properties were further compared with those measured in the presence of external lubricating fluids, such as Fluorinert® FC-40 and hexadecane.

Finally in **Chapter 6** we summarize the achievements in this thesis and their applicability for future application in MEMS/NEMS technology. Also, we discuss improvements of such type of coatings by considering additional approaches.

## 1.9 References

1. Feynman, R. P., There's plenty of room at the bottom. *Eng. Sci.* **1960**, 23, (5), 22-36.
2. Bhushan, B., *Handbook of Nanotechnology*. 2 ed.; Springer- Verlag: New York, **2007**.
3. Kim, N. K.; Cha, N. G.; Kim, K. C.; Kim, T. G.; Park, J. G., Chemical and nanomechanical characteristics of fluorocarbon thin films deposited by using plasma enhanced chemical vapor deposition. *J. Korean Phys. Soc* **2007**, 50, (4), 1113-1118.
4. Maboudian, R.; Howe, R. T., Critical Review: Adhesion in surface micromechanical structures. *J. Vac. Sci. Technol., B* **1997**, 15, (1), 1-20.
5. Maboudian, R.; Ashurst, W. R.; Carraro, C., Self-assembled monolayers as anti-stiction coatings for MEMS: characteristics and recent developments. *Sens. Actuators, A* **2000**, 82, (1-3), 219-223.
6. Bhushan, B.; Kasai, T.; Kulik, G.; Barbieri, L.; Hoffmann, P., AFM study of perfluoroalkylsilane and alkylsilane self-assembled monolayers for anti-stiction in MEMS/NEMS. *Ultramicroscopy* **2005**, 105, (1-4), 176-188.
7. Pujari, S. P.; Spruijt, E.; Cohen Stuart, M. A.; van Rijn, C. J. M.; Paulusse, J. M. J.; Zuilhof, H., Ultralow Adhesion and Friction of Fluoro-Hydro Alkyne-Derived Self-Assembled Monolayers on H-Terminated Si(111). *Langmuir* **2012**, 28, (51), 17690-17700.
8. Pujari, S. P.; Scheres, L.; Weidner, T.; Baio, J. E.; Cohen Stuart, M. A.; van Rijn, C. J. M.; Zuilhof, H., Covalently Attached Organic Monolayers onto Silicon Carbide from 1-Alkynes: Molecular Structure and Tribological Properties. *Langmuir* **2013**, 29, (12), 4019-4031.
9. Pujari, S. P.; Li, Y.; Regeling, R.; Zuilhof, H., Tribology and Stability of Organic Mono layers on CrN: A Comparison among Silane, Phosphonate, Alkene, and Alkyne Chemistries. *Langmuir* **2013**, 29, (33), 10405-10415.
10. Vyas, M. K.; Schneider, K.; Nandan, B.; Stamm, M., Switching of friction by binary polymer brushes. *Soft Matter* **2008**, 4, (5), 1024-1032.
11. Raviv, U.; Giasson, S.; Kampf, N.; Gohy, J.-F.; Jeome, R.; Klein, J., Lubrication by charged polymers. *Nature* **2003**, 425, 163-165.
12. Landherr, L. J. T.; Cohen, C.; Agarwal, P.; Archer, L. A., Interfacial Friction and Adhesion of Polymer Brushes. *Langmuir* **2011**, 27, (15), 9387-9395.
13. Perrine, K. A.; Teplyakov, A. V., Reactivity of selectively terminated single crystal silicon surfaces. *Chem. Soc. Rev.* **2010**, 39, (8), 3256-3274.
14. Gooding, J. J.; Darwish, N., The rise of self-assembled monolayers for fabricating electrochemical biosensors—an interfacial perspective. *Chem. Rec.* **2012**, 12, (1), 92-105.
15. Li, Y.; Calder, S.; Yaffe, O.; Cahen, D.; Haick, H.; Kronik, L.; Zuilhof, H., Hybrids of Organic Molecules and Flat, Oxide-Free Silicon: High-Density Monolayers, Electronic Properties, and Functionalization. *Langmuir* **2012**, 28, (26), 9920-9929.
16. Pensa, E.; Cortes, E.; Corthey, G.; Carro, P.; Vericat, C.; Fonticelli, M. H.; Benitez, G.; Rubert, A. A.; Salvarezza, R. C., The Chemistry of the Sulfur-Gold Interface: In Search of a Unified Model. *Acc. Chem. Res.* **2012**, 45, (8), 1183-1192.
17. Love, J. C.; Estroff, L. A.; Kriebel, J. K.; Nuzzo, R. G.; Whitesides, G. M., Self-assembled monolayers of thiolates on metals as a form of nanotechnology. *Chem. Rev.* **2005**, 105, (4), 1103-1169.
18. Hakkinen, H., The gold-sulfur interface at the nanoscale. *Nat. Chem.* **2012**, 4, (6), 443-455.
19. Haensch, C.; Hoeppener, S.; Schubert, U. S., Chemical modification of self-assembled silane based monolayers by surface reactions. *Chem. Soc. Rev.* **2010**, 39, (6), 2323-2334.

20. Wen, K.; Maoz, R.; Cohen, H.; Sagiv, J.; Gibaud, A.; Desert, A.; Ocko, B. M., Postassembly chemical modification of a highly ordered organosilane multilayer: New insights into the structure, bonding, and dynamics of self-assembling silane monolayers. *ACS Nano* **2008**, 2, (3), 579-599.
21. Sagiv, J., Organized Monolayers by Adsorption, I. Formation and Structure of Oleophobic Mixed Monolayers on Solid Surfaces. *J. Am. Chem. Soc.* **1978**, 102, (1), 92-98.
22. Linford, M. R.; Chidsey, C. E. D., Alkyl monolayers covalently bonded to silicon surfaces. *J. Am. Chem. Soc.* **1993**, 115, (26), 12631-12632.
23. Voicu, R.; Boukherroub, R.; Bartzoka, V.; Ward, T.; Wojtyk, J. T. C.; Wayner, D. D. M., Formation, characterization, and chemistry of undecanoic acid-terminated silicon surfaces: Patterning and immobilization of DNA. *Langmuir* **2004**, 20, (26), 11713-11720.
24. Sun, Q. Y.; de Smet, L. C. P. M.; van Lagen, B.; Giesbers, M.; Thune, P. C.; van Engelenburg, J.; de Wolf, F. A.; Zuilhof, H.; Sudholter, E. J. R., Covalently attached monolayers on crystalline hydrogen-terminated silicon: Extremely mild attachment by visible light. *J. Am. Chem. Soc.* **2005**, 127, (8), 2514-2523.
25. Scheres, L.; Giesbers, M.; Zuilhof, H., Organic Monolayers onto Oxide-Free Silicon with Improved Surface Coverage: Alkynes versus Alkenes. *Langmuir* **2010**, 26, (7), 4790-4795.
26. Alexander B. Sieval; Ricarda Opitz; Huub P. A. Maas; Michael G. Schoeman; Geert Meijer; Frank J. Vergeldt; Han Zuilhof; Sudholter, E. J. R., Monolayers of 1-Alkynes on the H-Terminated Si(100) Surface. *Langmuir* **2000**, 16, (26), 10359-10368.
27. Gooding, J. J.; Ciampi, S., The molecular level modification of surfaces: from self-assembled monolayers to complex molecular assemblies. *Chem. Soc. Rev.* **2011**, 40, (5), 2704-18.
28. Cattaruzza, F.; Cricenti, A.; Flamini, A.; Girasole, M.; Longo, G.; Mezzi, A.; Prosperi, T., Carboxylic acid terminated monolayer formation on crystalline silicon and silicon nitride surfaces. A surface coverage determination with a fluorescent probe in solution. *J. Mater. Chem.* **2004**, 14, (9), 1461-1468.
29. Zigah, D.; Herrier, C.; Scheres, L.; Giesbers, M.; Fabre, B.; Hapiot, P.; Zuilhof, H., Tuning the Electronic Communication between Redox Centers Bound to Insulating Surfaces. *Angew. Chem. Int. Ed.* **2010**, 49, (18), 3157-3160.
30. Yang, M.; Teeuwen, R. L. M.; Giesbers, M.; Baggerman, J.; Arafat, A.; de Wolf, F. A.; van Hest, J. C. M.; Zuilhof, H., One-Step Photochemical Attachment of NHS-Terminated Monolayers onto Silicon Surfaces and Subsequent Functionalization. *Langmuir* **2008**, 24, (15), 7931-7938.
31. Kolb, H. C.; Finn, M. G.; Sharpless, K. B., Click Chemistry: Diverse Chemical Function from a Few Good Reactions. *Angew. Chem. Int. Ed.* **2001**, 40, (11), 2004-2021.
32. Wang, Q.; Chan, T. R.; Hilgraf, R.; Fokin, V. V.; Sharpless, K. B.; Finn, M. G., Bioconjugation by Copper(I)-Catalyzed Azide-Alkyne [3 + 2] Cycloaddition. *J. Am. Chem. Soc.* **2003**, 125, (11), 3192-3193.
33. Laughlin, S. T.; Baskin, J. M.; Amacher, S. L.; Bertozzi, C. R., In vivo imaging of membrane-associated glycans in developing zebrafish. *Science* **2008**, 320, (5876), 664-667.
34. van Berkel, S. S.; Dirks, A. J.; Meeuwissen, S. A.; Pinggen, D. L. L.; Boerman, O. C.; Laverman, P.; van Delft, F. L.; Cornelissen, J. J. L. M.; Rutjes, F. P. J. T., Application of Metal-Free Triazole Formation in the Synthesis of Cyclic RGD-DTPA Conjugates. *ChemBioChem* **2008**, 9, (11), 1805-1815.



35. Shi, F.; Waldo, J. P.; Chen, Y.; Larock, R. C., Benzyne Click Chemistry: Synthesis of Benzotriazoles from Benzyne and Azides. *Org. Lett.* **2008**, 10, (12), 2409-2412.
36. Sawoo, S.; Dutta, P.; Chakraborty, A.; Mukhopadhyay, R.; Bouloussa, O.; Sarkar, A., A new bio-active surface for protein immobilisation via copper-free 'click' between azido SAM and alkynyl Fischer carbene complex. *Chem. Commun.* **2008**, (45), 5957-5959.
37. Dag, A.; Durmaz, H.; Hizal, G.; Tunca, U., Preparation of 3-arm star polymers (A3) via Diels–Alder click reaction. *J. Polym. Sci., Part A: Polym. Chem.* **2008**, 46, (1), 302-313.
38. Blackman, M. L.; Royzen, M.; Fox, J. M., Tetrazine Ligation: Fast Bioconjugation Based on Inverse-Electron-Demand Diels–Alder Reactivity. *J. Am. Chem. Soc.* **2008**, 130, (41), 13518-13519.
39. Inglis, A. J.; Sinnwell, S.; Stenzel, M. H.; Barner-Kowollik, C., Ultrafast Click Conjugation of Macromolecular Building Blocks at Ambient Temperature. *Angew. Chem. Int. Ed.* **2009**, 48, (13), 2411-2414.
40. Hoyle, C. E.; Bowman, C. N., Thiol-Ene Click Chemistry. *Angew. Chem. Int. Ed.* **2010**, 49, (9), 1540-1573.
41. Hoogenboom, R., Thiol-Yne Chemistry: A Powerful Tool for Creating Highly Functional Materials. *Angew. Chem. Int. Ed.* **2010**, 49, (20), 3415-3417.
42. Pounder, R. J.; Stanford, M. J.; Brooks, P.; Richards, S. P.; Dove, A. P., Metal free thiol-maleimide 'Click' reaction as a mild functionalisation strategy for degradable polymers. *Chem. Commun.* **2008**, (41), 5158-5160.
43. Ott, C.; Hoogenboom, R.; Schubert, U. S., Post-modification of poly(pentafluorostyrene): a versatile "click" method to create well-defined multifunctional graft copolymers. *Chem. Commun.* **2008**, (30), 3516-3518.
44. ten Brummelhuis, N.; Diehl, C.; Schlaad, H., Thiol–Ene Modification of 1,2-Polybutadiene Using UV Light or Sunlight. *Macromolecules* **2008**, 41, (24), 9946-9947.
45. Killops, K. L.; Campos, L. M.; Hawker, C. J., Robust, Efficient, and Orthogonal Synthesis of Dendrimers via Thiol-ene "Click" Chemistry. *J. Am. Chem. Soc.* **2008**, 130, (15), 5062-5064.
46. Lowe, A. B., Thiol-ene "click" reactions and recent applications in polymer and materials synthesis. *Polym. Chem.* **2010**, 1, (1), 17-36.
47. Campos, M. A. C.; Paulusse, J. M. J.; Zuilhof, H., Functional monolayers on oxide-free silicon surfaces via thiol-ene click chemistry. *Chem. Commun.* **2010**, 46, (30), 5512-5514.
48. Kohler, E. P.; Potter, H., The Properties of Unsaturated Sulfur Compounds. I. Alpha Beta Unsaturated Sulfones. *J. Am. Chem. Soc.* **1935**, 57, (7), 1316-1321.
49. Finzi, C.; Venturini, G.; L. Sartini, Thiophenols. Dithioflavone and linear dithioflavanone *Gazz. Chim. Ital.* **1930**, 60, 798-811.
50. Fairbanks, B. D.; Scott, T. F.; Kloxin, C. J.; Anseth, K. S.; Bowman, C. N., Thiol–Yne Photopolymerizations: Novel Mechanism, Kinetics, and Step-Growth Formation of Highly Cross-Linked Networks. *Macromolecules* **2009**, 42, (1), 211-217.
51. Hensarling, R. M.; Doughty, V. A.; Chan, J. W.; Patton, D. L., "Clicking" Polymer Brushes with Thiol-yne Chemistry: Indoors and Out. *J. Am. Chem. Soc.* **2009**, 131, (41), 14673-14675.
52. Wendeln, C.; Rinnen, S.; Schulz, C.; Arlinghaus, H. F.; Ravoo, B. J., Photochemical Microcontact Printing by Thiol-Ene and Thiol-Yne Click Chemistry. *Langmuir* **2010**, 26, (20), 15966-15971.

53. Rigoberto C. Advincula; William A. Rittain; Kenneth C. Caster; Richard A. He, . r., *Polymer Brushes: Synthesis, Characterization, Applications*. WILEY-VCH Verlag GmbH & Co. KGaA: 2004.
54. Hoy, O.; Zdyrko, B.; Lupitskyy, R.; Sheparovych, R.; Aulich, D.; Wang, J. F.; Bittrich, E.; Eichhorn, K. J.; Uhlmann, P.; Hinrichs, K.; Muller, M.; Stamm, M.; Minko, S.; Luzinov, I., Synthetic Hydrophilic Materials with Tunable Strength and a Range of Hydrophobic Interactions. *Adv. Funct. Mater.* **2010**, 20, (14), 2240-2247.
55. Banerjee, I.; Pangule, R. C.; Kane, R. S., Antifouling coatings: Recent developments in the design of surfaces that prevent fouling by proteins, bacteria, and marine organisms. *Adv. Mater.* **2011**, 23, (6), 690-718.
56. Stuart, M. A. C.; Huck, W. T. S.; Genzer, J.; Muller, M.; Ober, C.; Stamm, M.; Sukhorukov, G. B.; Szleifer, I.; Tsukruk, V. V.; Urban, M.; Winnik, F.; Zauscher, S.; Luzinov, I.; Minko, S., Emerging applications of stimuli-responsive polymer materials. *Nat Mater* **2010**, 9, (2), 101-113.
57. Bhairamadgi, N. S.; Pujari, S. P.; van Rijn, C. J. M.; Zuilhof, H., Adhesion and Friction Properties of Polymer Brushes: Fluoro versus Non-fluoro Polymer Brushes at Varying Thickness. *Langmuir* **2014**, 30, (8), 2068–2076.
58. Pidhatika, B.; Moller, J.; Vogel, V.; Konradi, R., Nonfouling surface coatings based on poly(2-methyl-2-oxazoline). *Chimia* **2008**, 62, (4), 264-269.
59. Senaratne, W.; Andruzzi, L.; Ober, C. K., Self-assembled monolayers and polymer brushes in biotechnology: Current applications and future perspectives. *Biomacromolecules* **2005**, 6, (5), 2427-2448.
60. Ayres, N., Polymer brushes: Applications in biomaterials and nanotechnology. *Polym. Chem.* **2010**, 1, (6), 769.
61. Brinks, M. K.; Studer, A., Polymer Brushes by Nitroxide-Mediated Polymerization. *Macromol. Rapid Commun.* **2009**, 30, (13), 1043-1057.
62. Arbey, R.; Avnand, .; Paripovic, D.; Scherer, N.; Sugnaux, C.; Tugulu, S.; Lok, H.-A., Polymer Brushes via Surface-Initiated Controlled Radical Polymerization: Synthesis, Characterization, Properties, and Applications. *Chem. Rev.* **2009**, 109, (11), 5437-5527.
63. Matyjaszewski, K., Atom Transfer Radical Polymerization (ATRP): Current Status and Future Perspectives. *Macromolecules* **2012**, 45, (10), 4015-4039.
64. Dowson, D., *History of Tribology*. 2nd Edition ed.; Professional Engineering Publishing: Distributed by ASTM, 1998.
65. Zeng, H., *Polymer Adhesion, Friction and Lubrication*. John Wiley & Sons, Inc.: Hoboken, New Jersey, **2013**.
66. Yoshizawa, H.; You-Lung, C.; Israelachvili, J., Recent advances in molecular level understanding of adhesion, friction and lubrication. *Wear* **1993**, 168, (1–2), 161-166.
67. Binnig, G.; Quate, C. F., Atomic Force Microscopy. *Phys. Rev. Lett.* **1986**, 56, (9), 930-933.
68. Giesbers, M. Surface Force Studied With Colloidal Probe Atomic Force Microscopy. Wageningen University, Wageningen, The Netherlands, **2001**.
69. Chung, K.-H.; Pratt, J. R.; Reitsma, M. G., Lateral Force Calibration: Accurate Procedures for Colloidal Probe Friction Measurements in Atomic Force Microscopy. *Langmuir* **2009**, 26, (2), 1386-1394.
70. F. T. Limpoco, R. C. A., and Scott S. Perry, Solvent Dependent Friction Force Response of Polystyrene Brushes Prepared by Surface Initiated Polymerization. *Langmuir* **2007**, 23, (24), 12196–12201.

71. Klein, J.; Kamiyama, Y.; Yoshizawa, H.; Israelachvili, J. N.; Fredrickson, G. H.; Pincus, P.; Fetters, L. J., Lubrication forces between surfaces bearing polymer brushes. *Macromolecules* **1993**, 26, (21), 5552-5560.
72. Klein, J.; Kumacheva, E.; Mahalu, D.; Perahla, D.; Fetters, L. J., Reduction of frictional forces between solid-surfaces bearing polymer brushes. *Nature* **1994**, 634-636.
73. Klein, J.; Perahia, D.; Warburg, S., Forces between polymer-bearing surfaces undergoing shear. *Nature* **1991**, 143-145.
74. Hurley, C. R.; Leggett, G. J., Influence of the Solvent Environment on the Contact Mechanics of Tip-Sample Interactions in Friction Force Microscopy of Poly(ethylene terephthalate) Films. *Langmuir* **2006**, 22, (9), 4179-4183.
75. Bielecki, R. M.; Benetti, E. M.; Kumar, D.; Spencer, N. D., Lubrication with Oil-Compatible Polymer Brushes. *Tribol Lett* **2012**, 45, (3), 477-487.
76. Wei, Q.; Cai, M.; Zhou, F.; Liu, W., Dramatically Tuning Friction Using Responsive Polyelectrolyte Brushes. *Macromolecules* **2013**, 46, (23), 9368-9379.
77. Sakata, H.; Kobayashi, M.; Otsuka, H.; Takahara, A., Tribological properties of poly(methyl methacrylate) brushes prepared by surface-initiated atom transfer radical polymerization. *Polym. J.* **2005**, 37, (10), 767-775.

# Chapter 2

---

## Efficient Functionalization of Oxide-free Silicon(111) Surfaces: Thiol-yne versus Thiol-ene Click Chemistry

### Abstract

Thiol-yne click (TYC) chemistry was utilized as a copper-free click reaction for the modification of alkyne-terminated monolayers on oxide-free Si(111) surfaces, and the results were compared with the analogous thiol-ene click (TEC) chemistry. A wide range of thiols such as 9-fluorenylmethoxy-carbonyl cysteine, thio- $\beta$ -D-glucose tetraacetate, thioacetic acid, thioglycerol, thioglycolic acid and 1H,1H,2H,2H-perfluorodecanethiol were immobilized using TYC under photochemical conditions, and all modified surfaces were characterized by static water contact angle measurements, X-ray photoelectron spectroscopy (including a simulation thereof by density functional calculations) and infrared absorption reflection spectroscopy. Surface-bound TYC proceeds with an efficiency up to 1.5 thiols per alkyne group. This high surface coverage proceeds without oxidizing the Si surface. TYC yielded consistently higher surface coverages than TEC, due to double addition of thiols to alkyne-terminated monolayers. This also allows for the sequential and highly efficient attachment of two different thiols onto an alkyne-terminated monolayer.

This chapter is published as:

*'Efficient Functionalization of Oxide-Free Silicon(111) Surfaces: Thiol-yne versus Thiol-ene Click Chemistry'*  
Bhairamadgi, N. S.; Gangarapu, S.; Campos, M. A. C.; Paulusse, J. M. J.; van Rijn, C. J. M.; Zuilhof, H.  
*Langmuir* **2013**, 29, 14, 4535-4542.

**Contents**

<b>2. Efficient Functionalization of Oxide-free Silicon(111) Surfaces: Thiol-yne versus Thiol-ene Click Chemistry .....</b>	<b>19</b>
Abstract .....	19
2.1 Introduction .....	21
2.2 Experimental Methods .....	22
2.2.1 Simulation of XPS Spectra.....	23
2.2.2 Monolayer Preparation.....	23
2.2.3 Thiol-yne Click Chemistry.....	24
2.3 Results and Discussion.....	24
2.3.1 Alkyne-Terminated Monolayers .....	24
2.3.2 Thiol-yne Click Chemistry.....	27
2.3.3 Thiol-ene versus Thiol-yne Click Chemistry .....	29
2.4 Conclusions .....	32
2.5 References .....	33

## 2.1 Introduction

In the last decade “click chemistries” have attracted significant attention in the fields of synthetic chemistry, chemical biology, pharmacology and materials science,<sup>1-8</sup> due to their unique advantages such as mild reaction conditions, a high degree of bio-orthogonality and high reaction yields.<sup>2,3,9-13</sup> While highly effective and most popular, the copper-catalyzed alkyne-azide cycloaddition (CuAAC) utilizes Cu(I) as catalyst, which can be disadvantageous for biological samples and surface properties.<sup>14-16</sup> Apart from the toxicity of Cu ions, the electronic properties of modified surfaces can also be seriously affected.<sup>17</sup> These limitations can be overcome by the Cu-free and strain-promoted cyclooctyne-azide click reaction (SPAAC).<sup>9, 18</sup> However, this method yields a reduced surface coverage compared to CuAAC, because of the steric bulk of cyclooctyne moieties in combination with some non-selective reactivity related to the high reactivity of these cyclooctynes. Recently, our group reported the modification of Si(111) surfaces and silicon nanoparticles using thiol-ene click (TEC) chemistry.<sup>19, 20</sup> Silicon surface modification via TEC approach resulted in good surface coverages (45% – 75%, depending on the thiol), and surfaces did not display oxidation after modification.<sup>20</sup> Yet, several aspects would favor further improvements: 1) some thiols react rather sluggishly in TEC, thus hampering the attachment – a speed-up would thus be desired; 2) silicon surfaces do react with 1-alkenes, but the packing density is sub-optimal, and can be improved by switching to 1-alkynes.<sup>21,22</sup> 3) TEC does not directly allow the binding of two different thiols onto one linker chain; such binding, however, may be advantageous to obtain surfaces with complex surface requirements.

To address all these issues at once, the current paper investigates thiol-yne click (TYC) chemistry onto alkyne-terminated monolayers derived from 1, $\omega$ -dialkynes. Terminal alkynes react more readily with the H-terminated Si surface, yielding a more densely packed surface modification with increased stability.<sup>21, 23-25</sup> In addition, alkynes typically react in TYC faster than the corresponding alkenes in TEC reactions,<sup>26</sup> while finally TYC would, in principle, allow the binding of two different groups onto one surface-terminal group.<sup>26-32</sup> Mechanistically, TYC is a radical chain process that proceeds as follows: in the first propagation step of the TYC reaction, vinyl sulfide radicals are formed by the addition of a thiol radical across the alkyne triple bond. A vinyl sulfide radical subsequently abstracts a hydrogen radical from a thiol, thus generating vinyl sulfide and another reactive thiol radical. If a second addition step is feasible, then next a thiol radical adds across the double bond of the vinyl sulfide leading to the formation of dithioether radical, which subsequently abstracts a hydrogen radical from thiol forming a 1,2-dithioether. An intermediate (vinyl sulfide) formed after the addition of thiol was nearly three times more reactive towards hydrothiolation than the initial yne moiety.<sup>33</sup> Ravoo et al.<sup>34</sup> reported the photochemical micro contact printing onto silane-coated silicon oxide

and glass surfaces via TEC and TYC chemistry with D,L-dithiothreitol, 3-mercaptopropionic acid, tetraacetylgalactoside-thiol conjugate, and a galactoside-thiol conjugate on alkyne-terminated monolayers. However, they did not observe any difference in reactivity between TEC and TYC reactions. In contrast, Minozzi et al. studied the thiol-yne click reaction in solution, and observed that both mono as well as bis-adducts are formed, depending on reaction conditions.<sup>35</sup> Silicon surfaces modified via TYC may provide improved access to further modification with biomolecules, which could find application in the development of biosensors and microelectronic devices.<sup>36, 37</sup>

Our aim in the current study was to compare the efficiency of surface-bound TYC versus TEC reactions, via the modification of Si(111) surfaces with alkyne-terminated monolayers, followed by attachment of various functional thiols (Figures 1 and 2). The resulting surfaces have been investigated by a range of surface-sensitive characterization techniques, including XPS, contact angle measurements and IR spectroscopy, so as to provide an unambiguous comparison of the surface-bound TEC and TYC reactions.

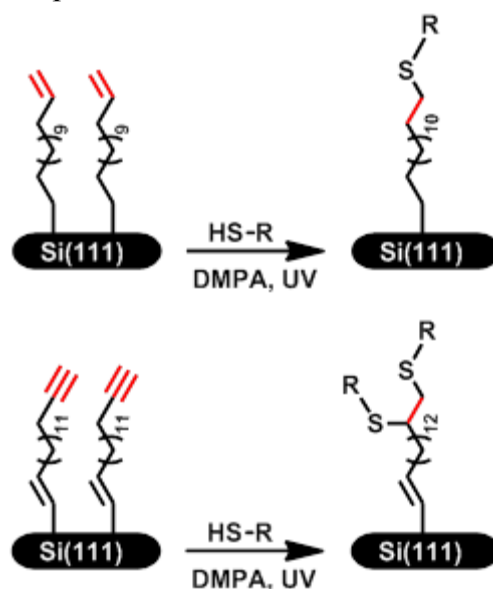


**Figure 1.** Comparison of surface-bound thiol-ene (above) and thiol-yne (below) chemistry under current study.

## 2.2 Experimental Methods

All materials were obtained from Sigma-Aldrich and used without further purification unless otherwise specified. Fmoc-protected cysteine (99.6%) was purchased from Chem-Impex International. Diethyl ether and dichloromethane were distilled before use. 1,15-Hexadecadiyne was prepared using a method adapted from the synthesis of analogous 1, $\omega$ -diynes.<sup>38</sup> (See Supporting Information for experimental details and spectral data.) Nuclear magnetic resonance ( $^1\text{H}/^{13}\text{C}$  NMR) spectra were recorded on a Bruker 400/100 MHz machine at room temperature using  $\text{CDCl}_3$  as internal reference. A Krüss DSA 100 goniometer was used to measure static water contact angles under ambient conditions. Droplets (3.0  $\mu\text{L}$ ) of deionized water were dispensed with a micro syringe. The errors in

the contact angles were  $\pm 1^\circ$ . X-ray photoelectron spectroscopy (XPS) measurements were performed on a JEOL JPS-9200 system (conditions: Al K $\alpha$  source with an X-ray power of 300 W, an analyzer pass energy of 10 eV, and energy resolution of  $< 0.65$  eV). Binding energies of C1s (C-C) peak was calibrated to 285.0 eV, data was analyzed using CasaXPS software. IRRAS spectra were recorded on a Bruker Tensor 27 FT-IR spectrometer using a commercially variable angle reflection unit (Auto Seagull, Harrick Scientific). A Harrick grid polarizer was installed in front of the detector and was used to measure spectra with *p*-polarized (parallel) radiation with respect to the plane of incidence at the sample surface. All spectra were obtained at an incident angle of  $68^\circ$  with 2048 scans recorded for each sample.

### 2.2.1 Simulation of XPS Spectra

Electronic core level calculations were used to simulate the core levels of C1s XPS spectra. The effect of Si-C bond monolayers are mimicked by binding of an alkyl chain to either a Si(SiH<sub>3</sub>)<sub>3</sub> (TMS) moiety,<sup>39</sup> or a ((Si(CH<sub>3</sub>)<sub>3</sub>)<sub>2</sub>CH<sub>3</sub>Si)<sub>2</sub>-Si(H)CH<sub>3</sub> structure used before to mimic the H-Si surface.<sup>40</sup> The geometries of the different systems were optimized at B3LYP/6-311G(d,p) level of theory and followed by natural bond order (NBO) analysis for the calculation of core orbital energies. All the calculations were carried out using the Gaussian 09 program.<sup>41</sup>

### 2.2.2 Monolayer Preparation

One-side polished Si(111) wafers (n-type, 475-550  $\mu\text{m}$  thick, resistivity 1.0-5.0  $\Omega\text{ cm}$ , Siltronic, France) were cut into  $1 \times 1\text{ cm}^2$  pieces and washed with acetone (semiconductor grade), and then sonicated for 10 min in acetone. The samples were cleaned using piranha acid (H<sub>2</sub>SO<sub>4</sub>:H<sub>2</sub>O<sub>2</sub>, 3:1) for 30 min. **Caution: Piranha solution reacts violently with organic materials and should be handled carefully!** Silicon substrates were rinsed with sufficient amounts of deionized water (18.3 M $\Omega\text{ cm}$  resistivity), dried with a stream of dry argon and etched in an argon-saturated 40% aqueous NH<sub>4</sub>F (semiconductor grade) solution for 15 min under an argon atmosphere. After taking them out, the substrates were rinsed with deionized water, dried under a stream of argon and rapidly transferred to a 25 mL three-necked flask (fitted with a capillary, a reflux condenser and connected to a vacuum pump) containing neat 1,15-hexadecadiyne (1.0 g) under an argon atmosphere for 30 min. After transferring the substrates, the capillary that slowly flows argon into the flask was moved away from the solution to avoid disturbance during monolayer formation. The reaction flask was kept at  $80^\circ\text{C}$  for 16 h under 4 mbar pressure with a gentle argon flow and under ambient light (i.e., the standard fluorescent lamps in the fume hood were kept on). After subsequently letting the reaction flask cool down to room temperature, the vacuum was released by purging argon and the silicon wafer was removed from the 1,15-hexadecadiyne. The functionalized silicon substrates were rinsed



with hexane followed by dichloromethane and dried with a stream of argon. Static water contact angle, XPS and IRRAS measurements were used for further characterization. Mixed monolayers were prepared in a similar way as described above, using a 1:1 mixture of 1, 15-hexadecadiyne and 1-dodecyne on H-Si(111) surfaces. The alkyne-terminated monolayer is referred to as **S-alkyne** and mixed monolayers as **S-mix**.

### 2.2.3 Thiol-yne Click Chemistry

Mixtures of a thiol (**1**, **2**, **3**, **4** or **5**; typically 0.072 – 7.22 mM) and 2,2-dimethoxy-2-phenylacetophenone (DMPA) as photoinitiator were prepared in a 1:0.2 molar ratio, in a minimal amount of chlorobenzene (ca. 1 mL) (Figure 2). The freshly prepared alkyne-terminated silicon substrates **S-alkyne** were rinsed with dichloromethane and dried with a stream of argon prior to further modification via TYC reaction. A few drops of freshly prepared thiol and initiator mixture were transferred onto an alkyne-terminated monolayer on Si(111) surfaces and irradiated with a 365 nm light (Power output 800  $\mu\text{W}/\text{cm}^2$ , distance between lamp and surface was 2 cm, Spectroline, Westbury, NY) for 1.5 h. Afterwards, the modified Si substrates were washed several times with chlorobenzene, and then with dichloromethane, and dried under a stream of argon. The thus modified Si substrates were characterized by static water contact angle measurements, IR and XPS.

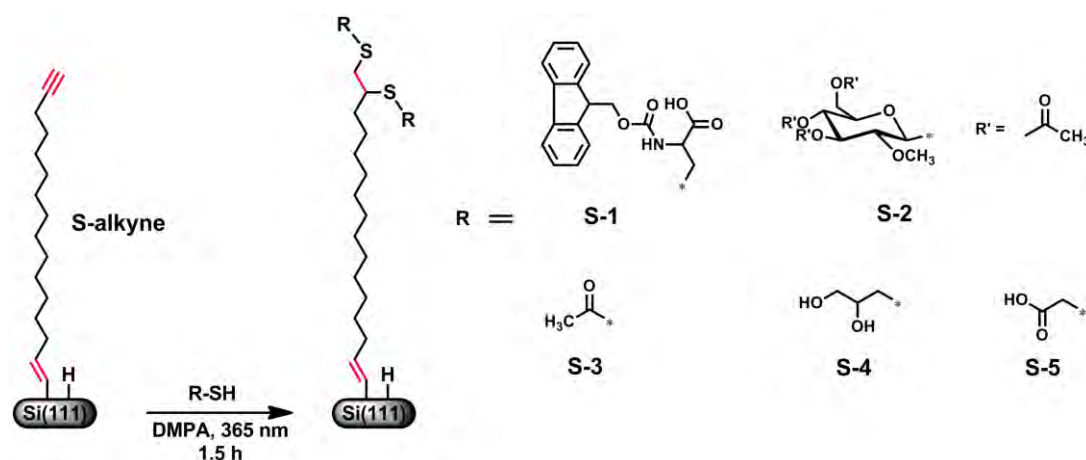


**Figure 2.** Modification of alkyne-terminated monolayers via thiol-yne click reaction.

## 2.3 Results and Discussion

### 2.3.1 Alkyne-Terminated Monolayers

Alkyne-terminated monolayers **S-alkyne** were prepared from the reaction of a H-terminated Si(111) surface with 1,15-hexadecadiyne. The H-terminated Si(111) surfaces were obtained by etching in argon-saturated 40%  $\text{NH}_4\text{F}$  solution for 15 min. 1,15-Hexadecadiyne was synthesized in two steps starting from 1,12-dodecadiol, via activation of the alcohol moieties by tosylation, followed by reacting these with  $\text{LiC}\equiv\text{CH}$ , to yield

$\text{HC}\equiv\text{C}(\text{CH}_2)_{12}\text{C}\equiv\text{CH}$ . This compound was then used to modify the freshly etched Si(111) surfaces under oxygen-free, thermal conditions (80 °C, 16 h, argon atmosphere). Upon modification, the surfaces became hydrophobic, with a static water contact angle of  $\sim 87^\circ$ . IRRAS results (Figure 3) showed the symmetric and anti-symmetric C-H stretching frequencies at  $2854\text{ cm}^{-1}$  and  $2925\text{ cm}^{-1}$ , respectively, which indicate the formation of covalently bound monolayers without much short-range order. Since 1-alkyne derived monolayers display a high degree of short-range order (e.g. indicated by corresponding C-H vibrations at  $2850\text{ cm}^{-1}$  and  $2918\text{ cm}^{-1}$ ),<sup>21</sup> we attribute this difference to mutual repulsions between  $\pi$ -bond orbitals at the top of the monolayer. The peak at  $3324\text{ cm}^{-1}$  is a characteristic  $\text{-C}\equiv\text{C-H}$  stretch peak, which indicates the presence of terminal  $\text{-C}\equiv\text{C-H}$  moieties on the surface.

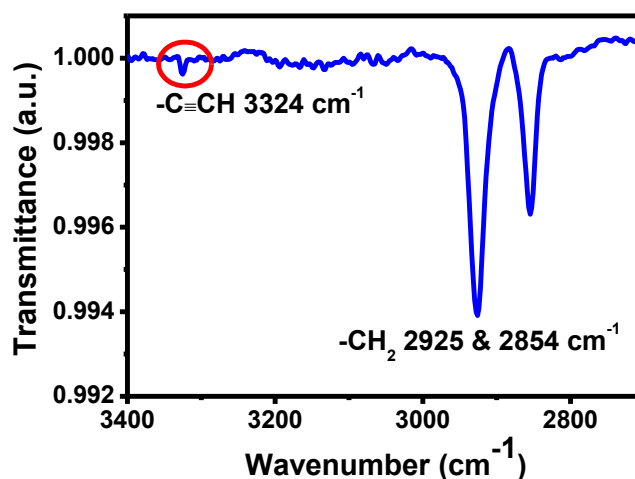


**Figure 3.** IRRAS spectrum of H-C $\equiv$ C-terminated monolayer derived from 1,15-hexadecadiyne on H-Si(111) (S-alkyne).

The XPS C1s narrow scan (Figure 4A) was deconvoluted into three peaks at 283.5 eV, 285.0 eV and 286.2 eV with an area ratio of 1:14:1, respectively, which is in line with the assignment to Si-C, C-C and C $\equiv$ C-C atoms, respectively. This indicates that per di-alkyne molecule, only one terminal alkyne group reacted with the silicon surface, in line with the IR data above, and that polymerization of terminal alkyne groups was not observed. Similar observations with 1,8-nonadiyne on H-Si(100) were reported before by Gooding and co-workers.<sup>42, 43</sup> In addition, density functional theory (DFT) was used to calculate the binding energies of distinct carbon atoms attached to the surface. As shown in detail elsewhere, B3LYP/6-311G(d,p) calculations provide an excellent and simple approach to obtain chemically reliable chemical shifts for the XPS C1s spectra.<sup>44</sup> The calculations showed that the carbons attached to Si(111) come at lower binding of 284.4 eV, aliphatic carbon atoms (C-C) come at 285 eV and terminal alkyne carbon comes at much lower binding energy of 284.3 eV, which yields an excellent agreement with the experimentally obtained spectrum/which allows unequivocal assignment of the experimental spectrum

(Figure 4B and details in Supporting Information, Figure SI-8 ). These results can be compared to the reported values in literature, and confirm the usefulness of DFT calculations for the assignment of C1s spectra of organic monolayers.<sup>45</sup> These alkyne-terminated silicon surfaces were stable to oxidation, as no silicon oxide peak was detected at 103 eV in XPS Si2p narrow scan (Supporting Information, Figure SI-1), also upon extensive storage (>1 month) under ambient conditions.

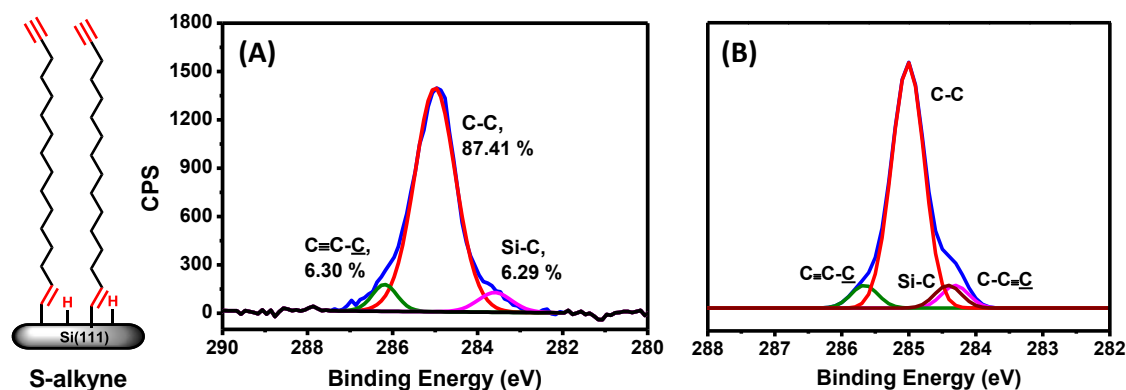


**Figure 4.** XPS spectrum of alkyne-terminated monolayer **S-alkyne**. (A) Experimental C1s narrow scan and (B) Simulated C1s spectrum from DFT (B3LYP/6-311G(d,p)) calculations.

Analogously, to obtain alkyne-terminated monolayers in which the terminal alkyne moieties can undergo subsequent reactions with less steric hindrance, we prepared mixed monolayers (**S-mix**) from a 1:1 mixture of 1,15-hexadecadiyne ( $C_{16}$ ) and 1-dodecyne ( $C_{12}$ ). The mixed monolayer showed a static water contact angle of  $95^\circ$ . The IR spectrum is similar to that **S-alkyne** (Figure 5), with an increased alkyne C-H stretch peak at  $3326\text{ cm}^{-1}$  and the appearance of a methyl peak at  $2965\text{ cm}^{-1}$ . The XPS spectrum (Figure 6A) now shows a 2:13:1 ratio for the  $\underline{\text{C}}\text{-Si} / \underline{\text{C}}\text{-C} / \underline{\text{C}}\text{-C}\equiv\text{C}$  (from alkyne-terminated monolayer) carbon atoms, in line with the formation of a 50% alkyne-terminated mixed monolayer. In addition, the simulated XPS spectrum from DFT calculations (Figure 6B) is in good agreement with experimentally obtained XPS spectrum of mixed monolayer.

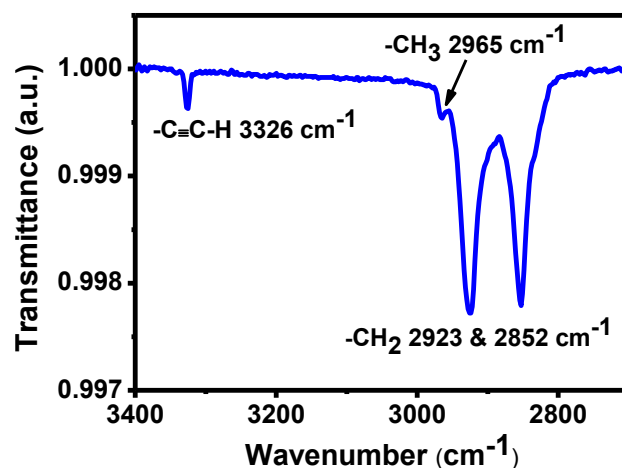


**Figure 5.** IRRAS spectrum of mixed monolayer **S-mix**.

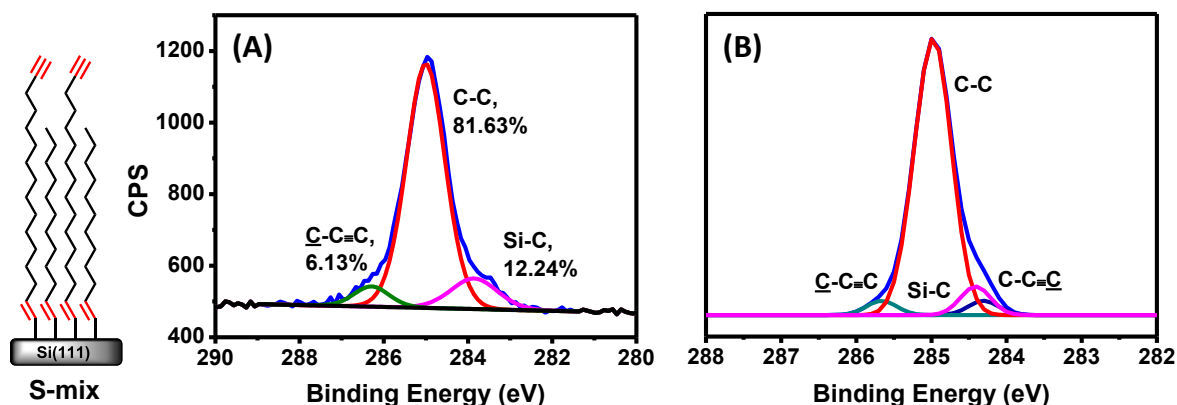


Figure 6. Experimental (A) and DFT-simulated (B) XPS C1s spectra of mixed monolayer **S-mix**.

### 2.3.2 Thiol-yne Click Chemistry

Alkyne-terminated silicon surfaces **S-alkyne** were treated with various thiols, such as 9-fluorenylmethoxy-carbonyl cysteine **1**, thio- $\beta$ -D-glucose tetraacetate **2**, thioacetic acid **3**, thioglycerol **4**, and thioglycolic acid **5** in the presence of DMPA as photo-initiator. A few drops (3 to 4) of a concentrated solution (details in Supporting Information) of DMPA and the thiol in chlorobenzene were transferred to an alkyne-terminated silicon surface, and TYC reactions were initiated by exposure to 365 nm light for 1.5 h under ambient conditions. Modification was monitored by measuring static water contact angles, which were decreased from initial contact angle of  $87^\circ$  (**S-alkyne**) to  $38^\circ$  -  $68^\circ$  (depending on thiols) after thiol-yne click modification (Table 1).

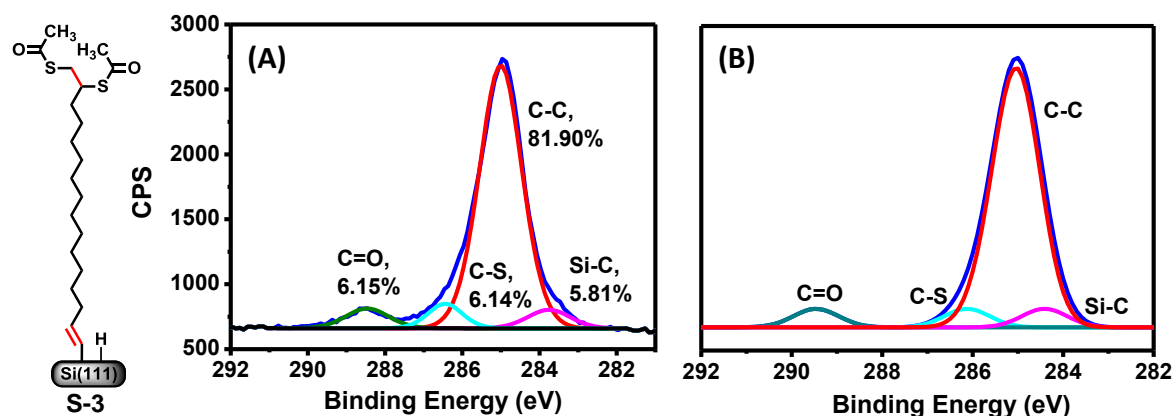


Figure 7. XPS spectrum of surface **S-3**. Experimental (A) and DFT-simulated (B) C1s narrow scan.

The thicknesses of modified surfaces were calculated by using the atomic ratio of C1s and Si2p from XPS survey scans with the help of Equation 1, building on the work of Wallart et al.<sup>46</sup>

$$d_{ML} (\text{\AA}) = \lambda_{ML}^{Si} \sin(\phi) \ln(1 + C/Si) \quad (1)$$

**Table 1.** Static water contact angle of Si(111) surfaces after modification.

Modified Si(111) surfaces	Static water contact angle ( $\theta^\circ$ )
<b>S-alkyne</b>	87
<b>S-1</b>	68
<b>S-2</b>	63
<b>S-3</b>	63
<b>S-4</b>	38
<b>S-5</b>	40
<b>S-mix<sup>a</sup></b>	95
<b>S-mix-3<sup>b</sup></b>	58
<b>S-mix-3/6<sup>c</sup></b>	103

<sup>a</sup> = Mixed monolayer, <sup>b</sup> = TYC with thiol **3** on mixed monolayer **S-mix**, <sup>c</sup> = TYC with sequential addition of thiol **3** and **6** on **S-mix**.

in which  $d_{ML}$  = thickness of monolayer,  $\lambda_{ML}^{Si}$  = attenuation length of Si2p photoelectrons in the organic monolayer (39.5 Å), and  $\phi$  = angle between the surface plane and detector (80°). The thickness of all modified surfaces is shown in Figure 8. Increase in thicknesses was observed after all TYC reactions when compared to the alkyne-terminated monolayer **S-alkyne**, and this was found to correlate to the size and surface coverage of the attached thiols. Successful surface-bound TYC chemistry of all modified surfaces was evidenced by the appearance of a S2s peak at 228.0 eV in the XPS survey scan (Supporting Information, Figure SI-1 to SI-5). In line with this, the XPS C1s narrow scan of e.g. thioacetic acid-modified surfaces (**S-3**) revealed a new peak at 288.5 eV, characteristic for a carbonyl carbon group ( $>C=O$ ), as present in the carboxylic acid group. The peak at 285.0 eV was deconvoluted into four peaks at 283.7 eV, 285.0 eV, 286.5 eV and 288.5 eV, corresponding to Si-C-, -C-C-, -C-S- and -C=O groups, respectively (Figure 7A). These experimental XPS binding energies of different carbon atoms are in good agreement with the calculated XPS binding energies from DFT calculations. The DFT calculations showed the peaks at 284.4 eV, 285.0 eV, 286.3 eV and 289.3 eV, corresponding to Si-C-, -C-C-, -C-S-, -C=O, respectively (Figure 7B, details Supporting Information, Figure SI-9, Table SI-3 and SI-4). Such deconvolution allows for the determination of the surface coverage of the attached groups, by considering the percentage ratio of area under well-separated -C=O peak with sum of area under -C-S-, - and -C-C peaks. The surface coverage of all thiol-modified surfaces was observed to be in the range of 48% - 146% (Figure 9). The Si2p narrow scan XPS data of all thiol-modified surfaces did not show any peak at 103 eV (shown in Supporting Information, Figure SI-1

to SI-5), which further showed that the modified silicon oxide-free surfaces were oxide-free even after exposing to 365 nm light for 1.5 h during TYC reaction.

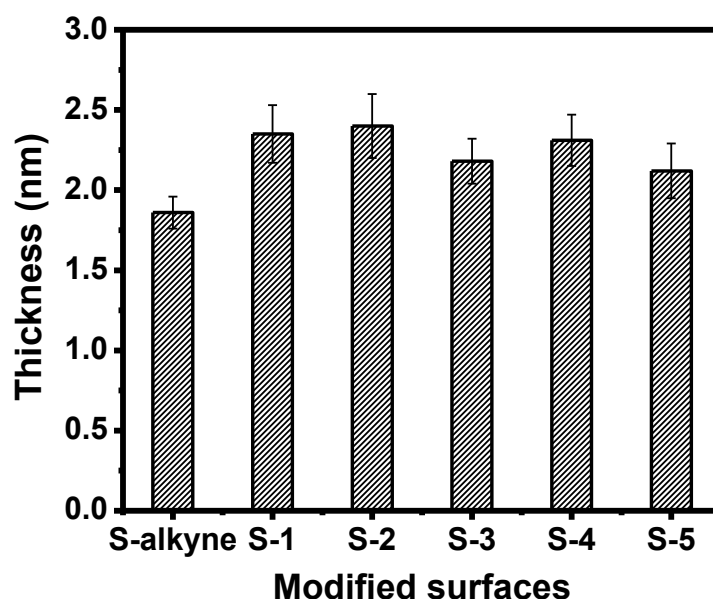


**Figure 8.** Thickness of modified surfaces calculated from the XPS-derived C/Si atomic ratio.

### 2.3.3 Thiol-ene versus Thiol-yne Click Chemistry

We compared surface coverages of TYC-modified surfaces with those obtained for TEC-modified surfaces, which were previously reported by our group.<sup>20</sup> In this, we consider the number of thiols reacting per alkyne/alkene functional group; a surface coverage of over 100% indicates that more than one thiol is bound to each alkyne/alkene group. In a TYC reaction, in principle, two thiol groups can react with one alkyne group, which consequently yields the potential to a higher surface coverage as compared to the TEC reaction.<sup>35, 36, 47-49</sup> Indeed, as found here, TYC chemistry on alkyne-terminated Si surfaces yielded for all thiols under investigation a consistently higher surface coverage of attached thiols than the corresponding TEC chemistry (Figure 9).<sup>20</sup> For example, in a TYC reaction 1 molecule of thiol [3] reacted per alkyne group, while in the analogous TEC reaction only ca. 0.5 thiol [3] molecules reacted per alkene moiety on alkene-terminated monolayer. In fact, a surface coverage of 100% or more was observed for all cases of the TYC reaction, apart from some particularly sterically hindered thiols (Figure 9). The observed surface coverages are not necessarily the maximally obtainable coverages, as apart from increased steric hindrance at the surface, the decreasing availability of thiols due to disulfide formation also plays a role.<sup>35</sup> This was, for example, inferred from the observation that the yield of these surface-bound click reactions could be pushed slightly higher by taking sample out of the solution, cleaning it with dichloromethane, and then continuing the reaction with fresh thiols (Supporting Information, Figure SI-6).

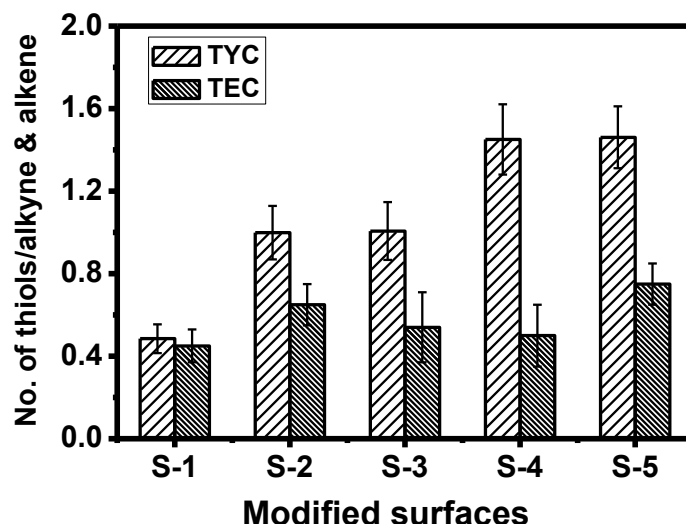


**Figure 9.** Surface reactivity: Thiol-ene versus thiol-yne click reactions.

An example of a thiol yielding a lower surface coverage is 9-fluorenylmethoxycarbonyl cysteine **1**, which did not show much difference in comparison to the TEC reaction. This might be due to the steric hindrance introduced by bulky molecule itself, while additionally the reaction rate of this thiol is reduced by deprotonation of a fraction of the thiols by the internal secondary amine functionality.<sup>26</sup> Apart from steric hindrance, radical stabilization might also play a role. This would explain why thioacetic acid **3**, which has roughly the same size as thiols **4** and **5**, still yielded a lower surface coverage than **4** and **5**. The stabilization of thioacetic acid radicals by resonance effects of the neighboring carbonyl moiety<sup>50-52</sup> yields a diminished reactivity.

The occurrence of >100% surface coverage, i.e. the reaction of more than one equivalent of thiols per alkyne moiety, induced us to investigate the formation of mixed monolayers with a high coverage of two different thiols. To this aim, we prepared Si(111) substrate with 50% alkyne-termination and 50% alkyl termination **S-mix**, in which the alkyne moieties stick out above the alkyl groups, yielding on average a reduced steric hindrance around the alkyne moiety. Onto this mixed monolayer we then attached thiols **3** (thioacetic acid) and **6** (1H,1H,2H,2H-perfluorodecanethiol) in a sequential manner (Figure 10). In first step, the alkyne-terminated mixed monolayer **S-mix** was reacted with thiol **3** in the presence of DMPA as a photoinitiator, yielding surface **S-mix-3**. The reduced static water contact angle (from 95° to 58°) suggested the successful attachment of thiol **3** on mixed monolayer. XPS survey scan showed the appearance of a new S2s peak at 228.0 eV from thiol **3**, while in the XPS C1s narrow scan a peak at 288.6 eV was observed, which is characteristic for the carbonyl carbon of thiol **3** (Figure 10A). A surface coverage of 83% was deduced from the ratio of the peak area at 288.6 eV (C=O) compared to the peak area of all other carbon atoms. A monolayer thickness of 2.0 nm was derived from the C/Si ratio from survey scan using Equation 1, which is a substantial

increase with respect to the XPS-derived thickness of the unreacted mixed monolayer 1.6 nm.

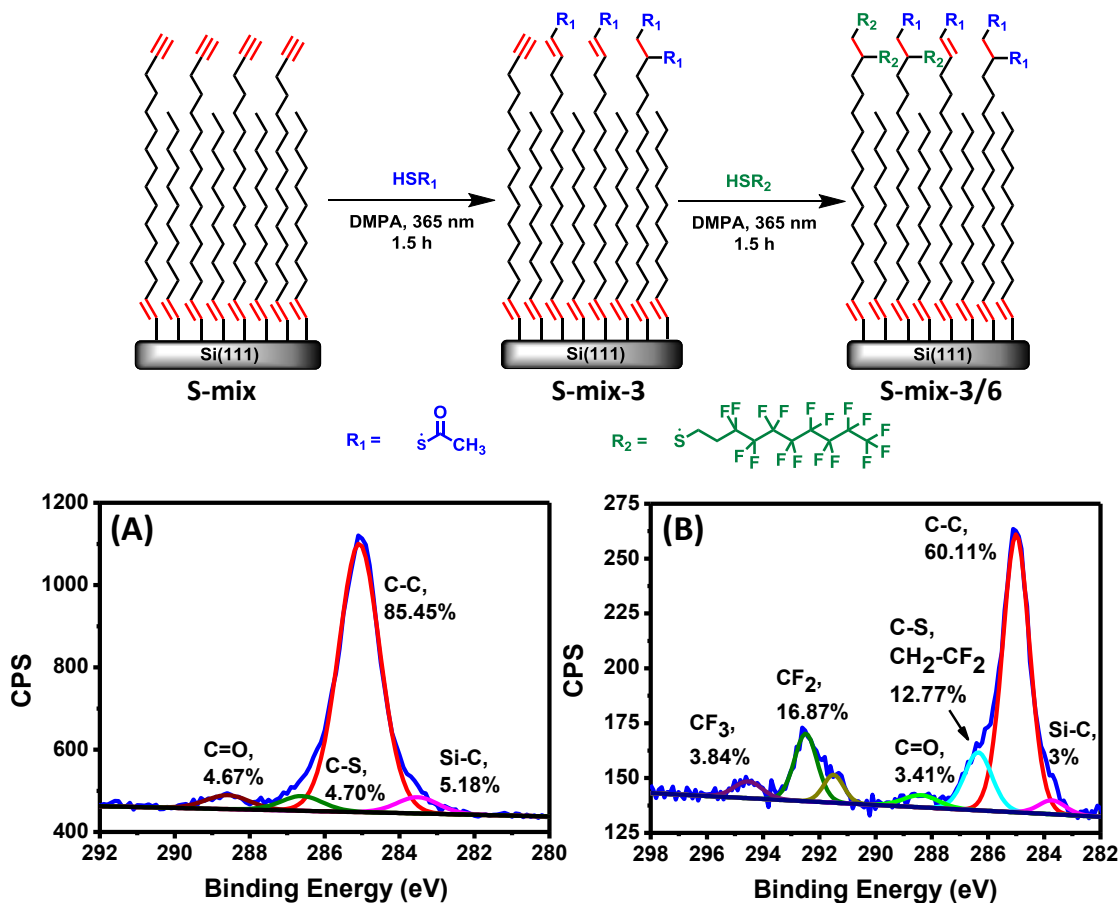


**Figure 10.** Top: Modification of mixed monolayer **S-mix** via thiol-ene click reaction with thiol **3** and subsequently with thiol **6**. Bottom: XPS C1s narrow scan of (A) **S-mix-3** and (B) **S-mix-3/6**.

In the second step thiol **6** was reacted to the surface that resulting after step 1 (**S-mix-3**) in the presence of DMPA as a photoinitiator. This second reaction increased the static water contact angle from  $58^\circ$  to  $103^\circ$  due to the highly apolar fluorinated chain.<sup>53</sup> In the XPS C1s narrow scan (Figure 10B), the region between 291.0 eV to 296.0 eV displays new peaks that correspond to carbons attached to two or three fluorine atoms ( $-\text{CF}_2-(\text{CF}_2)_6-\text{CF}_3$ ). These new peaks were deconvoluted into three peaks at 291.5, 292.5 and 294.5 eV, and attributed to  $-\text{CH}_2-\text{CF}_2-$ ,  $-\text{CF}_2-$ , and  $-\text{CF}_3$ , respectively. Of all the initially present alkyne moieties 63% reacted with this second thiol **6**, as was observed from the ratio of the peak area of all these carbon atoms attached to fluorine, to the peak area of the carbon atoms related to the original monolayer and thiol **3**. As a result, the XPS-derived thickness was increased from 2.0 nm to 2.3 nm upon reaction with thiol **6**. The formation of surface **S-mix-3/6** is supported by the contact angle of  $103^\circ$ , which can be compared with the contact angle obtained for monolayers with a high density of fluorinated chains (typically  $>110^\circ$ ).<sup>53</sup> Evidently, the construction of the terminal alkyne moieties above the alkyl chains allows them sufficient space to react even this second time with high efficiency.



## **2.4 Conclusions**

Thiol-yne click (TYC) chemistry between a thiol and a terminal alkyne moiety is a very efficient way to top-functionalize alkyne-terminated organic monolayers. The method allows for the attachment of up to 1.5 thiols per alkyne, proceeds both faster and with higher yields than the corresponding surface-bound thiol-ene click (TEC) reaction, and does not affect the surface properties of the underlying substrate. Since the initially formed vinyl sulfide can, in principle, react another time, the sequential use of two different thiols allows for the double addition onto alkyne-terminated monolayers, which makes it possible to easily construct complex surface architectures.

## 2.5 References

1. Ha, J. K.; Wooley, K. L.; Yström, A. M.; Burke, J. J.; Kade, M.; Hawker, J. J., Applications of Orthogonal “Click” Chemistries in the Synthesis of Functional Soft Materials. *Chem. Rev.* **2009**, 109, (11), 5620-5686.
2. Kolb, H. C.; Finn, M. G.; Sharpless, K. B., Click Chemistry: Diverse Chemical Function from a Few Good Reactions. *Angew. Chem. Int. Ed.* **2001**, 40, (11), 2004-2021.
3. Jewett, J. C.; Bertozzi, C. R., Cu-free click cycloaddition reactions in chemical biology. *Chem. Soc. Rev.* **2010**, 39, (4), 1272-1279.
4. Lallana, E.; Sousa-Herves, A.; Fernandez-Trillo, F.; Riguera, R.; Fernandez-Megia, E., Click chemistry for drug delivery nanosystems. *Pharm. Res.* **2012**, 29, (1), 1-34.
5. Aromí, G.; Barrios, L. A.; Roubeau, O.; Gamez, P., Triazoles and tetrazoles: Prime ligands to generate remarkable coordination materials. *Coord. Chem. Rev.* **2011**, 255, (5-6), 485-546.
6. Algar, W. R.; Prasuhn, D. E.; Stewart, M. H.; Jennings, T. L.; Blanco-Canosa, J. B.; Dawson, P. E.; Medintz, I. L., The controlled display of biomolecules on nanoparticles: A challenge suited to bioorthogonal chemistry. *Bioconjugate Chem.* **2011**, 22, (5), 825-858.
7. Pedersen, D. S.; Abell, A., 1,2,3-Triazoles in peptidomimetic chemistry. *Eur. J. Org. Chem.* **2011**, (13), 2399-2411.
8. Lau, Y. H.; Rutledge, P. J.; Watkinson, M.; Todd, M. H., Chemical sensors that incorporate click-derived triazoles. *Chem. Soc. Rev.* **2011**, 40, (5), 2848-2866.
9. Manova, R.; van Beek, T. A.; Zuilhof, H., Surface Functionalization by Strain-Promoted Alkyne–Azide Click Reactions. *Angew. Chem. Int. Ed.* **2011**, 50, (24), 5428-5430.
10. Golas, P. L.; Matyjaszewski, K., Click Chemistry and ATRP: A Beneficial Union for the Preparation of Functional Materials. *QSAR Comb Sci.* **2007**, 26, (11-12), 1116-1134.
11. Benzarling, J. M.; Moughity, V. A.; Han, J. W.; Patton, J. L., “Clicking” Polymer Brushes with Thiol-yne Chemistry: Indoors and Out. *J. Am. Chem. Soc.* **2009**, 131, (41), 14673-14675.
12. Gubbens, J.; Ruijter, E.; de Fays, L. E. V.; Damen, J. M. A.; de Kruijff, B.; Slijper, M.; Rijkers, D. T. S.; Liskamp, R. M. J.; de Kroon, A. I. P. M., Photocrosslinking and Click Chemistry Enable the Specific Detection of Proteins Interacting with Phospholipids at the Membrane Interface. *Chem Biol* **2009**, 16, (1), 3-14.
13. Beal, D. M.; Jones, L. H., Molecular scaffolds using multiple orthogonal conjugations: Applications in chemical biology and drug discovery. *Angew. Chem. Int. Ed.* **2012**, 51, (26), 6320-6326.
14. Wang, Q.; Chan, T. R.; Hilgraf, R.; Fokin, V. V.; Sharpless, K. B.; Finn, M. G., Bioconjugation by Copper(I)-Catalyzed Azide-Alkyne [3 + 2] Cycloaddition. *J. Am. Chem. Soc.* **2003**, 125, (11), 3192-3193.
15. Speers, A. E.; Adam, G. C.; Cravatt, B. F., Activity-Based Protein Profiling in Vivo Using a Copper(I)-Catalyzed Azide-Alkyne [3 + 2] Cycloaddition. *J. Am. Chem. Soc.* **2003**, 125, (16), 4686-4687.
16. Gierlich, J.; Burley, G. A.; Gramlich, P. M. E.; Hammond, D. M.; Carell, T., Click Chemistry as a Reliable Method for the High-Density Postsynthetic Functionalization of Alkyne-Modified DNA. *Org. Lett.* **2006**, 8, (17), 3639-3642.
17. McCarty, G. S., Molecular Lithography for Wafer-Scale Fabrication of Molecular Junctions. *Nano Lett.* **2004**, 4, (8), 1391-1394.

18. Manova, R. K.; Pujari, S. P.; Weijers, C. A. G. M.; Zuilhof, H.; van Beek, T. A., Copper-Free Click Biofunctionalization of Silicon Nitride Surfaces via Strain-Promoted Alkyne–Azide Cycloaddition Reactions. *Langmuir* **2012**, 28, (23), 8651-8663.
19. Ruizendaal, L.; Pujari, S. P.; Gevaerts, V.; Paulusse, J. M. J.; Zuilhof, H., Biofunctional Silicon Nanoparticles by Means of Thiol-Ene Click Chemistry. *Asian J. Chem.* **2011**, 6, (10), 2776-2786.
20. Caipa Campos, M. A.; Paulusse, J. M. J.; Zuilhof, H., Functional monolayers on oxide-free silicon surfaces via thiol-ene click chemistry. *Chem. Commun.* **2010**, 46, (30), 5512-5514.
21. Scheres, L.; Giesbers, M.; Zuilhof, H., Organic Monolayers onto Oxide-Free Silicon with Improved Surface Coverage: Alkynes versus Alkenes. *Langmuir* **2010**, 26, (7), 4790-4795.
22. Yaffe, O.; Scheres, L.; Puniredd, S. R.; Stein, N.; Biller, A.; Lavan, R. H.; Shpaisman, H.; Zuilhof, H.; Haick, H.; Cahen, D.; Vilan, A., Molecular Electronics at Metal/Semiconductor Junctions. Si Inversion by Sub-Nanometer Molecular Films. *Nano Lett.* **2009**, 9, (6), 2390-2394.
23. Gooding, J. J.; Ciampi, S., The molecular level modification of surfaces: from self-assembled monolayers to complex molecular assemblies. *Chem. Soc. Rev.* **2011**, 40, (5), 2704-2718.
24. Ciampi, S.; Harper, J. B.; Gooding, J. J., Wet chemical routes to the assembly of organic monolayers on silicon surfaces via the formation of Si-C bonds: surface preparation, passivation and functionalization. *Chem. Soc. Rev.* **2010**, 39, (6), 2158-2183.
25. Li, Y.; Calder, S.; Yaffe, O.; Cahen, D.; Haick, H.; Kronik, L.; Zuilhof, H., Hybrids of Organic Molecules and Flat, Oxide-Free Silicon: High-Density Monolayers, Electronic Properties, and Functionalization. *Langmuir* **2012**, 28, (26), 9920-9929.
26. Fairbanks, B. D.; Sims, E. A.; Anseth, K. S.; Bowman, C. N., Reaction Rates and Mechanisms for Radical, Photoinitiated Addition of Thiols to Alkynes, and Implications for Thiol–Yne Photopolymerizations and Click Reactions. *Macromolecules* **2010**, 43, (9), 4113-4119.
27. Han, J.; Zhao, B.; Gao, Y.; Tang, A.; Gao, C., Sequential click synthesis of hyperbranched polymers via the A<sub>2</sub> + CB<sub>2</sub> approach. *Polym. Chem.* **2011**, 2, (10), 2175-2178.
28. Liu, J.; Lam, J. W. Y.; Jim, C. K. W.; Ng, J. C. Y.; Shi, J.; Su, H.; Yeung, K. F.; Hong, Y.; Faisal, M.; Yu, Y.; Wong, K. S.; Tang, B. Z., Thiol-Yne click polymerization: Regio- and stereoselective synthesis of sulfur-rich acetylenic polymers with controllable chain conformations and tunable optical properties. *Macromolecules* **2011**, 44, (1), 68-79.
29. Dondoni, A.; Marra, A., Recent applications of thiol-ene coupling as a click process for glycoconjugation. *Chem. Soc. Rev.* **2012**, 41, (2), 573-586.
30. Lowe, A. B.; Hoyle, C. E.; Bowman, C. N., Thiol-yne click chemistry: A powerful and versatile methodology for materials synthesis. *J. Mater. Chem.* **2010**, 20, (23), 4745-4750.
31. Naik, S. S.; Chan, J. W.; Comer, C.; Hoyle, C. E.; Savin, D. A., Thiol-yne 'click' chemistry as a route to functional lipid mimetics. *Polym. Chem.* **2011**, 2, (2), 303-305.
32. Massi, A.; Nanni, D., Thiol-yne coupling: revisiting old concepts as a breakthrough for up-to-date applications. *Org. Biomol. Chem.* **2012**, 10, (19), 3791-3807.

33. Fairbanks, . . . Scott, T. F. Kloxin, . . . Anseth, K. S. Rowman, . . ., Thiol–Yne Photopolymerizations: Novel Mechanism, Kinetics, and Step-Growth Formation of Highly Cross-Linked Networks. *Macromolecules* **2008**, 42, (1), 211-217.
34. Wendeln, C.; Rinnen, S.; Schulz, C.; Arlinghaus, H. F.; Ravoo, B. J., Photochemical Microcontact Printing by Thiol–Ene and Thiol–Yne Click Chemistry. *Langmuir* **2010**, 26, (20), 15966-15971.
35. Minozzi, M.; Monesi, A.; Nanni, D.; Spagnolo, P.; Marchetti, N.; Massi, A., An Insight into the Radical Thiol/Yne Coupling: The Emergence of Arylalkyne-Tagged Sugars for the Direct Photoinduced Glycosylation of Cysteine-Containing Peptides. *J. Org. Chem.* **2010**, 76, (2), 450-459.
36. Norberg, O.; Lee, I. H.; Aastrup, T.; Yan, M.; Ramström, O., Photogenerated lectin sensors produced by thiol-ene/yne photo-click chemistry in aqueous solution. *Biosens. Bioelectron.* **2012**, 34, (1), 51-56.
37. Spangler, B. D.; Tyler, B. J., Capture agents for a quartz crystal microbalance-continuous flow biosensor: functionalized self-assembled monolayers on gold. *Anal. Chim. Acta* **1999**, 399, (1-2), 51-62.
38. Smith, W. N.; Beumel Jr, O. F., Preparation of Alkynes and Dialkynes by Reaction of Monohalo- and Dihaloalkanes with Lithium Acetylenide-Ethylenediamine Complex. *Synthesis* **1974**, 1974, (06), 441-443.
39. Stewart, M. P.; Buriak, J. M., Exciton-mediated hydrosilylation on photoluminescent nanocrystalline silicon. *J. Am. Chem. Soc.* **2001**, 123, (32), 7821-7830.
40. Rijksen, B.; van Lagen, B.; Zuilhof, H., Mimicking the Silicon Surface: Reactivity of Silyl Radical Cations toward Nucleophiles. *J. Am. Chem. Soc.* **2011**, 133, (13), 4998-5008.
41. Frisch, M. J. T., G. W.; Schlegel, H. B.; Scuseria, G. E.; Robb, M. A.; Cheeseman, J. R.; Scalmani, G.; Barone, V.; Mennucci, B.; Petersson, G. A.; Nakatsuji, H.; Caricato, M.; Li, X.; Hratchian, H. P.; Izmaylov, A. F.; Bloino, J.; Zheng, G.; Sonnenberg, J. L.; Hada, M.; Ehara, M.; Toyota, K.; Fukuda, R.; Hasegawa, J.; Ishida, M.; Nakajima, T.; Honda, Y.; Kitao, O.; Nakai, H.; Vreven, T.; Montgomery, Jr., J. A.; Peralta, J. E.; Ogliaro, F.; Bearpark, M.; Heyd, J. J.; Brothers, E.; Kudin, K. N.; Staroverov, V. N.; Kobayashi, R.; Normand, J.; Raghavachari, K.; Rendell, A.; Burant, J. C.; Iyengar, S. S.; Tomasi, J.; Cossi, M.; Rega, N.; Millam, N. J.; Klene, M.; Knox, J. E.; Cross, J. B.; Bakken, V.; Adamo, C.; Jaramillo, J.; Gomperts, R.; Stratmann, R. E.; Yazyev, O.; Austin, A. J.; Cammi, R.; Pomelli, C.; Ochterski, J. W.; Martin, R. L.; Morokuma, K.; Zakrzewski, V. G.; Voth, G. A.; Salvador, P.; Dannenberg, J. J.; Dapprich, S.; Daniels, A. D.; Farkas, Ö.; Foresman, J. B.; Ortiz, J. V.; Cioslowski, J.; Fox, D. J., Gaussian 09, Revision A.1., In Gaussian, Inc., Wallingford CT, 2009.
42. Ciampi, S.; Ames, M. Michaels, P. Gooding, . . ., Tandem “ Click” Reactions at Acetylene-Terminated Si(100) Monolayers. *Langmuir* **2011**, 27, (11), 6940-6949.
43. Ciampi, S.; Böcking, T.; Kilian, K. A.; James, M.; Harper, J. B.; Gooding, J. J., Functionalization of Acetylene-Terminated Monolayers on Si(100) Surfaces: A Click Chemistry Approach. *Langmuir* **2007**, 23, (18), 9320-9329.
44. Giesbers, M.; Marcelis, A. T. M.; Zuilhof, H., Simulation of XPS C1s Spectra of Organic Monolayers by Quantum Chemical Methods. *Langmuir* **2013**, 29, (15), 4782-4788.
45. Hu, A.; Griesing, S.; Rybachuk, M.; Lu, Q. B.; Duley, W. W., Nanobuckling and x-ray photoelectron spectra of carbyne-rich tetrahedral carbon films deposited by femtosecond laser ablation at cryogenic temperatures. *J. Appl. Phys.* **2007**, 102, (7).

46. Wallart, X.; Henry de Villeneuve, C.; Allongue, P., Truly Quantitative XPS Characterization of Organic Monolayers on Silicon: Study of Alkyl and Alkoxy Monolayers on  $-\text{Si}(111)$ . *J. Am. Chem. Soc.* **2005**, 127, (21), 7871-7878.
47. Türlüç, O.; Meier, M. A. R., A novel polymerization approach via thiol-yne addition. *J. Polym. Sci., Part A: Polym. Chem.* **2012**, 50, (9), 1689-1695.
48. Wu, J.-T.; Huang, C.-H.; Liang, W.-C.; Wu, Y.-L.; Yu, J.; Chen, H.-Y., Reactive Polymer Coatings: A General Route to Thiol-ene and Thiol-yne Click Reactions. *Macromol. Rapid Commun.* **2012**, 33, (10), 922-927.
49. Li, L.; Zahner, D.; Su, Y.; Gruen, C.; Davidson, G.; Levkin, P. A., A biomimetic lipid library for gene delivery through thiol-yne click chemistry. *Biomaterials* **2012**, 33, (32), 8160-8166.
50. Oswald, A. A.; Griesbaum, K.; Hudson, B. E.; Bregman, J. M., Organic Sulfur Compounds. XIII.1 Free-Radical Addition of Thiols to Phenylacetylene2. *J. Am. Chem. Soc.* **1964**, 86, (14), 2877-2884.
51. Griesbaum, K., Problems and Possibilities of the Free-Radical Addition of Thiols to Unsaturated Compounds. *Angew. Chem. Int. Ed.* **1970**, 9, (4), 273-287.
52. Fischer, J. A.; Zoldan, V. C.; Benitez, G.; Rubert, A. A.; Ramirez, E. A.; Carro, P.; Salvarezza, R. C.; Pasa, A. A.; Vela, M. E., Sulfidization of Au(111) from Thioacetic Acid: An Experimental and Theoretical Study. *Langmuir* **2012**, 28, (43), 15278-15285.
53. Pujari, S. P.; Spruijt, E.; Cohen Stuart, M. A.; van Rijn, C. J. M.; Paulusse, J. M. J.; Zuilhof, H., Ultralow Adhesion and Friction of Fluoro-Hydro Alkyne-Derived Self-Assembled Monolayers on H-Terminated Si(111). *Langmuir* **2012**, 28, (51), 17690-17700.

# Chapter 3

## Hydrolytic and Thermal Stability of Organic Monolayers on Various Inorganic Substrates

### Abstract

A comparative study is presented on the hydrolytic and thermal stability of 24 different kinds of monolayers on Si(111), Si(100), SiC, SiN, SiO<sub>2</sub>, CrN, ITO, PAO, Au and stainless steel surfaces. These surfaces were modified by utilizing appropriate organic compounds having a constant alkyl chain length (C<sub>18</sub>), but with different surface-reactive groups, such as 1-octadecene, 1-octadecyne, 1-octadecyltrichlorosilane, 1-octadecanethiol, 1-octadecylamine and 1-octadecylphosphonic acid. The hydrolytic stability of obtained monolayers was systematically investigated in triplicate in constantly flowing aqueous media at room temperature in acidic (pH 3), basic (pH 11), phosphate buffer saline (PBS) and deionized water (neutral conditions), for a period of 1 day, 7 days and 30 days, yielding 1152 data points for the hydrolytic stability. The hydrolytic stability was monitored by static water contact angle measurements and X-ray photoelectron spectroscopy (XPS). The covalently bound alkyne monolayers on Si(111), Si(100) and SiC were shown to be among the most stable monolayers under acidic and neutral conditions. Additionally, the thermal stability of 14 different monolayers was studied in vacuum using XPS at elevated temperatures (25 °C – 600 °C). Similar to the hydrolytic stability, the covalently bound both alkyne and alkene monolayers on Si(111), Si(100) and SiC started to degrade from temperatures above 260 °C, whereas on oxide surfaces (e.g., PAO) phosphonate monolayers even displayed thermal stability up to ~ 500 °C.

This chapter is published as:

*'Hydrolytic and Thermal Stability of Organic Monolayers on Various Inorganic Substrates'* Bhairamadgi, N. S.; Pujari, S. P.; Trovela, F. G.; Debrassi, A.; Khamis, A. A.; Alonso, J. M.; Al Zahrani, A. A., Wennekes, T.; Al-Turaif, H. A.; van Rijn, C. J. M.; Alhamed, Y. A.; Zuilhof, H. *Langmuir* **2014**, 30, 20, 5829–5839.

**Contents**

<b>3. Hydrolytic and Thermal Stability of Organic Monolayers on Various Inorganic Substrates .....</b>	<b>37</b>
Abstract .....	37
3.1 Introduction .....	39
3.2 Experimental Methods .....	43
3.2.1 Chemicals .....	43
3.2.2 Substrates .....	43
3.2.3 Contact Angle Measurements .....	43
3.2.4 X-ray Photoelectron Spectroscopy (XPS) .....	44
3.2.5 Hydrolytic Stability Tests .....	44
3.2.6 Thermal Stability Tests .....	45
3.2.7 Monolayer Preparation .....	45
3.3 Results and Discussion .....	46
3.3.1 Hydrolytic Stability .....	46
3.3.2 Thermal Stability .....	51
3.4 Conclusions .....	55
3.5 References .....	56

### 3.1 Introduction

Organic monolayers have found an impressive variety of applications in the fields of biosensors, micro- and nanoelectronics, chemical and biochemical sensors, nanotribology, lithographic patterning, wettability control, optoelectronics, biomedical appliances and so on.<sup>1-3</sup> For many of these applications inorganic substrates are used that are often based on silicon, metals or metal oxides. Here, the monolayer provide functionality and acts as an interfacial layer between the substrate and the surrounding environment, which can be either aqueous e.g., water under physiological conditions or gaseous e.g., air at various humidities and temperatures. Therefore the stability of this interfacial monolayer is crucial, as the performance and durability of such devices depend to a large degree on it.<sup>2</sup>

Several approaches with a wide range of surface-reactive groups have been taken toward the formation of stable monomolecular layers on inorganic surfaces.<sup>1</sup> Self-assembled monolayer (SAM)-forming monomers consist of three domains: a terminal functional group that ultimately defines the exposed surface functionality, a hydrocarbon chain (typically oligomethylene) to promote monolayer packing and organization, and an anchoring group responsible for the specific chemical interactions with the substrate. Various anchoring groups – such as thiol, alcohol, alkyne, alkene, silane and phosphonate – conveniently assemble on a wide variety of active surfaces, which can be terminated with metal atoms (e.g., Au), hydrogen atoms (e.g., Si-H), or metal-oxide or hydroxyl groups (e.g., glass and SiC). As a result, the addition of organic monolayers can function as a precise tool to make a substrate of choice amenable for a wide range of applications. For example, silane, thiol and phosphonate groups have been used to link molecules to inorganic surfaces, and are widely used in micro/nano-electromechanical systems (MEMS/NEMS).<sup>4</sup> Many types of monolayers have thus found application under different sorts of conditions. The range of these applications is typically determined by the intrinsic characteristics of the substrate (e.g., electrical conductivity, optical transparency, atomic smoothness, chemical robustness, hardness, etc.), and by the stability of the attachment of the monolayer to that substrate.

A characteristic limitation of attached monolayers involves hydrolysis and subsequent (partial) loss of functionality. Specifically, hydrolysis may become problematic in non-neutral media, such as at low or high pH or at elevated salt concentrations such as in phosphate-buffered saline (PBS) solutions. This stability issue therefore is highly relevant to optimize either the substrate or the attachment chemistry for the application at hand.

Monolayers on metals are frequently prepared by addition of thiolates. Several stability studies have been conducted on thiolate monolayers on gold to find the optimal conditions for use in certain applications.<sup>5, 6</sup> It was typically found that monodentate thiolate monolayers were rather unstable under mild chemical conditions, in biological media, under ultraviolet light irradiation and mild mechanical disturbance (gentle wiping), which e.g., hampers the sensing properties of sensing devices.<sup>7, 8</sup> Typically, for thiol monolayers



on other surfaces, such as Ag, Pt, Cr and Cu, the stability is even worse, as such monolayers desorbed within an hour of air exposure under ambient laboratory conditions or under vacuum.<sup>9-11</sup> Despite this stability issue, thiolate monolayers are still used in many studies. The probable reason is that they are easy to make on a variety of substrates, often-considered stable enough for use in non-demanding research laboratory applications, and if required, multivalent thiols can be used to achieve a higher stability.

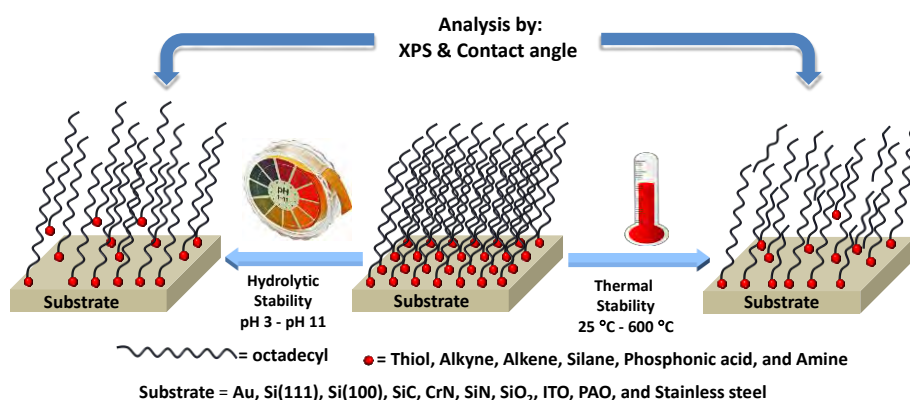
Modification of oxide surfaces has typically been performed using silanes, carboxylic acids and phosphonic acids.<sup>1</sup> Especially silanes form SAMs quite easily. The advantage of silane monolayers over thiolate monolayers is that silanes are mechanically as well as chemically more stable due to a cross-linked two-dimensional network with neighboring silanols.<sup>12</sup> However, a drawback of these monolayers is that they are bound to the substrate via Si-O-M bonds, which are prone to hydrolyze under aqueous and humid conditions.<sup>13, 14</sup> On the other hand, phosphonic acids form a strong bond with metal oxides, and the adsorption rate and stability strongly depends on the density of hydroxyl groups.<sup>15, 16</sup> Particularly, upon curing phosphonic acids may form additional P-O-M bonds (bi-dentate or tri-dentate) with hydroxyl groups on the surface, leading to a higher stability compared to silane and carboxylate monolayers on metal oxides.<sup>17-20</sup>

Recently our group has studied the hydrolytic stability of phosphonic acid and alkyne monolayers on porous aluminum oxide (PAO) and on chromium nitride (CrN) surfaces, in comparison with carboxylic acid,  $\alpha$ -hydroxycarboxylic acid, alkene, and silane monolayers at different pH and temperatures (40 °C, 60 °C and 80 °C).<sup>18, 19</sup> These results indicated that alkynes and phosphonates allow the formation of hydrolytically stable monolayers on oxide surfaces.

Despite the rapidly growing importance of surface modification, these isolated studies on a few specific surfaces actually highlighted the fact that, to the best of our knowledge, *no comprehensive comparative study* has been reported on the hydrolytic stability of a wide range of surfaces that are modified with an organic monolayer. In fact, a similar situation is present for the high-temperature stability of monolayer-modified surfaces. Such a high-temperature stability becomes increasingly important, because of a rapidly rising number of monolayer-based applications in the field of microelectronics and nanotechnology.<sup>21, 22</sup> The thin dielectric layers or primer layers in such devices are mostly made up of monolayers, and the stability thereof becomes crucial especially in the case of the subsequent deposition of high-k oxides in field-effect transistors (FETs), which is carried out at elevated temperatures.<sup>23-25</sup> Again, only limited studies have been conducted on the thermal stability of monolayers on various substrates at room temperature or elevated temperatures under ambient conditions, and these indicate that under such conditions monolayers mainly desorb due to oxidation rather than by thermally induced degradation.<sup>26-28</sup> Moreover, only a few studies present information on the thermal stability of monolayers under high vacuum conditions, using high-resolution electron energy loss

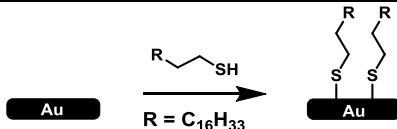
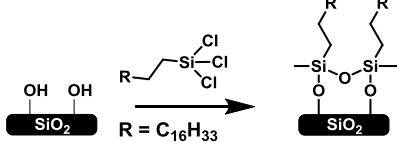
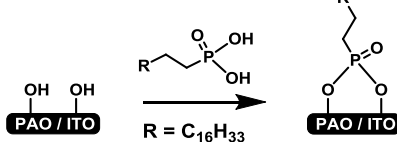
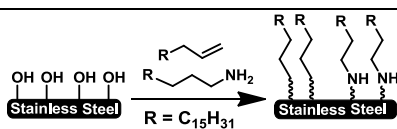
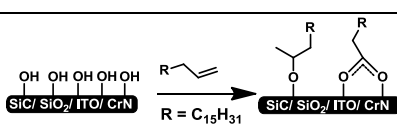
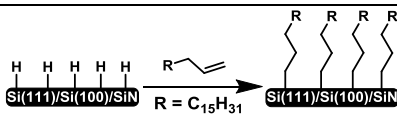
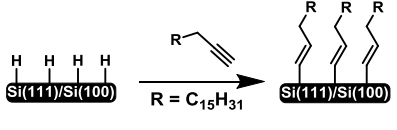
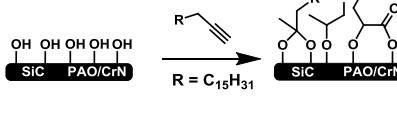
spectroscopy (HREELS) and X-ray photoelectron spectroscopy (XPS),<sup>25, 29, 30</sup> or quantitative *in-situ* infrared spectroscopy.<sup>31</sup>

Given the central role of monolayer stability for such a wide range of applications, and the current lack of relevant data that allows the direct comparison of monolayer stability on various substrates, the present study aims to fill that gap. Here we present the results of a comprehensive study of the hydrolytic stability of 24 different monolayer-substrate combinations, and the thermal stability of 14 of them. To this aim, we first prepared organic monolayers, all with a fixed alkyl chain length ( $C_{18}$ ) – as the length of the alkyl chain has been found to be an important variable for the monolayer stability. A wide range of surface-reactive linker groups was chosen depending on the substrate reactivity, i.e. thiolate on Au, silane on glass, phosphonate on hydroxyl-terminated PAO and ITO, amine on stainless steel (SS), alkene and alkyne on hydroxyl-terminated PAO, CrN,  $SiO_2$ , and SiC, and hydrogen-terminated Si(111), Si(100), and SiN surfaces. Subsequently, the loss of monolayer chains under the conditions of interest was studied. These modified surfaces were assessed for their hydrolytic stability by prolonged immersion in flowing water, under acidic (pH 3), neutral (pH 7; deionized water and PBS) and basic (pH 11) conditions, and subsequently studied throughout by static water contact angle and XPS measurements. Since all measurements were performed in triplicate, this yields 1152 measurements of the hydrolytic stability measured on one monolayer length and by a constant approach. For the thermal stability, 8 of these modified surfaces were heated inside a XPS system up to 600 °C, and the stability was then measured by the loss of the carbon signal. For these 8 modified surfaces ~200 XPS measurements thus provide an overview of the thermal stability. An overview of this study is presented in Figure 1, whereas a list of the modified surfaces under study together with the nomenclature used here is given in Table 1. All together, this study thus provides a benchmark for the comparison of monolayer stability on different substrates and using various attachment chemistries.



**Figure 1.** Study of the hydrolytic and thermal stability of organic monolayers (1-octadecanethiol, 1-octadecyne, 1-octadecene, 1-octadecyletrichlorosilane, 1-octadecylphosphonic acid and 1-octadecylamine) on a range of inorganic substrates (Au, Si(111), Si(100), SiC, CrN, SiN,  $SiO_2$ , ITO, PAO, and stainless steel).

**Table 1.** Monolayer-modified substrates under current study, together with a brief indication of their preparation.

Substrate-Monolayer	Scheme	Modification Conditions	Ref.
Au-Thiol		<ol style="list-style-type: none"> <li>1. Cleaned in air plasma (10 min).</li> <li>2. Reacted with 1mM 1-octadecanethiol in ethanol (24 h).</li> </ol>	32
SiO <sub>2</sub> -Silane		<ol style="list-style-type: none"> <li>1. Cleaned in air plasma (10 min).</li> <li>2. Reacted with 1mM 1-octadecyltrichlorosilane in cyclohexane (10 min).</li> </ol>	19
PAO/ITO-PA		<ol style="list-style-type: none"> <li>1. a) Immersed in mixture of 37% HCl &amp; methanol (1:1, v/v) (30 min) for PAO. b) Immersed in mixture of 25% NH<sub>4</sub>OH and 50% H<sub>2</sub>O<sub>2</sub> (1:1, v/v), at 90 °C (60 min) for ITO.</li> <li>2. Reacted with 1 mM 1-octadecylphosphonic acid (PA) in ethanol for PAO &amp; with 5 mM PA in THF for ITO (24 h).</li> <li>3. Cured at 140 °C (4 h).</li> </ol>	18, 33
SS-Amine/Alkene		<ol style="list-style-type: none"> <li>1. Immersed in mixture of 20% HCl and 20% H<sub>2</sub>SO<sub>4</sub>, at 80 °C (30 min).</li> <li>2. Reacted with 50 mM 1-octadecylamine in hexane (3 h).</li> <li>3. Reacted with neat 1-octadecene, UV (16 h).</li> </ol>	34
SiC/SiO <sub>2</sub> /ITO/CrN-Alkene		<ol style="list-style-type: none"> <li>1. a) Immersed in mixture of 25% NH<sub>4</sub>OH and 50% H<sub>2</sub>O<sub>2</sub> (1:1, v/v), at 90 °C (60 min) for ITO. b) Cleaned in air plasma (10 min) for SiC, SiO<sub>2</sub> &amp; CrN.</li> <li>2. Wet-etching in 2.5% HF (2 min) for SiC.</li> <li>3. Reacted with neat 1-octadecene, UV (SiO<sub>2</sub> &amp; ITO) or heating to 130 °C (SiC/SiO<sub>2</sub>/ITO/CrN) (16 h).</li> </ol>	19, 35-37
Si(111)/Si(100)/SiN-Alkene		<ol style="list-style-type: none"> <li>1. Cleaned in air plasma (10 min).</li> <li>2. Wet-etching in 40% NH<sub>4</sub>F (15 min) for Si(111) and Si(100) and in 2.5% HF for SiN (2 min).</li> <li>3. Reacted with neat 1-octadecene, UV or at 85 °C (16 h).</li> </ol>	38-41
Si(111)/Si(100)-Alkyne		<ol style="list-style-type: none"> <li>1. Cleaned in air plasma (10 min).</li> <li>2. Wet-etching in 40% NH<sub>4</sub>F (15 min).</li> <li>3. Reacted with neat 1-octadecyne at 85 °C (16 h).</li> </ol>	40, 42
SiC-PAO/CrN-Alkyne		<ol style="list-style-type: none"> <li>1. Cleaned in air plasma (10 min) for CrN &amp; SiC.</li> <li>2. Wet-etching in 2.5% HF (2 min) for SiC.</li> <li>3. Cleaned in mixture of 37% HCl &amp; methanol (1:1, v/v) (30 min) for PAO.</li> <li>4. Reacted with 1-octadecyne at 130 °C (16 h).</li> </ol>	18, 19, 43

Note: for all substrates cleaning and sonication in acetone was the first step and all photochemical modifications used 254 nm light.

## 3.2 Experimental Methods

### 3.2.1 Chemicals

1-Octadecyltrichlorosilane (silane), 1-octadecanethiol (thiol), 1-octadecylamine (amine), 1-octadecylphosphonic acid (PA) and 1-octadecene (alkene) were obtained from Sigma-Aldrich and used without further purification unless otherwise specified. 1-Octadecyne (alkyne) was prepared using a method adapted from the synthesis of analogous alkynes.<sup>19</sup> Acetone was obtained in semiconductor grade: VLSI PURANAL Honeywell 17617. Dichloromethane (distilled before use), ethanol, methanol and pentane were obtained from Sigma-Aldrich (all HPLC grade). Phosphate-buffered saline (PBS; pH 7) was obtained from Fluka; hydrochloric acid (HCl, 37%) and sodium hydroxide (NaOH, pellets) were obtained from Sigma-Aldrich.

### 3.2.2 Substrates

Silicon(111) wafers were (111)-oriented, single-side polished (500-550  $\mu\text{m}$  thick, n-type doping by phosphorus, AFM (See Supporting Information, Figure SI-21) root mean square (RMS) roughness = 0.2 nm), and resistivity of 2.0 - 8.0  $\Omega\text{ cm}$  (Siltronix, France). Silicon(100) wafers were (100)-oriented, single-side polished (500-550  $\mu\text{m}$  thick, n-type doping by phosphorus, RMS = 0.1 nm), and resistivity of 1.0 - 2.0  $\Omega\text{ cm}$  (Seltec Silicon, Mitsubishi Silicon America). Stoichiometric polycrystalline 3C-SiC films (SiC; thickness 183 nm, RMS = 2.3 nm) were obtained by chemical vapor deposition (CVD) of 1,3-disilabutane ( $\text{CH}_3\text{SiH}_2\text{CH}_2\text{SiH}_3$ , DSB) on Si(100),<sup>44</sup> and were received as a gift from Prof. Roya Maboudian (University of California, Berkeley). Chromium nitride (CrN) films (thickness 1  $\mu\text{m}$ , RMS = 5.0 nm) obtained by sputter deposition on Si(100) were obtained from ASML B.V., the Netherlands. Silicon-rich silicon nitride (SiN) samples (CVD  $\text{Si}_x\text{N}_4$ ,  $x > 3$ ) on Si(100), (thickness of 147 nm, RMS = 4.3 nm), were obtained from Lionix B.V., the Netherlands. Silicon oxide ( $\text{SiO}_2$ ) surfaces were synthetic fused silica slides (15  $\times$  25  $\text{mm}^2$ ), RMS = 2.5 nm obtained from Praezisions Glas and Optik, Iserlohn, Germany. Indium tin oxide (ITO) substrates were (25  $\times$  25  $\text{mm}^2$ ), RMS = 2.7 nm obtained from Sigma Aldrich, surface resistivity 8 – 12  $\Omega/\text{sq}$ . Porous aluminium oxide (PAO) samples (36  $\times$  8  $\text{mm}^2$ , Anopore) with an average pore size of 200 nm, RMS = 15 nm were obtained from Whatman Scientific. Gold (Au(111)) (25  $\times$  25  $\text{mm}^2$ ) substrates, RMS = 3.0 nm were obtained from Sigma Aldrich. Stainless steel (SS), RMS = 2.5 nm was used as 316L type (1  $\times$  1  $\text{cm}^2$ ).

### 3.2.3 Contact Angle Measurements

The contact angle measurements were performed using Krüss DSA 100 contact angle goniometer having automated drop dispenser and image/video capture system. The static contact angles were measured at six different places on a modified surface by dispensing

six small droplets (3.0  $\mu\text{L}$  volume of deionized water) with the help of an automated drop dispenser. The tangent 2 fitting model was implemented for contact angle measurements for all samples except PAO under hydrolytic study with accuracy of  $\pm 1^\circ$  or  $\pm 2^\circ$ . The PAO modified surfaces were best fitted with tangent 1 method, where the drop profiles were fitted with general conic-section equation by Drop Shape Analyzer (DSA, 100 version 1.9, Kruss) software.

### 3.2.4 X-ray Photoelectron Spectroscopy (XPS)

The X-ray photoelectron spectra at ambient temperature were obtained using a JPS-9200 photoelectron spectrometer (JEOL, Japan) for all the samples used in the study of the hydrolytic stability, unless otherwise specified. A monochromatic Al K $\alpha$  X-ray source ( $h\nu = 1486.7$  eV, 12 kV and 20 mA) with an analyzer pass energy of 10 eV was used. A base pressure of  $3 \times 10^{-7}$  Torr was maintained in the XPS chamber during measurements and the spectra were collected at room temperature. The X-ray incidence angle and the electron acceptance angle were  $80^\circ$  and  $10^\circ$  to the surface normal, respectively. Because of the electrostatic charging in the positive direction on the surface (specifically on non-conducting samples like PAO, SiN, ITO and SiO $_2$ ), a charge compensation was used during the XPS scans with an accelerating voltage of 2.8 eV and a filament current of 4.8 A. All XPS spectra were analyzed using the CasaXPS software. Details of the XPS equipment used at elevated temperatures are given below.

### 3.2.5 Hydrolytic Stability Tests

Hydrolytic stability experiments were carried out by placing the modified surfaces in rubber stopper glass vials. Four different aqueous environments were prepared containing deionized (DI) water, PBS at pH 7, an acidic (HCl) solution at pH 3, a basic (NaOH) solution at pH 11. The stability for all surfaces was investigated at constant temperature of 25  $^\circ\text{C}$ . The vials under study were continuously agitated at 25 rpm using an incubator shaker, benchtop Innova 4080 to mimic mechanical disturbances by flowing solvents; this approach also minimizes the deposition of adventitious carbon on surface. The stability of the functionalized surfaces under acidic, basic, PBS and neutral deionized water was monitored directly after preparation, and after 1 day, 7 days and 30 days of immersion in the described medium in a laboratory environment. In all cases before measurements the samples were taken from the medium, rinsed with fresh deionized water then sonicated in water, ethanol and dichloromethane for 5 min in each solvent, finally rinsed with dichloromethane, and dried in a flow of dry argon. The PAO surfaces were in this last step dried under high vacuum ( $\sim 10$  mbar) for 30 min before the contact angle and XPS measurements. The samples were returned to new vials filled with freshly prepared solutions for prolonged periods of this stability study.

### 3.2.6 Thermal Stability Tests

XPS measurements at elevated temperatures were carried out using a SPECS XPS spectrometer operating at a base pressure of  $4 \times 10^{-10}$  mbar. The monochromatic Al K $\alpha$  (1486.7 eV) X-ray source was operated in focusing mode to irradiate the sample surface with a spot size of  $0.2 \times 3.5$  mm and 13.5 kV, 150 Watt of X-ray power. The sample was tilted  $25^\circ$  from the x-axis, resulting in an electron take-off angle of  $65^\circ$  between the sample surface and the direction of photoelectrons detected by the analyzer. XPS data were collected utilizing a PHOIBOS 150 MCD-9 hemispherical energy analyzer operating in Fixed Analyzer Transmission (FAT) mode. For the measurements, the analyzer was set to the high magnification mode with a round entrance slit of 7.0 mm diameter and the iris aperture was closed to 30 mm. With this configuration, the accepted area from the sample was determined to be about  $0.5 \text{ mm}^2$  and acceptance angle  $\sim 9^\circ$ . For the high-resolution spectra, the analyzer pass energy was 23 eV, while an energy step of 25 - 30 meV and a dwell time of 100 msec was used. The total measurement time for two elemental regions (e.g., C1s and Si2p) in one scan each was kept as short as possible, which turned out to be about 2 to 3 min; during such a measurement the temperature was kept constant. For samples that require charge neutralization, the neutralizer settings of 2.2 filament current, 100.8  $\mu\text{A}$  emission current and 3.0 eV electron energy (i.e. accelerating voltage) were applied.

The heating of the samples was carried out by using an electron beam heater made from thoriated-tungsten wire underneath the molybdenum metal plate on which the samples were mounted. The samples were heated based on electron bombardment with grounded samples and a filament potential up to 1000 V. The heating control unit was operated in manual mode whereby the filament current and accelerating voltage were set manually. The samples were heated to various temperatures at a rate of about 2 to 3  $^\circ\text{C}/\text{min}$ . Once the desired temperature was reached, the *in-situ* XPS measurements were started. Each sample was analyzed at three different temperatures. New locations were used for each temperature: after about 1 min to stabilize the instrument, the temperature was maintained constant at a desired temperature for ca. 4 min, which allowed the collection of XPS data for two elemental regions. The heating process was then continued to reach the next (higher) temperature.

### 3.2.7 Monolayer Preparation

All the substrates were cut into  $1 \times 1 \text{ cm}^2$  pieces and modified according to reported literature procedures, unless otherwise specified (see Table 1). All monolayer-modified surfaces used in this study displayed static water within  $1^\circ$  of the reported static contact angles when such data were available. Modified substrates that did not fulfill this criterion were discarded.

### 3.3 Results and Discussion

#### 3.3.1 Hydrolytic Stability

Alkyl monolayer-modified surfaces were prepared on Si(111), Si(100), SiC, SiN, SiO<sub>2</sub>, CrN, ITO, PAO, Au and stainless steel surfaces according to procedures reported in literature (Table 1). To ensure the quality of the monolayers on these substrates the modified surfaces were characterized in detail with XPS and static water contact angle measurements before the stability study. Since none of the attachment chemistries yields high-quality monolayers on all surfaces, we focused on monolayer head groups with at least significant affinity towards specific surface sites, such as a thiolate monolayer on Au,<sup>32</sup> silane on glass,<sup>19</sup> phosphate on hydroxyl-terminated PAO<sup>18</sup> and ITO,<sup>33</sup> amine on steel,<sup>34</sup> alkene and alkyne monolayers on hydroxyl-terminated PAO,<sup>18</sup> CrN,<sup>19</sup> SiO<sub>2</sub>,<sup>36</sup> and SiC,<sup>35, 43</sup> and on hydrogen-terminated Si(111),<sup>40, 42</sup> Si(100)<sup>40</sup> and SiN<sup>39, 41</sup> surfaces.

To study the hydrolytic stability of monolayers, modified surfaces were immersed up to 30 days under constant agitation in four different aqueous media containing deionized (DI) water, PBS at pH 7.0, an acidic (HCl) solution at pH 3, a basic (NaOH) solution at pH 11. After 1 day, 7 days and 30 days samples were removed from the above solutions, cleaned with plenty of deionized water, and subsequently sonicated in water, ethanol and dichloromethane for 5 min each. The hydrolytic stability was followed by static water contact angle measurements and by carbon desorption rates, using the ratio of carbon to major substrate element from XPS survey scans. Specifically in deionized water and the PBS solution, agitation was essential to prevent adventitious carbon deposition from biological origin. However, it is known that the X-ray based techniques like XPS can damage monolayers.<sup>45, 46</sup> Therefore, to minimize such damage, we performed only survey scan XPS measurements for a short period of time (~120 sec) by keeping samples in same orientation (See Supporting Information, Figure SI-18A), therefore the monolayer degradation under this condition would be negligible.<sup>46</sup> To illustrate the type of data obtained, we present these in Figure 2 for three monolayers, with a relatively low, medium and high stability, respectively. A bar-graph representation of all the water contact angle based stability data for all the surfaces under study (with the exception of the PAO surfaces; Supporting Information, Figure SI-17) is shown in Figure 3. In addition, the water contact angles for PAO, and the XPS carbon-to-substrate element ratio for all surfaces is given in the Supporting Information (Figure SI-1 to SI-17). The water contact angle data for PAO start above 150° due to its porous structure,<sup>18</sup> and inclusion thereof in Figure 3 would have compressed the figure significantly, which would make it harder to read; part of these data are presented separately in Figure 2 and discussed in detail below.

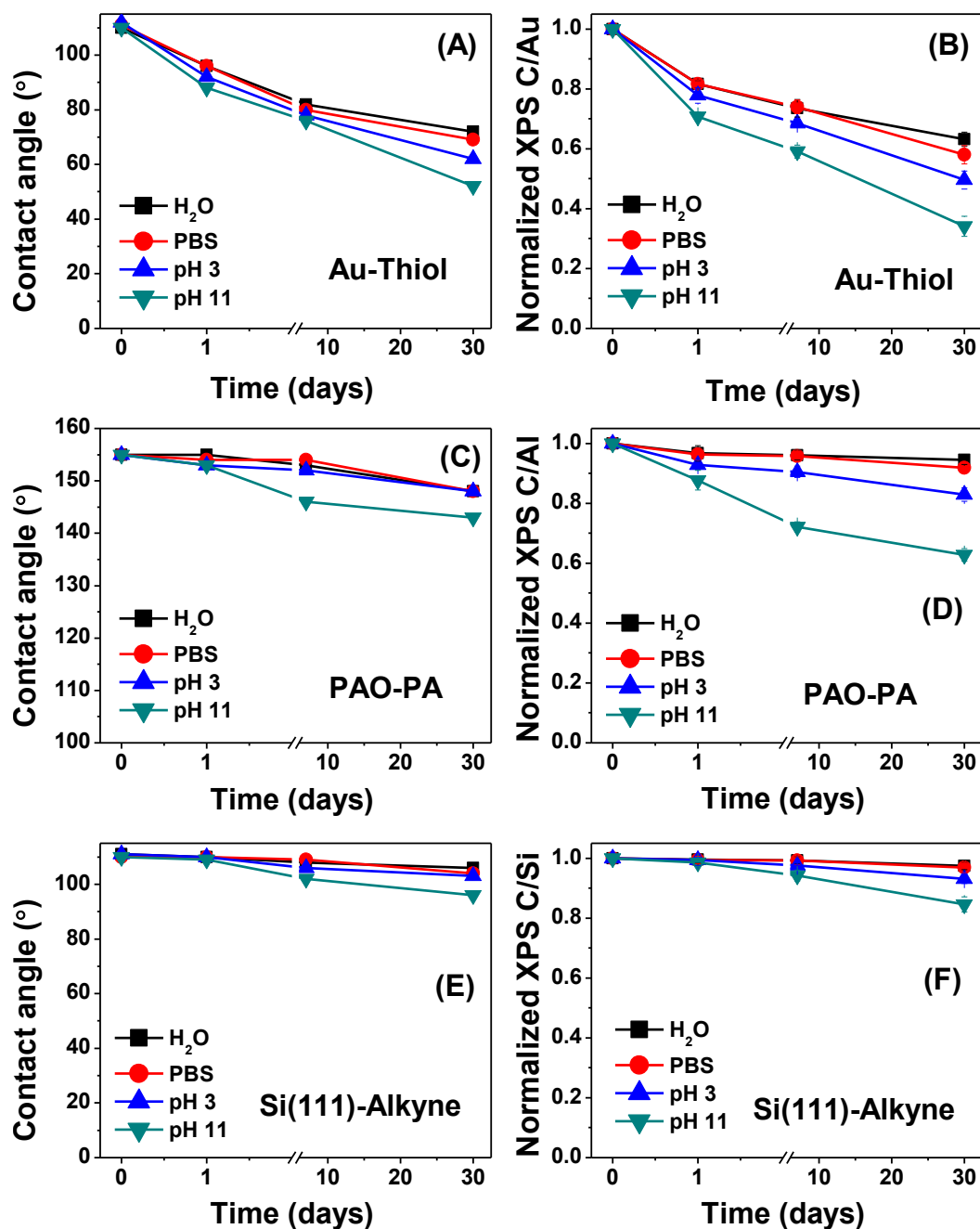


**Figure 2.** The hydrolytic stability of Au-thiol (A, B), PAO-PA (C, D) and Si(111)-Alkyne (E, F) monolayer-modified surfaces as followed by static contact angle measurements (A, C, E) and normalized C/(Au or Al or Si) ratio from XPS survey scan (B, D, F), respectively. Measurements were performed on cleaned surfaces after taking them out from H<sub>2</sub>O, PBS, pH 3 and pH 11 at the indicated time period (lines connecting data points are a mere guide to eye).

The stability of the thiolate monolayer on Au is represented in Figure 2A, which indicates that already after one day significant changes were observed. There was not much difference between pH 3, H<sub>2</sub>O and PBS solutions, in which the static contact angle lowered by  $17^\circ \pm 2^\circ$ . However, the decay was more pronounced in basic solution (pH 11), in which the contact angle was decreased by  $\sim 22^\circ$  from the initial value. This value



reduced further to  $52^\circ$  after 30 days of immersion. The contact angle results were supported by XPS data, which show prominent carbon desorption in basic (pH 11) solution (Figure 2B). After 1 day, immersion in  $\text{H}_2\text{O}$  and PBS up to  $\sim 19\%$  of carbon was desorbed, and 23% and 30% in case of pH 3 and pH 11, respectively. After prolonged immersion in  $\text{H}_2\text{O}$ , PBS, pH 3 and pH 11 for 30 days, desorption of  $\sim 37\%$ ,  $\sim 42\%$ ,  $\sim 51\%$  and  $\sim 66\%$ , respectively, was observed by XPS survey scans (Figure 2B). Our results are coherent with stability studied by other groups.<sup>7, 8</sup> However, these data contrast with those of Kong et al., who observed that 1-hexadecanethiol monolayers on Au were stable in basic solution (pH 12) for period of 1 week and are labile in basic solution having pH  $> 12$ .<sup>47</sup> During our studies we noted that without stirring/agitation significant atmospheric contamination of the surfaces can occur, which leads to clear increase in thickness,<sup>48, 49</sup> which hamper analysis of thickness or contact angle data in terms of stability effects. To minimize this deposition of adventitious carbon, constant agitation was therefore both crucial and used.

The phosphonate monolayers on PAO were stable for a week in  $\text{H}_2\text{O}$ , PBS and pH 3 solutions with only a small change, barely outside the error limit, in contact angle (Figure 2C) and C/Al ratio from XPS (Figure 2D). After 7 days of immersion in  $\text{H}_2\text{O}$ , PBS and pH 3 solutions, the contact angle had dropped by just  $2^\circ - 3^\circ$  and the XPS C/Al ratio by  $\sim 4\%$ ,  $\sim 5\%$  and  $\sim 10\%$ , respectively, from the initial value (Figure 2C and 2D). Even after prolonged immersion for 30 days in these solutions, the PAO-PA monolayer did not undergo big changes anymore, with a contact angle constant at  $148^\circ$ , and XPS C/Al ratio which only dropped by 6% ( $\text{H}_2\text{O}$ ), 9% (PBS) and 18% (pH 3) from the initial C/Al ratio. These results show that PAO-PA monolayers are extremely stable under acidic (pH 3),  $\text{H}_2\text{O}$  (neutral) and PBS (pH 7) conditions, which is in line with previous studies.<sup>18</sup> For alkaline conditions, a significantly lower stability was observed, although still better than for the thiol-Au combination. These observations are also consistent with the stability obtained of phosphonate monolayers on magnetron-sputtered aluminum in acidic and basic solutions.<sup>50</sup> The analogous phosphonate monolayers on ITO (ITO-PA) were not as stable as those on PAO surfaces (see Supporting Information, Figure SI-2 for detailed data). This could be caused by the intrinsic porosity and roughness of PAO surfaces, as this provides more surface area for phosphonate groups to form bi-dentate or tri-dentate binding with surface hydroxyl groups.<sup>17, 51</sup> Additionally, PAO is more basic as compared to ITO, and it has been reported that phosphonates form strong binding on basic surfaces as compared to less basic surfaces.<sup>52</sup>

Alkene and alkyne monolayers were prepared on both hydroxyl-terminated and hydrogen-terminated silicon surfaces. As a representative, we here discuss the one that appeared to be the most stable under hydrolytic stability conditions, namely a monolayer derived from 1-octadecyne on Si(111) (see Figure 2E and 2F). After immersion for 1 day in all four solutions, no change was observed in static contact angle as well as in the

carbon percentage as determined by XPS with respect to the starting situation. Even after 7 days of immersion in neutral or acidic media only minor changes were detected, whereas only in basic solution a small reduction in the water contact angle was observed: ca  $7^\circ$ , accompanied by a reduction of  $\sim 6\%$  in the carbon content as determined by XPS. After prolonged immersion for 30 days in  $\text{H}_2\text{O}$ , PBS and pH 3 the static contact angle had decreased by only  $4^\circ - 7^\circ$ , and the carbon content by  $\sim 3\%$  to  $\sim 7\%$ . This indicates that alkyne-derived monolayers on Si(111) surface are exceptionally stable in  $\text{H}_2\text{O}$ , PBS and acidic (pH 3) solutions. In pH 11 solution 16% of the carbon content desorbed after 30 days, but the surface was still hydrophobic as indicated by the eventual contact angle of  $96^\circ \pm 2^\circ$ . The method of preparation of such alkyne monolayers on Si(111) (thermal or photochemical) does not seem to be important in this respect, as there no significant difference in stability was observed (Figure 2E and Supporting Information, Figures SI-12). Similar results were also obtained on H-Si(100) surfaces modified with 1-octadecyne under thermal as well as photochemical conditions (Supporting Information, Figure SI-14). Slightly less stable monolayers were observed on H-Si(111), H-Si(100) and on SiN that were modified with 1-octadecene under both thermal as well as photochemical conditions (Supporting Information, Figure SI-4 to SI-6). We relate this difference in stability to the density of the monolayers: alkyne-derived monolayers are more densely packed as compared to alkene-derived monolayers (for  $\text{C}_{18}$  65% vs 55%).<sup>42</sup> In addition, the nature of the linking bond (Si bound to  $\text{sp}^2$ -hybridized C atom) adds to the stability.

This high hydrolytic stability of alkyne-linked monolayers was also found on other substrates such as Si(100), SiC, CrN and PAO (see Figure 3, and Supporting Information, Figure SI-13 to SI-16). Specifically, alkyne monolayers on SiC displayed an exceptional stability. SiC substrates yield  $-\text{OH}$  terminated SiC surface upon acid wet etching prior to the attachment process. This surface structure allows a specific reaction that links to the obtained high stability: alkynes react to form not just one C-O-C link, but actually two O-C bonds that form a acetal-containing six-membered ring via a double Markovnikov addition.<sup>41</sup> This different binding mode apparently leads to a highly stable monolayer attachment.

This hypothesis is substantiated by the stability studies on 1-octadecene-derived monolayers on hydroxyl-terminated surfaces like  $\text{SiO}_2$ , ITO, CrN, SiC and stainless steel. These layers are among the most stable ones included in this study, and no significant change was e.g., observed for SiC-alkene surfaces upon immersion for 1 day in  $\text{H}_2\text{O}$ , PBS and pH 3. Only in basic media we observed a small decrease in the static water contact angle ( $7^\circ \pm 1^\circ$ ) (Supporting Information, Figure SI-7). After prolonged immersion (30 days) in  $\text{H}_2\text{O}$ , PBS and pH 3 the static contact angle lowered only by  $8^\circ$  to  $10^\circ$ , indicating that monolayers obtained from-

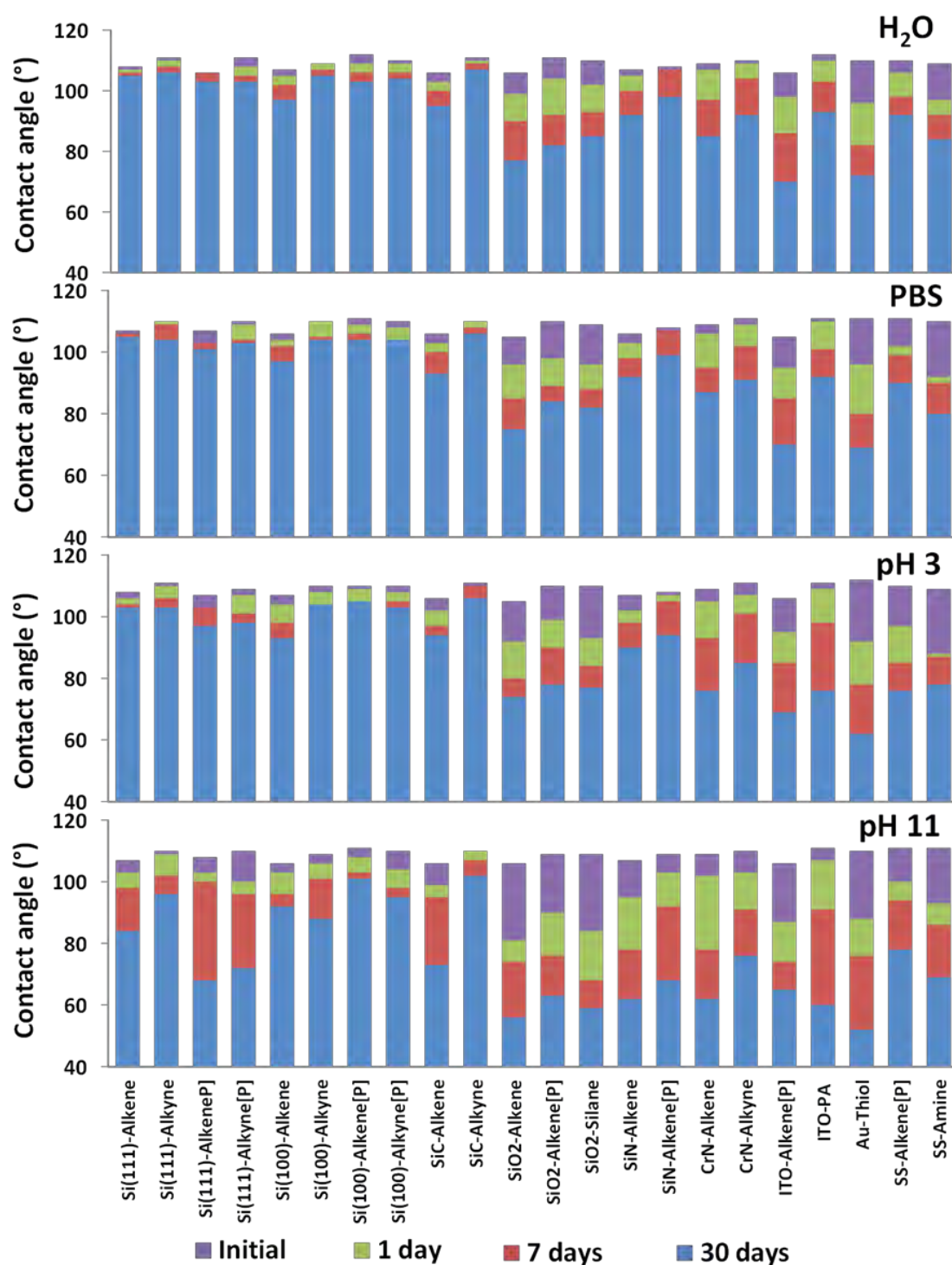


**Figure 3.** The hydrolytic stability of monolayers on different substrates was followed by static water contact angle measurements. Measurements were performed on cleaned surfaces after taking them out from H<sub>2</sub>O, PBS, pH 3 and pH 11 solutions at the indicated time period. [P] indicates surfaces modified under photochemical conditions.

-alkenes are stable in H<sub>2</sub>O, PBS and acidic conditions (see Figure 3, and Supporting Information, Figure SI-7). However, prolonged immersion in basic solution decreased the static contact angle to 73°, indicating that an octadecene-based monolayer obtained on

SiC is not as stable as in H<sub>2</sub>O, PBS and acidic (pH 3) solutions. As such, the SiC-alkene monolayers are not as stable as alkyne-derived ones, but are still stable compared to monolayers derived from e.g., thiols, silanes and phosphonates on Au, SiO<sub>2</sub>, and ITO surfaces (contact angles in Figure 3, XPS data in Figure 2A, and full data set in Supporting Information, Figures SI-1 and SI-2). These results are in accordance with previous results obtained by our group on 1-hexadecene-modified SiC surface under acid (2 M HCl at 90 °C) and basic (0.001 M NaOH at 60 °C) conditions.<sup>35</sup> The stability of octadecene-modified SiC was attributed to the formation of C-O-C instead of Si-O-C bond at the substrate-monolayer interface. Additionally, the Si-C and C-O-C bonds are basically unaffected by most nucleophiles, but Si-O bonds are labile to nucleophilic attacks under basic conditions.<sup>35, 53, 54</sup>

In summary, alkyne-based monolayers on hydrogen-terminated Si and especially on hydroxyl-terminated SiC are highly resistant towards hydrolysis in a wide range of media. This is due to a combination of the nature of the linkage (atoms involved, inertness towards most nucleophiles) and the packing of the monolayer. This extraordinary stability of alkyne-based monolayers thus opens up such modified surfaces to a wide range of new applications in micro and nanotechnology.

### 3.3.2 Thermal Stability

To explore further applications of organic monolayers in e.g., high performance-high temperature FETs and MEMS/NEMS devices, the thermal stability of modified surfaces was studied from 25 °C to 600 °C under ultra-high vacuum (UHV) conditions using XPS. To illustrate the type of information that is obtainable from there, the desorption behavior of alkyl monolayers of thiol on Au, PA on PAO and alkynes on Si(111) substrates is shown in Figure 4, as examples of weak, intermediate and highly stable monolayers.

The thermal stability was monitored by studying as a function of heating temperature to the desorption using the normalized C/substrate peak area ratio, i.e., for the systems in Figure 4, the ratio of C/Au, C/Al and C/Si for thiol, PA and alkyne monolayers on Au, PAO and Si(111), respectively. The XPS data were obtained using at least six samples (1 × 1 cm<sup>2</sup>) of each type of monolayer, and the XPS data were obtained at three different places on each sample to prevent any radiation-induced damage and thus change in the elemental composition. Stepped temperature series were employed on different samples to obtain comparative results and minimize thermal damage (so if 6 increasingly high temperatures were to be measured on 2 samples, on sample A temperatures 1, 3 and 5 would be measured, whereas on sample B temperatures 2, 4 and 6 would be measured; a more detailed schematic representation is given in the Supporting Information, Figure SI-18B). All data points were fitted with a Boltzmann-sigmoidal curve, which allows the determination of  $T_{10}$  and  $T_{50}$  values, i.e., the temperatures at which respectively 10% and 50% loss of monolayers is observed due to thermally induced desorption.

Figure 4A, D, and G show the desorption behavior of thiol monolayers, which are easily desorbed thermally from Au surfaces: the desorption starts at  $\sim 60^\circ\text{C}$  ( $T_{10} = 85^\circ\text{C}$ ) and was complete at  $120^\circ\text{C}$  ( $T_{50} = 106^\circ\text{C}$ ). This observation is consistent with values reported in literature.<sup>26, 28</sup> The low stability of thiol monolayers is attributed to the relatively weak Au-S bond (bond strength  $\sim 40$  kcal/mol).<sup>55</sup>

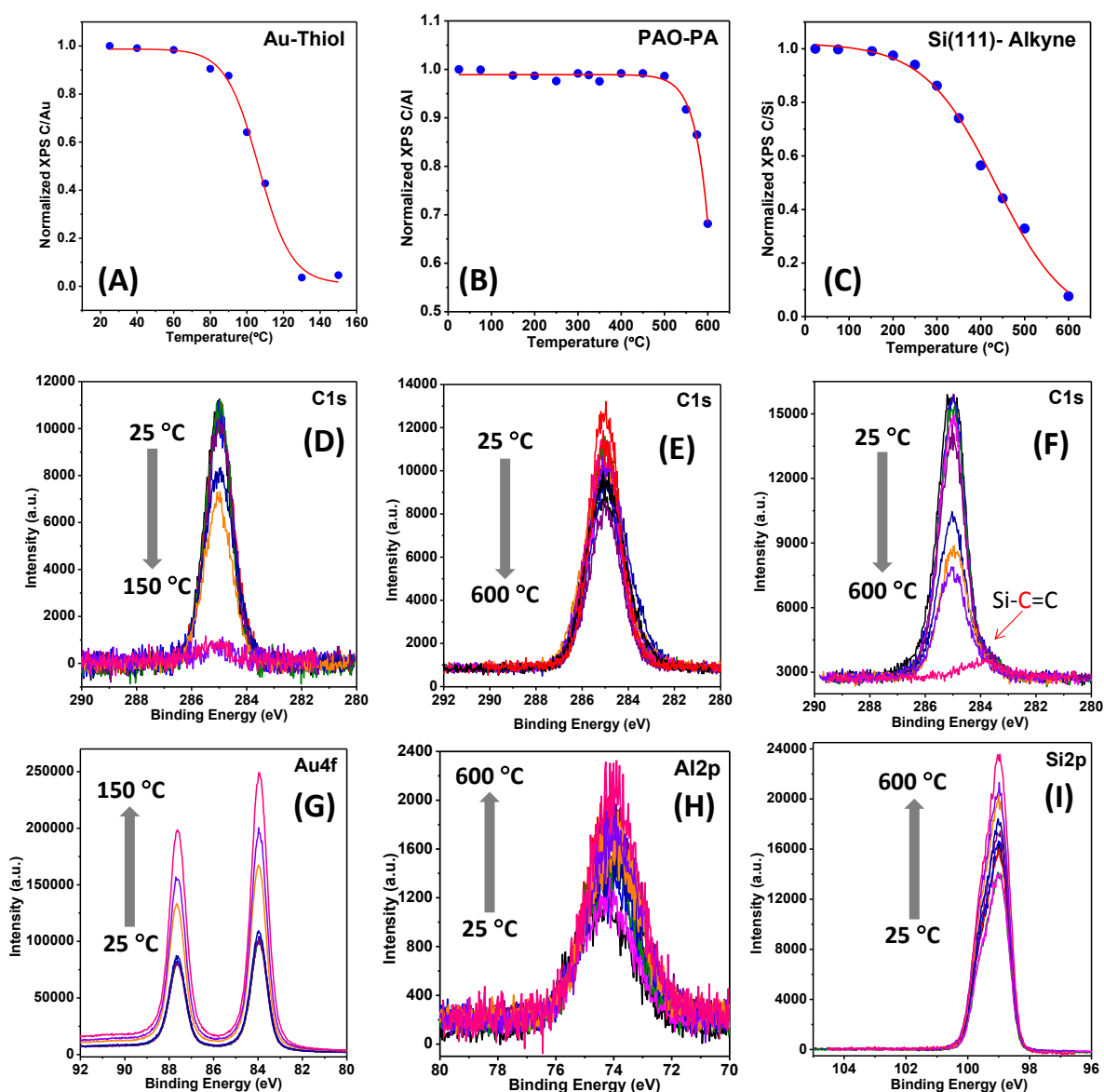


**Figure 4.** Thermal stability of (A) Au-thiol, (B) PAO-PA and (C) Si(111)-alkyne monolayers as followed by desorption of carbon using temperature-dependent XPS. The points were normalized by the peak areas as observed at  $25^\circ\text{C}$  and fitted with a Boltzmann-sigmoidal curve. The XPS C1s desorption (D, E, F) and concomitant increase in substrate element (G, H, I) with increased temperature correspond to Au-thiol, PAO-PA and Si(111)-alkyne, respectively.

The alkyne monolayers on Si(111) show a significantly higher stability: the desorption only starts well above  $200^\circ\text{C}$  ( $T_{10} = 265^\circ\text{C}$ ), but even then no sharp desorption peak is observed. Even upon heating to  $400^\circ\text{C}$  the desorption is still only partial ( $T_{50} = 433^\circ\text{C}$ ), as shown in Figure 4C. Interestingly, a shoulder peak at 284 eV (Figure 4F) corresponding

to Si-C=C was still present even after heating at 600 °C. The ratio of C-C/Si-C was gradually increasing after annealing from 94.4/5.6 (at 25 °C) to 16.0/84.0 (at 600 °C), indicating Si-C=C bond was still intact at elevated temperature up to 600 °C (Figure SI-20). It is of interest to note the difference in the stability observed between alkyne-derived and alkene-derived monolayers on Si(111): alkyne-derived monolayers are typically more strongly bound, which is attributed to a combination of stabilizing  $\pi$ - $\pi$  interactions with neighboring groups,<sup>49</sup> the higher packing density that increases interchain Van der Waals attractions, and the strength of the Si-C=C bond compared to the Si-C-C bond.<sup>42</sup> Nevertheless, the alkene monolayers showed under the UHV conditions employed here a significantly higher thermal stability compared to the reported thermal stability of analogous alkene-derived (under air, nitrogen, or argon/hydrogen mixture) monolayers on Si(111) that desorbed completely at ~350 °C (Supporting Information, Figure SI-19C).<sup>31</sup> Finally, the PA monolayers on PAO reveal an exceptionally high stability, which seems to characterize phosphonic acid-derived monolayers on some metal oxide surfaces (see also below PA on ITO, Table 2). The PA monolayers on PAO display almost no notable desorption even up to ~500 °C ( $T_{10}$  = 562 °C) (Figure 4B, E, and H). Apparently, under these conditions of slow heating in vacuo an optimal curing is effectively observed, which might lead to the formation of multi-dentated structures.<sup>56</sup>

The thermal desorption characteristics of all 14 monolayers under study are presented in Table 2 via their  $T_{10}$  and  $T_{50}$  temperatures. The complete degradation curves for all these substrates as a function of temperature are shown in Supporting Information, Figure SI-19. Noteworthy in view of the intermediate hydrolytic stability is the high thermal stability of silane-derived monolayers on SiO<sub>2</sub>:  $T_{10}$  was ~ 433 °C, but  $T_{50}$  was not even observed yet by heating up the sample to 600 °C. This observation is analogous to perfluoroalkylsiloxane monolayers (> 600 °C) on Si(100),<sup>57</sup> but in contrast with observations on octadecyltrichlorosilane monolayers, where > 50% monolayer was desorbed at ~500 °C under UHV.<sup>25</sup> Silane-derived monolayers possess the ability to form cross-linked 2D networks between neighboring Si-O groups at elevated temperatures, which is a process that depends on the processing of the monolayer and number of leaving groups in the original silane.<sup>1</sup> Like the Si-C bound monolayers, siloxane monolayers eventually desorb via C-C cleavage instead of Si-C or Si-O cleavage.<sup>25</sup>

As explained above, on oxides like PAO (and to a lesser degree: ITO) especially PA forms extremely stable monolayers, displaying  $T_{10}$  = 562 °C (ITO:  $T_{10}$  = 352 °C). An explanation for this very high temperature stability might be the ability of phosphonic acids to form multiple strong bonds to the PAO substrate via monodentated, bidentated or tridentated structures with the surface hydroxyl groups.<sup>20, 56</sup> Alkyne and alkene-derived monolayers on PAO and ITO substrates, respectively, show a relatively low  $T_{10}$  value (typically < 300 °C). Since e.g., alkynes also form bidentate structures to PAO,<sup>58</sup> just like

phosphonic acids may do,<sup>1</sup> it is the nature of the bonds (Al-O-C vs Al-O-P) that is determining this difference.<sup>18</sup> The monolayers derived from alkenes and alkynes on Si(111) and Si(100) have somewhat mixed stability and it is difficult to derive any conclusion based on  $T_{10}$  (Table 2). However, based on  $T_{50}$  it appears that alkynes derived monolayers were more stable at elevated temperature than alkene derived monolayers. Considering the substrate effect, these monolayers on Si(100) were having higher stability than on Si(111): as expected the  $T_{50}$  was higher for alkynes (545 °C on Si(100) > 433 °C for Si(111)) than alkenes (377 °C on Si(100) > 313 °C for Si(111)). Tentatively, this is attributed to the formation of doubly bound alkyne-derived structures on Si(100), which is easier on Si(100) than on Si(111).<sup>59</sup> Similarly alkene-derived monolayers on SiN surfaces were stable up to 200 °C ( $T_{10}$  = 228 °C and  $T_{50}$  = 349 °C). However, alkyne-derived monolayers were less stable ( $T_{10}$  = 272 °C and  $T_{50}$  = 398 °C) than alkene-derived monolayers ( $T_{10}$  = 284 °C and  $T_{50}$  = 480 °C) on SiC surfaces and not in line with hydrolytic stability. However, direct comparison will not possible because binding properties of alkyne and alkene-derived monolayers SiC were completely different from H-terminated surfaces.<sup>43</sup>

**Table 2.** Thermal desorption at 10% ( $T_{10}$  °C) and 50% ( $T_{50}$  °C) carbon loss with elevated temperature on various substrate and different head groups.

Monolayer	$T_{10}$ °C	$T_{50}$ °C
Au-Thiol	85	106
SiO <sub>2</sub> -Silane	433	>600
SiO <sub>2</sub> -Alkene	280	506
PAO-PA	562	>600
PAO- Alkyne	284	>600
ITO-PA	352	442
ITO- Alkene	195	368
Si(111)-Alkene	219	313
Si(111)-Alkyne	265	433
Si(100)- Alkene	306	377
Si(100)- Alkyne	223	545
SiC- Alkene	284	480
SiC- Alkyne	272	398
SiN- Alkene	228	349

### 3.4 Conclusions

Organic monolayers bound to inorganic substrates display a wide range of hydrolytic and thermal stabilities that depend on both the used attachment chemistry and the substrate characteristics. Despite the application of these monolayers in an ever-increasing range of high-end devices, to the best of our knowledge, the current paper presents the *first comprehensive comparative study*. While many organic monolayers hydrolyze quickly or upon prolonged immersion (30 days), alkyne-based (Si-C bound) monolayers on Si, and especially alkyne-based (C-O-C bound) monolayers on SiC display a superb hydrolytic stability, also under extreme pH conditions and under physiological conditions (PBS buffer). These two monolayers also display a good thermal stability in vacuum. A superb thermal stability was obtained for phosphonic acid-derived monolayers on a variety of oxide surfaces (such as PAO and ITO), but these phosphonic acid-derived monolayers display only an intermediate hydrolytic stability.

These results show that selecting the monolayer of choice strongly depends on the application of interest. The dataset obtained in this study (> 1400 measurements) discloses both the hydrolytic and thermal stability over a wide range of conditions for a comprehensive series of organic monolayers on inorganic substrates. This for the first time allows a proper comparative evaluation, expedites monolayer selection for future applications, and also highlights the great potential for several organic monolayer-substrate pairs.



### 3.5 References

1. Pujari, S. P.; Scheres, L.; Marcelis, A. T. M.; Zuilhof, H., Covalent Surface Modification of Oxide Surfaces. *Angew. Chem. Int. Ed.* **2014**, DOI: 10.1002/anie.201306709.
2. Kondo, T.; Yamada, R.; Uosaki, K., Self-Assembled Monolayer (SAM). In *Organized Organic Ultrathin Films*, Wiley-VCH Verlag GmbH & Co. KGaA: 2013; pp 7-42.
3. Förch, R.; Schönherr, H.; Jenkins, A. T. A., *Surface Design: Applications in Bioscience and Nanotechnology*. Wiley: 2009.
4. Maboudian, R.; Ashurst, W. R.; Carraro, C., Self-assembled monolayers as anti-stiction coatings for MEMS: characteristics and recent developments. *Sensor Actuat A-Phys* **2000**, 82, (1-3), 219-223.
5. Kafer, D.; Witte, G.; Cyganik, P.; Terfort, A.; Woll, C., A comprehensive study of self-assembled monolayers of anthracenethiol on gold: Solvent effects, structure, and stability. *J. Am. Chem. Soc.* **2006**, 128, (5), 1723-1732.
6. Chinwangso, P.; Jamison, A. C.; Lee, T. R., Multidentate Adsorbates for Self-Assembled Monolayer Films. *Acc. Chem. Res.* **2011**, 44, (7), 511-519.
7. Jans, K.; Bonroy, K.; Palma, R. D.; Reekmans, G.; Jans, H.; Laureyn, W.; Smet, M.; Borghs, G.; Maes, G., Stability of Mixed PEO-Thiol SAMs for Biosensing Applications. *Langmuir* **2008**, 24, (8), 3949 -3954.
8. Flynn, N. T.; Tran, T. N. T.; Cima, M. J.; Langer, R., Long-Term Stability of Self-Assembled Monolayers in Biological Media. *Langmuir* **2003**, 19, (26), 10909 - 10915.
9. Schoenfish, M. H.; Pemberton, J. E., Air stability of alkanethiol self-assembled monolayers on silver and gold surfaces. *J. Am. Chem. Soc.* **1998**, 120, (18), 4502-4513.
10. Singhana, B.; Jamison, A. C.; Hoang, J.; Lee, T. R., Self-Assembled Monolayer Films Derived from Tridentate Cyclohexyl Adsorbates with Alkyl Tailgroups of Increasing Chain Length. *Langmuir* **2013**, 29, (46), 14108-14116.
11. Clot, O.; Wolf, M. O., Spontaneous Adsorption of 4-Ferrocenylphenyl Isocyanide and 11-Mercaptoundecanoyl Ferrocene on Chromium. *Langmuir* **1999**, 15, (24), 8549-8551.
12. Herzer, N.; Hoeppener, S.; Schubert, U. S., Fabrication of patterned silane based self-assembled monolayers by photolithography and surface reactions on silicon-oxide substrates. *Chem. Commun.* **2010**, 46, (31), 5634-5652.
13. Silverman, B. M.; Wiegand, K. A.; Schwartz, J., Comparative Properties of Siloxane vs Phosphonate Monolayers on A Key Titanium Alloy. *Langmuir* **2005**, 21, (1), 225 - 228.
14. Seitz, O.; Fernandes, P. G.; Tian, R.; Karnik, N.; Wen, H.-C.; Stiegler, H.; Chapman, R. A.; Vogel, E. M.; Chabal, Y. J., Control and stability of self-assembled monolayers under biosensing conditions. *J. Mater. Chem.* **2011**, 21, (12), 4384-4392.
15. Giza, M.; Thissen, P.; Grundmeier, G., Adsorption Kinetics of Organophosphonic Acids on Plasma-Modified Oxide-Covered Aluminum Surfaces. *Langmuir* **2008**, 24, (16), 8688-8694.
16. Guerrero, G.; Alauzun, J. G.; Granier, M.; Laurencin, D.; Mutin, P. H., Phosphonate coupling molecules for the control of surface/interface properties and the synthesis of nanomaterials. *Dalton Trans.* **2013**, 42, (35), 12569-12585.
17. Bauer, T.; Schmaltz, T.; Lenz, T.; Halik, M.; Meyer, B.; Clark, T., Phosphonate- and carboxylate-based self-assembled monolayers for organic devices: a theoretical study of surface binding on aluminum oxide with experimental support. *ACS Appl. Mater. Interfaces* **2013**, 5, (13), 6073-6080.

18. Debrassi, A.; Ribbera, A.; Vos, W. M. d.; Wennekes, T.; Zuilhof, H., Stability of (Bio)Functionalized Porous Aluminum Oxide. *Langmuir* **2014**, 30, (5), 1311–1320.
19. Pujari, S. P.; Li, Y.; Regeling, R.; Zuilhof, H., Tribology and Stability of Organic Monolayers on CrN: A Comparison among Silane, Phosphonate, Alkene, and Alkyne Chemistries. *Langmuir* **2013**, 29, (33), 10405-10415.
20. Queffélec, C.; Petit, M.; Janvier, P.; Knight, D. A.; Bujoli, B., Surface Modification Using Phosphonic Acids and Esters. *Chem. Rev.* **2012**, 112, (7), 3777-3807.
21. Fabre, B., Ferrocene-Terminated Monolayers Covalently Bound to Hydrogen-Terminated Silicon Surfaces. Toward the Development of Charge Storage and Communication Devices. *Acc. Chem. Res.* **2010**, 43, (12), 1509-1518.
22. Cao, A.; Sudhölter, E. J.; de Smet, L. C., Silicon Nanowire-Based Devices for Gas-Phase Sensing. *Sensors* **2013**, 14, (1), 245-271.
23. Acton, B. O.; Ting, G. G.; Shamberger, P. J.; Ohuchi, F. S.; Ma, H.; Jen, A. K. Y., Dielectric Surface-Controlled Low-Voltage Organic Transistors via n-Alkyl Phosphonic Acid Self-Assembled Monolayers on High-k Metal Oxide. *ACS Appl. Mater. Interfaces* **2010**, 2, (2), 511-520.
24. Everaerts, K.; Emery, J. D.; Jariwala, D.; Karmel, H. J.; Sangwan, V. K.; Prabhumirashi, P. L.; Geier, M. L.; McMorro, J. J.; Bedzyk, M. J.; Facchetti, A.; Hersam, M. C.; Marks, T. J., Ambient-Processable High Capacitance Hafnia-Organic Self-Assembled Nanodielectrics. *J. Am. Chem. Soc.* **2013**, 135, (24), 8926-8939.
25. Kluth, G. J.; Sung, M. M.; Maboudian, R., Thermal Behavior of Alkylsiloxane Self-Assembled Monolayers on the Oxidized Si(100) Surface. *Langmuir* **1997**, 13, (14), 3775-3780.
26. Shadnam, M. R.; Amirfazli, A., Kinetics of alkanethiol monolayer desorption from gold in air. *Chem. Commun.* **2005**, (38), 4869-4871.
27. Weber, J.; Balgar, T.; Hasselbrink, E., Conformational disorder in alkylsiloxane monolayers at elevated temperatures. *J. Chem. Phys.* **2013**, 139, (24), 244902.
28. Shon, Y.-S.; Lee, T. R., Desorption and Exchange of Self-Assembled Monolayers (SAMs) on Gold Generated from Chelating Alkanedithiols. *J. Phys. Chem. B* **2000**, 104, (34), 8192-8200.
29. Sung, M. M.; Kluth, G. J.; Yauw, O. W.; Maboudian, R., Thermal Behavior of Alkyl Monolayers on Silicon Surfaces. *Langmuir* **1997**, 13, (23), 6164-6168.
30. Chandekar, A.; Sengupta, S. K.; Whitten, J. E., Thermal stability of thiol and silane monolayers: A comparative study. *Appl. Surf. Sci.* **2010**, 256, (9), 2742-2749.
31. Faucheux, A.; Gouget-Laemmel, A. C.; Allongue, P.; de Villeneuve, C. H.; Ozanam, F.; Chazalviel, J. N., Mechanisms of thermal decomposition of organic monolayers grafted on (111) silicon. *Langmuir* **2007**, 23, (3), 1326-1332.
32. Bain, C. D.; Troughton, E. B.; Tao, Y. T.; Evall, J.; Whitesides, G. M.; Nuzzo, R. G., Formation of monolayer films by the spontaneous assembly of organic thiols from solution onto gold. *J. Am. Chem. Soc.* **1989**, 111, (1), 321-335.
33. Paniagua, S. A.; Hotchkiss, P. J.; Jones, S. C.; Marder, S. R.; Mudalige, A.; Marrikar, F. S.; Pemberton, J. E.; Armstrong, N. R., Phosphonic Acid Modification of Indium-Tin Oxide Electrodes: Combined XPS/UPS/Contact Angle Studies. *J. Phys. Chem. C* **2008**, 112, (21) 7809 - 7817.
34. Ruan, C.-M.; Bayer, T.; Meth, S.; Sukenik, C. N., Creation and characterization of n-alkylthiol and n-alkylamine self-assembled monolayers on 316L stainless steel. *Thin Solid Films* **2002**, 419, (1-2), 95-104.
35. Rosso, M.; Arafat, A.; Schroën, K.; Giesbers, M.; Roper, C. S.; Maboudian, R.; Zuilhof, H., Covalent Attachment of Organic Monolayers to Silicon Carbide Surfaces. *Langmuir* **2008**, 24, (8), 4007 - 4012.

36. ter Maat, J.; Regeling, R.; Yang, M.; Mullings, M. N.; Bent, S. F.; Zuilhof, H., Photochemical Covalent Attachment of Alkene-Derived Monolayers onto Hydroxyl-Terminated Silica. *Langmuir* **2009**, 25, (19), 11592-11597.
37. Li, Y.; Zuilhof, H., Photochemical Grafting and Patterning of Organic Monolayers on Indium Tin Oxide Substrates. *Langmuir* **2012**, 28, (12), 5350-5359.
38. Arafat, A.; Schroën, K.; de Smet, L. C. P. M.; Sudhölter, E. J. R.; Zuilhof, H., Tailor-Made Functionalization of Silicon Nitride Surfaces. *J. Am. Chem. Soc.* **2004**, 126, (28), 8600-8601.
39. Rosso, M.; Giesbers, M.; Arafat, A.; Schroën, K.; Zuilhof, H., Covalently Attached Organic Monolayers on SiC and Si<sub>3</sub>N<sub>4</sub> Surfaces: Formation Using UV Light at Room Temperature. *Langmuir* **2009**, 25, (4), 2172-2180.
40. Sun, Q.-Y.; de Smet, L. C. P. M.; van Lagen, B.; Giesbers, M.; Thüne, P. C.; van Engelenburg, J.; de Wolf, F. A.; Zuilhof, H.; Sudhölter, E. J. R., Covalently Attached Monolayers on Crystalline Hydrogen-Terminated Silicon: Extremely Mild Attachment by Visible Light. *J. Am. Chem. Soc.* **2005**, 127, (8), 2514-2523.
41. Manova, R. K.; Pujari, S. P.; Weijers, C. A. G. M.; Zuilhof, H.; van Beek, T. A., Copper-Free Click Biofunctionalization of Silicon Nitride Surfaces via Strain-Promoted Alkyne–Azide Cycloaddition Reactions. *Langmuir* **2012**, 28, (23), 8651-8663.
42. Scheres, L.; Giesbers, M.; Zuilhof, H., Self-Assembly of Organic Monolayers onto Hydrogen-Terminated Silicon: 1-Alkynes Are Better Than 1-Alkenes. *Langmuir* **2010**, 26, (13), 10924-10929.
43. Pujari, S. P.; Scheres, L.; Weidner, T.; Baio, J. E.; Cohen Stuart, M. A.; van Rijn, C. J. M.; Zuilhof, H., Covalently Attached Organic Monolayers onto Silicon Carbide from 1-Alkynes: Molecular Structure and Tribological Properties. *Langmuir* **2013**, 29, (12), 4019-4031.
44. Roper, C. S.; Radmilovic, V.; Howe, R. T.; Maboudian, R., Single-source chemical vapor deposition of SiC films in a large-scale low-pressure CVD growth, chemical, and mechanical characterization reactor. *J. Electrochem. Soc.* **2006**, 153, (8), C562-C566.
45. Amy, F.; Chan, C. K.; Zhao, W.; Hyung, J.; Ono, M.; Sueyoshi, T.; Kera, S.; Nesher, G.; Salomon, A.; Segev, L.; Seitz, O.; Shpaisman, H.; Schöll, A.; Haeming, M.; Böcking, T.; Cahen, D.; Kronik, L.; Ueno, N.; Umbach, E.; Kahn, A., Radiation Damage to Alkyl Chain Monolayers on Semiconductor Substrates Investigated by Electron Spectroscopy. *J. Phys. Chem. B* **2006**, 110, (43), 21826-21832.
46. Frydman, E.; Cohen, H.; Maoz, R.; Sagiv, J., Monolayer Damage in XPS Measurements As Evaluated by Independent Methods. *Langmuir* **1997**, 13, (19), 5089-5106.
47. Kong, B.; Kim, Y.; Choi, I. S., pH-Dependent Stability of Self-Assembled Monolayers on Gold. *Bull. Korean Chem. Soc.* **2008**, 29, (9), 1843-1846.
48. Jiang, G.; Niederhauser, T. L.; Davis, S. D.; Lua, Y.-Y.; Cannon, B. R.; Dorff, M. J.; Howell, L. L.; Magleby, S. P.; Linford, M. R., Stability of alkyl monolayers on chemomechanically scribed silicon to air, water, hot acid, and X-rays. *Colloids Surf., A* **2003**, 226, (1-3), 9-16.
49. Puniredd, S. R.; Assad, O.; Haick, H., Highly Stable Organic Monolayers for Reacting Silicon with Further Functionalities: The Effect of the C–C Bond nearest the Silicon Surface. *J. Am. Chem. Soc.* **2008**, 130, (41), 13727-13734.
50. Liakos, I. L.; Newman, R. C.; McAlpine, E.; Alexander, M. R., Study of the Resistance of SAMs on Aluminium to Acidic and Basic Solutions Using Dynamic Contact Angle Measurement. *Langmuir* **2007**, 23, (3), 995-999.

51. Thissen, P.; Valtiner, M.; Grundmeier, G., Stability of phosphonic acid self-assembled monolayers on amorphous and single-crystalline aluminum oxide surfaces in aqueous solution. *Langmuir* **2010**, 26, (1), 156-64.
52. Marcinko, S.; Fadeev, A. Y., Hydrolytic Stability of Organic Monolayers Supported on TiO<sub>2</sub> and ZrO<sub>2</sub>. *Langmuir* **2004**, 20, (6), 2270 - 2273.
53. Sorarù, G. D.; Pederiva, L.; Latournerie, J.; Raj, R., Pyrolysis Kinetics for the Conversion of a Polymer into an Amorphous Silicon Oxycarbide Ceramic. *J. Am. Ceram. Soc.* **2002**, 85, (9), 2181-2187.
54. Lapin, N. A.; Chabal, Y. J., Infrared Characterization of Biotinylated Silicon Oxide Surfaces, Surface Stability, and Specific Attachment of Streptavidin. *J. Phys. Chem. B* **2009**, 113, (25), 8776-8783.
55. Nuzzo, R. G.; Dubois, L. H.; Allara, D. L., Fundamental studies of microscopic wetting on organic surfaces. 1. Formation and structural characterization of a self-consistent series of polyfunctional organic monolayers. *J. Am. Chem. Soc.* **1990**, 112, (2), 558-569.
56. Neves, B. R. A.; Salmon, M. E.; Russell, P. E.; Troughton, E. B., Thermal Stability Study of Self-Assembled Monolayers on Mica. *Langmuir* **2000**, 16, (6), 2409-2412.
57. Fréchette, J.; Maboudian, R.; Carraro, C., Thermal Behavior of Perfluoroalkylsiloxane Monolayers on the Oxidized Si(100) Surface. *Langmuir* **2006**, 22, (6), 2726-2730.
58. ter Maat, J.; Regeling, R.; Ingham, C. J.; Weijers, C. A. G. M.; Giesbers, M.; de Vos, W. M.; Zuilhof, H., Organic Modification and Subsequent Biofunctionalization of Porous Anodic Alumina Using Terminal Alkynes. *Langmuir* **2011**, 27, (22), 13606-13617.
59. Sieval, A. B.; Van den Hout, B.; Zuilhof, H.; Sudhölter, E. J. R., Molecular modeling of covalently attached alkyl monolayers on the hydrogen-terminated Si(111) surface. *Langmuir* **2001**, 17, (7), 2172-2181.



# Chapter 4

---

## Adhesion and Friction Properties of Polymer Brushes: Fluoro versus Non-fluoro Polymer Brushes at Varying Thickness

### Abstract

A series of different thicknesses of fluoro poly(2,2,2-trifluoroethyl methacrylate) and its analogous non-fluoro poly(ethyl methacrylate) polymer brushes were prepared via surface-initiated atom transfer radical polymerization (SI-ATRP) on Si(111) surfaces. The thiol-yne click (TYC) reaction was used to immobilize the SI-ATRP initiator with a high surface coverage, in order to achieve denser polymer brushes (grafting density from  $\sim 0.1$  to  $0.8$  chains/nm<sup>2</sup>). All polymer brushes were characterized by static water contact angle measurements, infrared absorption reflection spectroscopy, and X-ray photoelectron spectroscopy. Adhesion and friction force measurements were conducted with silica colloidal probe atomic force microscopy (CP-AFM) under ambient and dry (argon) conditions. The fluoro poly(2,2,2-trifluoroethyl methacrylate) polymer showed a decrease in adhesion and friction with increasing thickness. The analogous non-fluoro poly(ethyl methacrylate) polymer brushes showed a high adhesion and friction under ambient conditions. Friction coefficients down to 0.0057 (ambient conditions) and 0.0031 (dry argon) were obtained for poly(2,2,2-trifluoroethyl methacrylate) polymer brushes with 140 nm thickness, which are the lowest among these type of polymer brushes.

This chapter is published as:

*‘Adhesion and Friction Properties of Polymer Brushes: Fluoro versus Non-fluoro Polymer Brushes at Varying Thickness’ Bhairamadgi, N. S.; Pujari, S. P.; Leermakers, F. A. M.; van Rijn, C. J. M.; Zuilhof, H. Langmuir* **2014**, 30, 8, 2068–2076.

**Contents**

<b>4. Adhesion and Friction Properties of Polymer Brushes: Fluoro versus Non-fluoro Polymer Brushes at Varying Thickness .....</b>	<b>61</b>
Abstract .....	61
4.1 Introduction .....	63
4.2 Experimental Methods .....	65
4.2.1 Materials.....	65
4.2.2 Surface Functionalization.....	65
4.2.3 Initiator Immobilization .....	66
4.2.4 Preparation of Poly(ethyl methacrylate) Brushes.....	66
4.2.5 Preparation of Poly(2,2,2-trifluoroethyl methacrylate) Brushes .....	67
4.2.6 Contact Angle Measurements .....	67
4.2.7 Ellipsometry .....	67
4.2.8 Atomic Force Microscopy (AFM) .....	67
4.2.9 X-ray Photoelectron Spectroscopy (XPS).....	68
4.2.10 Fourier Transform Infrared Reflection Absorption Spectroscopy (FT-IRRAS) .....	68
4.3 Results and Discussion.....	69
4.3.1 Silicon Surface Functionalization .....	69
4.3.2 Initiator Immobilization .....	69
4.3.3 Preparation of Poly(ethyl methacrylate) Brushes.....	70
4.3.4 Preparation of Poly(2,2,2-trifluoroethyl methacrylate) Brushes .....	72
4.3.5 Adhesion and Friction .....	74
4.3.6 Adhesion .....	74
4.3.7 Friction .....	76
4.4 Conclusions .....	77
4.5 References .....	78

## 4.1 Introduction

Polymer brushes – tightly packed, surface-bound polymers<sup>1</sup> – are increasingly used due to their unique properties, which make them amenable for a wide range of applications. Their potential becomes evident from the range of fields in which they are currently studied: antifouling surfaces,<sup>2</sup> reversible switching behavior (depending on e.g., pH, heat or light),<sup>3, 4</sup> multivalent functionalization,<sup>5</sup> tunable wettability<sup>6, 7</sup> and lubrication,<sup>8</sup> and so forth. Therefore, polymer brushes find application in sensors,<sup>9, 10</sup> drug delivery,<sup>9</sup> and micro and nano fluidic devices.<sup>11</sup> Polymer brushes can be obtained quite easily via ‘grafting to’ and ‘grafting from’ approaches.<sup>12</sup> Covalently bound polymer brushes are mechanically and chemically more robust than coatings obtained via e.g., spin coating or other non-covalent coating methods.<sup>13, 14</sup> Therefore, such brushes may act as a very thin, yet stable lubricant that reduces the adhesive forces between two sliding substances in the presence of a good solvent.<sup>15, 16</sup> Landherr et al. prepared surface-tethered polydimethylsiloxane (PDMS), polystyrene (PS) and related co-polymers with different chain lengths and surface coverages via a ‘grafting to’ approach, and observed that increasing the grafting density (0.04 to 0.79 chains/nm<sup>2</sup>) yields a large reduction in the friction coefficient due to the formation of an uniform surface of stretched chains with a reduced surface viscosity.<sup>17</sup> McNamee et al. studied the effect of molecular weight on the friction force of surface-bound (via silane coupling agent) polyethylene glycol (PEG) with monomeric units PEG6, PEG43 and PEG113 in water.<sup>18</sup> They observed that the friction increased with an increase in molecular weight (chain length) in the order PEG6 < PEG43 < PEG113, which was attributed to increasing polymer entanglement and intermolecular hydrogen bonding. As an alternative to ‘grafting to’ approaches, surface-initiated controlled radical polymerization (SI-CRP) methods,<sup>19</sup> such as reversible-addition fragmentation chain transfer (SI-RAFT),<sup>20</sup> nitroxide-mediated polymerization (SI-NMP),<sup>21</sup> photoiniferter-mediated polymerization (SI-PIMP)<sup>22</sup> and atom transfer radical polymerization (SI-ATRP) are proving to be highly useful.<sup>21</sup> SI-ATRP is the most established technique to produce polymer brushes among the other controlled radical-based techniques.<sup>23-25</sup> Spencer and co-worker prepared hydrophobic polymer brushes via a grafting-from approach, which showed good lubrication properties in hexadecane.<sup>26</sup> The lubrication properties of the polymer brushes are highly dependent on the type of solvents used. In a good solvent, the polymer brush will swell and thus stretch away from the substrate and move freely with a sliding movement of the contacting substance. This is probably best shown via the long-lived zwitterionic hip implant coatings of Ishara’s group, in which in fact the hydrating layer around the polymer brush acts as a highly stable lubrication layer.<sup>27</sup> The use of a solvent, however, will strongly limit the application range of polymer brushes, especially in conditions where liquids cannot be introduced, such as in Micro and Nano electromechanical devices (MEMS and NEMS).<sup>28</sup> Currently, a thin film of polytetrafluoroethylene (PTFE) is typically used as the main coating material



in such devices to reduce adhesion and friction. PTFE has many highly relevant properties for lubrication purposes, but it is not covalently bound to the substrate. As a result, it displays a limited mechanical stability and wear resistance.<sup>28, 29</sup> Sakata et al. studied the tribo-properties of spin-coated poly(methyl methacrylate) (PMMA) and surface-anchored PMMA brushes. They observed that surface-tethered PMMA brushes showed a lower friction coefficient and a better wear resistance than the corresponding spin-coated PMMA film, which was attributed to the anchoring of the chain ends.<sup>13</sup> Sun et al. prepared polyglycidyl methacrylate (PGMA) via a grafting-from approach on a silicon surface, and then a polyimide (PI) film was covalently grafted onto the PGMA brushes. They compared the tribological behavior of PI grafted on PGMA surfaces with that of a PI film coated on a bare silicon surface, and observed that the PI grafted on PGMA brushes exhibited a lower friction and improved wear resistance than the PI film coated on a bare silicon surface.<sup>30</sup>

These studies suggest that the adhesion and friction properties of polymer brushes are dependent mainly on the type of surface anchoring, the density and thickness of polymer brushes, and the surface energy. However, the nano-tribological properties of polymer brushes under dry conditions have not been studied in detail yet, despite their potential for application in MEMS/NEMS. Recently our group achieved an ultra-low adhesion and friction coefficient on surfaces modified with covalently bound fluorinated organic monolayers (ca. 2 nm thick) on Si, SiC and CrN under dry conditions.<sup>31-33</sup> Specifically, on atomically flat Si, friction coefficients as low as 0.012 were obtained.<sup>31</sup> Such monolayers also proved to be extremely wear-resistant.<sup>32</sup> In general, these studies showed that ultra-low adhesion and strongly reduced friction can be achieved by an increased fluorine content in the monolayer. To obtain analogous lubrication properties for polymer brushes under ambient conditions, one would thus need to combine covalent attachment with control over the thickness, grafting density and fluorine content. To the best of our knowledge, there are no studies that combine these features.

The aim of this paper is therefore to combine all these properties via the preparation, characterization, and tribology studies of covalently bound polymer brushes with varying thickness and fluorine content. To this aim we prepared covalently bound, alkyne-terminated monolayers on oxide-free Si(111), onto which an initiator was subsequently attached via a thiol-yne click (TYC) reaction.<sup>34</sup> This then allowed follow-up SI-ATRP reactions with ethyl methacrylate (EMA) and 2,2,2-trifluoroethyl methacrylate (TFEMA) and the preparation of the corresponding high-density brushes (Figure 1). The resulting polymer brushes were characterized in detail by ellipsometry, X-ray photoelectron spectroscopy (XPS), Fourier transform infrared reflection absorption spectroscopy (FT-IRRAS), and static water contact angle measurements (CA). Finally, the adhesion and friction properties were investigated by colloidal probe atomic force microscopy (CP-AFM) under ambient (relative humidity (RH) =  $44 \pm 2\%$ ) and dry (RH < 5%) conditions.

The ultra-low adhesion and friction forces of these polymer brushes will be helpful in designing highly robust thin films for a range of applications.

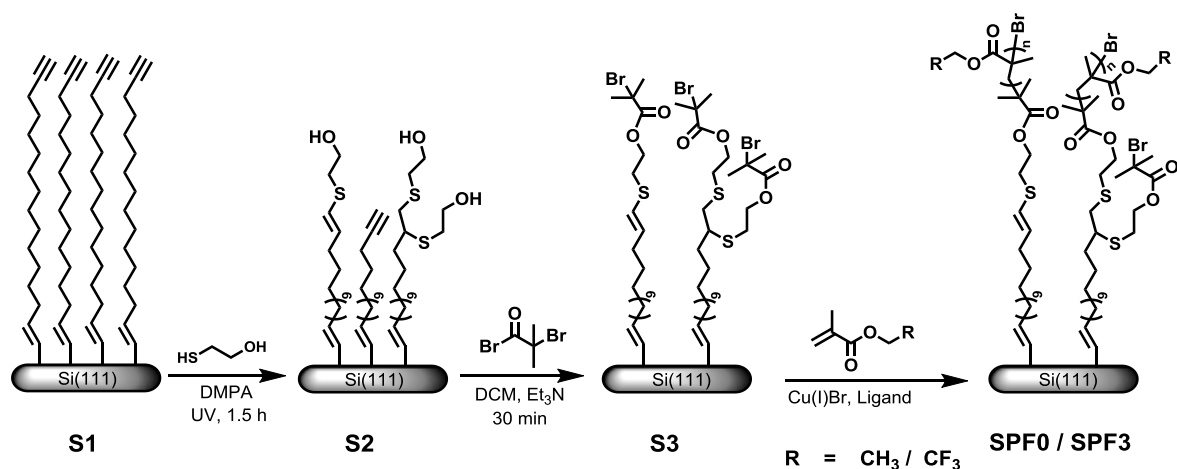


**Figure 1.** Surface functionalization via TYC chemistry, initiator immobilization and preparation of polymer brushes on Si(111) surfaces.

## 4.2 Experimental Methods

### 4.2.1 Materials

1,15-Hexadecadiyne was synthesized according to a literature procedure.<sup>34</sup> Chlorobenzene,  $\alpha,\alpha,\alpha$ -trifluorotoluene (TFT), tetrahydrofuran (THF), 2-mercaptoethanol, Cu(I)Br, N,N,N',N'',N''-pentamethyldiethylenetriamine (PMDETA), 4,4'-dinonyl-2,2'-bipyridine (dNbpy),  $\alpha$ -bromoisobutyryl bromide, ethyl methacrylate (EMA) and 2,2,2-trifluoroethyl methacrylate (TFEMA) were obtained from Sigma-Aldrich, and were used as received, unless otherwise specified. Monomers EMA and TFEMA were filtered through a basic alumina column to remove inhibitors before utilizing them for polymerization.

### 4.2.2 Surface Functionalization

Alkyne-terminated monolayers were prepared on oxide-free  $1 \times 1 \text{ cm}^2$  pieces of one-side polished Si(111) wafers (n-type, thickness 475-550  $\mu\text{m}$  and resistivity 1.0 - 5.0  $\Omega \text{ cm}$ , Siltronix, France) using with 1,15-hexadecadiyne.<sup>34</sup> The resulting alkyne-terminated Si substrates (denoted as **S1**) were rinsed with dichloromethane and dried under a stream of argon. The alkyne-terminated monolayers were further modified via a TYC reaction to obtain hydroxyl-terminated monolayers using freshly prepared mixtures of 2-mercaptoethanol and 2,2-dimethoxy-2-phenylacetophenone (DMPA) as photoinitiator in a 1:0.2 molar ratio. Alkyne-terminated surfaces were covered with a few drops (3 to 4) of thiol/initiator mixture. The TYC reaction was initiated by irradiation with handheld UV light 365 nm (Spectroline, Westbury, NY; power output 800  $\mu\text{W}/\text{cm}^2$ , distance between lamp and surface 2 cm) for 1.5 h. Afterwards, the modified Si substrates were rinsed a few

times with THF, sonicated for 5 min in THF and rinsed with dichloromethane, and dried under a stream of argon. The hydroxyl-terminated surfaces, designated as **S2**, were further characterized by contact angle and XPS measurements.

#### 4.2.3 Initiator Immobilization

A 5 ml vial containing 0.5 ml of dichloromethane and a clean hydroxyl-terminated surface (**S2**) was flushed using a stream of dry argon for 5 min. Initiator  $\alpha$ -bromoisobutyryl bromide (1 ml) and triethylamine (2 to 3 drops) were added into the vial. The inert atmosphere was maintained by a continuous flow of argon. After 30 min, the resulting initiator-functionalized surface (labelled **S3**) was washed using dichloromethane and dried with a stream of argon. Further characterization of the initiator-immobilized surface was performed using contact angle and XPS measurements.

#### 4.2.4 Preparation of Poly(ethyl methacrylate) Brushes

Seven initiator-immobilized ( $1 \times 1 \text{ cm}^2$ ) silicon substrates (**S3**) were fitted into a 50 mL custom-made reaction vessel containing a magnetic stirring bar (see Figure SI-1 in the Supporting Information for a schematic diagram of the reaction vessel). Subsequently, CuBr (50.0 mg, 0.35 mmol) was added under an argon atmosphere, and the reaction vessel was subsequently evacuated and backfilled with argon three times. Into another 50 mL Schlenk tube equipped with a magnetic stirring bar, an inhibitor-free monomer EMA (4.36 mL, 35 mmol) was placed together with the ligand PMDETA (62.4 mg, 0.36 mmol) and chlorobenzene as solvent (10 mL), and argon was bubbled through for at least 1 h. Afterwards, the content was cannulated into the custom-made reaction vessel containing the initiator-immobilized substrate (**S3**) and CuBr. The polymerization was carried out at 90 °C. To obtain various thicknesses of the resulting polymer brushes, the polymerization was carried out for set times on separate substrates. The custom-made reaction vessel allowed us to gradually immerse initiator-functionalized surface into the reaction mixture one after another (e.g., if with only two samples we would immerse only the bottom one for e.g., 4 h, then also immerse the next one for 2 h, we would thus have obtained reaction times of 6 and 2 h, respectively). As a result, we obtained polymer brushes with various thicknesses under near-identical conditions in one attempt. The polymerization was stopped after a fixed time by exposing the reaction mixture to air. The substrates were taken out from the reaction mixture, copiously rinsed with chlorobenzene and THF, sonicated for 15 min in THF to remove any physisorbed reaction components, and dried under a stream of argon. The modified substrates (**SPF0**) were subsequently dried under vacuum ( $< 5 \text{ mbar}$ ) at room temperature for 8 h before further study.

#### 4.2.5 Preparation of Poly(2,2,2-trifluoroethyl methacrylate) Brushes

The poly(2,2,2-trifluoroethyl methacrylate) brushes were prepared analogously, with some slight variations: seven initiator-immobilized Si substrates (**S3**) ( $1 \times 1 \text{ cm}^2$ ) were immersed one by one in a solution of CuBr (50.0 mg, 0.35 mmol), inhibitor-free TFEMA (5.0 mL, 35 mmol), the ligand dNnbp (147 mg, 0.36 mmol) and  $\alpha,\alpha,\alpha$ -trifluorotoluene (TFT) (10 mL). Modified surfaces (**SPF3**) were cleaned with TFT, sonicated for 15 min in THF, and then dried under vacuum for at least 8 h before further study.

#### 4.2.6 Contact Angle Measurements

The static water contact angle of modified surfaces was measured using a Kruss DSA 100 goniometer having an automated drop dispenser and an image capture system. A small droplet (3.0  $\mu\text{L}$ ) of water was dispensed via a microliter syringe, and static contact angles of these droplets were measured using a tangent 2 fitting model. The error in the measurement was  $\pm 1^\circ$  with five repeated measurements.

#### 4.2.7 Ellipsometry

The thickness of all modified surfaces was measured on a Sentech Instruments type SE-400 ellipsometer. The ellipsometer was operated at 632.8 nm (He-Ne laser) with a fixed incidence angle of  $70^\circ$ . A freshly etched (40%  $\text{NH}_4\text{F}$ )  $1 \times 1 \text{ cm}^2$  H-terminated Si(111) substrate was used to determine the optical constants ( $n = 3.821$  and  $k = 0.057$ ). The refractive index (RI) and thicknesses were obtained assuming a planar isotropic, three layer (ambient, polymer and substrate) model. The thicknesses of all modified surfaces were an average of six different measurements at six different places with a variation of  $\pm 0.1 \text{ nm}$  for monolayers and ca. 5% for polymer brushes. The swollen thickness of polymer brushes was measured using ellipsometry following literature procedure.<sup>35</sup> Acetone was used as a good solvent for swelling both polymer brushes ( $n \approx 1.36$ ) in a custom-made liquid cell, having  $70^\circ$  sloped windows.

#### 4.2.8 Atomic Force Microscopy (AFM)

All adhesion and friction forces were measured on a MFP-3D atomic force microscope (Asylum Research, Santa Barbara, CA) according to a procedure reported previously.<sup>31</sup> Both adhesion and friction measurements were carried out on micro scale under ambient (in air at a RH of  $44 \pm 2\%$ ) and dry (in a closed fluid cell, Asylum Research, Santa Barbara, CA, RH  $< 5\%$ ) conditions i.e. without using any solvents. To control the humidity, a flow (1 ml/min) of dry argon was passed continuously through a closed fluid cell (instead of the liquid that is typically used in such devices). The colloidal probe and sample under study were mounted into the fluid cell and the cell was closed, flushed with dry argon for at least 1 h before the measurements. Next, the outlet of the cell was closed and the argon flow was kept minimal ( $< 1 \text{ ml/min}$ ). Triangular silicon nitride cantilevers

(Bruker probes, NP-B, spring constant between 0.10 and 0.16 N/m) were modified with spherical silica particles ( $R = 3.0 \mu\text{m}$ , rms roughness value of  $6.83 \pm 2.06 \text{ nm}$ ) using Norland optical adhesive 61, and cured by exposure to UV light (365 nm) for 10 min. Prior to use, the cantilevers to which a silica sphere was attached (colloidal probes) were rinsed with ethanol and then cleaned using air plasma for 5 min.

The adhesion forces were measured using at least 200 separate force curves at three different places on each modified surface. A scan range of  $5.0 \mu\text{m}$  with 0.5 Hz was used for all modified surfaces. The normal spring constant of silica sphere-attached cantilevers was determined with the help of thermal tuning and following the Hutter and Bechhoefer method for each cantilever.<sup>36</sup> The spring constants were calibrated using deflection sensitivity of supported cantilever. The overall error limit is estimated to be 10% based on the error in measurement of the adhesion forces.<sup>31</sup>

The friction forces were measured using lateral force images, which were derived from trace and retrace tracks of  $20 \times 20 \mu\text{m}^2$  under variable loads ( $F_N = 10$  to  $95 \text{ nN}$ ). The lateral friction forces were obtained with a constant speed of  $5 \mu\text{m/s}$  at  $90^\circ$  angle to the cantilevers long axis. The average lateral force ( $[\mu_{\text{trace}} - \mu_{\text{retrace}}]/2$ , in V) signals were transformed into friction forces. To calibrate the cantilevers, the reversible bending of an  $8.9 \mu\text{m}$  thick glass fiber was used,<sup>37</sup> which leads to a conversion factor of  $17.7 \pm 2.6 \text{ nN/V}$ .<sup>31</sup>

#### 4.2.9 X-ray Photoelectron Spectroscopy (XPS)

All modified surfaces, i.e. at each step of the modification sequence, were characterized by XPS using a JEOL JPS-9200 photoelectron spectrometer. XPS measurements were performed on  $1 \times 1 \text{ cm}^2$  samples at room temperature using an monochromatic Al  $K\alpha$  X-ray source ( $h\nu = 1486.7 \text{ eV}$ , 12 kV, 20 mA), analyzer pass energy of 10 eV, base pressure in the chamber  $< 3 \times 10^{-7}$  torr, and angle between sample and the detector (takeoff angle,  $\phi$ )  $80^\circ \pm 1^\circ$ . To facilitate peak assignment, XPS C1s spectra were also simulated using DFT electronic core level calculations according to previously reported procedure.<sup>34, 38</sup>

#### 4.2.10 Fourier Transform Infrared Reflection Absorption Spectroscopy (FT-IRRAS)

IRRA spectra of modified surfaces were measured using a Bruker Tensor 27 FT-IR spectrometer with a variable-angle reflection unit (Auto Seagull, Harrick Scientific), at room temperature under ambient conditions. A Harrick grid polarizer was installed in front of the detector and spectra was recorded with p-polarized (parallel) light with respect to the plane of incidence at the sample surface. The IRRAS data for all modified surfaces were obtained at an incident angle of  $68^\circ$  (2048 scans) and  $4 \text{ cm}^{-1}$  resolution. IRRAS data of unmodified and oxidized surfaces were used as reference surfaces, which were subtracted from the spectra of all the samples.

## 4.3 Results and Discussion

### 4.3.1 Silicon Surface Functionalization

Covalently bound alkyne-terminated monolayers on oxide-free Si(111) surfaces were prepared as reported previously.<sup>34</sup> Briefly, alkyne-terminated monolayers were obtained from the reaction of a H-terminated Si(111) surface with 1,15-hexadecadiyne at 80 °C for 16 h under an argon atmosphere, and displayed the expected C1s XPS spectrum and static water contact angle of  $87^\circ \pm 1^\circ$ .<sup>34</sup> The reacting alkyne moiety provides access to a densely packed monolayer and the strong Si-C bond (306 kJ/mol, compared to e.g., Si-O at 243 kJ/mol) mediates anchoring to the Si substrate and protects the Si surface from oxidation.<sup>39,40</sup> Here, especially the strong anchoring is necessary to enhance the tribological properties of modified surfaces.<sup>13</sup> Additionally, this dense monolayer allows the attachment of initiator with a high surface coverage, and this will yield densely grafted polymer brushes, with concomitantly lower adhesion and friction properties.<sup>41</sup> To achieve this, we used the TYC reaction – which yields a high surface coverage with up to two thiols bound per alkyne<sup>34</sup> as compared to other surface-bound reactions such as the thiol-ene click reaction – to couple alkyne-terminated monolayers **S1** with 2-mercaptoethanol to obtain hydroxyl-terminated monolayers. As a result, the static water contact angle dropped from  $87^\circ$  to  $38^\circ (\pm 1^\circ)$  (Table 1). The ellipsometric thickness of this OH-terminated monolayer (**S2**) was  $2.0 \pm 0.2$  nm, and the C1s XPS data could be properly deconvoluted into four peaks at 283.4, 285.0, 286.0 and 287.0 eV corresponding to Si-C, C-C, C-S and C-O, respectively (Figure 2A). On average 1.5 thiols were reacted with one terminal alkyne group, as calculated by comparing the theoretical and experimental (C-O)/(all other C atoms) area ratio in the XPS C1s narrow scan (Supporting Information Table SI-9). The experimentally obtained XPS C1s spectra were in good agreement with the simulated XPS spectrum using DFT calculations (Supporting Information, Figure SI-7, Table SI-1 and Table SI-2),<sup>34, 38</sup> which supports the assignment of the resulting coatings.

### 4.3.2 Initiator Immobilization

To obtain the initiator-terminated surfaces, 2-bromoisobutrylbromide was coupled to OH-terminated Si(111) substrate **S2**, yielding surface **S3** with a static water contact angle of  $73^\circ \pm 1^\circ$  and ellipsometric thickness increase from 2.0 nm to 2.4 nm ( $\pm 0.2$  nm). An XPS survey scan (Supporting Information, Figure SI-3A) shows the appearance of a new peak at 69 eV, corresponding to Br3d from the initiator. The XPS C1s narrow scan (Figure 2B) was deconvoluted into six peaks at 283.5, 285.0, 286.0, 286.5, 287.3 and 289.8 eV, which corresponds to Si-C, C-C, C-S, C-Br, C-O, and C=O, respectively. From the (C=O)/(all other carbon atoms) ratio, on average  $\sim 1.5$  initiator molecules were immobilized on the **S2** monolayer (Supporting Information, Table SI-9). XPS C1s binding

energies were in accordance with simulated XPS C1s spectra obtained by DFT calculations (Supporting Information, Figure SI-8, Table SI-3 and Table SI-4).

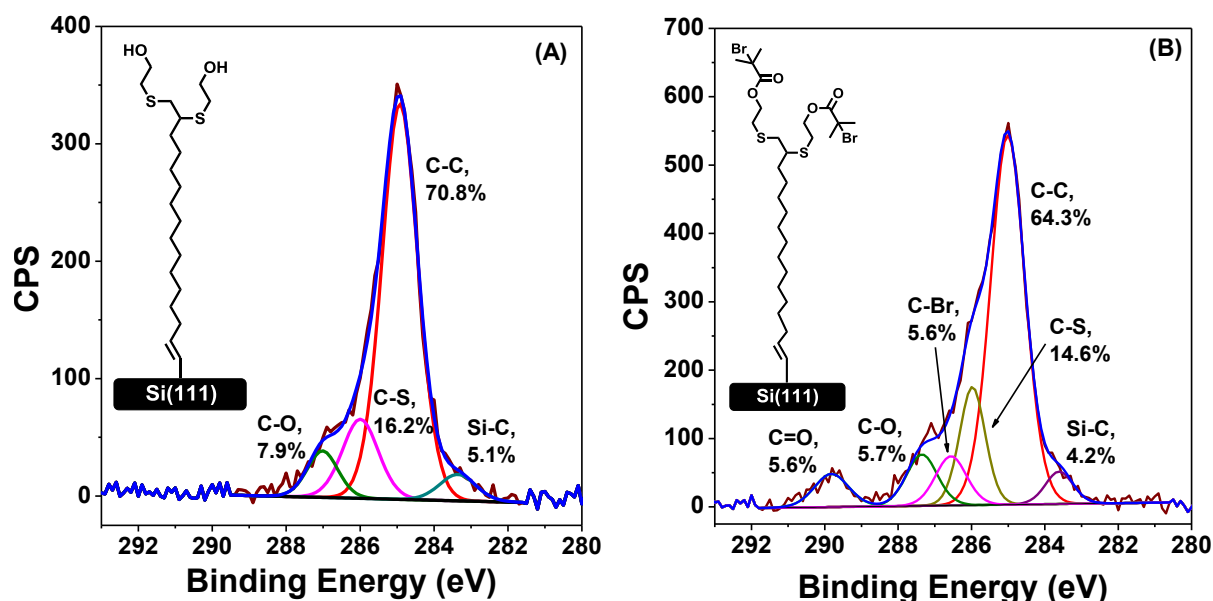


**Figure 2.** XPS C1s spectrum of (A) 2-mercaptoethanol-terminated surface S2 and (B)  $\alpha$ -bromoisobutryl bromide-immobilized surfaces S3.

**Table 1.** Static water contact angles of monolayers and polymer brushes on Si(111) surfaces.

Modified surfaces	Water static contact angle ( $^{\circ}$ )
S1	87 ( $\pm 1^{\circ}$ )
S2	38 $^{\circ}$ ( $\pm 1^{\circ}$ )
S3	73 $^{\circ}$ ( $\pm 1^{\circ}$ )
SPF0*	86 $^{\circ}$ ( $\pm 2^{\circ}$ )
SPF3*	98 $^{\circ}$ ( $\pm 2^{\circ}$ )

\*The CA would typically increase by  $1^{\circ}$  or  $2^{\circ}$  in case of polymer brushes upon increasing the thickness from 15 to  $>100$  nm.

### 4.3.3 Preparation of Poly(ethyl methacrylate) Brushes

Non-fluorinated **SPF0** brushes were prepared via SI-ATRP using ethyl methyl acrylate, CuBr, PMDETA and chlorobenzene as solvent at 90  $^{\circ}$ C. To obtain the different thickness of polymer brushes, the polymerization was carried out for various polymerization times in a custom-made reaction vessel to allow precise tuning of the polymerization times (Supporting Information for schematic diagram of vessel, Figure SI-1). The static water contact angle was  $86^{\circ} \pm 2^{\circ}$ . The thickness of dry polymer brushes was measured with ellipsometry (Figure 3). While overall the kinetics are nearly linear, the polymerization slows down in later stages due to inaccessible active polymerization sites or termination,

in line with the absence of either sacrificial initiator or deactivator [e.g. Cu(II)], which are typically used to control the polymerization rate.<sup>42</sup>

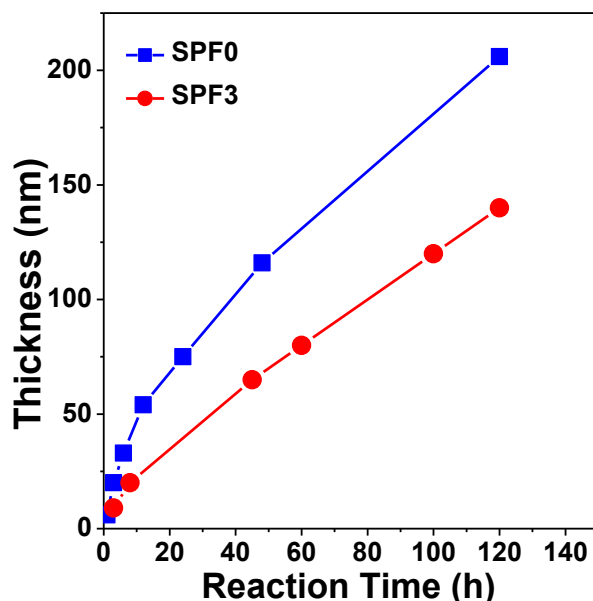


**Figure 3.** Development of the thickness of polymer brushes **SPF0** and **SPF3** as a function of reaction time (lines are merely a guide to the eye).

The IRRAS spectrum for **SPF0** brushes (Figure 4) shows the characteristic IR stretching of the carbonyl moiety at  $1739\text{ cm}^{-1}$ , and the C-H stretching vibrations between  $2800 - 3050\text{ cm}^{-1}$ . The intensity of IR peaks clearly increased with an increase in the thickness of the polymer brushes.

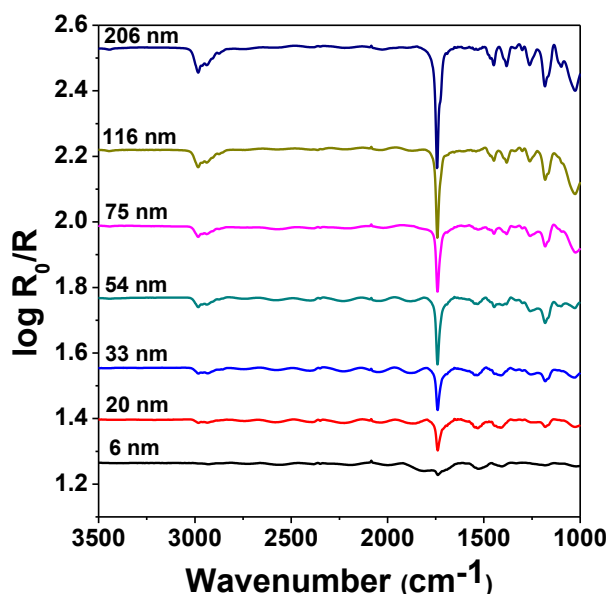


**Figure 4.** IRRAS of polymer brushes (**SPF0**) with varied thicknesses.

The composition of **SPF0** brushes was characterized using XPS. The C1s (285.0 eV) and O1s (532.0) peaks were evidently observed in the XPS survey scan (Figure 5A), displaying an atomic ratio of 3 : 1 for C/O, which matches with the theoretically expected



ratio. The XPS C1s narrow scan (Figure 5B) was deconvoluted into three peaks at 285.0, 286.4 and 288.7 eV, corresponding to  $\text{C-C}$ ,  $\text{C-O}$  and  $\text{C=O}$ , respectively. The atomic percentage under these peaks was 67.2%, 16.5% and 16.3%, respectively, which is in excellent agreement with the composition of a single monomer unit, namely 4:1:1. Additionally, the experimental C1s spectrum of **SPF0** brushes again correlates well with the simulated XPS spectrum using the DFT electronic core level calculations (Supporting Information, Figure SI-9, Table SI-5 and Table SI-6), showing that this approach is not just applicable to monolayers, but is also highly useful for the analysis of polymeric layers on a surface.

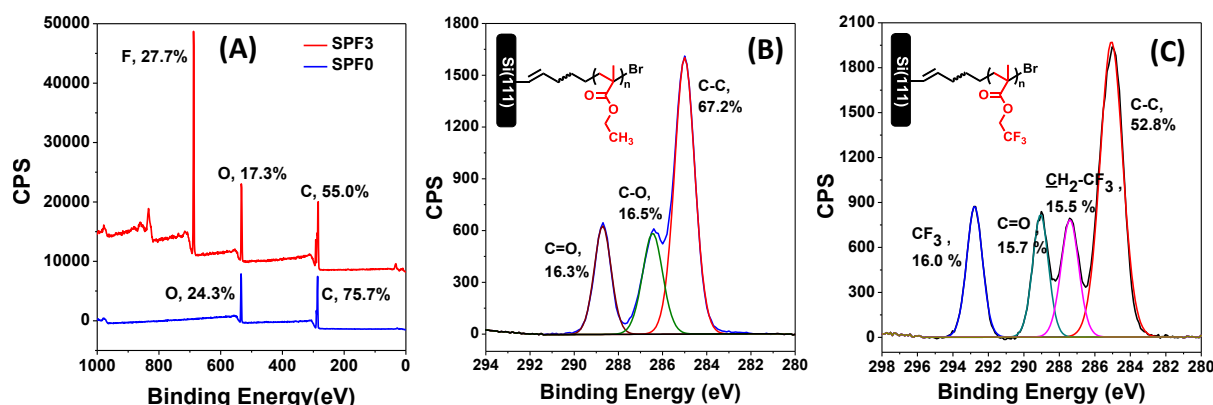


**Figure 5.** XPS survey scan (A) and C1s narrow scan spectra of **SPF0** (B) and **SPF3** (C).

#### 4.3.4 Preparation of Poly(2,2,2-trifluoroethyl methacrylate) Brushes

The **SPF3** brushes were analogously prepared via SI-ATRP using 2,2,2-trifluoroethyl methyl acrylate, CuBr, dNbpy and  $\alpha,\alpha,\alpha$ -trifluorotoluene (TFT) as solvent at 90 °C. Here, TFT was needed instead of chlorobenzene, as used for the synthesis of **SPF0**, due to solubility issues in chlorobenzene. At room temperature, in ambient air, the static water contact angle of the polymer layers was  $98^\circ \pm 2^\circ$ , which was higher than **SPF0** due to fluorine substitution in the brushes. Different polymer thicknesses were again obtained via tuning of the reaction time (Figure 3), and their near-linear growth again indicates controlled polymerization. Typically, after longer reaction times the polymerization slowed down, which is attributed to an increase in the deactivator concentration or loss of active chain ends, which, in turn, slows down the polymer brush growth.<sup>43</sup> Additionally, it seems that the growth of **SPF0** is faster than that of **SPF3**, but a direct comparison<sup>44</sup> is difficult due to the use of different ligands and solvents. The grafting density and molecular weight is given in Table 2. Similar to **SPF0**, the thinner **SPF3** brushes displayed a lower grafting density (0.09 chains/nm<sup>2</sup>; **SPF3** thickness = 9 nm) than thick ones (0.73 chains/nm<sup>2</sup>; **SPF3** thickness = 140 nm). The steady growth of the polymer thickness was further supported by IRRAS data (see Supporting Information, Figure SI-

6), which showed the increase in the intensity of characteristic IR peaks<sup>45</sup> upon prolonged reaction times.

The composition of **SPF3** brushes was characterized using XPS. The intensity of the C1s (285.0 eV), O1s (532.0 eV), and F1s (688.0 eV) peaks closely matches the theoretically expected 6:2:3 ratio (Figure 5A). In addition, deconvolution of the XPS C1s narrow scan (Figure 5C) yields four peaks, at 285.0 (C-C), 287.4 (CH<sub>2</sub>-CF<sub>3</sub>), 289.0 (C=O) and 292.7 eV (CF<sub>3</sub>), in an atomic percentage ratio of 52.8%, 15.5%, 15.7% and 16.0%, respectively, which matches the theoretically expected 3:1:1:1 ratio. The simulated XPS C1s spectrum for **SPF3** brushes mimics the experimentally obtained XPS spectrum (Supporting Information, Figure SI-10, Table SI-7 and Table SI-8) very well, confirming the assignment.

**Table 2.** The swelling ratio, grafting density (chains/nm<sup>2</sup>) and molecular weight (g/mol) as determined for **SPF0** and **SPF3** via swelling in acetone.

<b>SPF0</b>				<b>SPF3</b>			
Dry thickness $h_{dry}$ (nm)	Swelling ratio	Grafting density (chains/nm <sup>2</sup> ) <sup>a</sup>	Molecular weight (g/mol) <sup>b</sup>	Dry thickness $h_{dry}$ (nm)	Swelling ratio	Grafting density (chains/nm <sup>2</sup> ) <sup>a</sup>	Molecular weight (g/mol) <sup>b</sup>
6	4.42	0.16	25800	9	5.61	0.09	69000
20	3.32	0.28	48600	20	4.02	0.18	79000
33	2.73	0.41	54100	65	2.38	0.52	89500
54	2.33	0.56	64500	80	2.21	0.60	95500
75	2.17	0.64	78100	120	2.09	0.67	127000
116	2.03	0.74	105000	140	2.00	0.73	137000
206	1.92	0.82	167000				

<sup>a</sup> Estimated from equation (1) and <sup>b</sup> Estimated from equation (2) after determining polymer grafting density.

The grafting density of polymer brushes was determined via the swelling ratio of polymer brushes according to Malham et al.<sup>46</sup> using equation (1),

$$\alpha = \left(\frac{d}{a}\right)^{3-1/\nu} \quad (1)$$

where  $\alpha$  is swollen ratio ( $h_{swell} / h_{dry}$ ) of polymer brushes, acetone was used as good solvent to obtain swollen thickness,<sup>35</sup> the grafting density  $1/d^2$  was obtained using the average distance  $d$  between anchoring sites of neighboring polymer chains,  $a$  is the size of the monomer (EMA = 0.57 nm and TFEMA = 0.58 nm, as determined from their respective structures modeled as in a polymer backbone in ChemBio3D Ultra 13.0), while finally the exponent  $\nu$  was assumed to be  $\sim 1/2$  (theta solvent) for dense polymer brushes.<sup>46</sup>

Accordingly, using this grafting density we also determined the molecular weight ( $M_w$ ) of grafted polymer brushes following equation (2),

$$M_w = \frac{h_{dry}\rho N_A}{(1/d^2)} \quad (2)$$

where  $\rho$  = bulk density of the polymer (1.11 g/cm<sup>3</sup> for **SPF0** and 1.18 g/cm<sup>3</sup> for **SPF3**), and  $N_A$  = Avogadro's number.

The grafting density and molecular weight are given in Table 2. The highest grafting density of 0.82 chains/nm<sup>2</sup> was found for  $h_{dry}$  206 nm **SPF0**, and the lowest of 0.16 chains/nm<sup>2</sup> for  $h_{dry}$  6 nm **SPF0**, indicating polymer brushes were densely grafted and were in a stretched brush regime. This relatively high density of the polymer brushes is the result of the dense immobilization of the initiator via a TYC reaction, as it known that the initial initiator density is crucial for the maximum density of polymer brushes.<sup>47</sup> The grafting densities obtained here on polymer brushes were close to the graft densities obtained for analogous polymer brushes like PMMA<sup>35</sup> and PTFEMA.<sup>48</sup> However, the estimated graft densities in Table 2 are dependent on the value of exponent  $\nu$  in eq. 1, such that when e.g., a value of  $\nu = 3/5$  is used (assumption of semidilute brush),<sup>46</sup> the estimated grafting density would differ accordingly.

#### 4.3.5 Adhesion and Friction

To study the tribological properties of the **SPF0** and **SPF3** brushes, the adhesion and frictional forces were studied under various normal loads on the nN scale under ambient (RH = 44 ± 2%) and dry (RH < 5%) conditions. The adhesion and friction properties were analyzed using colloidal probe atomic force microscopy, as outlined in more detail elsewhere.<sup>31</sup>

#### 4.3.6 Adhesion

Figure 6A illustrates the adhesion of a silica probe particle to **SPF3** polymer brushes under ambient conditions. The brushes were compressed upon applying increasing normal loads under ambient conditions. At first, polymer brushes compress upon applied normal loads from 5 to 40 nN, which lead to a larger contact area between probe and polymer brushes, yielding increased adhesion forces.<sup>49, 50</sup> Further increase of the load (up to 150 nN) only marginally increases the adhesion, as further compression becomes increasingly difficult due to entropic penalties associated with increased crowding.<sup>50</sup> However, a reduced increase in adhesion was observed with an increase of the polymer thickness: at a normal load of 10 nN, the adhesion force for a 9 nm brush was 16.70 nN, while for a 140 nm brush this was only 9.75 nN (Figure 6A, inset). This has been related to the brush structure: at lower thicknesses, polymer brushes are less dense and disordered, while upon prolonged polymerization the brushes become increasingly dense and stretch out.<sup>17</sup> This higher graft density then leads to a reduced compressibility and lower adhesion.<sup>49</sup> In addition, the colloidal probe forms hydrogen bonds with hydrophilic functional groups such as the ester moiety, as these can get expose to the probe in horizontal alignments of parts of specifically thin polymer films. In thicker, more densely packed brushes (0.52 to 0.73 chains/nm<sup>2</sup>), the backbones are on average more perpendicular to the substrate and in

stretched conformation, and therefore such functional groups are not as much exposed to the probe.<sup>17, 51, 52</sup> Additionally, with increased thickness, the number of highly apolar  $-\text{CF}_3$  functional groups in the backbone of the brush increases, which may also diminish the H-bonding interactions. Finally, since the fluoro groups diminish the formation of a water meniscus in such AFM experiments, not much effect is observed upon decreasing the humidity from  $44 \pm 2\%$  to  $<5\%$ : the adhesion forces of **SPF3** coatings of various thicknesses are unaffected (Figure 6B).

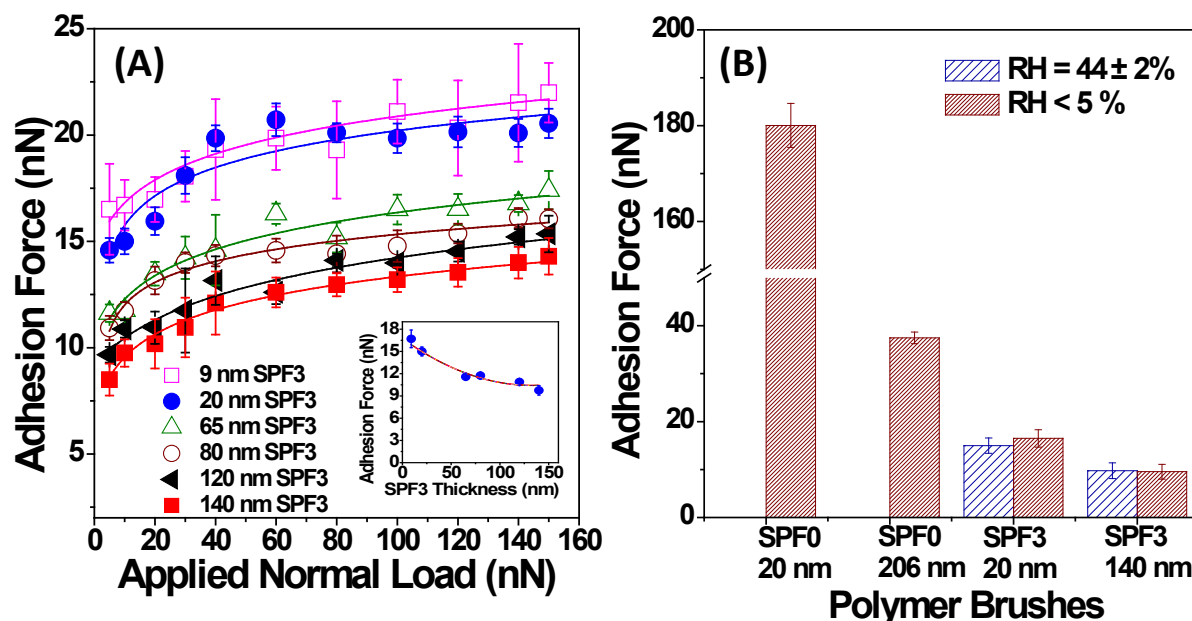


**Figure 6.** (A) Adhesion (pull-off) forces derived from force-distance curves following different applied normal loads (5 to 150 nN) on a colloidal silica probe, and in inset at constant applied normal load 10 nN on **SPF3** with different thicknesses (lines are guide to the eye). (B) Thickness-dependent adhesion forces at constant applied normal load 10 nN on **SPF0** and **SPF3** at various relative humidities ( $\text{RH} = 44 \pm 2\%$  or  $< 5\%$ ).

In contrast, for the non-fluoro polymer brushes **SPF0** the analogous adhesion forces were simply too high to measure in our set-up under ambient conditions: when the probe was brought near **SPF0** brushes, it was strongly attracted towards the polymer brushes and could not be pulled away from the polymer brushes due to the low spring constant of the AFM tip, which limits the pull of force. This is attributed to the water meniscus that forms between the colloidal probe and the surface under the experimentally used relative humidity of  $44 \pm 2\%$ .<sup>53, 54</sup> Similar polymers like poly(methyl methacrylate) PMMA are susceptible to such environmental effects ( $\text{RH} > 30\%$ ) and tend to show a higher adhesion under humid conditions.<sup>52, 55</sup> Under dry conditions ( $\text{RH} < 5\%$ ) this water meniscus effect is clearly diminished, and adhesion forces of 180 nN and 37 nN could be obtained for **SPF0** of 20 nm and 206 nm, respectively. In comparison with **SPF3**, the **SPF0** surfaces display a much larger thickness dependence, as the lower polarizability of  $-\text{CF}_3$  groups compared to  $-\text{CH}_3$  groups diminishes the meniscus effect.<sup>28, 31</sup>

### 4.3.7 Friction

The lateral friction forces were measured against a non-modified silica probe on both **SPF0** and **SPF3** polymer brushes under ambient conditions ( $RH = 44 \pm 2\%$ ) by applying normal loads ranging from 10 to 90 nN at a scan rate of 0.5 Hz. The lateral friction forces obtained for **SPF3** as a function of the applied load are presented in Figure 7, together with the friction coefficients derived from the slope of such a linear plot for a range of thicknesses. The lateral friction for **SPF3** brushes shows a linear increase with an increase in applied load (Figure 7A), analogous to the adhesion measurements on **SPF3** brushes (Figure 6A), as dynamic molecular bonding/debonding events occur. Similarly, the friction decreased with increasing the **SPF3** thickness, which was attributed to the increased density and reduced interaction with the hydrophilic silica probe. These observations are coherent with results obtained by Casoli et al., who concluded that higher external stresses are necessary to attain lateral movement in long chain polymer brushes, due to the solid-like behavior of longer polymer brushes.<sup>56</sup>

A lowest friction coefficient of 0.0057 was obtained for 140 nm **SPF3** brushes under ambient conditions (Figure 7B), which is among the lowest friction coefficient obtained on polymer brushes without a solvent. Far more frequently, friction forces of polymer brushes are studied in solvents, which add an additional lubricant to the system. This situation is, however, of limited relevance for MEMS/NEMS applications. A nice exception is a study by Landherr et al., who studied friction forces of polydimethylsiloxane brushes against a polystyrene bead ( $RH = 35\%$  to  $40\%$ ), and observed a lowest friction coefficient of 0.0024. It is difficult to directly compare this with our measurements, as in that study polystyrene beads were used, which have a low interaction with PDMS brushes, as well as with a humid environment.<sup>17,57</sup>

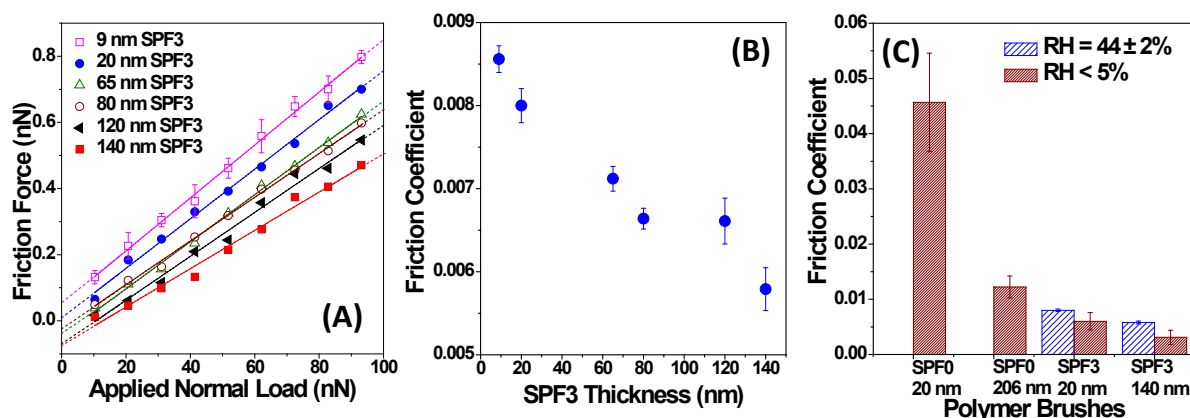


**Figure 7.** Friction of SPF0 and SPF3 coatings under dry ( $RH < 5\%$ ) and ambient ( $RH = 44 \pm 2\%$ ) conditions. (A) Lateral friction force for SPF3 as a function of the applied normal load;  $RH = 44 \pm 2\%$ . [The error bars represent the typical standard deviations in the mean friction force of three independent measurements.] (B) Friction coefficient for SPF3 of various thicknesses as derived from the slopes in (A); (C) Thickness dependence of the friction coefficient against a colloidal silica probe on SPF0 and SPF3 films under different humidity conditions ( $RH = 44 \pm 2\%$  or  $< 5\%$ ).

This humidity effect is indeed borne out by measurements under dry conditions ( $RH < 5\%$ ) (Figure 7C), which yield a friction coefficient down to values as low as 0.0031 for 140 nm **SPF3** brushes, and confirm the effect of the water meniscus.<sup>58</sup>

In case of the non-fluoro **SPF0** brushes with  $RH = 44 \pm 2\%$ , the friction pair (i.e. colloidal probe and polymer brushes) remains in a stick state, due to the high adhesion associated with these **SPF0** brushes. As a result, the friction force obtained here has only limited significance,<sup>53</sup> but is obviously much higher than for **SPF3**. Under dry conditions ( $RH < 5\%$ ), the friction can be properly studied, and shows that – analogous to **SPF3** coating – the friction coefficient goes down with increasing film thickness but remains 4 – 10 times (for **SPF0** at 206 nm 0.0122, and at 20 nm 0.0456) as high as for **SPF3** (Figure 7C). Additionally, the molecular bonding-debonding mechanism operative under dry conditions mainly depends on interfacial properties such as functional groups and capillary forces and relatively weak Van der Waals forces. Under humid conditions the polymer brushes show a high friction due to strong Van der Waals interactions and hydrogen bonding in the contact with moisture, resulting in strong interactions of the polymer brushes with the colloidal probe.<sup>59</sup> As an additional effect, the crystallinity increases with increasing grafting density of polymer brushes, which minimizes the friction due to enhanced oscillatory stick-slip dynamics effects<sup>60</sup> and bonding-debonding events, as is observed for both **SPF0** and **SPF3**.

With such ultralow adhesion and friction properties under ambient conditions, covalently bound fluoropolymer brushes will be an alternative to non-covalently bound PTFE-like coatings as are typically used in MEMS/NEMS. The covalently bound fluorinated coatings involve more deposition steps, but will be stronger than non-covalent coatings. Fluorination of covalently bound polymer films can therefore be used for a substantial decrease in adhesion and friction forces, and continues to be studied in our laboratories.

#### 4.4 Conclusions

Covalently bound fluoro and non-fluoro polymer brushes with varying thickness and high graft density ( $\sim 0.1$  to  $0.8$  chains/nm<sup>2</sup>) were grown by surface-initiated ATRP on silicon surfaces. High-grafting density films could be obtained via the efficient attachment of an ATRP initiator by thiol-yne click chemistry. AFM-based tribology studies with a colloidal probe show that especially the fluorinated polymer brushes, which contain a CF<sub>3</sub> moiety in each monomer, yield very low adhesion forces (down to 9.75 nN at 10 nN applied normal load for 140 nm polymer films) and friction coefficients (0.0057 and 0.0031, for ambient ( $RH = 44 \pm 2\%$ ) and dry ( $RH < 5\%$ ) conditions, respectively). Our data clearly indicate the importance of thickness, grafting density and meniscus effects in adhesion and friction behavior under ambient conditions, especially in non-fluoro polymer

brushes and point to the high potential of high-density fluorinated polymer brushes as ‘solid-state’ lubricants for MEMS/NEMS and applications.

#### 4.5 References

1. Advincula, R. C.; Brittain, W. J.; Caster, K. C.; R  he, J., *Polymer Brushes: Synthesis, Characterization, Applications*. Wiley-VCH Verlag GmbH & Co. KGaA: Weinheim, **2005**.
2. Banerjee, I.; Pangule, R. C.; Kane, R. S., Antifouling coatings: Recent developments in the design of surfaces that prevent fouling by proteins, bacteria, and marine organisms. *Adv. Mater.* **2011**, 23, (6), 690-718.
3. Dai, S.; Ravi, P.; Tam, K. C., Thermo- and photo-responsive polymeric systems. *Soft Matter* **2009**, 5, (13), 2513-2533.
4. Stuart, M. A. C.; Huck, W. T. S.; Genzer, J.; Muller, M.; Ober, C.; Stamm, M.; Sukhorukov, G. B.; Szleifer, I.; Tsukruk, V. V.; Urban, M.; Winnik, F.; Zauscher, S.; Luzinov, I.; Minko, S., Emerging applications of stimuli-responsive polymer materials. *Nat. Mater.* **2010**, 9, (2), 101-113.
5. Toomey, R.; Tirrell, M., Functional polymer brushes in aqueous media from self-assembled and surface-initiated polymers. *Annu. Rev. Phys. Chem.* **2008**, 59, 493-517.
6. Zhou, F.; Huck, W. T. S., Surface grafted polymer brushes as ideal building blocks for "smart" surfaces. *PCCP* **2006**, 8, (33), 3815-3823.
7. Hoy, O.; Zdyrko, B.; Lupitsky, R.; Sheparovych, R.; Aulich, D.; Wang, J. F.; Bittrich, E.; Eichhorn, K. J.; Uhlmann, P.; Hinrichs, K.; Muller, M.; Stamm, M.; Minko, S.; Luzinov, I., Synthetic Hydrophilic Materials with Tunable Strength and a Range of Hydrophobic Interactions. *Adv. Funct. Mater.* **2010**, 20, (14), 2240-2247.
8. Qiang-bing, W.; Cai, M. R.; Zhou, F., Progress on surface grafted polymer brushes for biomimetic lubrication. *Acta Polym. Sin.* **2012**, (10), 1102-1107.
9. Cabane, E.; Zhang, X.; Langowska, K.; Palivan, C. G.; Meier, W., Stimuli-responsive polymers and their applications in nanomedicine. *Biointerphases* **2012**, 7, (1-4), 9.
10. Senaratne, W.; Andruzzi, L.; Ober, C. K., Self-assembled monolayers and polymer brushes in biotechnology: Current applications and future perspectives. *Biomacromolecules* **2005**, 6, (5), 2427-2448.
11. Tagliazucchi, M.; Szleifer, I., Stimuli-responsive polymers grafted to nanopores and other nano-curved surfaces: Structure, chemical equilibrium and transport. *Soft Matter* **2012**, 8, (28), 7292-7305.
12. Minko, S., Grafting on Solid Surfaces: “Grafting to” and “Grafting from” Methods. In *Polymer Surfaces and Interfaces*, Stamm, M., Ed. Springer Berlin Heidelberg: **2008**; pp 215-234.
13. Sakata, H.; Kobayashi, M.; Otsuka, H.; Takahara, A., Tribological properties of poly(methyl methacrylate) brushes prepared by surface-initiated atom transfer radical polymerization. *Polym. J.* **2005**, 37, (10), 767-775.
14. Tranchida, D.; Sperotto, E.; Chateauminois, A.; Schoenherr, H., Entropic Effects on the Mechanical Behavior of Dry Polymer Brushes During Nanoindentation by Atomic Force Microscopy. *Macromolecules* **2011**, 44, (2), 368-374.
15. Nomura, A.; Okayasu, K.; Ohno, K.; Fukuda, T.; Tsujii, Y., Lubrication Mechanism of Concentrated Polymer Brushes in Solvents: Effect of Solvent Quality and Thereby Swelling State. *Macromolecules* **2011**, 44, (12), 5013-5019.
16. Granick, S.; Binder, K.; Gennes, P. G.; Giannelis, E. P.; Grest, G. S.; Hervet, H.; Krishnamoorti, R.; L  ger, L.; Manias, E.; Rapha  l, E.; Wang, S. Q.; L  ger, L.; Rapha  l, E.; Hervet, H., Surface-Anchored Polymer Chains: Their Role in Adhesion

- and Friction. In *Polymers in Confined Environments*, Springer Berlin Heidelberg: **1999**; Vol. 138, pp 185-225.
17. Landherr, L. J. T.; Cohen, C.; Agarwal, P.; Archer, L. A., Interfacial Friction and Adhesion of Polymer Brushes. *Langmuir* **2011**, 27, (15), 9387-9395.
  18. McNamee, C. E.; Yamamoto, S.; Higashitani, K., Preparation and characterization of pure and mixed monolayers of poly(ethylene glycol) brushes chemically adsorbed to silica surfaces. *Langmuir* **2007**, 23, (8), 4389-4399.
  19. Pintauer, T.; Matyjaszewski, K., Atom Transfer Radical Polymerization (ATRP) and Addition (ATRA) and Applications. In *Encyclopedia of Radicals in Chemistry, Biology and Materials*, John Wiley & Sons, Ltd: **2012**.
  20. Gurbuz, N.; Demirci, S.; Yavuz, S.; Caykara, T., Synthesis of cationic N-[3-(dimethylamino)propyl]methacrylamide brushes on silicon wafer via surface-initiated RAFT polymerization. *J. Polym. Sci., Part A: Polym. Chem.* **2011**, 49, (2), 423-431.
  21. Barbey, R.; Lavanant, L.; Paripovic, D.; Schuwer, N.; Sugnaux, C.; Tugulu, S.; Klok, H. A., Polymer Brushes via Surface-Initiated Controlled Radical Polymerization: Synthesis, Characterization, Properties, and Applications. *Chem. Rev.* **2009**, 109, (11), 5437-5527.
  22. Krause, J. E.; Brault, N. D.; Li, Y.; Xue, H.; Zhou, Y.; Jiang, S., Photoiniferter-Mediated Polymerization of Zwitterionic Carboxybetaine Monomers for Low-Fouling and Functionalizable Surface Coatings. *Macromolecules* **2011**, 44, (23), 9213-9220.
  23. Gualandi, C.; Vo, C. D.; Focarete, M. L.; Scandola, M.; Pollicino, A.; Di Silvestro, G.; Tirelli, N., Advantages of Surface-Initiated ATRP (SI-ATRP) for the Functionalization of Electrospun Materials. *Macromol. Rapid Commun.* **2013**, 34, (1), 51-56.
  24. Fristrup, C. J.; Jankova, K.; Hvilsted, S., Surface-initiated atom transfer radical polymerization-a technique to develop biofunctional coatings. *Soft Matter* **2009**, 5, (23), 4623-4634.
  25. Matyjaszewski, K., Atom Transfer Radical Polymerization (ATRP): Current Status and Future Perspectives. *Macromolecules* **2012**, 45, (10), 4015-4039.
  26. Bielecki, R. M.; Benetti, E. M.; Kumar, D.; Spencer, N. D., Lubrication with Oil-Compatible Polymer Brushes. *Tribol. Lett.* **2012**, 45, (3), 477-487.
  27. Kyomoto, M.; Moro, T.; Saiga, K.; Hashimoto, M.; Ito, H.; Kawaguchi, H.; Takatori, Y.; Ishihara, K., Biomimetic hydration lubrication with various polyelectrolyte layers on cross-linked polyethylene orthopedic bearing materials. *Biomaterials* **2012**, 33, (18), 4451-4459.
  28. Palacio, M.; Bhushan, B., Ultrathin Wear-Resistant Ionic Liquid Films for Novel MEMS/NEMS Applications. *Adv. Mater.* **2008**, 20, (6), 1194-1198.
  29. Biswas, S. K.; Vijayan, K., Friction and wear of PTFE — a review. *Wear* **1992**, 158, (1-2), 193-211.
  30. Sun, C.; Zhou, F.; Shi, L.; Yu, B.; Gao, P.; Zhang, J.; Liu, W., Tribological properties of chemically bonded polyimide films on silicon with polyglycidyl methacrylate brush as adhesive layer. *Appl. Surf. Sci.* **2006**, 253, (4), 1729-1735.
  31. Pujari, S. P.; Spruijt, E.; Stuart, M. A. C.; van Rijn, C. J. M.; Paulusse, J. M. J.; Zuilhof, H., Ultralow Adhesion and Friction of Fluoro-Hydro Alkyne-Derived Self-Assembled Monolayers on H-Terminated Si(111). *Langmuir* **2012**, 28, (51), 17690-17700.
  32. Pujari, S. P.; Scheres, L.; Weidner, T.; Baio, J. E.; Stuart, M. A. C.; Van Rijn, C. J. M.; Zuilhof, H., Covalently attached organic monolayers onto silicon carbide from 1-alkynes: Molecular structure and tribological properties. *Langmuir* **2013**, 29, (12), 4019-4031.



33. Pujari, S. P.; Yan, L.; Regeling, R.; Zuilhof, H., Tribology and Stability of Organic Monolayers on CrN: A Comparison among Silane, Phosphonate, Alkene, and Alkyne Chemistries. *Langmuir* **2013**, 29, (33), 10405-10415.
34. Bhairamadgi, N. S.; Gangarapu, S.; Caipa Campos, M. A.; Paulusse, J. M. J.; van Rijn, C. J. M.; Zuilhof, H., Efficient Functionalization of Oxide-Free Silicon(111) Surfaces: Thiol-yne versus Thiol-ene Click Chemistry. *Langmuir* **2013**, 29, (14), 4535-4542.
35. Moh, L. C. H.; Losego, M. D.; Braun, P. V., Solvent Quality Effects on Scaling Behavior of Poly(methyl methacrylate) Brushes in the Moderate- and High-Density Regimes. *Langmuir* **2011**, 27, (7), 3698-3702.
36. Hutter, J. L.; Bechhoefer, J., Calibration of atomic-force microscope tips. *Rev. Sci. Instrum.* **1993**, 64, (7), 1868-1873.
37. Liu, W. H.; Bonin, K.; Guthold, M., Easy and direct method for calibrating atomic force microscopy lateral force measurements. *Rev. Sci. Instrum.* **2007**, 78, (6), 063707.
38. Giesbers, M.; Marcelis, A. T. M.; Zuilhof, H., Simulation of XPS C1s Spectra of Organic Monolayers by Quantum Chemical Methods. *Langmuir* **2013**, 29, (15), 4782-4788.
39. Scheres, L.; Giesbers, M.; Zuilhof, H., Organic Monolayers onto Oxide-Free Silicon with Improved Surface Coverage: Alkynes versus Alkenes. *Langmuir* **2010**, 26, (7), 4790-4795.
40. Pujari, S. P.; Zuilhof, H., Highly wear-resistant ultra-thin per-fluorinated organic monolayers on silicon(111) surfaces. *Appl. Surf. Sci.* **2013**, 287, 159-164.
41. Yamamoto, S.; Ejaz, M.; Tsujii, Y.; Fukuda, T., Surface Interaction Forces of Well-Defined, High-Density Polymer Brushes Studied by Atomic Force Microscopy. 2. Effect of Graft Density. *Macromolecules* **2000**, 33, (15), 5608-5612.
42. Matyjaszewski, K.; Miller, P. J.; Shukla, N.; Immaraporn, B.; Gelman, A.; Luokala, B. B.; Siciolvan, T. M.; Kickelbick, G.; Vallant, T.; Hoffmann, H.; Pakula, T., Polymers at Interfaces: Using Atom Transfer Radical Polymerization in the Controlled Growth of Homopolymers and Block Copolymers from Silicon Surfaces in the Absence of Untethered Sacrificial Initiator. *Macromolecules* **1999**, 32, (26), 8716-8724.
43. He, G. P.; Zhang, G. W.; Hu, J. W.; Sun, J. P.; Hu, S. Y.; Li, Y. H.; Liu, F.; Xiao, D. S.; Zou, H. L.; Liu, G. J., Low-fluorinated homopolymer from heterogeneous ATRP of 2,2,2-trifluoroethyl methacrylate mediated by copper complex with nitrogen-based ligand. *J. Fluorine Chem.* **2011**, 132, (9), 562-572.
44. Qiu, J.; Matyjaszewski, K., Polymerization of substituted styrenes by atom transfer radical polymerization. *Macromolecules* **1997**, 30, (19), 5643-5648.
45. Liu, X.; Chen, J.; Sun, P.; Liu, Z.-W.; Liu, Z.-T., Grafting modification of ramie fibers with poly(2,2,2-trifluoroethyl methacrylate) via reversible addition-fragmentation chain transfer (RAFT) polymerization in supercritical carbon dioxide. *React. Funct. Polym.* **2010**, 70, (12), 972-979.
46. Malham, I. B.; Bureau, L., Density Effects on Collapse, Compression, and Adhesion of Thermoresponsive Polymer Brushes. *Langmuir* **2009**, 26, (7), 4762-4768.
47. Jones, D. M.; Brown, A. A.; Huck, W. T. S., Surface-Initiated Polymerizations in Aqueous Media: Effect of Initiator Density. *Langmuir* **2002**, 18, (4), 1265-1269.
48. Chen, R.; Feng, W.; Zhu, S.; Botton, G.; Ong, B.; Wu, Y., Surface-initiated atom transfer radical polymerization grafting of poly(2,2,2-trifluoroethyl methacrylate) from flat silicon wafer surfaces. *J. Polym. Sci., Part A: Polym. Chem.* **2006**, 44, (3), 1252-1262.
49. Yamamoto, S.; Ejaz, M.; Tsujii, Y.; Matsumoto, M.; Fukuda, T., Surface Interaction Forces of Well-Defined, High-Density Polymer Brushes Studied by Atomic Force Microscopy. 1. Effect of Chain Length. *Macromolecules* **2000**, 33, (15), 5602-5607.

50. Coad, B. R.; Lu, Y.; Glattauer, V.; Meagher, L., Substrate-Independent Method for Growing and Modulating the Density of Polymer Brushes from Surfaces by ATRP. *ACS Appl. Mater. Interfaces* **2012**, 4, (5), 2811-2823.
51. Li, L.; Li, J.; Lukehart, C. M., Graphitic carbon nanofiber-poly(acrylate) polymer brushes as gas sensors. *Sens. Actuator B-Chem.* **2008**, 130, (2), 783-788.
52. Lee, W.-J.; Chang, J.-G.; Ju, S.-P., Hydrogen-bond structure at the interfaces between water/poly(methyl methacrylate), water/poly(methacrylic acid), and water/poly(2-aminoethylmethacrylamide). *Langmuir* **2010**, 26, (15), 12640–12647.
53. Yu, J.; Chen, L.; Qian, L.; Song, D.; Cai, Y., Investigation of humidity-dependent nanotribology behaviors of Si(100)/SiO<sub>2</sub> pair moving from stick to slip. *Appl. Surf. Sci.* **2013**, 265, 192-200.
54. Wei, Z.; Zhao, Y.-P., Growth of liquid bridge in AFM. *J. Phys. D: Appl. Phys.* **2007**, 40, (14), 4368-4375.
55. Lancaster, J. K., A review of the influence of environmental humidity and water on friction, lubrication and wear. *Tribol. Int.* **1990**, 23, (6), 371-389.
56. Casoli, A.; Brendlé, M.; Schultz, J.; Auroy, P.; Reiter, G., Friction Induced by Grafted Polymeric Chains. *Langmuir* **2000**, 17, (2), 388-398.
57. Vyas, M. K.; Schneider, K.; Nandan, B.; Stamm, M., Switching of friction by binary polymer brushes. *Soft Matter* **2008**, 4, (5), 1024-1032.
58. Bhushan, B.; Burton, Z., Adhesion and friction properties of polymers in microfluidic devices. *Nanotechnology* **2005**, 16, (4), 467-478.
59. Deng, Z.; Smolyanitsky, A.; Li, Q.; Feng, X.-Q.; Cannara, R. J., Adhesion-dependent negative friction coefficient on chemically modified graphite at the nanoscale. *Nat. Mater.* **2012**, 11, (12), 1032-1037.
60. Dong, Y.; Li, Q.; Martini, A., Molecular dynamics simulation of atomic friction: A review and guide. *J. Vac. Sci. Technol., A* **2013**, 31, 030801.



# Chapter 5

---

## Adhesion and Friction Properties of Fluoropolymer Brushes: On the Tribological Inertness of Fluorine

### Abstract

The effects of fluorination on the adhesion and friction properties of covalently bound poly(fluoroalkyl methacrylate) polymer brushes (thickness  $\sim 80$  nm) were systematically investigated. Si(111) surfaces were functionalized with a covalently bound initiator via a thiol-yne click reaction to have a high surface coverage for initiator immobilization. Surface-initiated atom-transfer radical polymerization (SI-ATRP) was employed for the synthesis of four different fluoropolymer brushes (SPF $x$ , where  $x = 0, 3, 7$  or  $17$  F atoms per monomer), based on fluoroalkyl methacrylates. All polymer brushes were characterized with static contact angle measurements, X-ray photoelectron spectroscopy (XPS), and infrared absorption reflection spectroscopy (IRRAS). The polymer brushes exhibited an excellent hydrophobicity, with static water contact angles of up to  $121^\circ$  depending on the number of fluorine atoms per side chain in fluoroalkyl methacrylate. The degree of swelling was precisely studied by using ellipsometry in different solvents such as acetone, hexadecane, hexafluoroisopropanol, nonafluorobutyl methyl ether and Fluorinert<sup>®</sup> FC-40. The polymer brushes have shown nano-scale swelling behavior in all solvents except hexadecane. The grafting density decreased upon increasing fluorine content in polymer brushes from  $0.65$  chains/nm<sup>2</sup> (SPF0) to  $0.10$  chains/nm<sup>2</sup> (SPF17) as observed in Fluorinert<sup>®</sup> FC-40 as a good solvent. Adhesion and friction force measurements were conducted with silica colloidal probe atomic force microscopy (CP-AFM) under ambient, dry (argon) and lubricating fluid conditions. SPF17 showed the lowest coefficient of friction  $0.005$  under ambient condition ( $RH = 44 \pm 2\%$ ) and a further decrease with  $50\%$  under fluidic conditions. These polymer brushes also showed adhesion forces as low as  $6.900$  nN under ambient conditions, which further went down to  $0.003$  nN under fluidic conditions (Fluorinert<sup>®</sup> FC-40 and hexadecane) at  $10$  nN force.

## Contents

<b>5. Adhesion and Friction Properties of Fluoropolymer Brushes: On the Tribological Inertness of Fluorine .....</b>	<b>83</b>
Abstract.....	83
5.1 Introduction .....	85
5.2 Experimental Methods .....	86
5.2.1 Materials.....	86
5.2.2 Surface Functionalization and Initiator Immobilization.....	87
5.3 Preparation of Polymer Brushes.....	87
5.3.1 Poly(2,2,3,3,4,4,4-heptafluorobutyl methacrylate) Brushes (SPF7) .....	87
5.3.2 Poly(2-perfluorooctylethyl methacrylate) Brushes (SPF17) .....	88
5.3.3 Surface Characterization .....	88
5.3.4 Adhesion and Friction Measurements .....	89
5.4 Results and Discussion.....	89
5.4.1 Preparation and Characterization of Polymer Brushes.....	89
5.4.2 Adhesion and Friction .....	94
5.4.3 Adhesion .....	94
5.4.4 Friction .....	96
5.5 Conclusions .....	98
5.6 References .....	99

This chapter is submitted for publication as:

*'Adhesion and Friction Properties of Fluoropolymer Brushes: On the Tribological Inertness of Fluorine'*  
Bhairamadgi, N. S.; Pujari, S. P.; van Rijn, C. J. M.; Zuilhof, H. *Langmuir* **2014**, submitted.

## 5.1 Introduction

Fluorine-containing materials are well recognized due to their outstanding properties such as optical clarity, water repellence, resistance to weather influences, thermal and chemical resistance, flame retardation, non-adhesive, low friction, etc.<sup>1</sup> Therefore they are used for a wide range of applications, including coatings,<sup>2</sup> energy storage devices,<sup>3</sup> artificial joints,<sup>4</sup> pharmaceuticals,<sup>5, 6</sup> agrochemicals,<sup>7</sup> nonfouling materials<sup>8</sup> and a wide range of polymer-based materials.<sup>1, 9</sup> This potential of fluorinated materials is mainly enabled by the unique properties of C-F bonds, specifically the high binding energy and low polarizability, which are also crucial to obtain chemically resistant, low-dielectric constant materials to be used as low-friction coatings.<sup>10, 11</sup>

Fluorinated polymers are emerging as solid lubricants, and frequently used as fillers in many composites due to their low friction coefficients.<sup>12, 13</sup> Furthermore, fluoropolymers like polytetrafluoroethylene (PTFE) are widely used in micro/nano-electromechanical systems (MEMS/NEMS) as low-friction and anti-stiction coatings to improve the device performance.<sup>14, 15</sup> These coatings are generally obtained via chemical vapor deposition (CVD), spin coating or spray coatings.<sup>16</sup> The coatings obtained via these methods are, however, mechanically unstable and display limited resistance to wear during device operation.<sup>17</sup> The wear resistance can be improved by the use of covalently bound polymers or self-assembled monolayers.<sup>18</sup> Recently, our group has achieved ultralow friction and adhesion, combined with a high wear resistance, on covalently bound fluorinated monolayers on Si(111), SiC and CrN surfaces.<sup>19-22</sup> For example, a friction coefficient against a colloidal SiO<sub>2</sub> probe, without solvent, of only 0.012 was obtained on perfluoroalkyl (F<sub>17</sub>) monolayers on Si(111).<sup>19</sup> To investigate whether it would be possible to further improve these tribological properties, these studies were extended towards covalently bound polymeric systems. Using thiol-yne click chemistry to induce a high density of the surface-coupled initiator,<sup>23</sup> surface-initiated atom transfer radical polymerization (SI-ATRP) yielded a series (9 – 200 nm thickness) of densely grafted and well-defined trifluoro (**SPF3**) and non-fluoropolymer (**SPF0**) brushes on Si(111).<sup>23</sup> Apart from decreasing friction and adhesion forces with increasing brush thickness, we found a threefold reduction in the friction coefficient on 140 nm **SPF3** compared to the already very low friction coefficient of a perfluoroalkyl (F<sub>17</sub>) monolayer on Si(111) under ambient conditions (air, relative humidity RH = 44%). In contrast, the non-fluoropolymer brush showed a high adhesion, because of water meniscus effects under ambient conditions. This adhesion strongly reduces under dry conditions (RH ≤ 5%), but remained ~3 to ~8 times higher than on **SPF3**.

This significant effect of fluorination brought up the question whether a further decrease of the adhesion and friction forces could be observed upon further increased fluorination. Honda et al. studied the effect of fluorination on molecular aggregation of thin spin-casted films by varying the fluoroalkyl side chain length (n = 1 - 10) using wide-angle X-ray

diffraction. They observed ordered and crystallized films with increasing fluoroalkyl side chain length ( $n > 8$ ),<sup>24</sup> and this crystallinity can lower the friction and improve the wear resistance due to an increased hardness and elastic modulus of the polymer.<sup>25,26</sup> This suggested that further fluorination might influence the adhesion and friction properties of the polymer brushes.

Here we investigate the tribological properties of covalently bound fluoropolymer brushes with increasing fluoroalkyl side chain length (**SPF<sub>x</sub>** where  $x = 0, 3, 7$ , and  $17$ ; Figure 1) at a constant brush thickness ( $\sim 80$  nm). The fluoropolymer brushes were grown on Si(111) surfaces via a “grafting from” approach using SI-ATRP. The tribological properties of these polymer brushes were analyzed by adhesion and friction force measurements using colloidal probe atomic microscopy (CP-AFM) under ambient ( $RH = 44 \pm 2\%$ ) and dry ( $RH < 5\%$ ) conditions, and with and without the use of any external lubricants. The resulting data provide evidence for the potential of fluorination of polymer brushes to optimize the tribology of surface-bound materials.

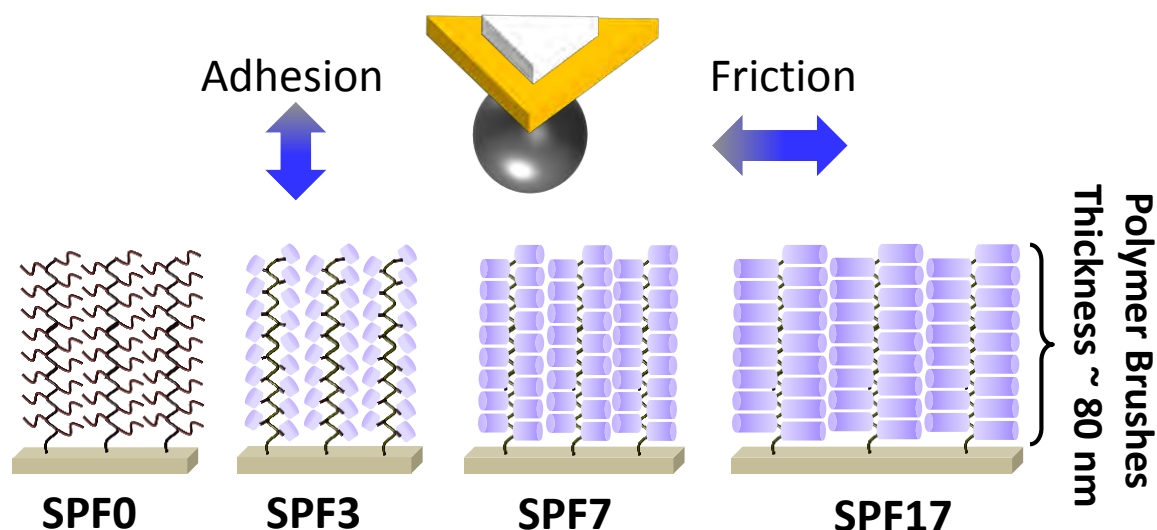


**Figure 1.** Schematic representation of covalently bound fluorinated polymer brushes at constant thickness ( $\sim 80$  nm) but with varying fluorine content to study the effects of fluorination in polymer on the adhesion and friction properties.

## 5.2 Experimental Methods

### 5.2.1 Materials

1,15-Hexadecadiyne was synthesized following previously reported procedure.<sup>23, 27</sup>  $\alpha,\alpha,\alpha$ -trifluorotoluene (TFT), dichloromethane (DCM), chlorobenzene, tetrahydrofuran (THF), mercaptoethanol, acetone (semiconductor grade VLSI PURANAL™), hexafluoroisopropanol (HFP), nonafluorobutyl methyl ether (NFE)  $\alpha$ -bromoisobutyryl bromide, 2,2-dimethoxy-2-phenylacetophenone (DMPA), N,N,N',N'',N'''-

pentamethyldiethylenetriamine (PMDETA), 4,4'-dinonyl-2,2'-bipyridine (dNbpy),  $\alpha$ -bromoisobutyryl bromide, copper(I) bromide (Cu(I)Br), ethyl methacrylate (EMA), 2,2,2-trifluoroethyl methacrylate (TFEMA), 2,2,3,3,4,4,4-heptafluorobutyl methacrylate (HFMA) and 2-perfluorooctylethyl methacrylate (FOEMA) were purchased from Sigma-Aldrich and used without further purification unless otherwise specified. DCM and THF were distilled before use. The inhibitors from monomers EMA, TFEMA, HFMA and FOEMA were removed by passing through a basic alumina column.

### 5.2.2 Surface Functionalization and Initiator Immobilization

The surface functionalization and initiator immobilization was performed as per the procedure reported previously.<sup>23, 27</sup> Briefly, one side polished Si(111) wafers (n-type, 475-550  $\mu\text{m}$  thick, resistivity 1.0 - 5.0  $\Omega\text{ cm}$ , Siltronix, France) were cut into  $1 \times 1\text{ cm}^2$  pieces, etched with 40%  $\text{NH}_4\text{F}$  to obtain oxide-free hydrogen-terminated Si(111) surfaces, and reacted with 1,15-hexadecadiyne at 80  $^\circ\text{C}$  for 16 h to yield alkyne-terminated monolayers (**S1**).<sup>27</sup> These surfaces were further functionalized via a photochemical thiol-yne click (TYC) reaction with 2-mercaptoethanol to obtain hydroxyl-terminated surfaces (**S2**), and reacted with  $\alpha$ -bromoisobutyryl bromide to obtain initiator-terminated Si(111) surfaces (**S3**), with properties as reported before.<sup>23</sup> Generically the procedure is as illustrated in Figure 2.

### 5.3 Preparation of Polymer Brushes

The poly(ethyl methacrylate) brushes (**SPF0**) and poly(2,2,2-trifluoroethyl methacrylate) brushes (**SPF3**) were prepared according to previously reported procedures.<sup>23</sup>

#### 5.3.1 Poly(2,2,3,3,4,4,4-heptafluorobutyl methacrylate) Brushes (SPF7)

A 50 mL Schlenk flask containing an initiator-immobilized surface (**S3**) and CuBr (50.0 mg, 0.35 mmol) was subsequently evacuated and backfilled with argon (3 times), and subsequently kept under an argon atmosphere. In another Schlenk flask, equipped with a magnetic stirring bar, monomer HFMA (7 mL, 17.5 mmol) was placed together with the ligand dNbpy (172 mg, 0.42 mmol) and 10 mL of TFT as solvent, and argon was bubbled through under stirring for at least 1 h. Subsequently, the content was cannulated to the Schlenk flask containing **S3** and CuBr. The Schlenk flask containing the reaction mixture and the initiator-terminated surfaces (**S3**) was slowly shaken on auto-shaker to homogenize the reaction mixture. The polymerization was initiated by heating to 110  $^\circ\text{C}$  for 72 h. The polymerization was terminated by exposing the reaction mixture to air and cooling the reaction mixture to room temperature. The substrates were removed from the reaction mixture and cleaned with TFT and sonicated in TFT for 15 min to remove any traces of physisorbed reaction components. Finally, the resulting modified polymer



surfaces (**SPF7**) were rinsed with TFT and THF, vacuum dried at room temperature at least for 8 h before further characterization.

### 5.3.2 Poly(2-perfluorooctylethyl methacrylate) Brushes (**SPF17**)

Poly(2-perfluorooctyl)ethyl methacrylate brushes were prepared analogously to **SPF7**. The polymerization was carried out on initiator-immobilized S3 surfaces in the presence of CuBr (50.0 mg, 0.35 mmol), monomer FOEMA (5.8 mL, 17.5 mmol) and the ligand dNbpy (147 mg, 0.36 mmol). Modified surfaces (**SPF17**) were cleaned with Fluorinert® FC-40 (Sigma-Aldrich) and sonicated for 15 min in the same solvent. Finally rinsed with TFT and THF and dried under vacuum for at least 8 h.

### 5.3.3 Surface Characterization

A Krüss DSA 100 goniometer was used for to measure the static water contact angle on at least six different places on a modified surface, by dispensing 3.0  $\mu\text{L}$  droplets of deionized water, hexadecane and Fluorinert® FC-40 with the help of an automated drop dispenser. The Tangent 2 fitting model was implemented for triplicate contact angle measurements (thus:  $6 \times 3$ ) with the accuracy of  $\pm 1^\circ$ . A Bruker Tensor 27 FT-IR spectrometer was used to obtain infrared reflection absorption spectra (IRRAS) of polymer brushes, at an incident angle of  $68^\circ$  (2048 scans) and  $4\text{ cm}^{-1}$  resolution. The IRRAS of piranha-treated unmodified Si(111) surface was used as reference and was subtracted from the IRRA spectra of modified surfaces. The thicknesses of polymer brushes were measured using a Sentech Instruments type SE-400 ellipsometer. An incident angle of  $70^\circ$  and the He-Ne laser source at 632.8 nm was used. The optical constants ( $n = 3.821$  and  $k = 0.057$ ) were determined using freshly etched  $1 \times 1\text{ cm}^2$  H-Si(111) surfaces. The obtained thicknesses were an average of six measurements at six different places, and yielded a typical deviation of ca. 5%. The swollen thickness of polymer brushes was measured using ellipsometry in different solvents such as Acetone (Refractive Index = 1.35), HFP (RI = 1.27), NFE (RI = 1.3) and FC-40 (RI = 1.29) in a custom-made liquid cell, having  $70^\circ$  sloped windows following a literature procedure.<sup>23, 28</sup> A JEOL JPS-9200 X-ray photoelectron spectroscopy (XPS) was utilized to monitor changes in the chemical composition during each step of the modification. The XPS data were obtained at room temperature using monochromatic Al  $K\alpha$  X-ray source ( $h\nu = 1486.7\text{ eV}$ , 12 kV, 20 mA) and an analyzer pass energy of 10 eV. The base pressure in the chamber  $< 3 \times 10^{-7}$  Torr was maintained during measurements. The obtained XPS C1s spectra were correlated with simulated core levels of C1s spectra using density functional theory (DFT) as reported previously.<sup>27, 29</sup>

### 5.3.4 Adhesion and Friction Measurements

The adhesion and friction measurements were performed using an Asylum Research MFP-3D atomic force microscope (AFM), under ambient conditions (Relative Humidity =  $44 \pm 2\%$ ), dry conditions ( $RH < 5\%$ ), and in solvents such as hexadecane and FC-40 at room temperature. The measurements under controlled humidity were performed in a closed fluid cell (Asylum Research). The humidity was controlled in a closed fluid cell with continuous flow (1 mL/min) of dry argon (instead of the liquid that is typically used in such devices). Similarly, for measurements in solvents, the same fluid cell was used and instead of argon, the cell was filled with the solvent under study. A detailed description of the adhesion and friction measurement setup has been reported elsewhere.<sup>19, 23</sup> Under all three conditions the adhesion and friction measurements were performed using spherical silica colloidal probes. These colloidal probes were prepared by attaching spherical silica particles (radius = 3.0  $\mu\text{m}$ , rms roughness value of  $6.83 \pm 2.06$  nm) to triangular silicon nitride cantilevers (Bruker probes, NP-B, spring constant between 0.10 and 0.16 N/m for all measurements, to allow comparative measurements) using Norland optical adhesive 61, and cured by exposure to UV light (365 nm). The colloidal probes were cleaned with ethanol and air plasma for 5 min before use.

The adhesion forces were measured at three different locations and minimum 200 force curves were obtained at each place. The scan range 5.0  $\mu\text{m}$  with scan rate of 0.5 Hz was used for measurements under all three conditions. The normal spring constant was determined using the Hutter and Bechhoefer method for each cantilever.<sup>30</sup> The calibration of the obtained spring constant was performed using the deflection sensitivity of the supported cantilever, and the overall error was estimated to be  $\sim 10\%$ .<sup>19</sup> The friction forces were measured using lateral force images of  $20 \times 20 \mu\text{m}^2$  under variable loads ( $F_N = 10 - 95$  nN). A constant speed of 5  $\mu\text{m/s}$  at a  $90^\circ$  angle to the cantilevers long axis was used for obtaining lateral friction forces. Following Liu et al.,<sup>31</sup> the average lateral force ( $[\mu_{\text{trace}} - \mu_{\text{retrace}}]/2$ , in V) signals were transformed into friction forces. The cantilevers were calibrated using conversion factor  $17.7 \pm 2.6$  nN/V, which was obtained by bending 8.9  $\mu\text{m}$  thick glass fiber.<sup>19</sup>

## 5.4 Results and Discussion

### 5.4.1 Preparation and Characterization of Polymer Brushes.

Polymer brushes with various fluorine content and a thickness of ca. 80 nm were prepared on Si(111) surfaces, according to the scheme given in Figure 2. First, Si(111) surfaces were functionalized with 1,15-hexadecadiyne to obtain alkyne-terminated surfaces (S1). These were further functionalized via a TYC reaction with mercaptoethanol to obtain a high surface coverage of covalently bound hydroxyl-terminated surfaces.<sup>27</sup> The resultant hydroxyl-terminated surfaces (S2) were treated with  $\alpha$ -bromoisobutyryl bromide

to obtain initiator-functionalized surfaces (**S3**) according to previously reported methods.<sup>23</sup> Using these **S3** surfaces in a SI-ATRP reaction in combination with the indicated methyl acrylate derivatives yielded the non-fluoropolymer surface **SPF0**, and the three fluorinated polymer brush surfaces **SPF3**, **SPF7** and **SPF17**, which have 3, 7 and 17 fluorine atoms per monomer, respectively. The preparation and characterization of non-fluoropolymer (**SPF0**) and fluoropolymer (**SPF3**) have been described previously.<sup>23</sup> A dry film thickness of ~80 nm as measured with ellipsometry was achieved by stopping the polymerization after a specific reaction time (Table 1). The roughness of polymer brushes was between 0.8 to 1.8 nm, indicating the uniform growth of polymer brushes (Table 1, whereas topography images are shown in Supporting Information Figure SI-1).<sup>32</sup>

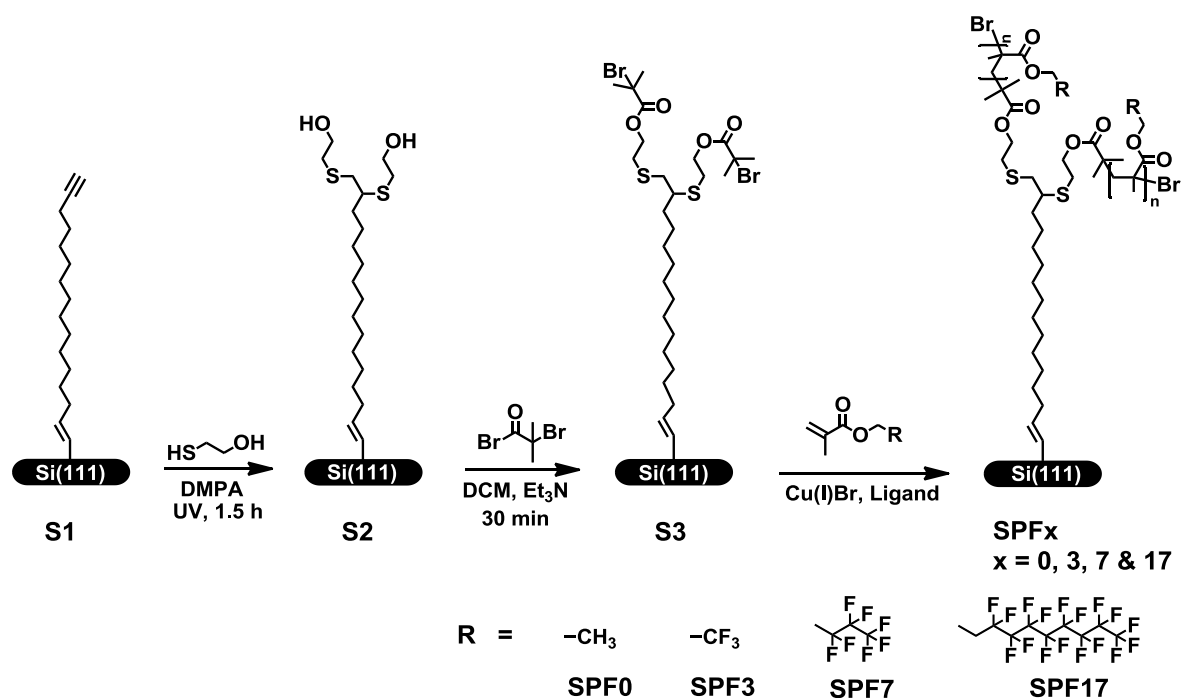


**Figure 2.** Schematic representation of the preparation of the polymer brushes.

The **SPF7** and **SPF17** surface were prepared using 2,2,3,3,4,4,4-heptafluorobutyl methacrylate (HFMA) and 3,3,4,4,5,5,6,6,7,7,8,8,9,9,10,10,10-heptafluorodecyl methacrylate (FOEMA), respectively (see Experimental Section), and a thickness of the polymer brushes of ca. 80 nm was obtained by adjusting the polymerization time. In general, the longer/more fluorinated materials yield a somewhat slower polymerization.<sup>33-35</sup> The static water (surface tension = 72 mN/m) contact angle was observed to increase with fluorine content in polymer brushes, from 88° on **SPF0** to 121° on **SPF17** (Table 1). This enhanced hydrophobicity by the relatively rigid fluoroalkyl side ( $\text{C}_8\text{F}_{17}$ ) chains might be due to the formation of a perpendicular orientation of the fluoroalkyl side chains in polymer brushes relative to the substrate ( $-\text{CF}_3$  outer side). Takahara and co-workers reported that  $\text{C}_8\text{F}_{17}$  chains form a hexagonally packed structure due to the low surface free

energy, in which these side chains were oriented almost perpendicular to the substrate to afford a lamellar structure.<sup>35</sup>

In addition, the contact angles were also measured in hexadecane (HD) (surface tension = 27 mN/m) and perfluorinated liquids FC-40 (surface tension = 17.1 mN/m). With an increased fluorine content,  $\theta_{\text{HD}}$  increases from  $<10^\circ$  (**SPF0**), via  $50^\circ$  (**SPF3**) to  $71^\circ$  (**SPF17**) (Table 1). The fluoropolymer brushes **SPF3**, **SPF7** and **SPF17** completely wetted in FC-40, whereas **SPF0** showed static contact angle of  $< 20^\circ$ . These contact angles indicate that HD and FC-40 are good lubricating fluids for the polymer brushes under study.

The IRRA spectra of the polymer brushes (Figure 3A) show peaks between 2818 - 3070  $\text{cm}^{-1}$  that can be assigned to the aliphatic CH and  $\text{CH}_2$  stretching vibrations, whereas the intense peak at  $\sim 1751 \text{ cm}^{-1}$  corresponds to the C=O moiety from ester carbonyl groups. Characteristic C-F peaks for fluoropolymers **SPF3**, **SPF7** and **SPF17** were observed between 1094 - 1382  $\text{cm}^{-1}$ . Additionally, the elemental compositions of all four polymer brushes were further verified by XPS survey scans, as shown in Figure 3B. In the XPS survey scan of non-fluoro **SPF0**, two peaks were detected at 285.0 eV (C1s) and 532.0 eV (O1s), in a percentage ratio 75:25, which matches the expected carbon to oxygen ratio per monomeric unit in EMA. Similarly, three peaks at 285.0, 532.0 and 589.0 eV for C1s, O1s and F1s, respectively, are observed in fluoropolymer brushes **SPF3**, **SPF7** and **SPF17**. The experimentally determined elemental composition is given in Supporting Information Table SI-1 and matches the expected elemental composition in all three fluoropolymer brushes. The XPS chemical shifts for all polymer brushes was further studied with C1s narrow scans, and is illustrated in Figure 4. The XPS C1s spectrum for **SPF0** and **SPF3** have been reported previously.<sup>23</sup>

**Table 1.** Static ( $\theta$ ) contact angle measured on polymer brushes using polar and non-polar solvents, ellipsometric thickness, and AFM-determined surface roughness of dry polymer brushes.

Polymer Brushes	Thickness (nm)	Reaction time (h)	$\theta_{\text{H}_2\text{O}}$ ( $^\circ$ )	$\theta_{\text{HD}}$ ( $^\circ$ )	$\theta_{\text{FC-40}}$ ( $^\circ$ )	RMS (nm)
<b>SPF0</b>	75	24	88	-	$< 20$	0.8
<b>SPF3</b>	80	60	98	50	-	0.7
<b>SPF7</b>	78	72	110	66	-	0.6
<b>SPF17</b>	80	96	121	71	-	1.8

The XPS C1s narrow scan of **SPF7** (Figure 4A) can be deconvoluted in five peaks at 285.0, 287.2, 288.9, 290.9 and 293.4 eV, corresponding to  $\text{CH}_2\text{-}\underline{\text{C}}\text{H-CH}_3$ ,  $\underline{\text{C}}\text{H}_2\text{-CF}_2$ ,  $\underline{\text{C}}=\text{O}$ ,  $\underline{\text{C}}\text{F}_2$  and  $\underline{\text{C}}\text{F}_3$ , respectively. The experimental ratio of the deconvoluted C1s XPS peaks under these peaks were 3.3:0.9:1.1:0.9, which closely matches the 3:1:1:2:1 ratio

expected from the monomeric unit of **SPF7** brushes. Analogously, the XPS C1s spectrum of **SPF17** was also deconvoluted; here seven peaks could be discerned corresponding to carbons having different chemical environments (Figure 4B): 285.0 eV ( $\text{CH}_3\text{-CH}_2\text{-CH}_2$ ), 286.9 eV ( $\text{CH}_2\text{-O}$ ), 285.8 eV ( $\text{CH}_2\text{-CF}_2$ ), 288.5 eV ( $\text{C=O}$ ), 289.6 eV ( $\text{-CF}_2\text{-CF}_2\text{-CH}_2\text{-}$ ), 291.1 eV ( $\text{CF}_2$ ) and 293.3 eV ( $\text{CF}_3$ ). The experimental percentage area under these deconvoluted peaks again closely corresponds to the expected ratio of different carbons in a single monomeric unit of **SPF17** brushes. The experimental XPS C1s spectral assignments were in good agreements with simulated core levels of C1s spectra (Supporting Information Table SI-1 and Figure SI-2).<sup>29</sup>

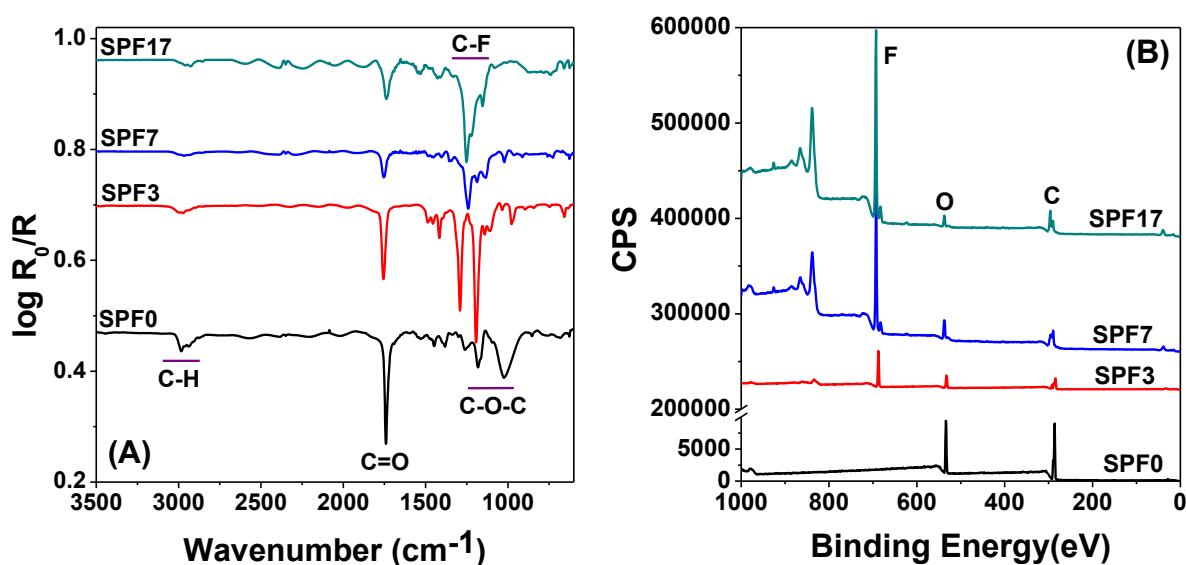


Figure 3. IRRA spectra (A) and (B) XPS survey scan of **SPF0**, **SPF3**, **SPF7** and **SPF17** polymer brushes.

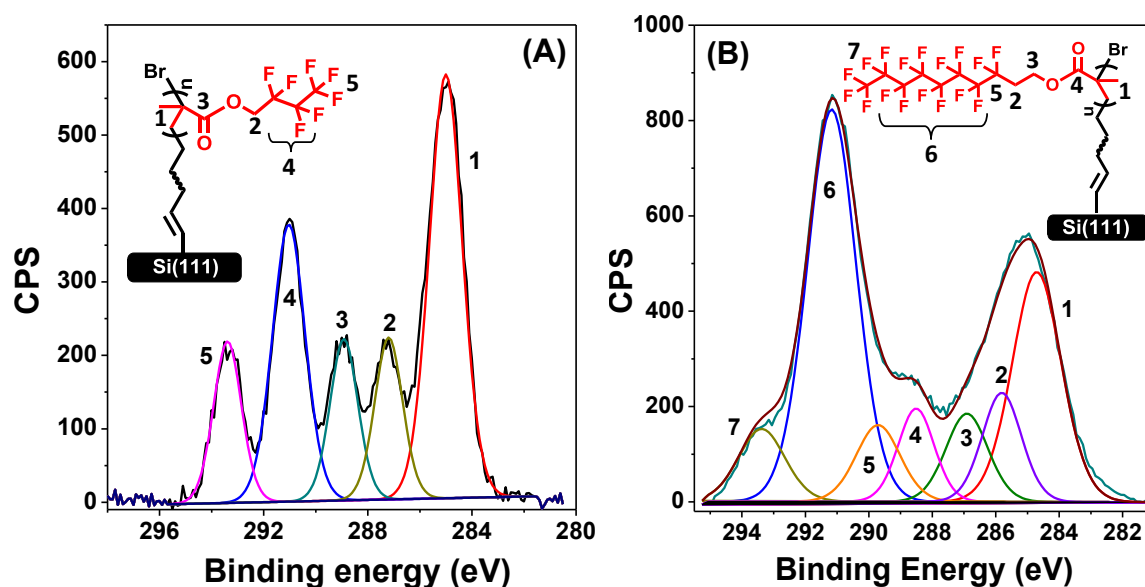


Figure 4. The XPS C1s spectra of **SPF7** (A) and **SPF17** (B) polymer brushes.

The grafting density of polymer brushes was determined according to Malham et al.<sup>36</sup> using Equation 1. The grafting density that is obtained using this method is derived from the observed swelling of polymer brushes in good solvents; therefore we used different solvents (acetone, HFP, NFE and FC-40) to obtain the grafting density, and from there the molecular weight (Equation 2).

$$\alpha = \left(\frac{d}{a}\right)^{3-1/\nu} \quad (1)$$

where,  $\alpha$  = swollen ratio ( $h_{\text{swell}} / h_{\text{dry}}$ , where  $h$  = polymer layer thickness (in nm) measured with ellipsometry) of polymer brushes in different solvents,  $1/d^2$  = grafting density, with an average distance  $d$  between tethered points of neighboring polymer chains,  $a$  = monomer size (EMA = 0.57 nm, TFEMA = 0.58 nm, HFMA = 0.76 nm, and FOEMA = 1.58 nm, obtained from their respective modeled structures as in a polymer backbone in ChemBio3D Ultra 13.0), while finally the exponent  $\nu$  was assumed to be 1/2 for theta solvent-behavior for densely grafted polymer brushes, according to Malhan et al.<sup>36</sup> The molecular weight ( $M_w$ ) of polymer brushes was determined using the grafting density of grafted polymer brushes from Equation (2):

$$M_w = \frac{h_{\text{dry}} \rho N_A}{(1/d^2)} \quad (2)$$

where  $\rho$  = bulk density of the polymer (1.11 g/cm<sup>3</sup> for **SPF0**, 1.18 g/cm<sup>3</sup> for **SPF3**, 1.34 g/cm<sup>3</sup> and 1.60 g/cm<sup>3</sup> for **SPF17**), and  $N_A$  = Avogadro's number.

The resulting grafting density and molecular weight of the **SPFx** polymer brushes under study is given in Table 2. A grafting density of  $\sim 0.50$  to  $\sim 0.70$  chains/nm<sup>2</sup> was observed for **SPF0** and **SPF3** in all four solvents. The grafting density decreased from 0.20 – 0.50 chains/nm<sup>2</sup> for **SPF7** to 0.10 – 0.20 chains/nm<sup>2</sup> for **SPF17** upon increasing the size and number of fluorine atoms in the fluoroalkyl side chain of polymer brushes. The polymer brushes with a smaller number of fluorine atoms (**SPF0** and **SPF3**) were swollen equally ( $\alpha = 2.2$  to 2.4) in all four solvents, so that the corresponding molecular weight can be obtained as the average of the molecular weights obtained in differed solvents, to be  $81 \times 10^3$  g/mol for **SPF0** and  $88 \times 10^3$  g/mol for **SPF3**, respectively. In contrast, polymer brushes with more highly fluorinated side chains showed a clear solvent-dependent swelling ( $\alpha = 1.36$  to 2.56), due to the difference in solvation of the fluoroalkyl chains by the various solvents. This thus yields different grafting densities for **SPF7** and **SPF17**, as derived from the swelling data obtained in different solvents, and correspondingly different molecular weights (Table 2). All polymer brushes swelled more in HFP compared than in FC-40; in hexadecane no swelling was observed. This swelling is, apart from the grafting density, dependent on the diffusion of solvent through polymer chains, the solvent-side chain interaction, which relates strongly to the number of fluorine atoms per solvent molecule.

**Table 2.** The swelling ratio, grafting density (chains/nm<sup>2</sup>) and molecular weight (g/mol) as determined for polymer brushes by swelling in different solvents.

Polymer brushes	Solvents	Swelling ratio ( $\alpha$ )	Grafting density (chains/nm <sup>2</sup> ) <sup>a</sup>	Molecular weight (g/mol) <sup>b</sup>
<b>SPF0</b>	Acetone	2.17	0.64	78000
	HFP	2.40	0.53	94000
	NFE	2.13	0.68	74000
	FC-40	2.17	0.65	77000
<b>SPF3</b>	Acetone	2.21	0.60	95000
	HFP	2.29	0.57	100000
	NFE	2.15	0.64	74000
	FC-40	2.08	0.69	83000
<b>SPF7</b>	Acetone	1.78	0.55	115000
	HFP	2.56	0.26	246000
	NFE	2.00	0.43	149000
	FC-40	2.99	0.19	330000
<b>SPF17</b>	Acetone	1.36	0.22	360000
	HFP	2.44	0.07	1140000
	NFE	2.16	0.09	890000
	FC-40	2.04	0.10	800000

<sup>a</sup> Estimated from Equation 1; <sup>b</sup> Estimated from Equation (2) after determining polymer grafting density.

### 5.4.2 Adhesion and Friction

The adhesion and friction properties of non-fluoro (**SPF0**) and fluoropolymer (**SPF3**) brushes with varying thickness under ambient (RH = 44 ± 2%) and dry (RH < 5 %) conditions were reported earlier.<sup>23</sup> We observed that adhesion and friction properties of polymer brushes were thickness dependent. Additionally, it was also found that especially the non-fluoropolymers were susceptible to environmental conditions, i.e. a substantially increased adhesion under humid conditions (RH = 44 ± 2% rather than < 5%). Contrary to this, there was no significant effect of the humidity on the adhesion and friction properties of fluoropolymer (**SPF3**) brushes. Here we study the effect of the increasing number of fluorine atoms in polymer brushes with constant thickness on their adhesion and friction properties under dry and ambient conditions. Additionally, to know their responses in solvents, we also studied adhesion and friction properties of these polymer brushes in hexadecane and Fluorinert<sup>®</sup> FC-40.

### 5.4.3 Adhesion

Figure 5 represents the adhesion forces on polymer brushes **SPF0**, **SPF3**, **SPF7** and **SPF17** with increasing normal loads from 5 nN to 150 nN under dry, ambient and solvents conditions (adhesion forces on the non-fluoropolymer brushes **SPF0** were only

obtained only under dry conditions ( $RH < 5\%$ ) due to the high adhesion associated with the meniscus effect between probe and surface). Three features are remarkable here. First, the adhesion of especially the **SPF17** surface is very low (all data after application of 10 nN applied load): 6.890 nN under ambient conditions, down to 0.049 nN in hexadecane and – in our set up – not measurably different from zero in the fluorinated solvent FC-40:  $0.003 \pm 0.007$  nN. As the number all go up gradually with less fluorination (see Figure 5D for an overview), this is attributed to what can be labelled as the tribological inertness of F atoms.

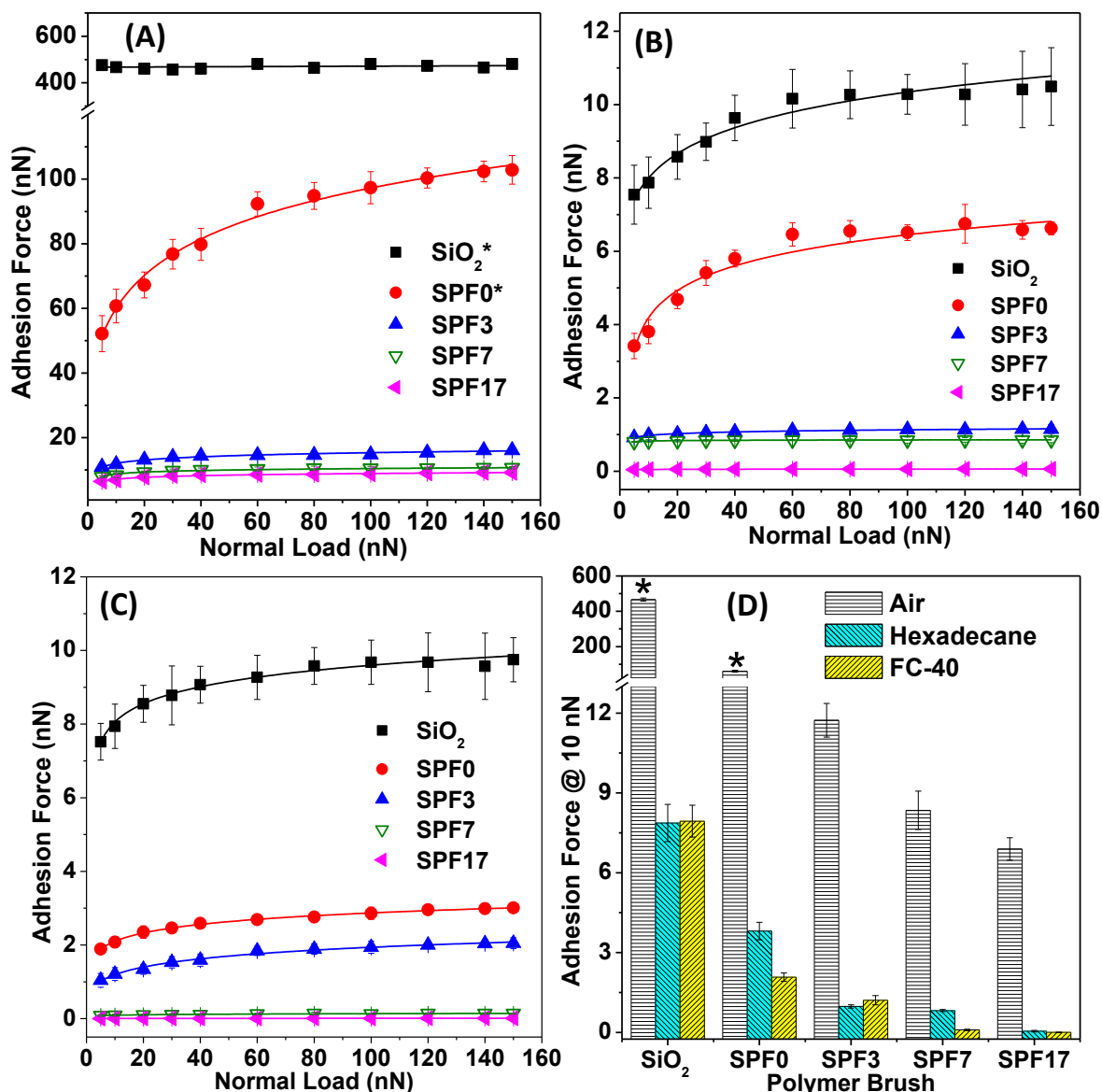


**Figure 5.** Adhesion (pull-off) forces at various applied normal load (5 nN to 150 nN) obtained on polymer brushes under (A) ambient ( $RH = 44 \pm 2\%$ ) \*dry ( $RH < 5\%$ ), (B) hexadecane, (C) FC-40 and (D) the adhesion forces obtained at 10 nN applied normal load.

Second, with increasing fluorination, the effects of increased normal loads seems to disappear: for **SPF0** the adhesion forces are not only much larger, but also increasing the



applied normal load from 5 to 150 nN roughly doubles the subsequently measured adhesion force, irrespective of whether this is measured under ambient conditions or in hexadecane or FC-40. However, for **SPF7** and especially **SPF17** such an effect of increased normal loads is nearly absent. Apparently, for **SPF0** the higher applied load increases the contact area between the colloidal tip and the polymer surface up to a maximum, thereby increasing the adhesion force.<sup>23,37</sup> This effect is nearly absent upon increased fluorination, which we attribute to the near-crystallinity of the side chains in especially the F<sub>17</sub> polymer, which is related to the low flexibility of perfluorinated side chains in dense polymer brushes.<sup>24</sup> For the bulk polymethacrylate with C<sub>8</sub>F<sub>17</sub> side chains a melting point of 348 K has been observed, whereas neither the CF<sub>3</sub> and C<sub>3</sub>F<sub>7</sub> side chain bulk polymer show only a glass transition temperature (CF<sub>3</sub>: T<sub>g</sub> = 259 K, C<sub>3</sub>F<sub>7</sub>: T<sub>g</sub> = 249 K), nor does crystallization occur for the analogous bulk polymer with C<sub>8</sub>H<sub>17</sub> side chains (T<sub>g</sub> = 221 K). In addition, it is known that the polymer brushes are spatially constrained, which leads to higher a T<sub>g</sub> or T<sub>m</sub> than for free polymers,<sup>38, 39</sup> which substantiates crystallinity for **SPF17** at room temperature. A similar correlation of adhesion with T<sub>g</sub> has also been observed by Spencer and co-workers for non-fluoropolymer brushes with increasing alkyl chain side chain (C<sub>6</sub>H<sub>14</sub>, C<sub>12</sub>H<sub>26</sub> and C<sub>18</sub>H<sub>38</sub>) in methacrylates.<sup>40</sup> Finally, even though the side chains in **SPF3** and **SPF7** are not expected to be crystalline, they nevertheless display a low adhesion compared to **SPF0**. This can be attributed to the diminished flexibility of also short fluoroalkyl side chains in fluoropolymer brushes.<sup>24</sup>

Third, significant medium effects are observed. In air, the humidity has a significant effect on non-fluorinated brushes, but the humidity plays hardly any role anymore upon fluorination. In fact, whereas the adhesion forces in air for **SPF3** were already the lowest measured for any flat surface when reported in 2013,<sup>23</sup> for **SPF17** a further reduction of 40% was observed, down to 6.890 nN. The reduction to near-zero values in the fluorinated solvent FC-40 indicates that the adhesion can be truly minimized given the right solvent. It is known that in good solvents, the polymer brushes swell and stretch out from substrates, causing them to experience lower forces than the actual applied normal loads.<sup>41</sup> Clearly FC-40 is a good solvent for these fluorinated brushes, and significantly better than the non-fluorinated analogue hexadecane. However, for most practical purposes the ambient adhesion data are probably more useful.

#### 5.4.4 Friction

The friction forces were obtained under ambient and dry conditions in air, and in hexadecane and FC-40; the results are illustrated in Figure 6. A linear increase in friction force with increasing applied normal loads was observed for all polymer brushes under ambient conditions (Figure 6A), regardless of the brush compression as seen for some brushes at low normal loads (< 40 nN) during the adhesion force measurements (Figure 5A). As explained above, the **SPF0** brushes showed an immense adhesion due to

meniscus effect associated with high humidity ( $RH = 44 \pm 2\%$ ). Therefore, the friction obtained under ambient condition on non-fluoropolymer brushes has no significance.<sup>23</sup> To still allow some comparison the friction forces on **SPF0** were obtained under dry conditions ( $RH < 5\%$ ). The friction coefficient on **SPF0** was 0.013, which is roughly twice as high as that for the fluoropolymer brushes under current study, with the lowest friction coefficient of 0.005 observed on **SPF17**. We interpret this ultralow friction in terms of the semi-crystallinity of the fluorinated side-chains in the polymer brushes.<sup>24, 35, 42</sup>

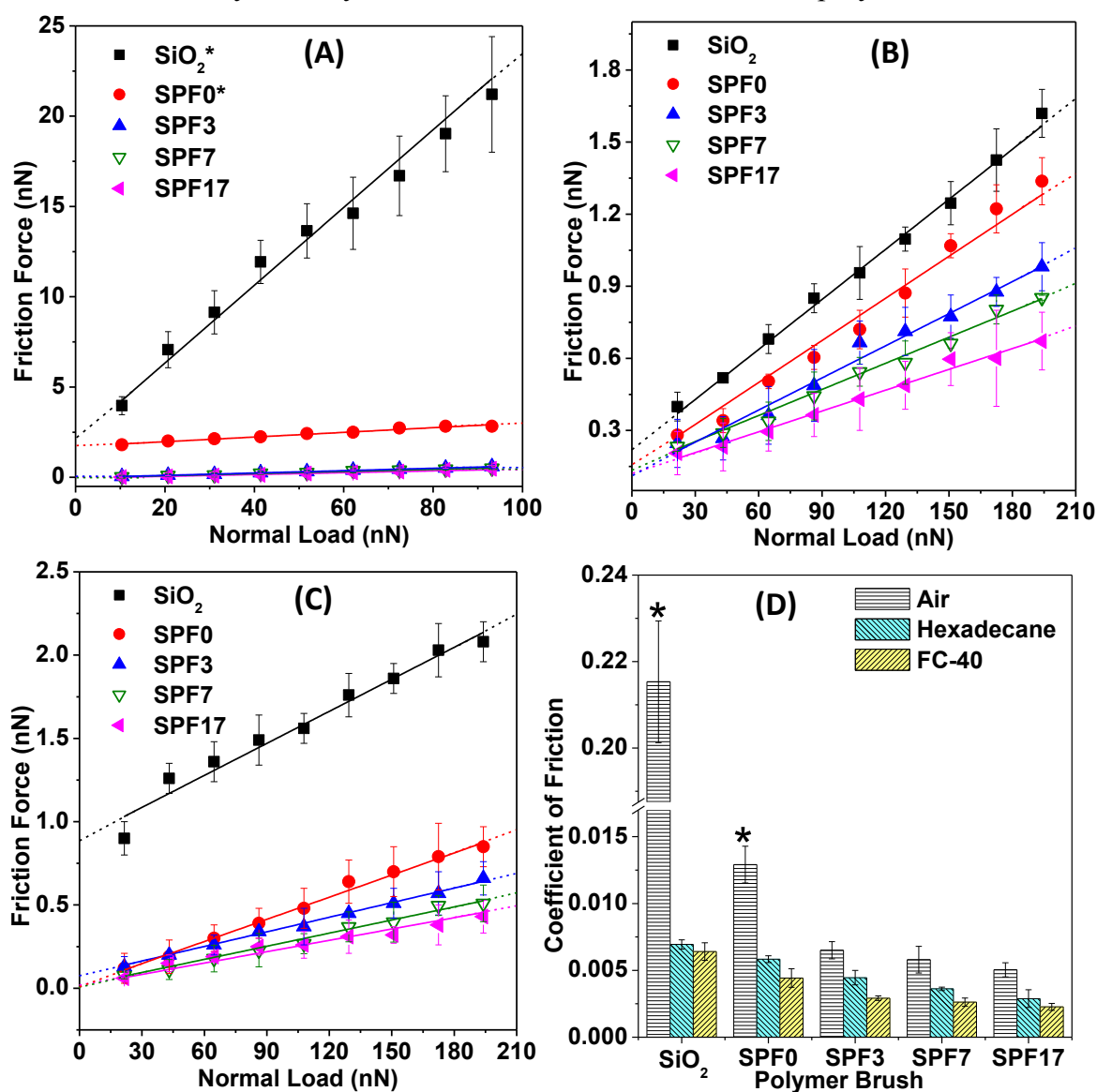


**Figure 6.** Friction forces versus applied normal load obtained under (A) ambient conditions ( $RH = 44 \pm 2\%$ ) [Note: \* = dry conditions;  $RH < 5\%$ ], (B) in hexadecane, (C) in FC-40. (D) The friction coefficient under all above conditions obtained from the slope of plots of the friction force versus normal load.

Similarly, the friction forces on these polymer brushes were also measured in fluoro and non-fluoro solvents. Figure 6B and 6C demonstrates friction forces obtained in hexadecane and FC-40 solvent as a function of applied normal load. Similar to the friction obtained under ambient/dry conditions, a linear friction force was obtained in both solvent

systems. The perfluoropolymer **SPF17** brushes has shown lowest friction coefficient 0.002 in FC-40 and 0.003 in hexadecane (Figure 6D). To a somewhat lesser extent, this is also observed for **SPF3** and **SPF7** the friction was reduced approximately by half ( $\sim 0.004$  in HD and  $\sim 0.003$  in FC-40), as compared to friction observed under ambient ( $\sim 0.006$ ) conditions on same polymer brushes. With proper solvation (here especially with FC-40 that swell the F-containing polymers well, see Table 1), the polymer brushes are in a stretched state, which apparently leads to a solvent cushion around the brush, which minimizes the friction. Similar effects have, for example, also been observed for zwitterionic polymers, which are highly hydrated in water, and display a correspondingly low friction coefficient in water.<sup>43</sup>

Finally, in addition to the solubility of polymer brushes, these solvents themselves act as lubricants, as can be seen on non-modified Si(111), which showed low friction in the presence of these solvents. An indication of the remarkably low friction coefficient in air of fluorinated brushes like **SPF17** is thus probably seen best by noting that this friction coefficient in air (0.005) is just twofold higher than that observed in solvent conditions. The low adhesion and friction properties of pefluoropolymer (**SPF17**) brushes thus significantly extend the range of tribological properties by acting as truly solid-bound, lubricating polymer films under dry as well as wet conditions, which will allow their use in a wide range of applications in microfluidics and in MEMS/NEMS.

## 5.5 Conclusions

High-density covalently bound fluoro and non-fluoropolymer brushes (**SPF<sub>x</sub>** with  $x = 0, 3, 7$ , and  $17$  F atoms per monomer) can be grown by SI-ATRP on Si(111) surfaces via thiol-yne click chemistry. The adhesion and friction forces of such polymer brushes can be tuned to progressively smaller values with increasing fluorine content. In fact, very low adhesion forces were found for **SPF17**: in air, hexadecane (poor solvent) and fluorinated solvent FC-40 (good solvent) values of only 6.89, 0.049 and 0.003 nN were observed, respectively, upon a 10 nN applied normal load. In addition, a friction coefficient of only 0.005 was obtained under ambient conditions on **SPF17**. These values are (among) the lowest ones for polymer brushes under ambient, solvent-free conditions. Therefore, these **SPF17** polymer brushes have great potential as dry lubricants.

## 5.6 References

1. Hougham, G.; Cassidy, P. E.; Johns, K.; Davidson, T., *Fluoropolymers 2 Properties*. Kluwer Academic Publishers: New York, **2002**.
2. Malshe, V. C.; Sangaj, N. S., Fluorinated acrylic copolymers Part 1: Study of clear coatings. *Prog. Org. Coat.* **2005**, 53, (3), 207-211.
3. Amatucci, G. G.; Pereira, N., Fluoride based electrode materials for advanced energy storage devices. *J. Fluorine Chem.* **2007**, 128, (4), 243-262.
4. Hougham, G.; Cassidy, P. E.; Johns, K.; Davidson, T., *Fluoropolymers 1 Synthesis*. Kluwer Academic Publishers: New York.
5. Müller, K.; Faeh, C.; Diederich, F., Fluorine in Pharmaceuticals: Looking Beyond Intuition. *Science* **2007**, 317, (5846), 1881-1886.
6. Purser, S.; Moore, P. R.; Swallow, S.; Gouverneur, V., Fluorine in medicinal chemistry. *Chem. Soc. Rev.* **2008**, 37, (2), 320-330.
7. Jeschke, P., The Unique Role of Fluorine in the Design of Active Ingredients for Modern Crop Protection. *ChemBioChem* **2004**, 5, (5), 570-589.
8. Schmidt, D. L.; Coburn, C. E.; DeKoven, B. M.; Potter, G. E.; Meyers, G. F.; Fischer, D. A., Water-based non-stick hydrophobic coatings. *Nature* **1994**, 368, 39-41.
9. Smith, D. W.; Iacono, S. T.; Boday, D. J.; Kettwick, S. C., *Advances in Fluorine-Containing Polymers*. ACS Sym Ser: **2013**; Vol. 1106.
10. Cui, J.; Qiang, L.; Zhang, B.; Yang, T.; Zhang, J., Lower friction and higher wear resistance of fluorine-incorporated amorphous carbon films. *Surf. Interface Anal.* **2013**, 45, (9), 1329-1333.
11. Rubio-Roy, M.; Portal, S.; Polo, M. C.; Pascual, E.; Bertran, E.; Andujar, J. L., Fluorination effects on tribological characteristics of hydrogenated amorphous carbon thin films. *Nsti Nanotech* **2008**, 1, 479-482.
12. Zheng, J.; Zhou, H.; Wan, Z.; Sang, R., The Tribological Properties of Several PTFE based self-lubricating composites in vacuum. In *Adv. Mater. Res.* **2012**; Vol. 535-537, pp 144-148.
13. Ji, K.; Shan, W.; Xia, Y.; Dai, Z., The Tribological Behaviors of Self-Lubricating Composites as Filler in Copper Foam. *Tribol. T* **2012**, 55, (1), 20-31.
14. Doms, M.; Feindt, H.; Kuipers, W. J.; Shewtanasoontorn, D.; Matar, A. S.; Brinkhues, S.; Welton, R. H.; Mueller, J., Hydrophobic coatings for MEMS applications. *J. Micromech. Microeng.* **2008**, 18, (5), 055030.
15. Bouaidat, S.; Winther-Jensen, B.; Christensen, S. F.; Jonsmann, J., Plasma-polymerized coatings for bio-MEMS applications. *Sensor. Actuat. A-Phys.* **2004**, 110, (1-3), 390-394.
16. Bhushan, B., Nanotribology and nanomechanics of MEMS/NEMS and BioMEMS/BioNEMS materials and devices. *Microelectron. Eng.* **2007**, 84, (3), 387-412.
17. Spengen, W. M. v., MEMS reliability from a failure mechanisms perspective. *Microelectron. Reliab.* **2003**, 43, (7), 1049-1060.
18. Sakata, H.; Kobayashi, M.; Otsuka, H.; Takahara, A., Tribological properties of poly(methyl methacrylate) brushes prepared by surface-initiated atom transfer radical polymerization. *Polym. J.* **2005**, 37, (10), 767-775.
19. Pujari, S. P.; Spruijt, E.; Cohen Stuart, M. A.; van Rijn, C. J. M.; Paulusse, J. M. J.; Zuilhof, H., Ultralow Adhesion and Friction of Fluoro-Hydro Alkyne-Derived Self-Assembled Monolayers on H-Terminated Si(111). *Langmuir* **2012**, 28, (51), 17690-17700.
20. Pujari, S. P.; Zuilhof, H., Highly wear-resistant ultra-thin per-fluorinated organic monolayers on silicon(111) surfaces. *Appl. Surf. Sci.* **2013**, 287, 159-164.

21. Pujari, S. P.; Scheres, L.; Weidner, T.; Baio, J. E.; Cohen Stuart, M. A.; van Rijn, C. J. M.; Zuilhof, H., Covalently Attached Organic Monolayers onto Silicon Carbide from 1-Alkynes: Molecular Structure and Tribological Properties. *Langmuir* **2013**, 29, (12), 4019-4031.
22. Sidharam P. Pujari, Y. L., Remco Regeling, and Han Zuilhof, Tribology and Stability of Organic Monolayers on CrN: A Comparison among Silane, Phosphonate, Alkene, and Alkyne Chemistries. *Langmuir* **2013**, 29, (33), 10405-10415.
23. Bhairamadgi, N. S.; Pujari, S. P.; Leermakers, F. A. M.; van Rijn, C. J. M.; Zuilhof, H., Adhesion and Friction Properties of Polymer Brushes: Fluoro versus Non-fluoro Polymer Brushes at Varying Thickness. *Langmuir* **2014**, 30, (8), 2068–2076.
24. Honda, K.; Morita, M.; Otsuka, H.; Takahara, A., Molecular Aggregation Structure and Surface Properties of Poly(fluoroalkyl acrylate) Thin Films. *Macromolecules* **2005**, 38, (13), 5699-5705.
25. Yamada, Y.; Tanaka, K., Effect of The Degree of Crystallinity on Friction and wear of Poly(ethylene-terephthalate). *ACS Sym Ser* **1985**, 287, 363-374.
26. Karuppiyah, K. S. K.; Bruck, A. L.; Sundararajan, S.; Wang, J.; Lin, Z.; Xu, Z.-H.; Li, X., Friction and wear behavior of ultra-high molecular weight polyethylene as a function of polymer crystallinity. *Acta Biomater.* **2008**, 4, (5), 1401-1410.
27. Bhairamadgi, N. S.; Gangarapu, S.; Campos, M. A. C.; Paulusse, J. M. J.; van Rijn, C. J. M.; Zuilhof, H., Efficient Functionalization of Oxide-Free Silicon(111) Surfaces: Thiol-yne versus Thiol-ene Click Chemistry. *Langmuir* **2013**, 29, (14), 4535-4542.
28. Moh, L. C. H.; Losego, M. D.; Braun, P. V., Solvent Quality Effects on Scaling Behavior of Poly(methyl methacrylate) Brushes in the Moderate- and High-Density Regimes. *Langmuir* **2011**, 27, (7), 3698-3702.
29. Giesbers, M.; Marcelis, A. T. M.; Zuilhof, H., Simulation of XPS C1s Spectra of Organic Monolayers by Quantum Chemical Methods. *Langmuir* **2013**, 29, (15), 4782-4788.
30. Hutter, J. L.; Bechhoefer, J., Calibration of atomic-force microscope tips. *Rev. Sci. Instrum.* **1993**, 64, (7), 1868-1873.
31. Liu, W. H.; Bonin, K.; Guthold, M., Easy and direct method for calibrating atomic force microscopy lateral force measurements. *Rev. Sci. Instrum.* **2007**, 78, (6), 063707.
32. Li, X.; Wei, X.; Husson, S. M., Thermodynamic Studies on the Adsorption of Fibronectin Adhesion-Promoting Peptide on Nanothin Films of Poly(2-vinylpyridine) by SPR. *Biomacromolecules* **2004**, 5, (3), 869-876.
33. Rastogi, A.; Paik, M. Y.; Ober, C. K., Development of a directly patterned low-surface-energy polymer brush in supercritical carbon dioxide. *ACS Appl. Mater. Interfaces* **2009**, 1, (9), 2013-20.
34. Bruno, A., Controlled Radical (Co)polymerization of Fluoromonomers. *Macromolecules* **2010**, 43, (24), 10163-10184.
35. Yamaguchi, H.; Honda, K.; Kobayashi, M.; Morita, M.; Masunaga, H.; Sakata, O.; Sasaki, S.; Takahara, A., Molecular Aggregation State of Surface-grafted Poly{2-(perfluorooctyl)ethyl acrylate} Thin Film Analyzed by Grazing Incidence X-ray Diffraction. *Polym. J.* **2008**, 40, (9), 854-860.
36. Malham, I. B.; Bureau, L., Density Effects on Collapse, Compression, and Adhesion of Thermoresponsive Polymer Brushes. *Langmuir* **2010**, 26, (7), 4762-4768.
37. Coad, B. R.; Lu, Y.; Glattauer, V.; Meagher, L., Substrate-Independent Method for Growing and Modulating the Density of Polymer Brushes from Surfaces by ATRP. *ACS Appl. Mater. Interfaces* **2012**, 4, (5), 2811-2823.
38. David S. Fryer; Richard D. Peters; Eui Jun Kim; Jeanne E. Tomaszewski; Juan J. de Pablo; Nealey, P. F.; White, C. C.; Wu, W.-l., Dependence of the Glass Transition

- Temperature of Polymer Films on Interfacial Energy and Thickness. *Macromolecules* **2001**, 34, (16), 5627–5634.
39. Yamamoto, S.; Tsujii, Y.; Fukuda, T., Glass Transition Temperatures of High-Density Poly(methyl methacrylate) Brushes. *Macromolecules* **2002**, 35, (16), 6077-6079.
  40. Bielecki, R. M.; Benetti, E. M.; Kumar, D.; Spencer, N. D., Lubrication with Oil-Compatible Polymer Brushes. *Tribol Lett* **2012**, 45, (3), 477-487.
  41. Limpoco, F. T.; Rigoberto C. Advincula; Perry, S. S., Solvent Dependent Friction Force Response of Polystyrene Brushes Prepared by Surface Initiated Polymerization. *Langmuir* **2007**, 23, (24), 12196 - 12201.
  42. Honda, K.; Morita, M.; Masunaga, H.; Sasaki, S.; Takata, M.; Takahara, A., Room-temperature nanoimprint lithography for crystalline poly(fluoroalkyl acrylate) thin films. *Soft Matter* **2010**, 6, (5), 870-875.
  43. Raviv, U.; Giasson, S.; Kampf, N.; Gohy, J.-F.; Jérôme, R.; Klein, J., Lubrication by charged polymers. *Nature* **2003**, 425, 163-165



# Chapter 6

---

## General Discussion

In this chapter we discuss an overview of achievements as described in this thesis along with some remaining and unanswered issues, new approaches and recommendations for further research.



## Contents

<b>6. General Discussion .....</b>	<b>103</b>
6.1 Introduction .....	105
6.2 Functional Monolayers.....	105
6.3 Stability of Monolayers.....	106
6.4 Polymer Brushes and Tribological Applications .....	107
6.5 Conclusions .....	110
6.6 References .....	111

## 6.1 Introduction

Micro and nano top-down technology has nowadays been able to downscale feature sizes far less than a micron. In this process the surface-area to volume ratio increases and thereby surface forces like capillary, van der Waals, and electrostatic forces become dominant over body/bulk forces. This leads to unwanted stiction and high friction, ultimately affecting the performance of the moving parts in the device negatively. Therefore low-adhesion, low-friction and stable coating materials are needed for today's high performance technological devices. Conventional approaches to overcome these effects involve the application of coatings exhibiting low adhesion and low friction. The mostly used low adhesion and friction materials are based on fluoropolymers e.g., PTFE.<sup>1</sup> Self-assembly of thiol/silane based monolayers are an alternative for overcoming stiction on microscale devices.<sup>2</sup> Both of these coatings are effective in eliminating stiction and friction, but they are not durable, as the former is susceptible to wear and the latter is chemically unstable under critical device operation conditions. Here we discuss the methods achieved in this thesis to overcome these issues and their further applicability in nanotechnology.

## 6.2 Functional Monolayers

As described in this thesis we developed surfaces functionalization methods that give stable, densely packed, and further functionalizable monolayers on oxide-free Si(111) surfaces. The obtained monolayers were covalently bound to the Si surface via Si-C bonds, which renders them stronger than the monolayers derived from thiols or silanes. Therefore, monolayers with Si-C bonds have potential applications in micro/nano electromechanical (MEMS/NEMS) devices where thiol- and silane- derived monolayers fail. Because, thiol- and silane- derived monolayers tend to degrade under device operating conditions like ambient, humid, liquids and elevated temperatures.<sup>3-8</sup>

The formation of functional monolayers is discussed in detail in **Chapter 2**, where we investigated Si(111) surface functionalization via 1,15-hexadecadiyne. The possibility of further functionalizing alkyne-terminated monolayers was evaluated by reacting them with various thiols via the thiol-yne click (TYC) reaction, which often yielded > 100% surface coverage, e.g., two thiols react with one alkyne group. Such a high surface coverage is not possible by using the well-known copper catalyzed alkyne-azide cycloaddition (CuAAC) reaction, where each alkyne will react with maximally one azide.

The combination of an alkyne-terminated monolayer and a TYC approach would allow the immobilization of organic biomolecules containing free thiols onto silicon surfaces. The alkyne-terminated monolayers are not only accessed by a TYC reaction, but also by well-known CuAAC reactions for further functionalization, depending on which set of reaction conditions suits the final application (Figure 1). Therefore, alkyne-terminated monolayers on Si(111) open up new fields of nanotechnology for developing biosensors

using functional monolayers to immobilize biomolecules of interest by choosing either TYC or CuAAC reactions. The advantage of utilizing TYC over CuAAC is that the TYC reaction does not require any toxic metal catalysts and gives high surface coverage. The high surface coverage result in high signal-to-noise ratio when using modified surfaces for biosensor applications.<sup>9,10</sup>

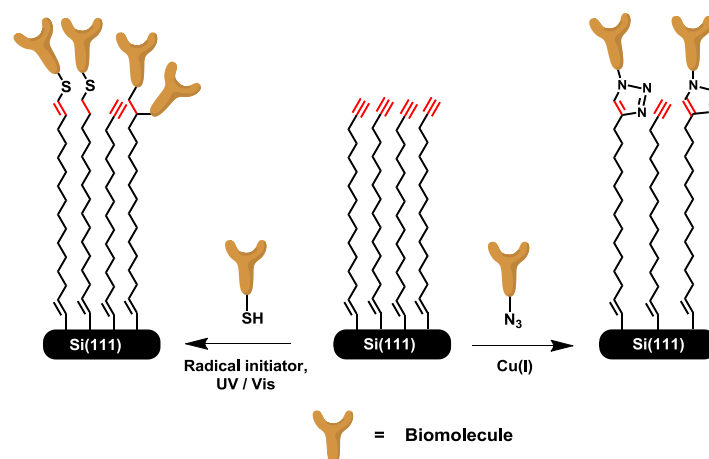


**Figure 1.** Surface functionalization via TYC and CuAAC reaction.

In biosensors, the receptor molecules are immobilized on a transducer surface, which converts the target binding event into a measurable electric signal.<sup>9</sup> Therefore an optimal orientation combined with a high concentration of receptor molecules on the transducer surface is crucial. With an oriented and highly concentrated immobilization of biomolecules (proteins) on a transducer surface, it will be possible to miniaturize the biosensor without losing sensitivity.<sup>11</sup> The thiol-containing amino acids like cysteine are less abundant in natural proteins, which allow the oriented immobilization of such proteins on surfaces via TYC click reaction without modification of proteins. In addition, the site-specific introduction of functional groups like azides, adds another route to allow oriented immobilization of proteins (using CuAAC or SPAAC reactions) on alkyne-terminated surfaces.

### 6.3 Stability of Monolayers

In **Chapter 3** we investigated stability of the monolayers using different combinations of monolayers and substrates under acidic (pH 3), neutral (pH 7), basic (pH 11), physiological (PBS) and under thermal conditions in a temperature range from 25 °C to 600 °C using the *in-situ* heating system in X-ray photoelectron spectroscopy (XPS). A compressive and comparative stability study enabled us to find a proper monolayer-substrate combination for specific applications. As explained above for biosensor applications monolayers must be stable under physiological conditions<sup>12</sup> and in case of high temperature field effect transistors (FETs) monolayers are expected to be stable at device operation temperatures.<sup>13, 14</sup> Here (**Chapter 3**) we followed the monolayer stability

using limited characterization techniques, without probing for an in-depth mechanistic understanding of monolayer degradation under specific conditions. To improve our understanding of the degradation of monolayers, a detailed stability study of monolayers using different surface-sensitive characterization techniques such as contact angle, infrared reflection absorption spectroscopy (IRRAS), atomic force microscopy (AFM), ellipsometry and XPS, etc., is required.

Our stability study was conducted with a constant monolayer chain length and with same terminal groups ( $-\text{CH}_3$ ). However, it would be interesting to measure the stability of monolayers with varying chain length ( $\text{C}_6$  to  $\text{C}_{18}$ ), different binding groups ( $\text{X} = -\text{SH}$ , -alkene, -alkyne, -acid, etc.) and terminal functional-groups ( $\text{R} = \text{CF}_3$ ,  $-\text{OH}$ ,  $-\text{COOH}$ , etc.) as shown in Figure 2. These parameters are important in determining the stability of monolayers, and show up in a wide range of applications. Though perhaps of limited scientific value, in practical view this will be highly valued information.

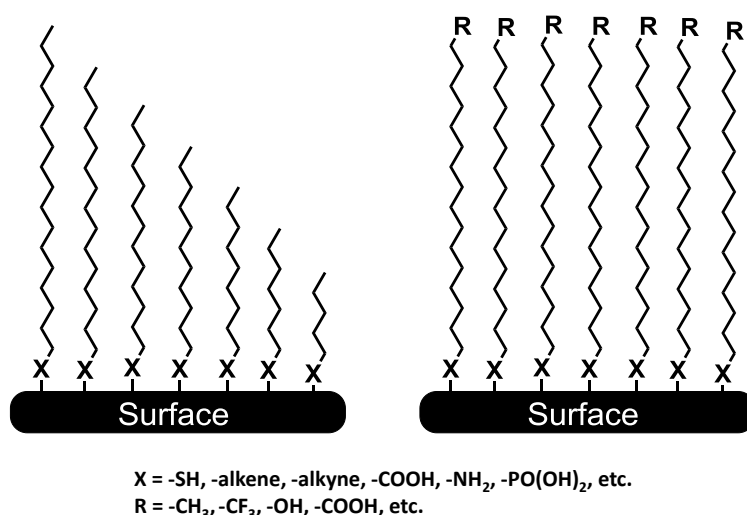


**Figure 2.** A new approach of monolayer stability study with varied chain length and head/anchoring, and terminal groups in monolayers.

## 6.4 Polymer Brushes and Tribological Applications

In **Chapter 4 and 5** the adhesion and friction properties of fluoropolymer brushes are evaluated and compared with non-fluoropolymer brushes, with respect to thickness and degree of fluorination of the polymer brushes. It was found that the adhesion and friction properties of non-fluoropolymer brushes were highly influenced by environmental conditions; under high humidity conditions, non-fluoro polymer brushes showed an immense adhesion due to capillary bridge formation between surface and colloidal probe, whereas this effect was insignificant on fluoro polymer brushes. The adhesion and friction properties of both polymer types were thickness dependent (**Chapter 4**) and a lower adhesion and friction was obtained with increasing fluorine content in the polymer brushes (**Chapter 5**). The polymer types studied in this thesis have potential application

as self-lubricating (in absence of external lubricants e.g., oil/grease) coatings in high-performance heavy duty industrial bearings and MEMS devices (Figure 3).

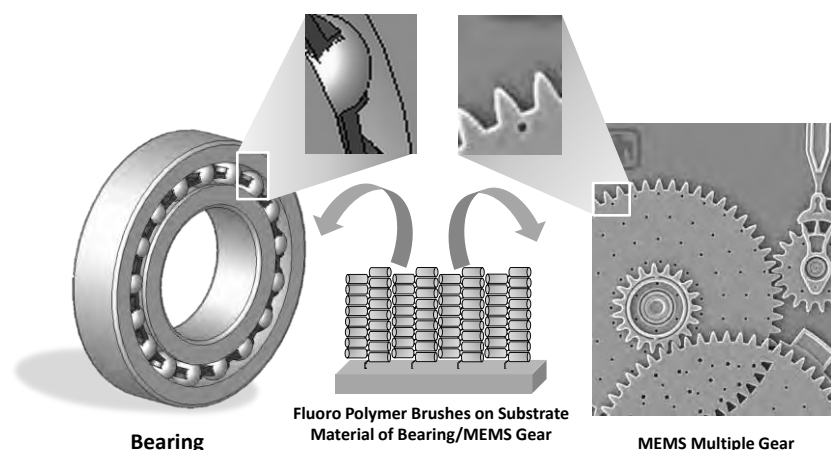


**Figure 3.** Application of covalently bound fluoropolymer films as self-lubricating thin film in bearing and MEMS gears (Sandia National Laboratories [www.mems.sandia.gov](http://www.mems.sandia.gov)).

The wear resistance is an important aspect for any coating material to be used for mechanical performance. The wear of polymer brushes was not studied for polymer brushes mentioned in this thesis. It is known that increasing fluorine content in monolayers results in higher wear resistance, due to increasing rigidity and crystallinity of the monolayers.<sup>15, 16</sup> The polymer brushes obtained from (2-perfluorooctyl) ethyl methacrylate (**SPF17**) (**Chapter 5**) were crystalline in nature;<sup>17</sup> therefore they are expected to have high wear resistance. The wear resistance of polymer brushes can be further improved by incorporating cross-linker in polymer brushes because the cross-linked network improve the shear strength of polymer brushes (Figure 4).<sup>18</sup> However, highly cross-linked polymer films will be brittle and have low wear resistance. Therefore, proper control of cross-linking network is necessary.

One of the current issues of polymer brushes characterization currently is the estimation of molecular weight and molecular weight distribution. There are theoretical methods known today to estimate molecular weight and grafting density.<sup>19, 20</sup> An alternative method is to synthesize free polymer simultaneously during the growth of polymer brush by addition of a sacrificial initiator. It is assumed that the free polymers generated in solution from sacrificial initiator and the surface grafted polymers have the same molecular weight and molecular weight distribution, but this is not always true.<sup>21, 22</sup> In case of high-surface area materials, like nanoparticles, however, the molecular weight of polymer brushes can be estimated after cleaving the brushes from the surface, e.g., by dissolving the nanoparticles in corrosive media like hydrofluoric acid.<sup>23</sup> However, the analysis of polymer brushes cleaved by this method on flat surfaces is more challenging than on nanoparticles, because a very small amount of polymer released from flat surfaces, which sometimes is insufficient for characterization.

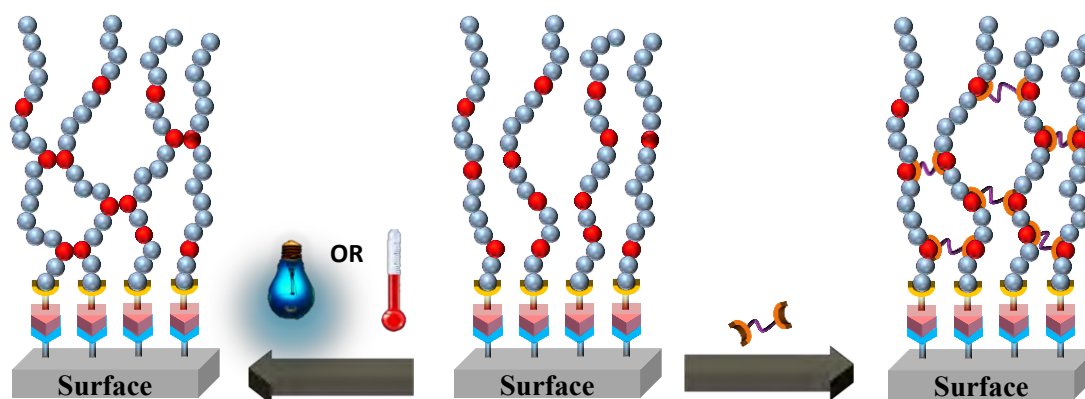


**Figure 4.** Cross linking of polymer brush using cross linker (right) and using either thermal or photochemical curing conditions (left).

In literature few approaches were proposed, where polymer brushes were cleaved from surfaces and molecular weight of cleaved polymer was determined using gel permeation chromatography (GPC) as depicted in Figure 5. Acid sensitive cleavable linkers were incorporated in initiator and these initiators then grafted on surfaces. The polymer brushes were grown from the cleavable initiator and then polymer brushes were immersed in suitable acidic solution to cleave them from cleavable linker.<sup>22, 24</sup>

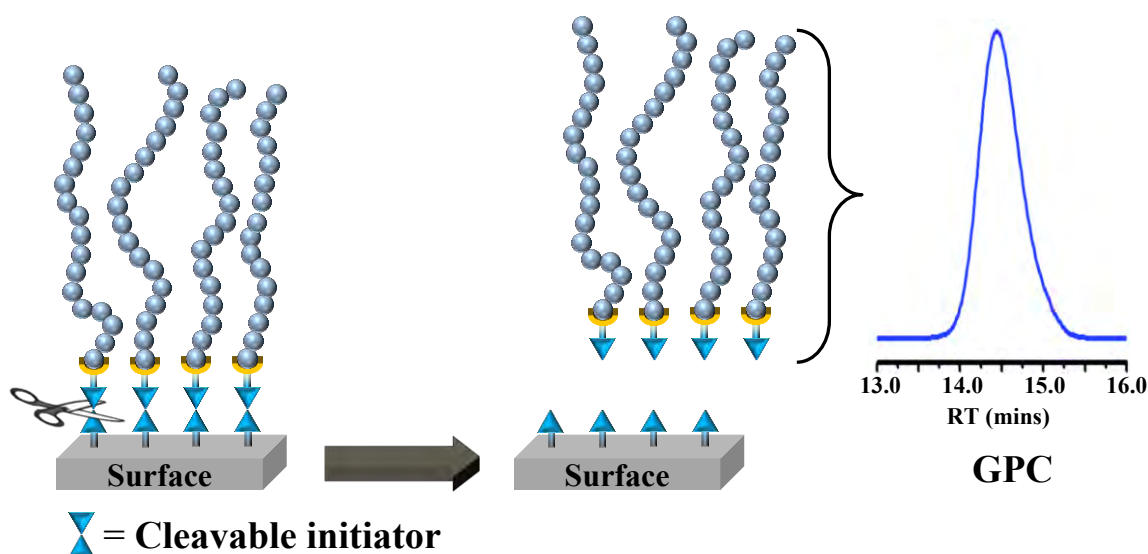


**Figure 5.** Polymer brushes with cleavable linker in initiator can be cleaved by exposure to a suitable solution and cleaved free polymer can be characterized by various polymer characterization techniques.

Chengjun et al. recently reported molecular weight determination of polymer brushes, which involved introduction of a photo-cleavable linker in the initiator and cleavage of the polymer brushes grown from these photosensitive initiators upon exposure to UV light.<sup>25</sup> However, the cleavage efficiency of the above mentioned method depends upon the diffusion of the cleaving solution through the polymer brushes and the penetration of light through the polymer film. When the polymer is not compatible with the cleaving medium

the latter will not diffuse through the polymer brushes; likewise, if the polymer brushes are highly dense, light will not penetrate them, leading to inefficient cleavage.

To effectively characterize polymer brushes, the media used for cleavage must be compatible with the polymers on the surface and should be milder. The amount of polymer obtained after cleavage must be high enough for characterization.

## **6.5 Conclusions**

In this thesis, a variety of aspects of surface chemistry were described, which include: functionalization of oxide-free silicon surfaces; use of TYC reaction for further functionalization; stability of monolayers on different substrates and preparation of fluoro- and non-fluoro polymer brushes. These approaches demonstrate insightful applications in nanotechnology. The functionalization of oxide-free silicon surfaces and the use of TYC enable the construction of more complex architecture for biosensor applications. Understanding monolayer stability can help in the selection of monolayer and substrate for specific applications under specific conditions. Finally, fluoro and non-fluoro polymer brushes with low adhesion and friction properties open a new era of lubricating polymer films under both dry and wet conditions for applications in MEMS/NEMS and microfluidics.

## 6.6 References

1. Sinha, S. K.; Satyanarayana, N.; Lim, S. c., Nano-tribology and Materials in MEMS. In Springer: Heidelberg, 2013.
2. Si-Li, R.; Sheng-Rong, Y.; Jin-Qing, W.; Wei-Min, L.; Ya-Pu, Z., Preparation and Tribological Studies of Stearic Acid Self-Assembled Monolayers on Polymer-Coated Silicon Surface. *Chem. Mater.* **2004**, 16, 428-434.
3. Gnanappa, A. K.; O'Murchu, C.; Slattery, O.; Peters, F.; O'Hara, T.; Aszalos-Kiss, B.; Tofail, S. A. M., Improved aging performance of vapor phase deposited hydrophobic self-assembled monolayers. *Appl. Surf. Sci.* **2011**, 257, (9), 4331-4338.
4. Kafer, D.; Witte, G.; Cyganik, P.; Terfort, A.; Woll, C., A comprehensive study of self-assembled monolayers of anthracenethiol on gold: Solvent effects, structure, and stability. *J. Am. Chem. Soc.* **2006**, 128, (5), 1723-1732.
5. Ang, X. F.; Li, F. Y.; Wei, J.; Tan, W. L.; Wong, C. C., A thermal and passivation study of self-assembled monolayers on thin gold films. *Thin Solid Films* **2008**, 516, (16), 5721-5724.
6. Schoenfish, M. H.; Pemberton, J. E., Air stability of alkanethiol self-assembled monolayers on silver and gold surfaces. *J. Am. Chem. Soc.* **1998**, 120, (18), 4502-4513.
7. Fr  chette, J.; Maboudian, R.; Carraro, C., Thermal Behavior of Perfluoroalkylsiloxane Monolayers on the Oxidized Si(100) Surface. *Langmuir* **2006**, 22, (6), 2726-2730.
8. Chandekar, A.; Sengupta, S. K.; Whitten, J. E., Thermal stability of thiol and silane monolayers: A comparative study. *Appl. Surf. Sci.* **2010**, 256, (9), 2742-2749.
9. Sadik, O. A.; Aluoch, A. O.; Zhou, A., Status of biomolecular recognition using electrochemical techniques. *Biosens. Bioelectron.* **2009**, 24, (9), 2749-2765.
10. Arya, S. K.; Solanki, P. R.; Datta, M.; Malhotra, B. D., Recent advances in self-assembled monolayers based biomolecular electronic devices. *Biosens. Bioelectron.* **2009**, 24, (9), 2810-2817.
11. O'Kennedy, R.; Townsend, S.; Donohoe, G. G.; Leonard, P.; Hearty, S.; Byrne, B., Speedily, Small, Sensitive, and Specific-Reality OR Myth for Future Analytical Methods. *Anal. Lett.* **2010**, 43, (10-11), 1630-1648.
12. Gooding, J. J.; Darwish, N., The rise of self-assembled monolayers for fabricating electrochemical biosensors—an interfacial perspective. *Chem Record* **2012**, 12, (1), 92-105.
13. Yokota, T.; Kuribara, K.; Tokuhara, T.; Zschieschang, U.; Klauk, H.; Takimiya, K.; Sadamitsu, Y.; Hamada, M.; Sekitani, T.; Someya, T., Flexible Low-Voltage Organic Transistors with High Thermal Stability at 250 °C. *Adv. Mater.* **2013**, 25, (27), 3639-3644.
14. Kuribara, K.; Wang, H.; Uchiyama, N.; Fukuda, K.; Yokota, T.; Zschieschang, U.; Jaye, C.; Fischer, D.; Klauk, H.; Yamamoto, T.; Takimiya, K.; Ikeda, M.; Kuwabara, H.; Sekitani, T.; Loo, Y.-L.; Someya, T., Organic transistors with high thermal stability for medical applications. *Nat. Commun.* **2012**, 3, 723.
15. Pujari, S. P.; Zuillhof, H., Highly Wear-Resistant Ultra-Thin Per-fluorinated Organic Monolayers on Silicon (111) Surfaces. *Appl. Surf. Sci.* **2013**, 287, (0), 159-164.
16. Patois, T.; Et Taouil, A.; Lallemand, F.; Carpentier, L.; Roizard, X.; Hihn, J.-Y.; Bondeau-Patissier, V.; Mekhalif, Z., Microtribological and corrosion behaviors of 1H,1H,2H,2H-perfluorodecanethiol self-assembled films on copper surfaces. *Surf. Coat. Technol.* **2010**, 205, (7), 2511-2517.
17. Yamaguchi, H.; Honda, K.; Kobayashi, M.; Morita, M.; Masunaga, H.; Sakata, O.; Sasaki, S.; Takahara, A., Molecular Aggregation State of Surface-grafted Poly{2-



- (perfluorooctyl)ethyl acrylate} Thin Film Analyzed by Grazing Incidence X-ray Diffraction. *Polym. J.* **2008**, 40, (9), 854-860.
18. Kobayashi, M.; Terada, M.; Takahara, A., Polyelectrolyte brushes: a novel stable lubrication system in aqueous conditions. *Faraday Discuss.* **2012**, 156, (0), 403-412.
  19. de Gennes, P. G., Conformations of Polymers Attached to an Interface. *Macromolecules* **1980**, 13, (5), 1069-1075.
  20. Malham, I. B.; Bureau, L., Density Effects on Collapse, Compression, and Adhesion of Thermoresponsive Polymer Brushes. *Langmuir* **2009**, 26, (7), 4762-4768.
  21. Turgman-Cohen, S.; Genzer, J., Simultaneous Bulk- and Surface-Initiated Controlled Radical Polymerization from Planar Substrates. *J. Am. Chem. Soc.* **2011**, 133, (44), 17567-17569.
  22. Koylu, D.; Carter, K. R., Stimuli-Responsive Surfaces Utilizing Cleavable Polymer Brush Layers. *Macromolecules* **2009**, 42, (22), 8655-8660.
  23. Pyun, J.; Jia, S. J.; Kowalewski, T.; Patterson, G. D.; Matyjaszewski, K., Synthesis and characterization of organic/inorganic hybrid nanoparticles: Kinetics of surface-initiated atom transfer radical polymerization and morphology of hybrid nanoparticle ultrathin films. *Macromolecules* **2003**, 36, (14), 5094-5104.
  24. Jayachandran, K. N.; Chatterji, P. R., Synthesis of dense brush polymers with cleavable grafts. *Eur. Polym. J.* **2000**, 36, (4), 743-749.
  25. Kang, C.; Crockett, R. M.; Spencer, N. D., Molecular-Weight Determination of Polymer Brushes Generated by SI-ATRP on Flat Surfaces. *Macromolecules* **2014**, 47, (1), 269-275.

# Appendix A

## Supporting Information: Chapter 2

### A.1 Synthesis of 1, 15-hexadecadiyne

#### A.1.1 Synthesis of Bis-(*p*-toluene sulfonate) dodecane

A 1 L three-necked round-bottom flask containing 300 mL THF was charged with 60.0 g of 1, 12-dodecanediol (296 mmol) and 124.0 g *p*-toluenesulfonyl chloride (651 mmol). The reaction mixture was stirred until the solution become clear and was cooled to 0 °C using an ice bath. Anhydrous potassium hydroxide (133.0 g, 2370 mmol) was added in small portions, maintaining the temperature <5 °C, after which the reaction mixture was stirred for another 3 h at room temperature. The reaction mixture was then filtered to remove remaining salts, and the solvents in the filtrate were removed under reduced pressure. The crude product was extracted with diethyl ether and the organic layer was washed first with water (3 × 100 mL) and then with brine (1 × 100 mL) solution. The organic layer extract was dried (MgSO<sub>4</sub>), concentrated in vacuo, and the crude product was purified by using silica gel column chromatography afforded 13.11 g (121 g, 237 mmol; 80%) of the bis-(*p*-toluene sulfonate) dodecane.

<sup>1</sup>H-NMR (δ<sub>ppm</sub>): 7.80-7.78 (d, 4H, Ph); 7.36-7.34 (d, 4H, Ph); 4.04-4.01(t, 4H, CH<sub>2</sub>-OTs); 2.46 (s, 6H, Ph-CH<sub>3</sub>); 1.67-1.60(m, 4H, CH<sub>2</sub>); 1.31-1.21(m, 16H, CH<sub>2</sub>).

<sup>13</sup>C-NMR (δ<sub>ppm</sub>): 144.57 (2C, Ph); 133.32 (2C, Ph); 129.77 (2C, Ph); 127.86 (2C, Ph); 70.66 (2C, CH<sub>2</sub>-OTs); 29.37 (2C, CH<sub>2</sub>); 29.31(4C, CH<sub>2</sub>); 28.88(4C, CH<sub>2</sub>); 28.81(2C, CH<sub>2</sub>); 25.31 (2C, CH<sub>2</sub>); 21.60 (2C, CH<sub>2</sub>).

#### A.1.2 Synthesis of 1,15-hexadecadiyne

A 1 L three-necked round-bottom flask fitted with a pressure-equalizing dropping funnel, condenser, stirrer and thermometer was flushed with argon and charged with lithium acetylide complex (37.7 g, 410 mmol). 200 ml DMSO was added and slurry with the acetylide lithium complex was formed. The solution was stirred and cooled in an ice bath. Bis-(*p*-toluene sulfonate) dodecane (100 g, 196 mmol) was added over 1 h maintaining the reaction temperature at 8 °C with external cooling. After complete addition of the bis-(*p*-toluene) dodecane, the reaction mixture was stirred for 1 h at room temperature. The reaction mixture was hydrolyzed with 100 mL of water and extracted with heptane, and the combined organic layers were dried (with magnesium sulfate), filtered and the solvent was removed under reduced pressure. Further purification was

carried out using column chromatography (with hexane as an eluent) and followed by recrystallization in hexane, to yield 42.7 g of 1,15-hexadecadiyne (117 mmol, 60% yield)

$^1\text{H-NMR}$  ( $\delta_{\text{ppm}}$ ): 2.18 (m, 4H  $\text{HC}\equiv\text{C-CH}_2\text{-CH}_2$ ); 1.93 (t, 2H,  $\text{HC}\equiv\text{C-CH}_2$ ); 1.53 (m, 4H  $\text{HC}\equiv\text{C-CH}_2\text{-CH}_2$ ); 1.22-1.45 (m, 16H, alkyl backbone).

$^{13}\text{C-NMR}$  ( $\delta_{\text{ppm}}$ ): 84.78 (2C,  $\text{R-C}\equiv\text{C-H}$ ); 68.00 (2C,  $\text{R-C}\equiv\text{C-H}$ ); 29.54 (2C,  $\text{CH}_2$ ); 29.46 (2C,  $\text{CH}_2$ ); 29.08 (2C,  $\text{CH}_2$ ); 28.74 (2C,  $\text{CH}_2$ ); 28.49 (2C,  $\text{CH}_2$ ); 18.38 (2C,  $-\text{CH}_2\text{-C}\equiv\text{C-H}$ ).

## A.2 Surface modification via thiol-yne click (TYC) reaction

### A.2.1 Thioglycolic acid (S-5)

Amounts employed: thioglycolic acid 0.5 mL (665 mg, 7.22 mmol), DMPA (370 mg, 1.44 mmol) in chlorobenzene (1 mL). Static water contact angle of resulting monolayer:  $40^\circ$ .

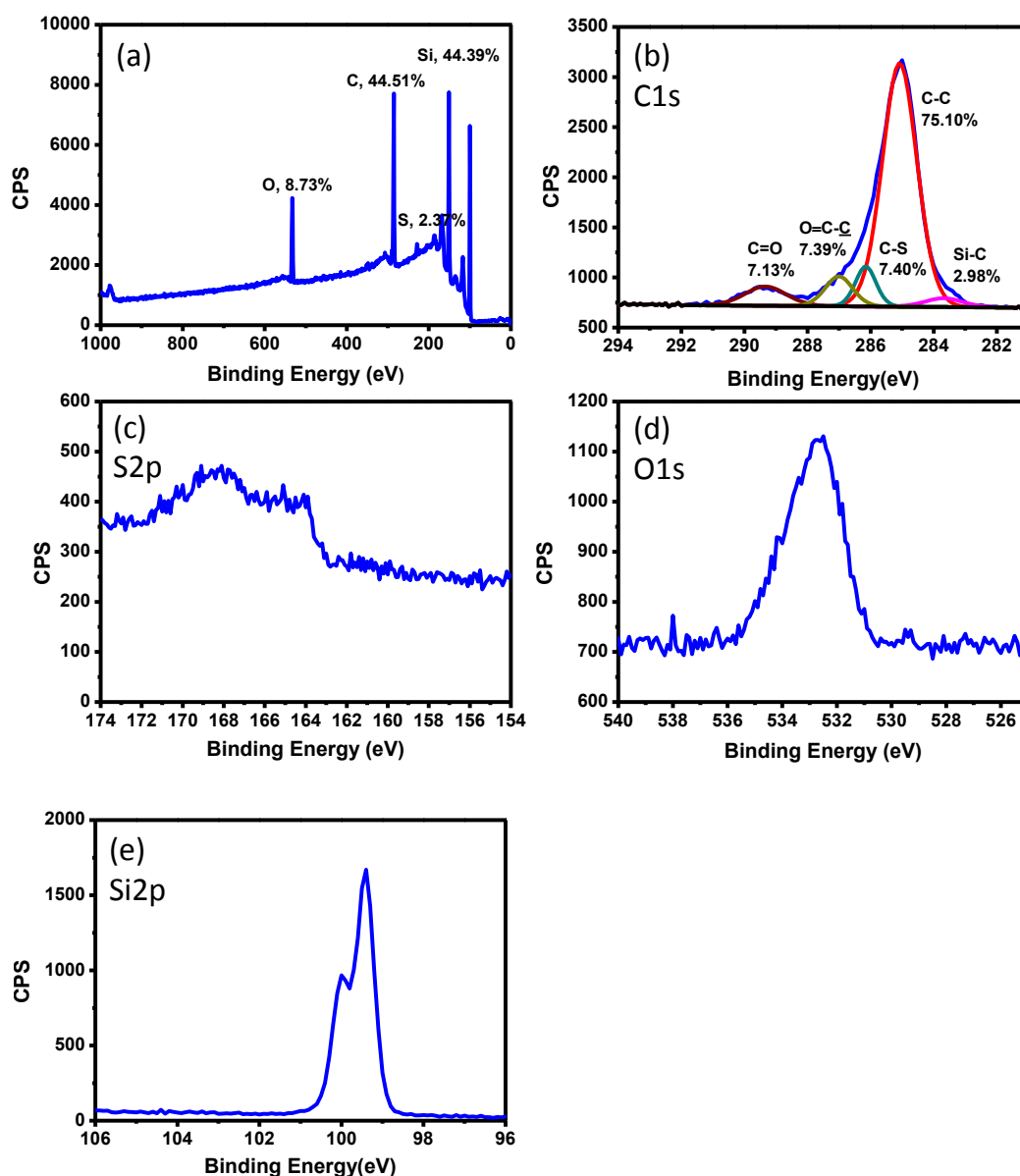


Figure SI-1. XPS spectrum of thioglycolic acid modified Si(111) surface (S-5).

### A.2.2 Thioacetic acid (S-3)

Amounts employed: 0.25 mL (264 mg, 3.47 mmol) thiolacetic acid, (177 mg, 0.70 mmol) DMPA in 0.5 mL chlorobenzene. Static water contact angle of resulting monolayer: 63°

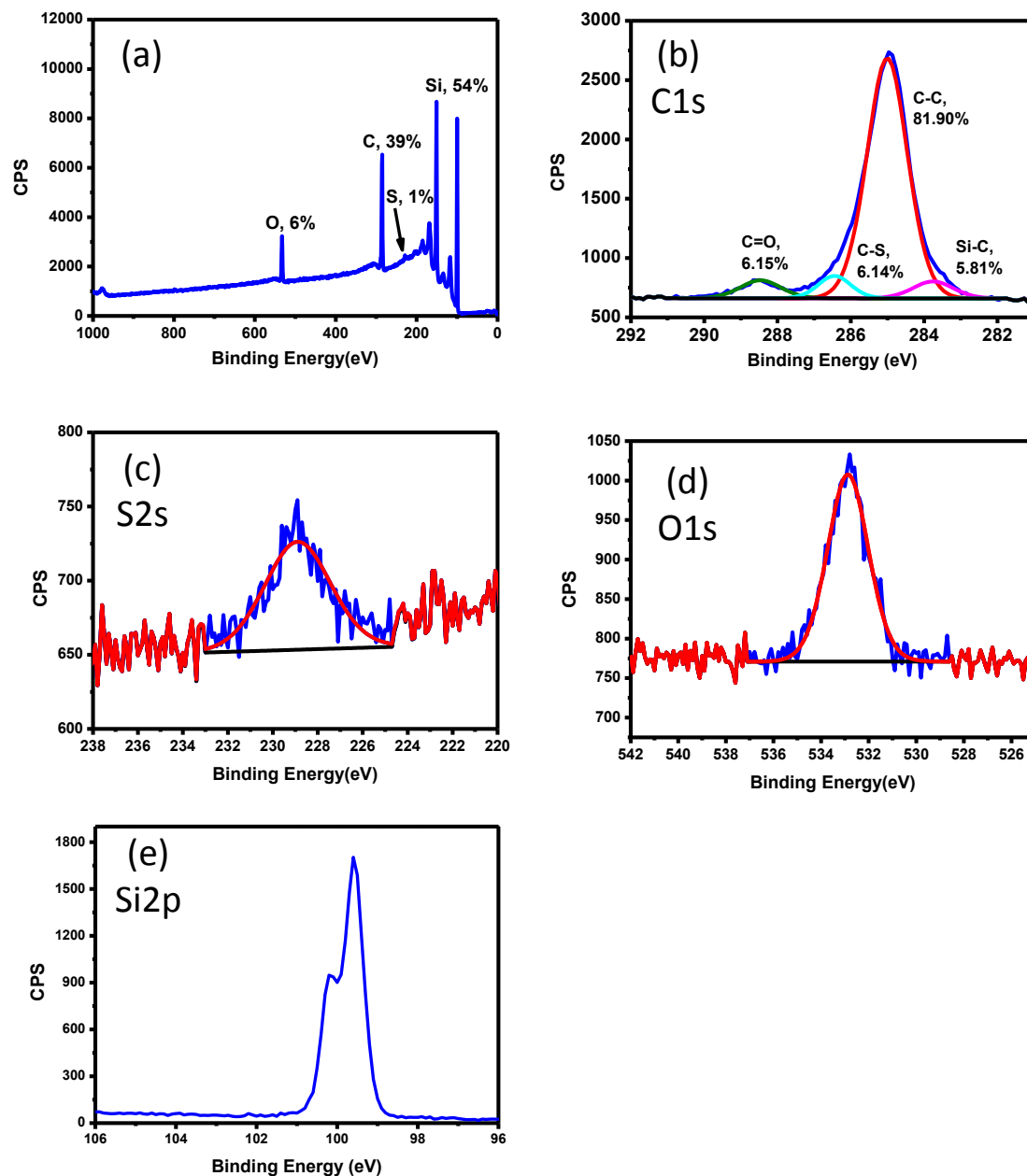


Figure SI-2. XPS spectrum of thioacetic acid modified Si(111) surface (S-3).

### A.2.3 Thioglycerol (S-4)

Amounts employed: 0.25 mL (311 mg, 2.86 mmol) thioglycerol, (147 mg, 0.57 mmol) DMPA in 0.5 mL chlorobenzene. Static water contact angle of resulting monolayer: 38°.

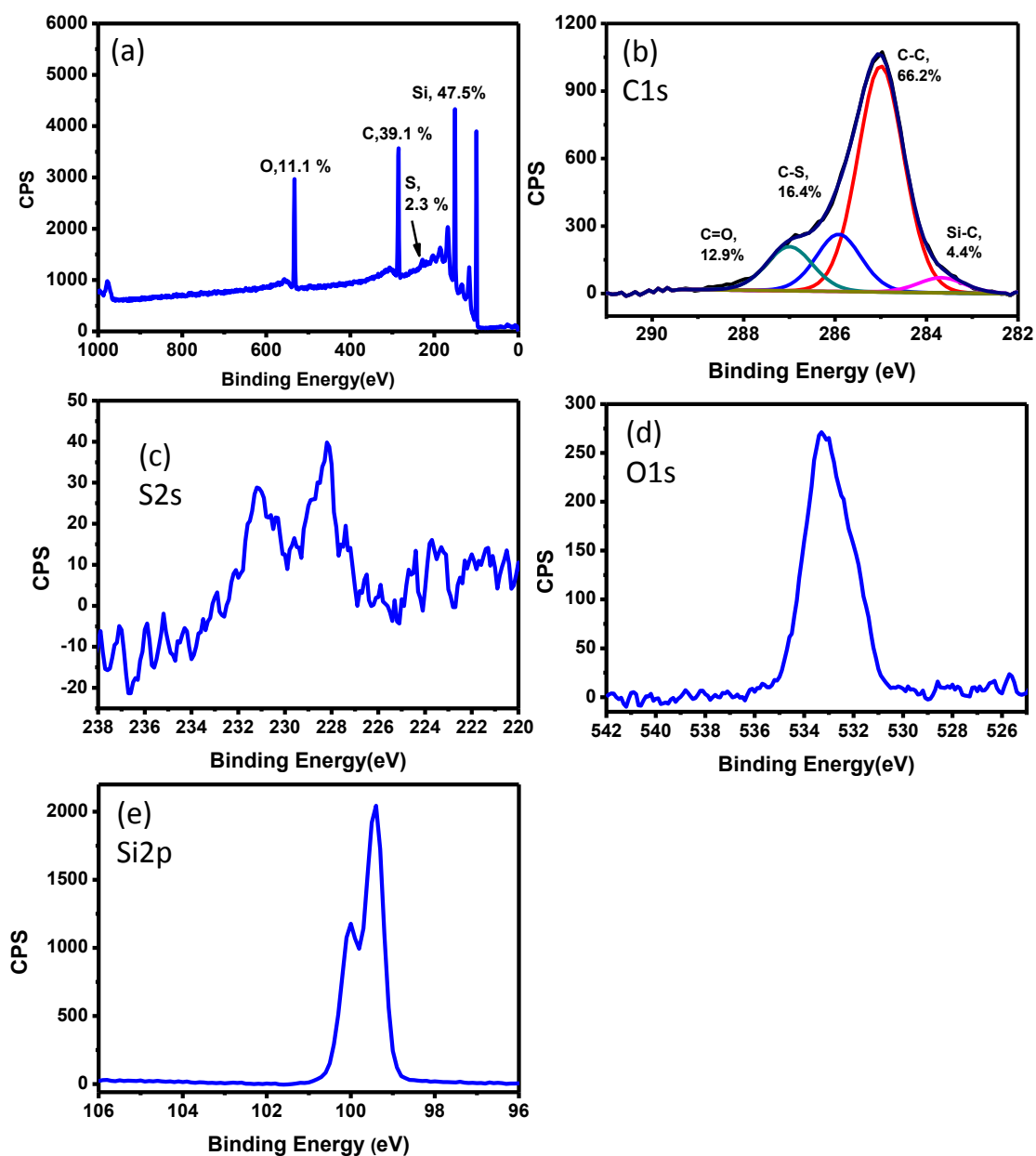


Figure SI-3. XPS spectrum of Thioglycerol modified Si(111) surface (S-4).

### A.2.4 Thio- $\beta$ -D-glucose Tetraacetate (S-2)

Amounts employed: 50 mg (1.14 mmol) thio-  $\beta$ -D-glucose, (7.02 mg, 0.027 mmol) DMPA in 0.5 mL chlorobenzene. Static water contact angle of resulting monolayer: 63°.

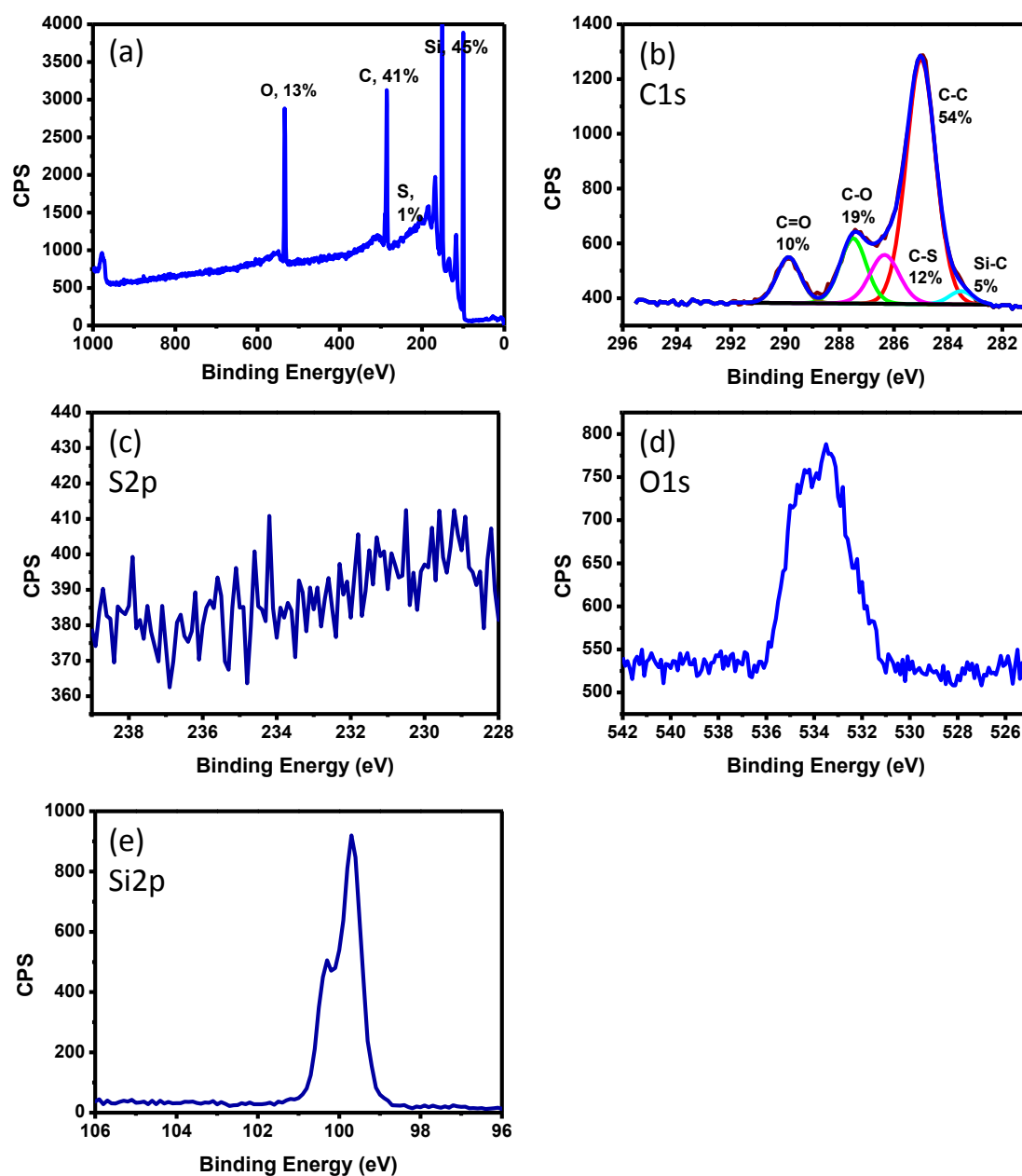


Figure SI-4. XPS spectrum of Thio- $\beta$ -D-glucose Tetraacetate Si(111) surface (S-2).

### A.2.5 9-Fluorenylmethoxy-carbonyl cysteine (S-1)

Amounts employed: 25 mg (0.072 mmol) Fmoc-Cys, (3.73 mg, 0.014 mmol) DMPA in 0.5 mL chlorobenzene. Static water contact angle of resulting monolayer: 68°.

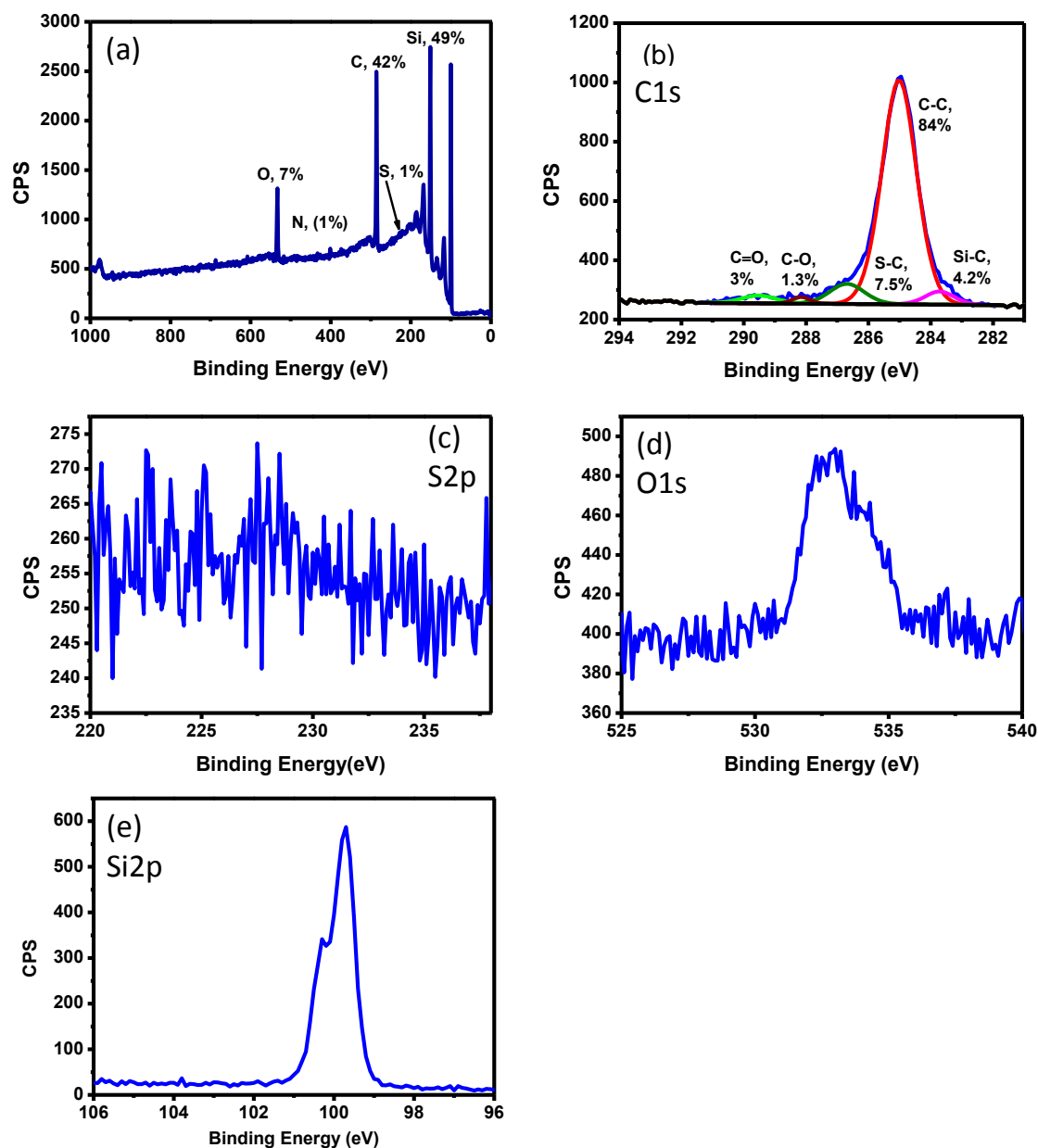


Figure SI-5. XPS spectrum of 9-fluorenylmethoxy-carbonyl cysteine Si(111) surface (S-1).

### A.2.6 Thioacetic acid (S-mix-3-II)

Amounts employed: 0.25 mL (264 mg, 3.47 mmol) thioacetic acid, (177 mg, 0.70 mmol) DMPA in 0.5 mL chlorobenzene and irradiated with a 365 nm light for 1.5 h and modified surface was noted as to **S-mix-3-I**. The modified **S-mix-3-I** substrates were washed several times with chlorobenzene, and then with dichloromethane, and dried under a stream of argon. The thus modified Si substrates were characterized by XPS. The **S-mix-3-I** surface was further modified with freshly prepared 0.25 mL (264 mg, 3.47 mmol) thiolacetic acid, (177 mg, 0.70 mmol) DMPA in 0.5 mL chlorobenzene and irradiated with a 365 nm light for 1.5 h and modified surface was noted as to **S-mix-3-II**. The modified **S-mix-3-II** substrates were washed several times with chlorobenzene, and then with dichloromethane, and dried under a stream of argon. The thus modified Si substrates were characterized by XPS.

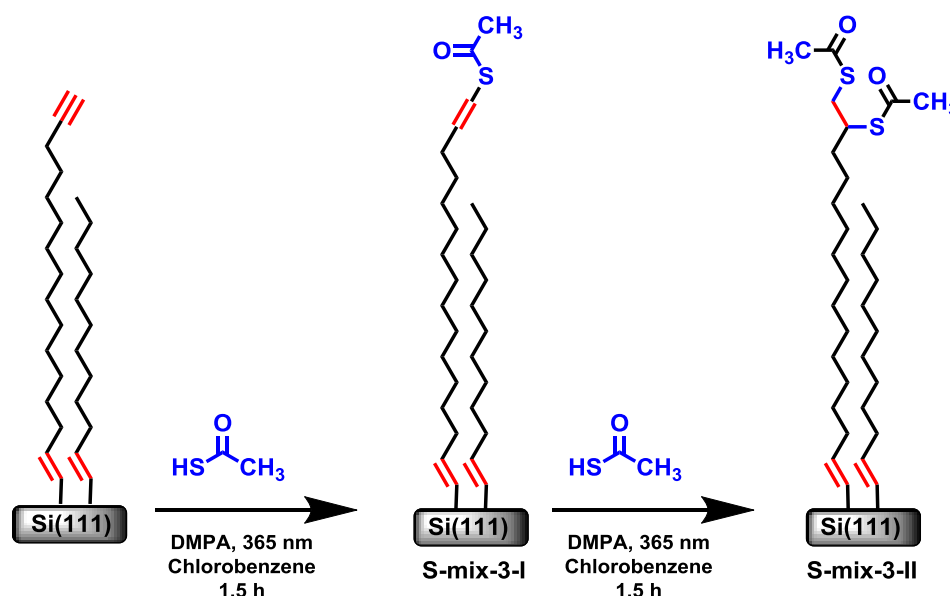


Figure SI-6: Modification of mixed monolayer (S-mix) via thiol-yne click reaction with thiol 3 in two steps.

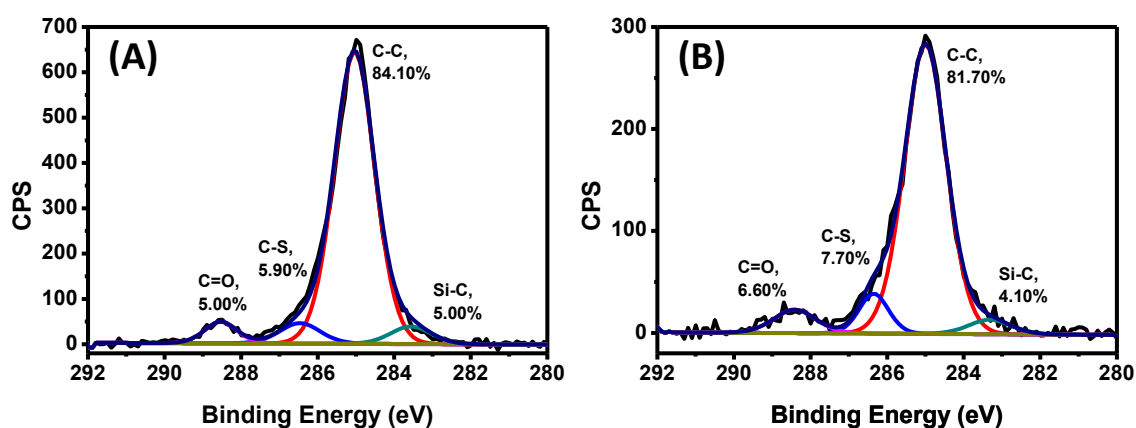
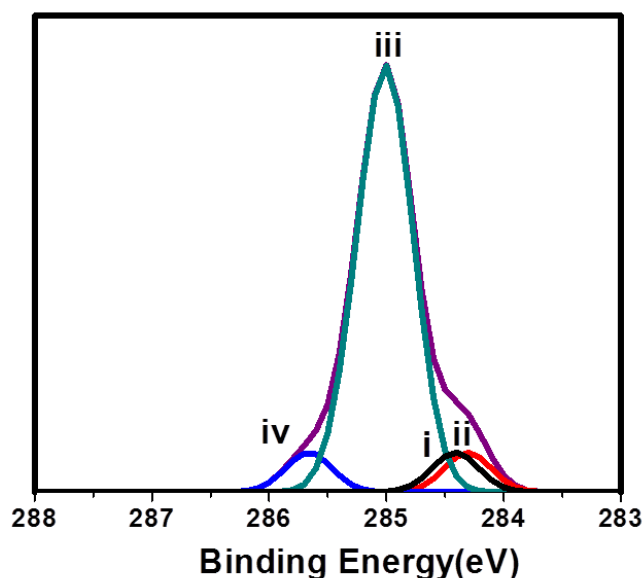


Figure SI-7. XPS spectrum of thiol (3) on **S-mix** surface. (A) C1s spectrum of **S-mix-3-I** and (B) C1s spectrum of **S-mix-3-II**.



### A.3 Electronic core level calculations

#### A.3.1 Alkyne terminated Monolayer (S-alkyne):



**Figure SI-8.** Simulated core level C 1s XPS-spectra for alkyne terminated monolayer. Simulation data was calculated based on DFT calculations of the C 1s core level energies for the C16 alkyne capped with a  $(\text{SiCH}_3)_3\text{Si-}$  group except for silicon bound carbon atom. The binding energy of Si bound carbon atom was calculated with  $\text{Si}_3$  structure with central Si-H centre, which was appended with four TMS groups. The spectra has been divided into different coloured curves based on the assigned numbers i-iv ( which are shown in Table SI-1) for different carbon atoms.

**Table SI-1.** Calculated  $\Delta\text{BE}$  of carbon atoms in Alkyne terminated monolayer (S-alkyne).

Carbon Type	Atom No.	$\Delta\text{BE}(\text{eV})$	Structure
CH <sub>2</sub>	1	-0.02	
CH <sub>2</sub>	2	0.05	
CH <sub>2</sub>	3	0.23	
CH <sub>2</sub>	4	0.66	
C $\equiv$ (-CH <sub>2</sub> )	5	-0.24	
C $\equiv$ C	6	-0.69	
CH <sub>2</sub>	7	-0.05	
CH <sub>2</sub>	8	-0.07	
CH <sub>2</sub>	9	-0.07	
CH <sub>2</sub>	10	-0.06	
CH <sub>2</sub>	11	-0.03	
CH <sub>2</sub>	12	0.02	
CH <sub>2</sub>	13	0.17	
CH <sub>2</sub>	14	0.24	
C=C	15	0.04	
=C-(Si)	16	-0.58	

**Table SI-2.** Analysis of the simulated C1s spectra and comparison with experimental data (relative to 285 eV) for alkyne terminated monolayer.

XPS peak	iv	ii	i	iii
Assigned carbons	4	6	16	1-3
Calculated (average) $\Delta$ BE(eV)	0.66	-0.69	-0.58	0.09
Experimental BE(eV)	286.2	-	283.5	285.00
Experimental $\Delta$ BE(eV)	1.2	-	-1.4	0.00

### A.3.2 Thioacetic acid terminated Monolayer (S-3)

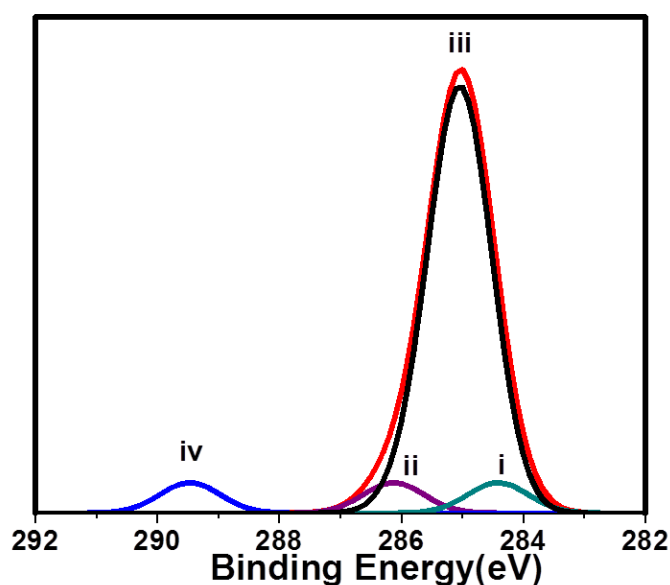


**Figure SI-9.** Simulated core level C1s XPS-spectra for thioacetic acid terminated monolayer. Simulation data was calculated based on DFT calculations of the C1s core level energies for the thioacetic acid capped with a  $(\text{SiCH}_3)_3\text{Si-}$  group except for silicon bound carbon atom. The binding energy of Si bound carbon atom was calculated with  $\text{Si}_3$  structure with central Si-H centre, which was appended with four TMS groups. The spectra has been divided into different coloured curves based on the assigned numbers i-iv (which are shown in Table SI- 4) for different carbon atoms.

**Table SI-3.** Calculated  $\Delta BE$  of carbon atoms in thioacetic acid terminated monolayer (**S-3**).

Carbon Type	Atom No.	$\Delta BE(eV)$	Structure
CH <sub>2</sub>	1	-0.09	
CH <sub>2</sub>	2	-0.05	
CH <sub>2</sub>	3	0.06	
CH <sub>2</sub>	4	0.21	
C= (-CH <sub>2</sub> )	5	0.19	
C= (-S)	6	1.99	
CH <sub>2</sub>	7	-0.11	
CH <sub>2</sub>	8	-0.11	
CH <sub>2</sub>	9	-0.11	
CH <sub>2</sub>	10	-0.08	
CH <sub>2</sub>	11	-0.05	
CH <sub>2</sub>	12	0.01	
CH <sub>2</sub>	13	0.16	
CH <sub>2</sub>	14	0.23	
C=C	15	0.04	
C=C-(Si)	16	-0.58	
C=O	22	4.46	
CH <sub>3</sub>	23	0.64	

**Table SI-4.** Analysis of the simulated C1s spectra and comparison with experimental data (relative to 285 eV) for thioacetic acid terminated monolayer (**S-3**).

XPS peak	iv	ii	i	iii
Assigned carbons	22	6	16	1-5 7-15 23
Calculated (average) $\Delta BE(eV)$	4.46	1.99	-0.58	0.06 0.00 0.64
Experimental BE(eV)	288.5	286.5	283.7	285.00
Experimental $\Delta BE(eV)$	3.50	1.50	-1.30	0.00

### A.3.3 Thioglycolic acid terminated Monolayer (S-5)

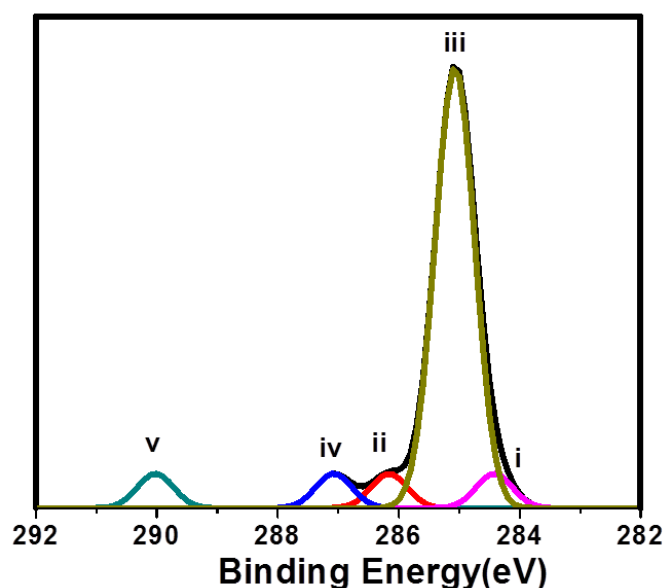


**Figure SI-10.** Simulated core level C1s XPS-spectra for thioglycolic acid terminated monolayer. Simulation data was calculated based on DFT calculations of the C1s core level energies for the thioglycolic acid capped with a  $(\text{SiCH}_3)_3\text{Si}$ - group except for silicon bound carbon atom. The binding energy of Si bound carbon atom was calculated with  $\text{Si}_3$  structure with central Si-H centre, which was appended with four TMS groups. The spectra has been divided into different coloured curves based on the assigned numbers i-v (which are shown in Table SI-6) for different carbon atoms.

**Table SI-5.** Calculated  $\Delta\text{BE}$  of carbon atoms in thioglycolic acid terminated monolayer (S-5).

Carbon Type	Atom No.	$\Delta\text{BE}(\text{eV})$	Structure
CH <sub>2</sub>	1	-0.01	
CH <sub>2</sub>	2	0.03	
CH <sub>2</sub>	3	0.16	
CH <sub>2</sub>	4	0.29	
C= (-CH <sub>2</sub> )	5	0.26	
C= (-S)	6	1.16	
CH <sub>2</sub>	7	-0.04	
CH <sub>2</sub>	8	-0.06	
CH <sub>2</sub>	9	-0.06	
CH <sub>2</sub>	10	-0.04	
CH <sub>2</sub>	11	-0.01	
CH <sub>2</sub>	12	0.04	
CH <sub>2</sub>	13	0.19	
CH <sub>2</sub>	14	0.26	
C=C	15	0.05	
C=C-(Si)	16	-0.58	
CH <sub>2</sub> ( -S)	22	2.07	
C=O	23	5.02	

**Table SI-6.** Analysis of the simulated C1s spectra and comparison with experimental data (relative to 285 eV) for thioglycolic acid terminated monolayer (S-5).

XPS peak	v	iv	ii	i	iii	
Assigned carbons	23	22	6	16	1-5	7-15
Calculated (average) $\Delta$ BE(eV)	5.06	2.07	1.16	-0.58	0.14	0.03
Experimental BE(eV)	289.30	287.0	286.15	283.69	285.00	
Experimental $\Delta$ BE(eV)	4.30	2.00	1.15	-1.31	0.00	

### A.3.4 Thioglucose terminated Monolayer (S-2)

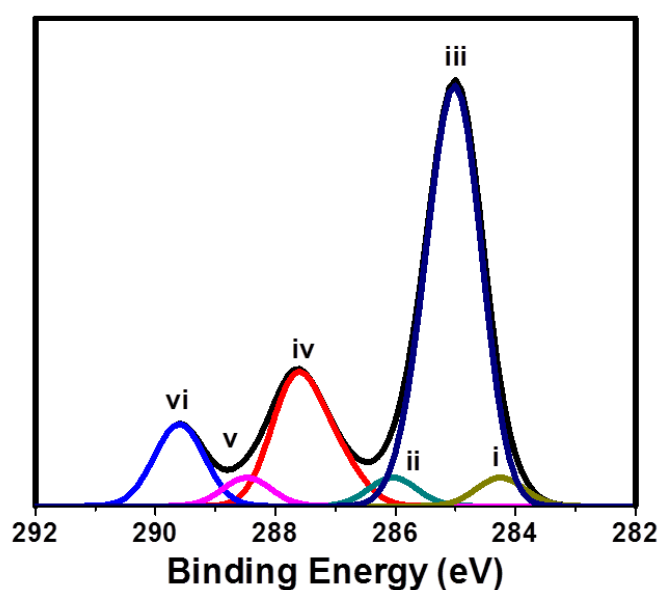


**Figure SI-11.** Simulated core level C1s XPS-spectra for thioglucose terminated monolayer. Simulation data was calculated based on DFT calculations of the C1s core level energies for the thioglucose capped with a  $(\text{SiCH}_3)_3\text{Si-}$  group except for silicon bound carbon atom. The binding energy of Si bound carbon atom was calculated with  $\text{Si}_3$  structure with central Si-H centre, which was appended with four TMS groups. The spectra has been divided into different coloured curves based on the assigned numbers i-vi (which are shown in Table SI-8) for different carbon atoms.

**Table SI-7.** Calculated  $\Delta BE$  of carbon atoms in thioglucose terminated monolayer (S-2)

Carbon Type	Atom No.	$\Delta BE(eV)$	Structure
CH <sub>2</sub>	1	-0.11	
CH <sub>2</sub>	2	-0.06	
CH <sub>2</sub>	3	0.06	
CH <sub>2</sub>	4	0.20	
C= (-CH <sub>2</sub> )	5	0.19	
C= (-S)	6	1.04	
CH <sub>2</sub>	7	-0.15	
CH <sub>2</sub>	8	-0.17	
CH <sub>2</sub>	9	-0.18	
CH <sub>2</sub>	10	-0.17	
CH <sub>2</sub>	11	-0.14	
CH <sub>2</sub>	12	-0.08	
CH <sub>2</sub>	13	0.05	
CH <sub>2</sub>	14	0.12	
C=C	15	-0.11	
C=C-(Si)	16	-0.75	
CH <sub>2</sub> ( sugar)	22	2.64	
CH <sub>2</sub> ( sugar)	23	2.74	
CH <sub>2</sub> ( sugar)	24	2.74	
CH <sub>2</sub> ( sugar)	25	3.47	
CH <sub>2</sub> ( sugar)	27	2.66	
CH <sub>2</sub> (-O)	29	2.23	
C=O	32	4.50	
-CH <sub>3</sub>	33	0.44	
C=O	35	4.77	
-CH <sub>3</sub>	36	0.54	
C=O	38	4.52	
-CH <sub>3</sub>	40	0.41	
-CH <sub>3</sub> ( -O)	42	1.87	

**Table SI-8.** Analysis of the simulated C1s spectra and comparison with experimental data (relative to 285 eV) for thioglucose terminated monolayer.

XPS peak	vi	v	iv	ii	i	iii
Assigned carbons	32,35,38	25	22-24,27,29,42	6	16	1-15 33,36,40
Calculated (average) $\Delta BE(eV)$	4.60	3.47	2.48	1.06	-0.75	-0.05 0.47
Experimental BE(eV)	289.89	-	287.50	286.39	283.61	285.00
Experimental $\Delta BE(eV)$	4.89	-	2.5	1.39	-1.39	0.00

### A.3.5 Thioglycerol terminated Monolayer (S-4)

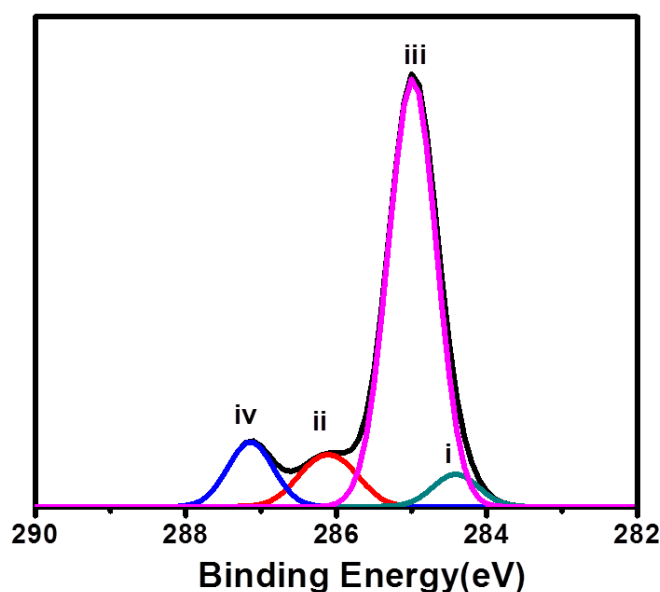


**Figure SI-12.** Simulated core level C 1s XPS-spectra for thioglycerol terminated monolayer. Simulation data was calculated based on DFT calculations of the C 1s core level energies for the thioglycerol capped with a  $(\text{SiCH}_3)_3\text{Si-}$  group except for silicon bound carbon atom. The binding energy of Si bound carbon atom was calculated with  $\text{Si}_3$  structure with central Si-H centre, which was appended with four TMS groups. The spectra has been divided into different coloured curves based on the assigned numbers i-iv (which are shown in Table SI-10) for different carbon atoms.

**Table SI-9.** Calculated  $\Delta\text{BE}$  of carbon atoms in thioglycerol terminated monolayer (S-4)

Carbon Type	Atom No.	$\Delta\text{BE}(\text{eV})$	Structure
CH2	1	-0.11	
CH2	2	0.07	
CH2	3	0.00	
CH2	4	0.12	
C= (-CH2)	5	-0.02	
C= (-S)	6	0.90	
CH2	7	-0.11	
CH2	8	-0.12	
CH2	9	-0.11	
CH2	10	-0.08	
CH2	11	-0.05	
CH2	12	0.01	
CH2	13	0.16	
CH2	14	0.23	
C=C	15	0.04	
C=C-(Si)	16	-0.58	
CH2 ( -S)	22	1.30	
CH2 (-O)	23	2.12	
CH2 (-O)	25	2.15	

**Table SI-10.** Analysis of the simulated C1s spectra and comparison with experimental data (relative to 285 eV) for thioglycerol terminated monolayer (S-4).

XPS peak	iv	ii	i	iii	
Assigned carbons	23,25	6,22	16	1-5	7-15
Calculated (average) $\Delta$ BE(eV)	2.13	1.10	-0.58	-0.01	0.00
Experimental BE(eV)	287.06	285.98	283.59	285.00	
Experimental $\Delta$ BE(eV)	2.06	0.98	-1.41	0.0	

### A.3.6 Fmoc-Cysteine terminated Monolayer (S-1)

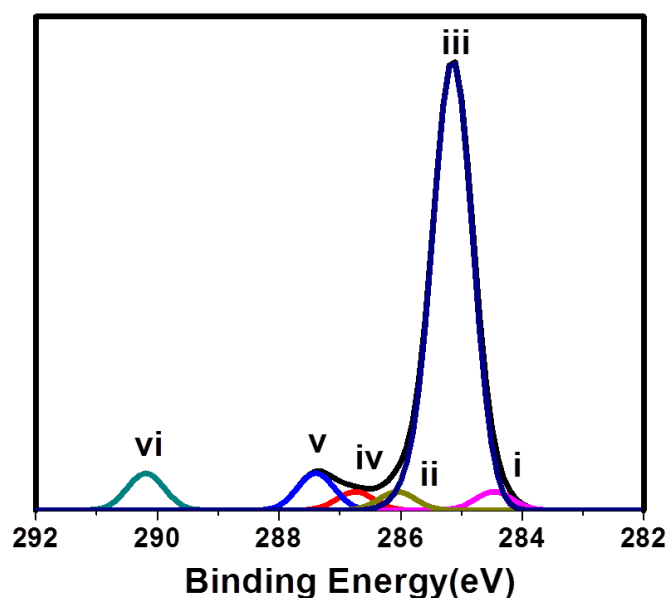


**Figure SI-13.** Simulated core level C 1s XPS-spectra for Fmoc-Cysteine terminated monolayer. Simulation data was calculated based on DFT calculations of the C 1s core level energies for the Fmoc-Cysteine capped with a  $(\text{SiCH}_3)_3\text{Si}$ - group except for silicon bound carbon atom. The binding energy of Si bound carbon atom was calculated with  $\text{Si}_3$  structure with central Si-H centre, which was appended with four TMS groups. The spectra has been divided into different coloured curves based on the assigned numbers i-vi (which are shown in Table SI-12) for different carbon atoms.



**Table SI-11.** Calculated  $\Delta BE$  of carbon atoms in Fmoc-Cysteine terminated monolayer (S-1)

Carbon Type	Atom No.	$\Delta BE(eV)$	Structure
CH <sub>2</sub>	1	-0.10	
CH <sub>2</sub>	2	-0.05	
CH <sub>2</sub>	3	0.05	
CH <sub>2</sub>	4	0.19	
C= (-CH <sub>2</sub> )	5	0.00	
C= (-S)	6	1.28	
CH <sub>2</sub>	7	-0.12	
CH <sub>2</sub>	8	-0.14	
CH <sub>2</sub>	9	-0.13	
CH <sub>2</sub>	10	-0.11	
CH <sub>2</sub>	11	-0.08	
CH <sub>2</sub>	12	-0.01	
CH <sub>2</sub>	13	0.09	
CH <sub>2</sub>	14	0.20	
C=C	15	0.10	
C=C-(Si)	16	-0.53	
CH <sub>2</sub> ( -S)	22	1.92	
CH <sub>2</sub> (-N)	23	2.55	
C=O	25	4.89	
C=O	26	4.67	
CH <sub>2</sub> (-O)	30	2.16	
CH <sub>2</sub>	32	0.45	
Ar-H	33	0.07	
Ar-H	34	-0.25	
Ar-H	35	-0.25	
Ar-H	36	0.08	
Ar-H	37	0.30	
Ar-H	38	0.30	
Ar-H	39	0.28	
Ar-H	40	0.10	
Ar-H	41	0.09	
Ar-H	42	0.28	
Ar-H	43	0.29	
Ar-H	44	0.29	

**Table SI-12.** Analysis of the simulated C1s spectra and comparison with experimental data (relative to 285 eV) for Fmoc-Cysteine terminated monolayer (S-1).

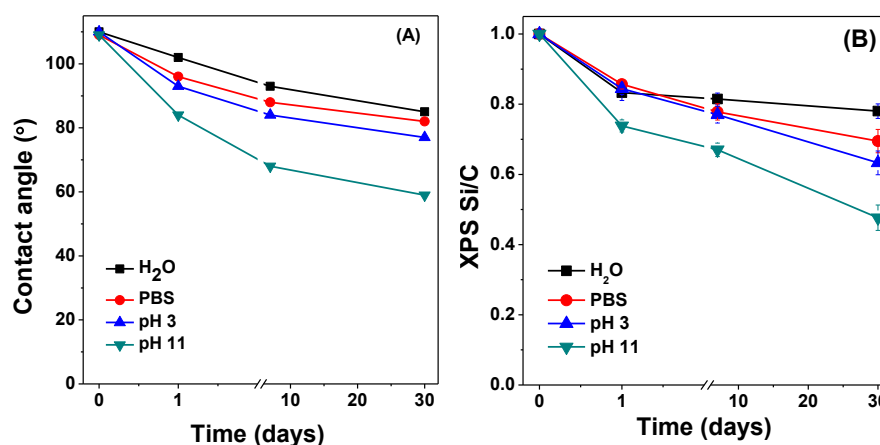
XPS peak	vi	v	iv	ii	i	iii
Assigned carbons	25,26	23,30	22	6	16	1-15 32-44
Calculated (average) $\Delta BE(eV)$	4.78	2.35	1.92	1.28	-0.53	0.00 0.15
Experimental BE(eV)	289.52	288.16	286.67	286.67	283.71	285.00
Experimental $\Delta BE(eV)$	4.52	3.16	1.67	1.67	-1.29	0.00

# Appendix B

## Supporting Information: Chapter 3

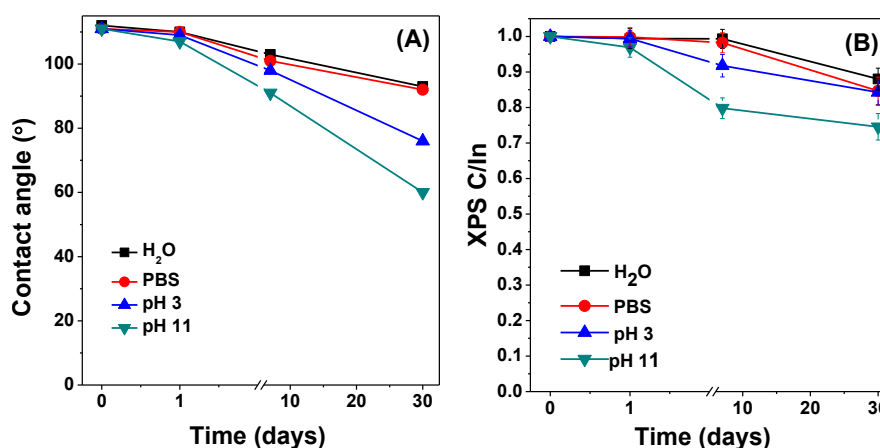
### B.1 Hydrolytic stability

#### B.1.1 1-Octadecyltrichlorosilane on glass ( $\text{SiO}_2$ ) [ $\text{SiO}_2$ -Silane]



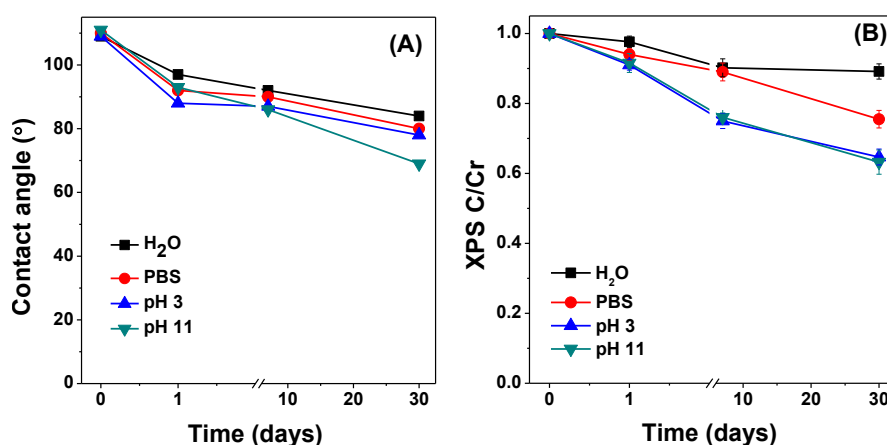
**Figure SI-1.** The stability of  $\text{SiO}_2$ -Silane was followed by static contact angle measurements (A) and normalized C/Si ratio from XPS survey scan (B). Measurements were performed on cleaned surfaces after taking them out from  $\text{H}_2\text{O}$ , PBS, pH 3 and pH 11 solutions at the indicated time period (lines connecting data points are mere guide to eye).

#### B.1.2 1-Octadecylphosphonic acid on hydroxyl-terminated ITO (ITO-PA)



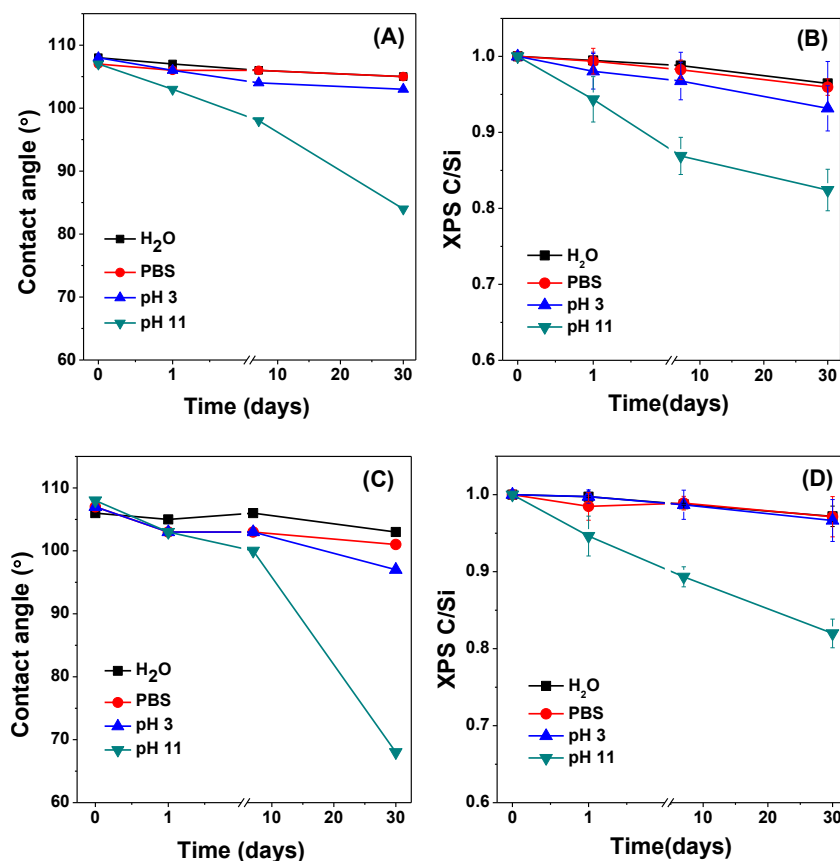
**Figure SI-2.** The stability of ITO-PA was followed by static contact angle measurements (A) and normalized C/In ratio from XPS survey scan (B). Measurements were performed on cleaned surfaces after taking them out from  $\text{H}_2\text{O}$ , PBS, pH 3 and pH 11 solutions at the indicated time period (lines connecting data points are mere guide to eye).

### B.1.3 1-Octadecamine on stainless steel [SS-Amine]



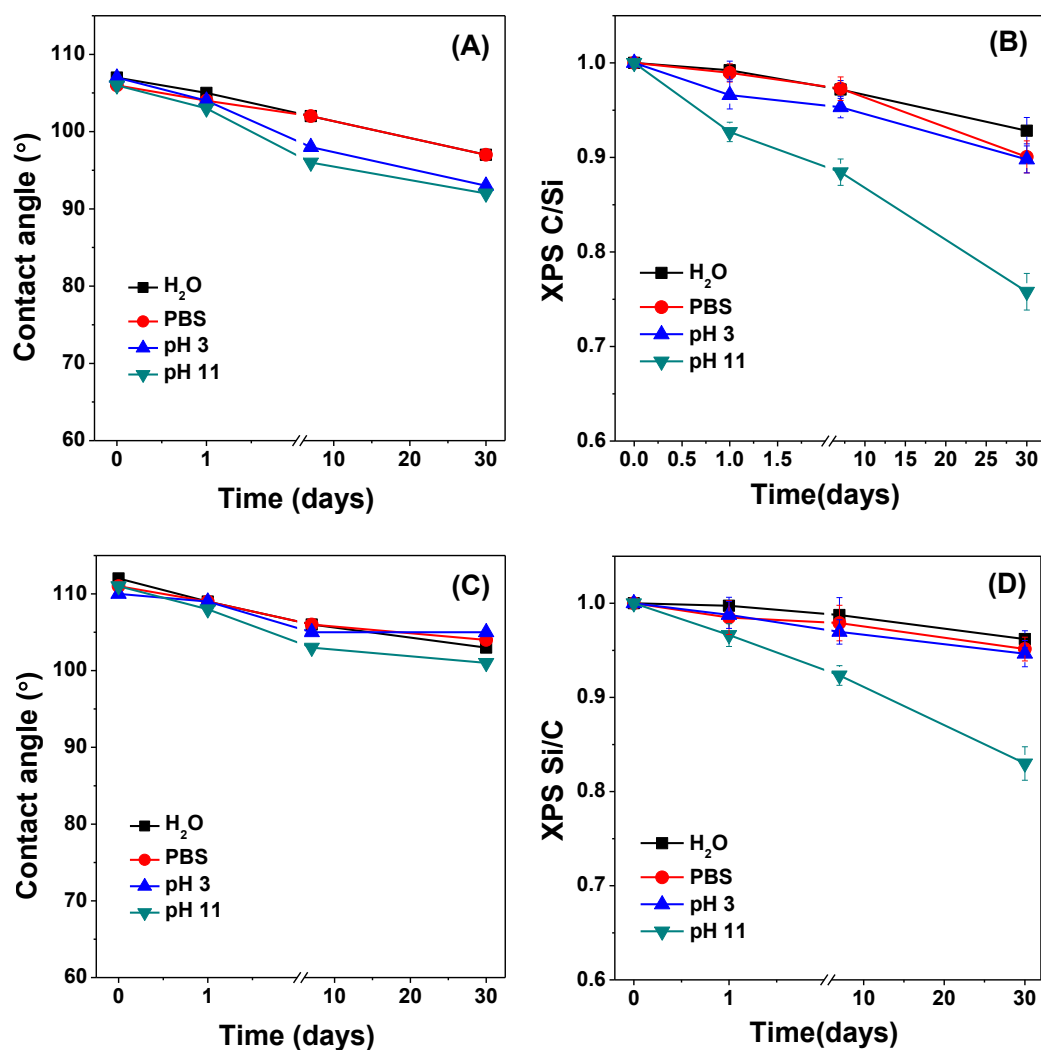
**Figure SI-3.** The stability of SS-Amine was followed by static contact angle measurements (A) normalized C/Cr ratio from XPS survey scan (B). Measurements were performed on cleaned surfaces after taking them out from H<sub>2</sub>O, PBS, pH 3 and pH 11 solutions at the indicated time period (lines connecting data points are mere guide to eye).

### B.1.4 1-Octadecene on hydrogen-terminated Si(111) [Si(111)-Alkene]



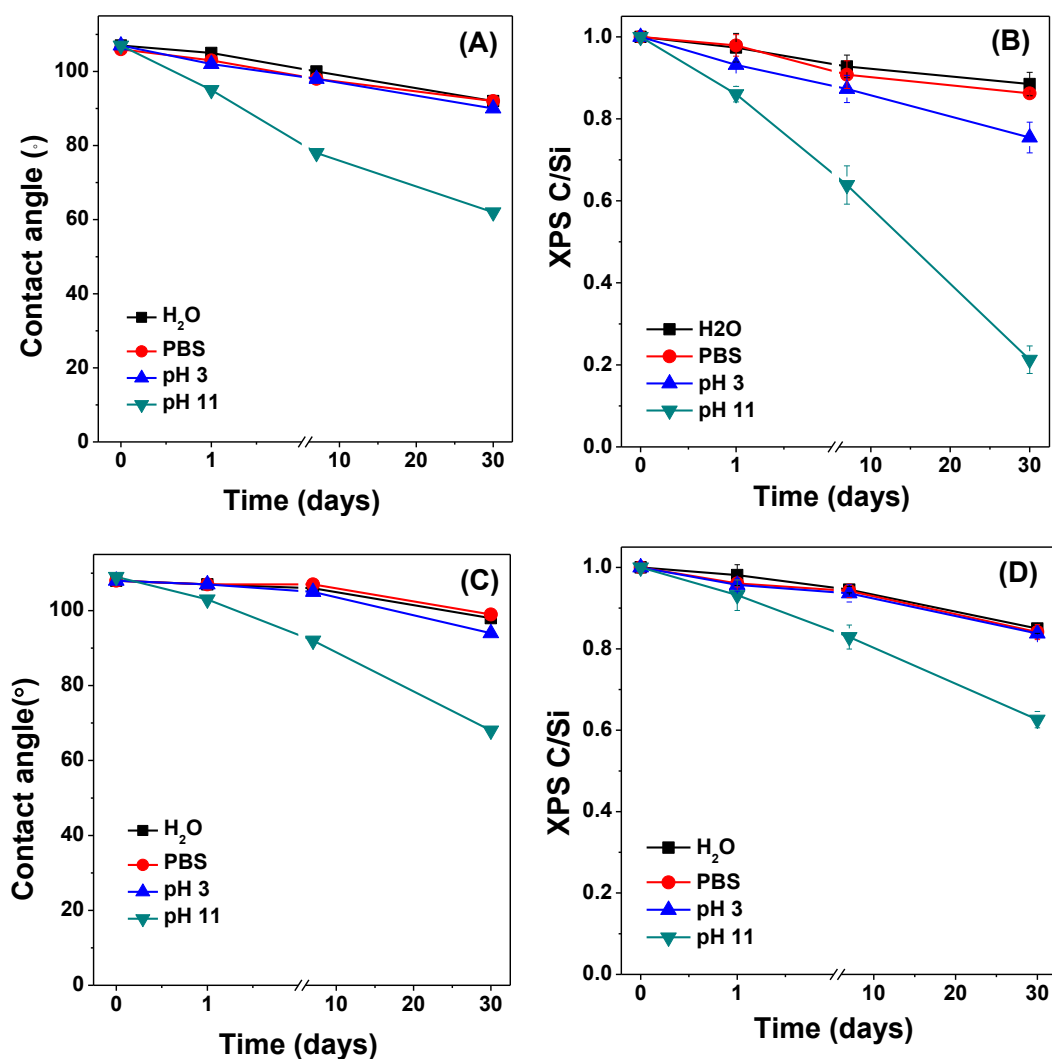
**Figure SI-4.** The stability of Si(111)-Alkene was followed by static contact angle measurements (A, monolayers prepared under thermal conditions and C, monolayer prepared under photochemical conditions) and normalized C/Al ratio from XPS survey scan (B, monolayers prepared under thermal conditions and D, monolayer prepared under photochemical conditions). Measurements were performed on cleaned surfaces after taking them out from H<sub>2</sub>O, PBS, pH 3 and pH 11 at the indicated time period (lines connecting data points are mere guide to eye).

## B.1.5 1-Octadecene on hydrogen-terminated Si(100)[Si(100)-Alkene]



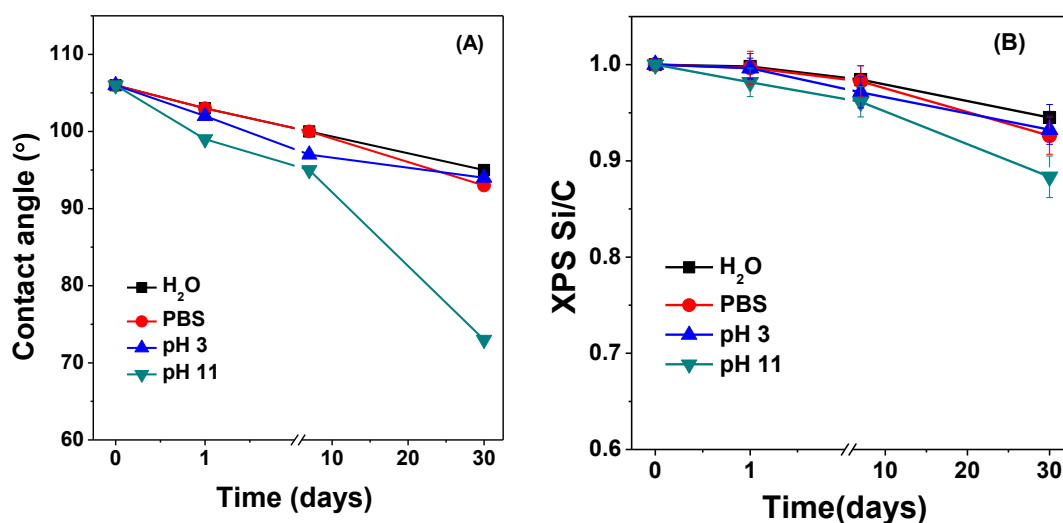
**Figure SI-5.** The stability of Si(100)-Alkene was followed by static contact angle measurements (A, monolayers prepared under thermal conditions and C, monolayer prepared under photochemical conditions) and normalized C/Al ratio from XPS survey scan (B, monolayers prepared under thermal conditions and D, monolayer prepared under photochemical conditions). Measurements were performed on cleaned surfaces after taking them out from H<sub>2</sub>O, PBS, pH 3 and pH 11 at the indicated time period (lines connecting data points are mere guide to eye).

## B.1.6 1-Octadecene on SiN [SiN-Alkene]



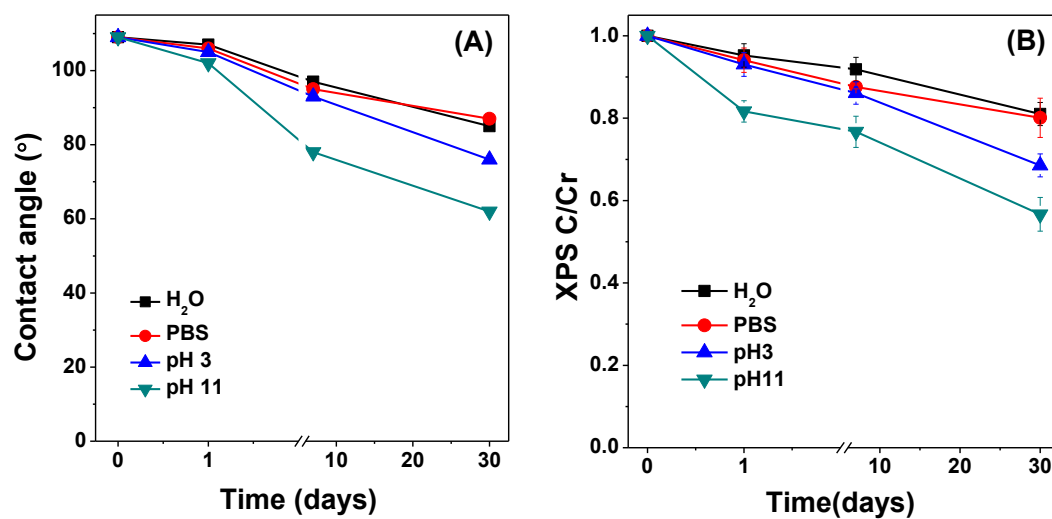
**Figure SI-6.** The stability of SiN-Alkene was followed by static contact angle measurements (A, monolayers prepared under thermal conditions and C, monolayer prepared under photochemical conditions) and normalized C/Si ratio from XPS survey scan (B, monolayers prepared under thermal conditions and D, monolayer prepared under photochemical conditions). Measurements were performed on cleaned surfaces after taking them out from H<sub>2</sub>O, PBS, pH 3 and pH 11 at the indicated time period (lines connecting data points are mere guide to eye).

### B.1.7 1-Octadecene on hydroxyl-terminated SiC [SiC-Alkene]

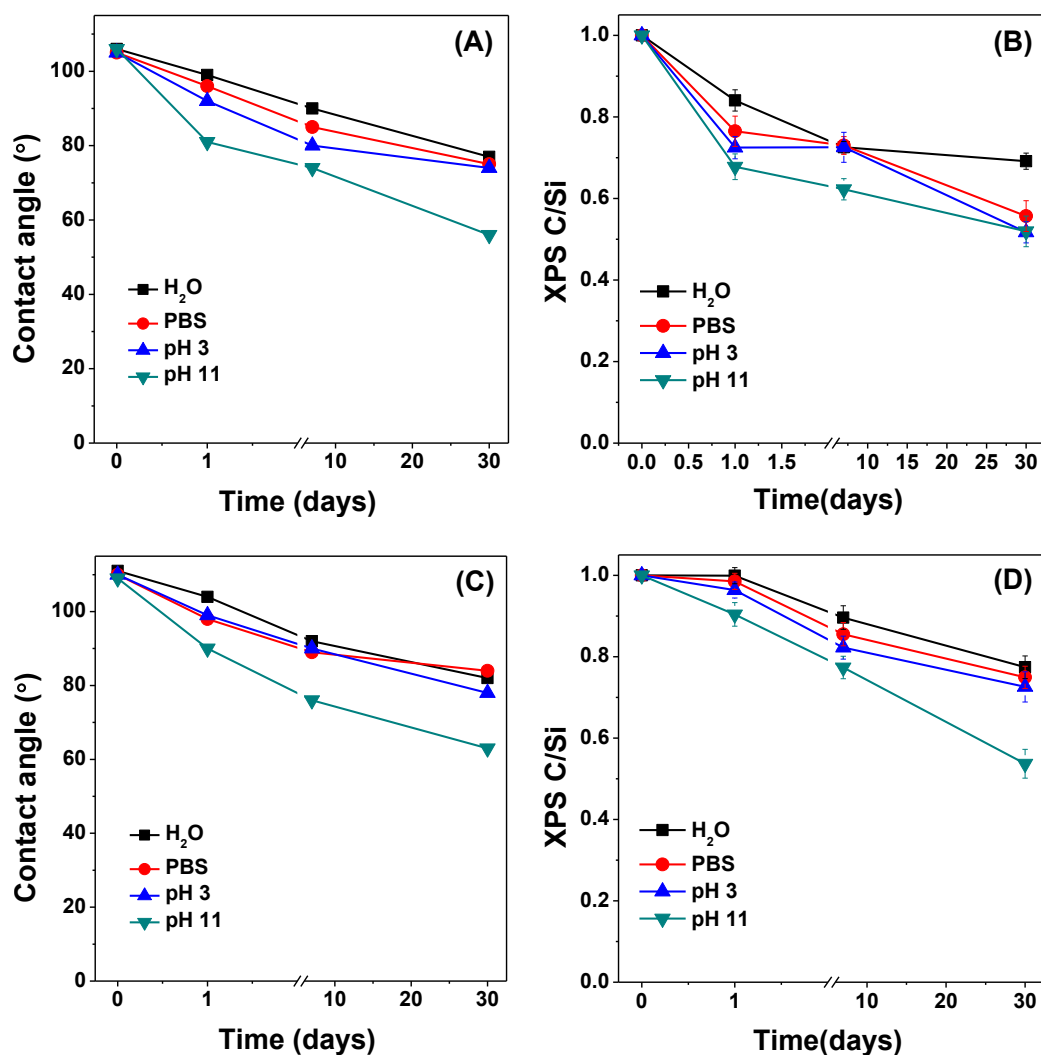


**Figure SI-7.** The stability of SiC-Alkene was followed by static contact angle measurements (A) and normalized C/Si ratio from XPS survey scan (B). Measurements were performed on cleaned surfaces after taking them out from H<sub>2</sub>O, PBS, pH 3 and pH 11 at the indicated time period (lines connecting data points are mere guide to eye).

### B.1.8 1-Octadecene on hydroxyl-terminated CrN [CrN-Alkene]



**Figure SI-8.** The stability of CrN-Alkene was followed by static contact angle measurements (A) and normalized C/Cr ratio from XPS survey scan (B). Measurements were performed on cleaned surfaces after taking them out from H<sub>2</sub>O, PBS, pH 3 and pH 11 at the indicated time period (lines connecting data points are mere guide to eye).

**B.1.9 1-Octadecene on hydroxyl-terminated SiO<sub>2</sub> [SiO<sub>2</sub>-Alkene]**

**Figure SI-9.** The stability of SiO<sub>2</sub>-Alkene was followed by static contact angle measurements (A, monolayers prepared under thermal conditions and C, monolayer prepared under photochemical conditions) and normalized C/Al ratio from XPS survey scan (B, monolayers prepared under thermal conditions and D, monolayer prepared under photochemical conditions). Measurements were performed on cleaned surfaces after taking them out from H<sub>2</sub>O, PBS, pH 3 and pH 11 at the indicated time period (lines connecting data points are mere guide to eye).

### B1.10 1-Octadecene on hydroxyl-terminated ITO (ITO-Alkene)

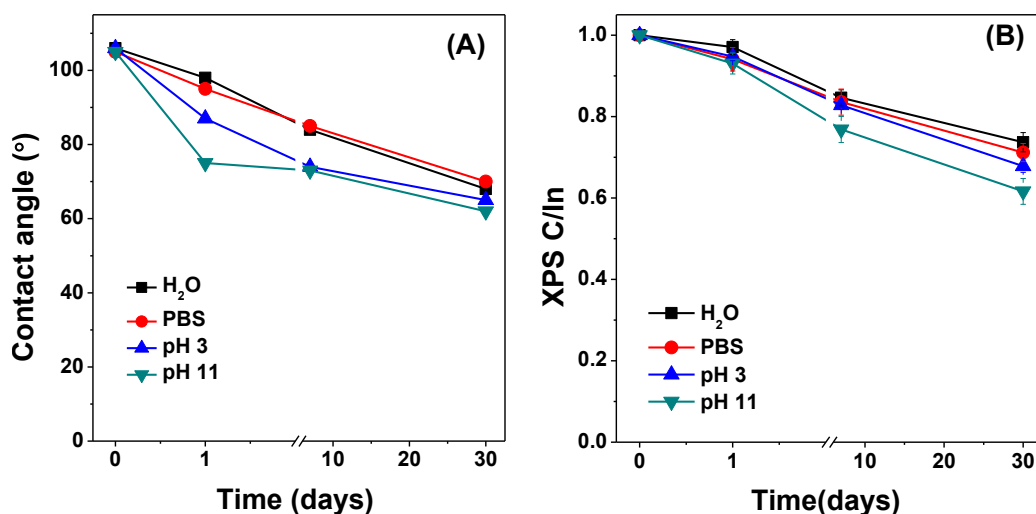


**Figure SI-10.** The stability of ITO-Alkene was followed by static contact angle measurements (A) and normalized C/In ratio from XPS survey scan (B). Measurements were performed on cleaned surfaces after taking them out from H<sub>2</sub>O, PBS, pH 3 and pH 11 solutions at the indicated time period (lines connecting data points are mere guide to eye).

### B.1.11 1-Octadecene on stainless steel (SS) under photochemical conditions [SS-Alkene]

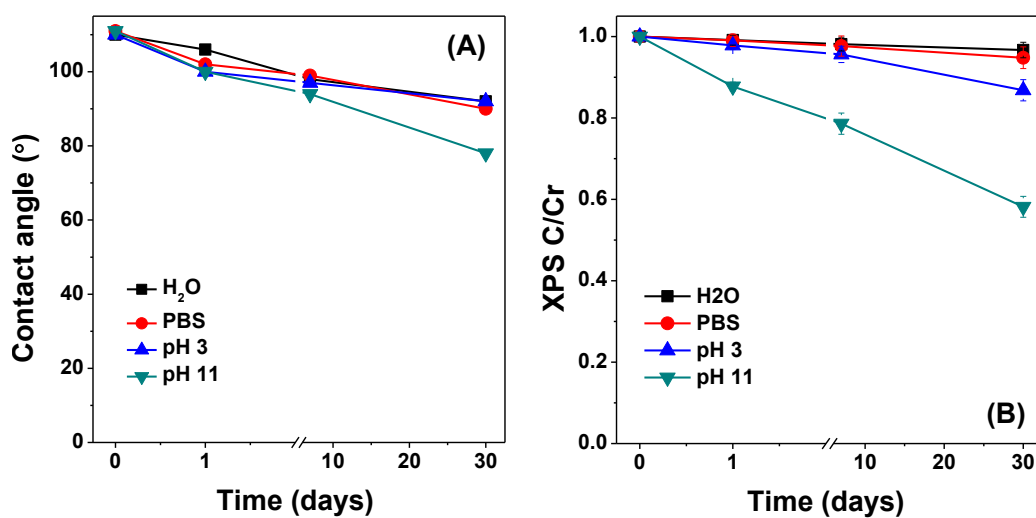


**Figure SI-11.** The stability of SS-Alkene was followed by static contact angle measurements (A) and normalized C/Cr ratio from XPS survey scan (B). Measurements were performed on cleaned surfaces after taking them out from H<sub>2</sub>O, PBS, pH 3 and pH 11 solutions at the indicated interval (lines connecting data points are mere guide to eye).



### B.1.12 1-Octadecyne on hydrogen-terminated Si(111) under photochemical conditions [Si(111)-Alkyne]

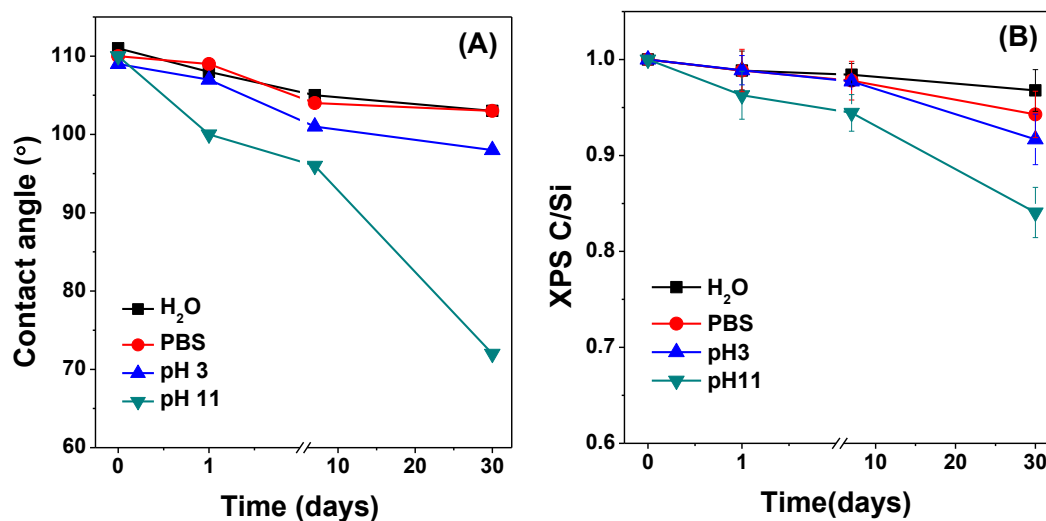


**Figure SI-12.** The stability of Si(111)-Alkyne was followed by static contact angle measurements (A) and normalized C/Si ratio from XPS survey scan (B). Measurements were performed on cleaned surfaces after taking them out from H<sub>2</sub>O, PBS, pH 3 and pH 11 solutions at the indicated interval (lines connecting data points are mere guide to eye).

### B.1.13 1-Octadecyne on hydroxyl-terminated SiC [SiC-Alkyne]

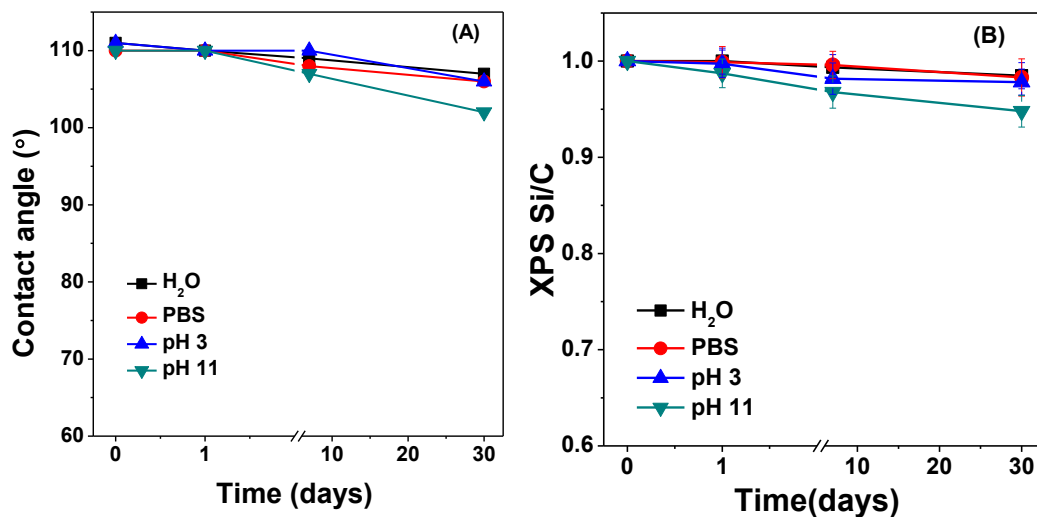


**Figure SI-13.** The stability of SiC-Alkyne was followed by static contact angle measurements (A) and normalized C/Si ratio from XPS survey scan (B). Measurements were performed on cleaned surfaces after taking them out from H<sub>2</sub>O, PBS, pH 3 and pH 11 at the indicated time period (lines connecting data points are guide to eye).

## B.1.14 1-Octadecyne on hydrogen-terminated Si(100) [Si(100)-Alkyne]

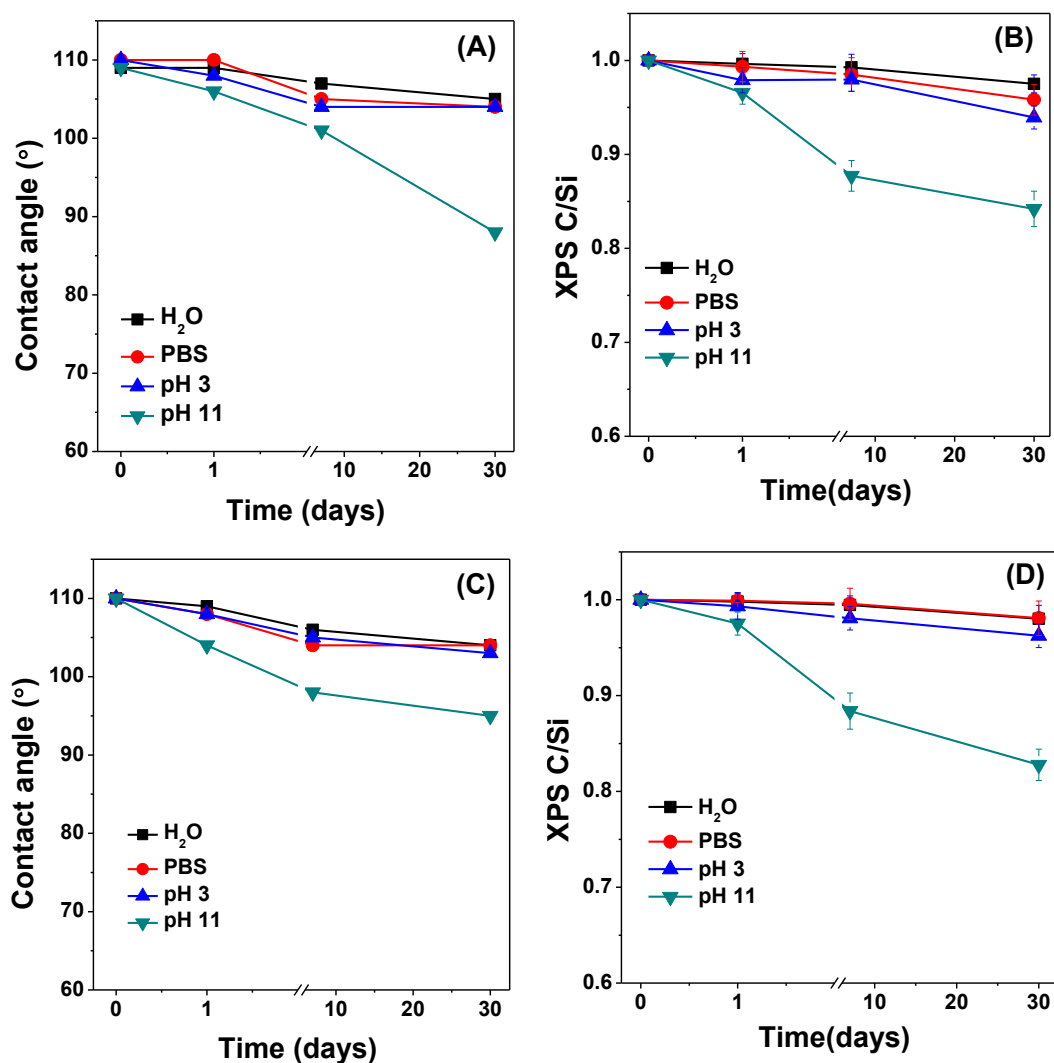


**Figure SI-14.** The stability of Si(100)-Alkyne was followed by static contact angle measurements (A, monolayers prepared under thermal conditions and C, monolayer prepared under photochemical conditions) and normalized C/Si ratio from XPS survey scan (B, monolayers prepared under thermal conditions and D, monolayer prepared under photochemical conditions). Measurements were performed on cleaned surfaces after taking them out from H<sub>2</sub>O, PBS, pH 3 and pH 11 at the indicated time period (lines connecting data points are guide to eye).

### B.1.15 1-Octadecyne on hydroxyl-terminated CrN under thermal conditions [CrN-Alkyne]

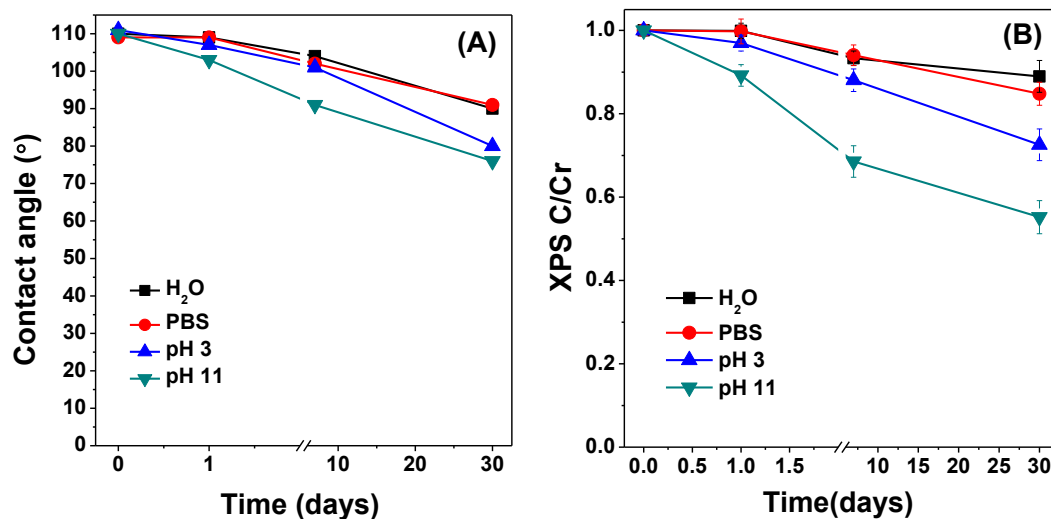


**Figure SI-15.** The stability of CrN-Alkyne was followed by static contact angle measurements (A) normalized C/Cr ratio from XPS survey scan (B). Measurements were performed on cleaned surfaces after taking them out from H<sub>2</sub>O, PBS, pH 3 and pH 11 at the indicated time period (lines connecting data points are guide to eye).

### B. 1.16 1-Octadecyne on hydroxyl-terminated porous aluminium oxide (PAO) [PAO-Alkyne]

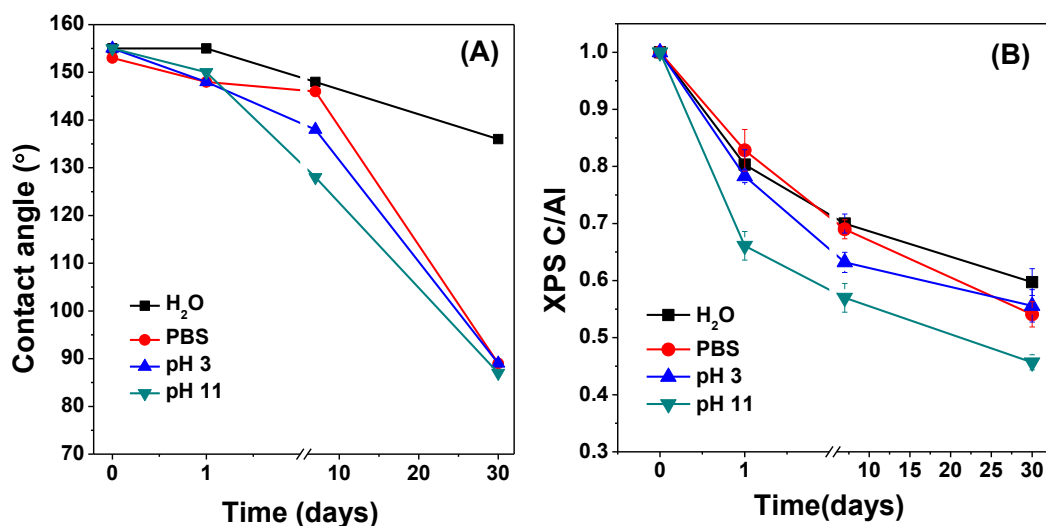


**Figure SI-16.** The stability of PAO-Alkyne was followed by static contact angle measurements (A) and normalized C/Al ratio from XPS survey scan (B). Measurements were performed on cleaned surfaces after taking them out from H<sub>2</sub>O, PBS, pH 3 and pH 11 at the indicated time period (lines connecting data points are mere guide to eye).

### B.1.17 Static water contact angle on PAO-PA and PAO-Alkyne before and after stability tests

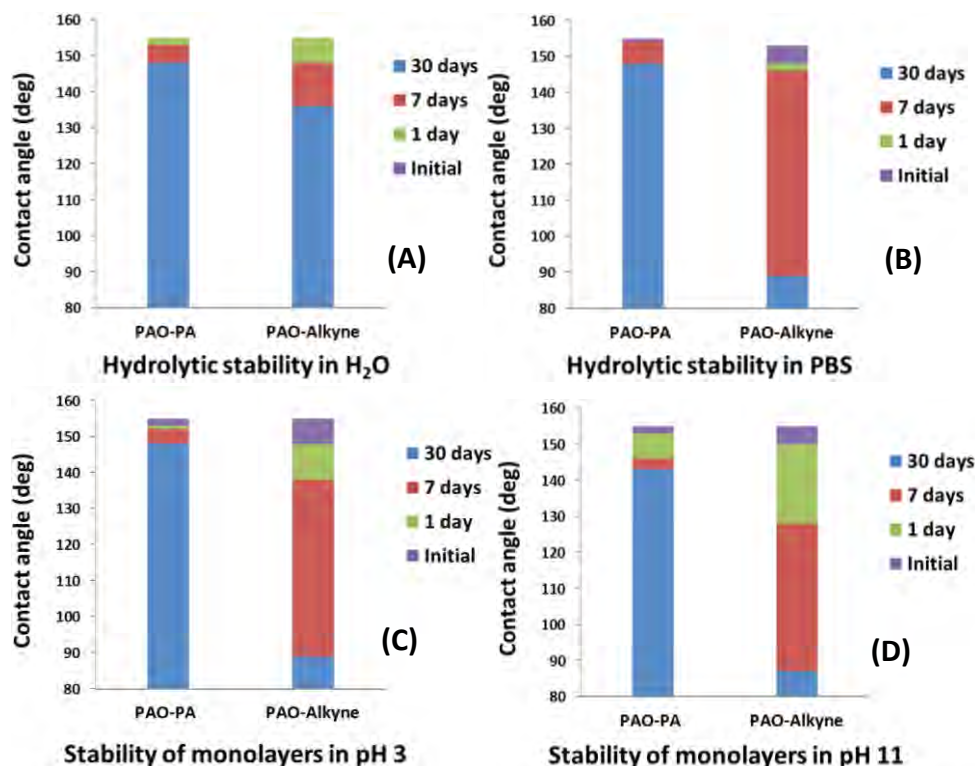


**Figure SI-17.** The hydrolytic stability of monolayers on PAO-PA and PAO-Alkyne were followed by static water contact angle measurements. Measurements were performed on cleaned surfaces after taking them out from H<sub>2</sub>O, PBS, pH 3 and pH 11 at the indicated time period.

## B.2. Thermal stability

### B.2.1 Schematic representation of thermal stability measurements using XPS

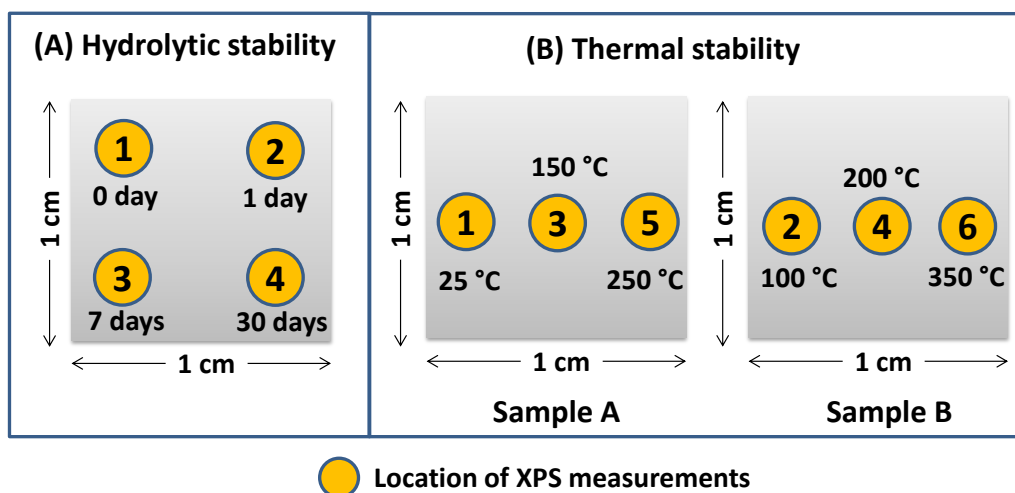


**Figure SI-18.** Schematic representation of XPS measurement locations for hydrolytic stability (A) and thermal stability (B) tests. The XPS was measured on different locations and repeated measurements on same place were avoided to minimize the X-ray induced degradation of monolayers.

## B.2.2 Monolayer desorption followed with XPS

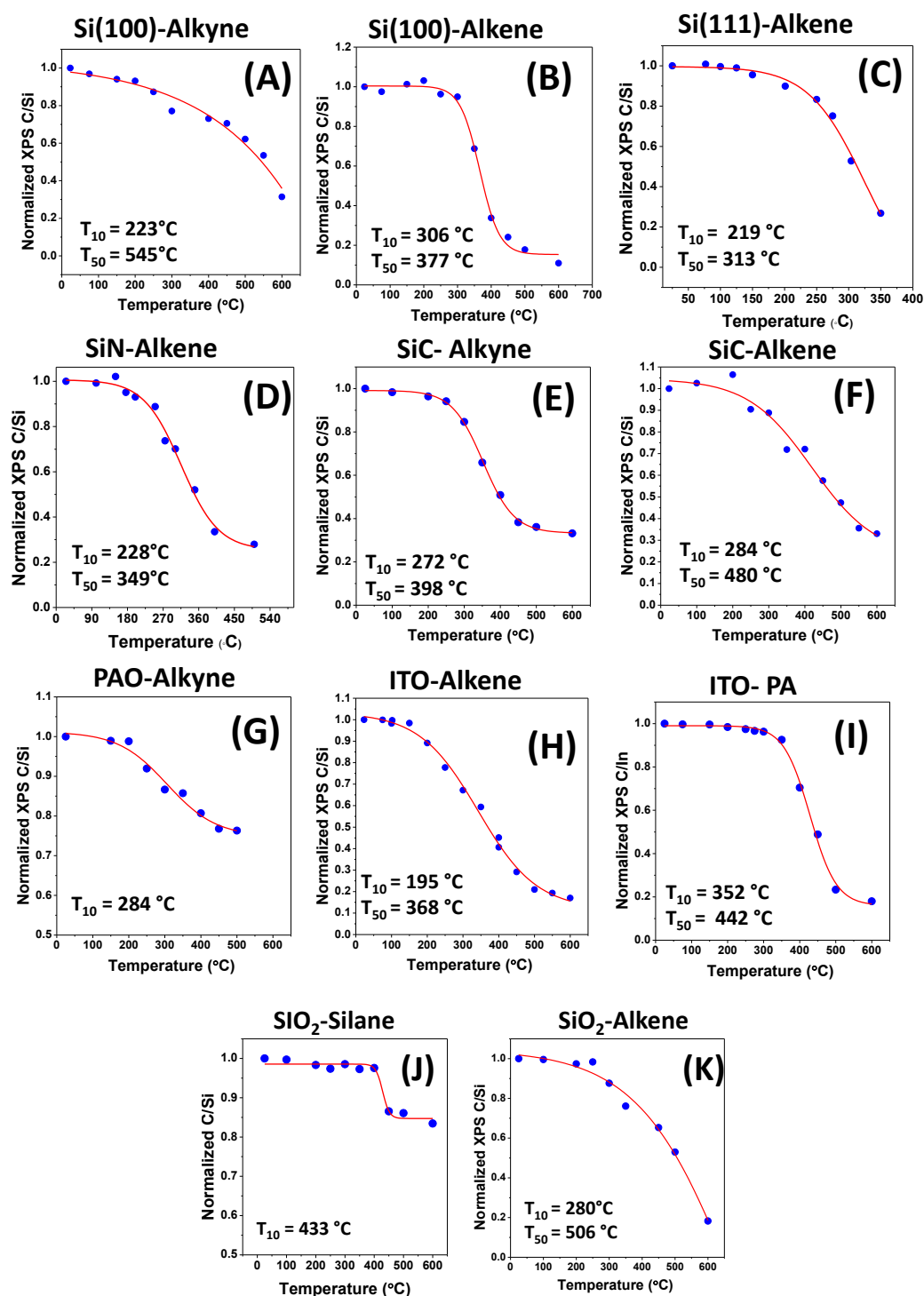


**Figure SI-19.** The normalized XPS data of (A) Si(100)-Alkyne, (B) Si(100)-Alkene, (C) Si(111)-Alkene, (D) SiN-Alkene, (E) SiC-Alkyne, (F) SiC-Alkene, (G) PAO-Alkyne, (H) ITO-Alkene, (I) ITO-PA, (J) SiO<sub>2</sub>-Silane and (K) SiO<sub>2</sub>-Alkene surfaces. The thermal stability was followed by desorption of carbon using XPS equipment provided with a heating control system. The samples were heated to a certain temperature at the rate of 2 °C/min and hold for ~2 minutes for stabilization before the XPS measurement was performed. All carbon desorption points were fitted with a Boltzmann-sigmoidal curve.

### B.2.3 XPS C1s of Si(111)-Alkyne spectra after heating from 25 °C to 600 °C.

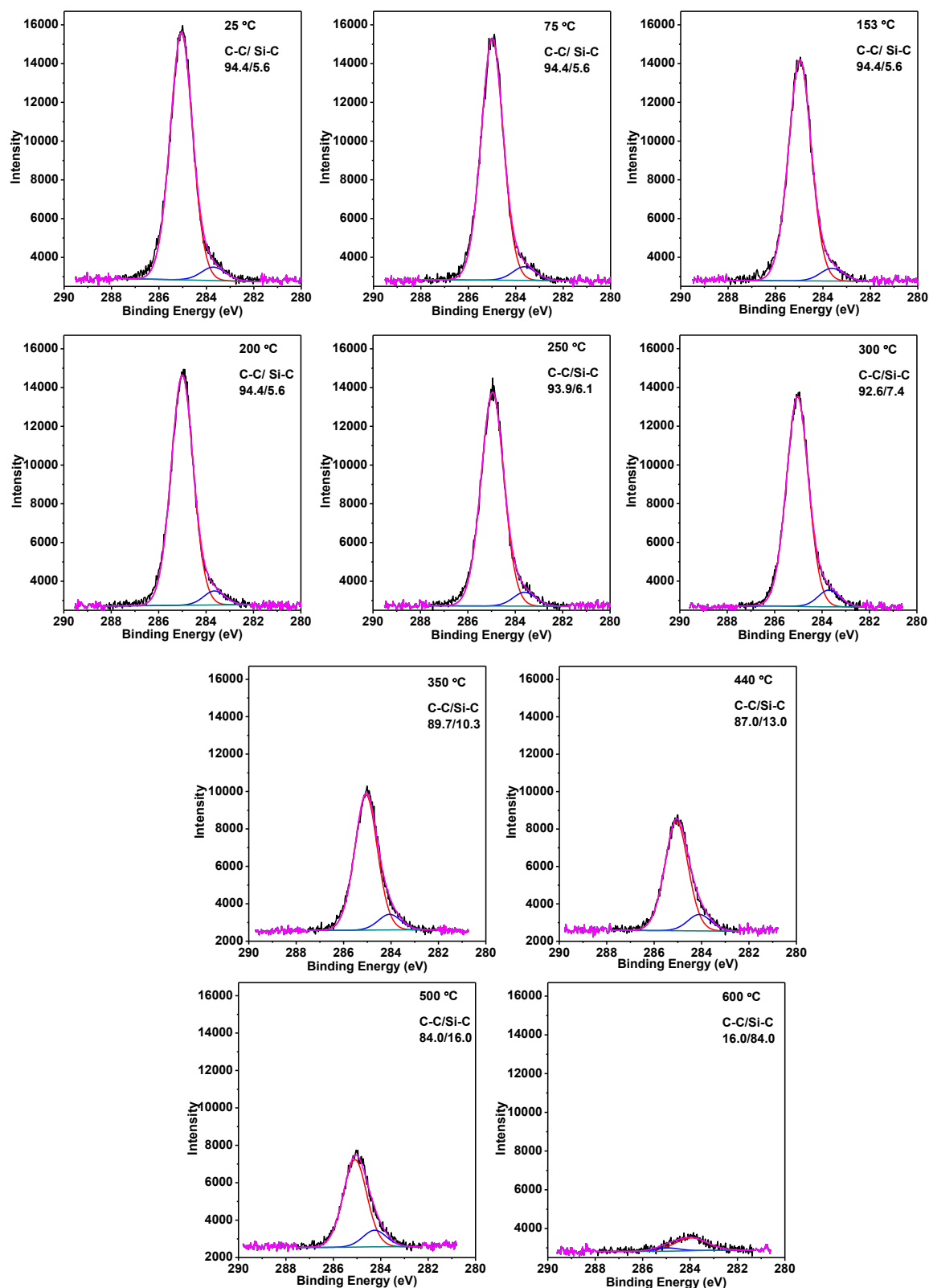


**Figure SI-20.** The XPS C1s spectra showing carbon desorption after samples were heated during XPS measurement from 25 °C to 600 °C. The presence of peak at 284 eV hold indicates Si-C=C bond was intact up 600 °C.



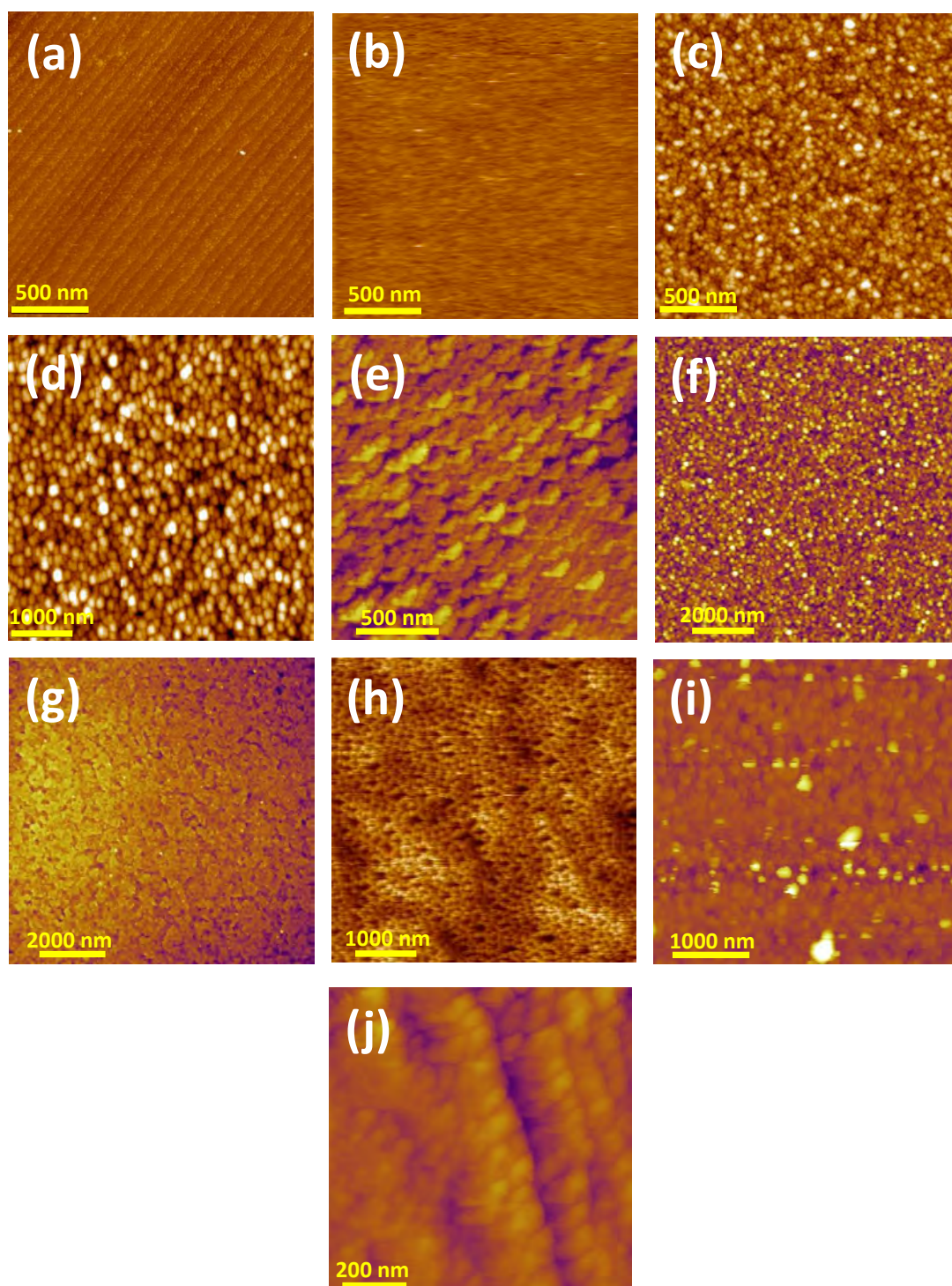


**Figure SI-21.** AFM topographic images of (a) Si(111), root mean square (RMS) roughness = 0.2 nm after etched in 40%  $\text{NH}_4\text{F}$  for 15 min; (b) Si(100), RMS = 0.1 nm after etched in 40%  $\text{NH}_4\text{F}$  for 15 min; (c) SiC, RMS = 2.3 nm after etched in 2.5 HF for 2 min; (d) SiN, RMS = 4.3 nm after etched in 2.5 HF for 2 min; (e)  $\text{SiO}_2$ , RMS = 2.5 after cleaned in air plasma for 10 min; (f) CrN, RMS = 5.0 nm after cleaned in air plasma for 10 min; (g) ITO, RMS = 2.7 nm after cleaned in mixture of 25%  $\text{NH}_4\text{OH}$  and 50%  $\text{H}_2\text{O}_2$  (1:1,v/v), at 90 °C for 60 min; (h) PAO, RMS = 15.0 nm after cleaned in mixture of 37% HCl & methanol (1:1,v/v) for 30 min; (i) Au, RMS = 3.0 nm after cleaned in air plasma (10 min); and (j) Stainless steel, RMS = 2.5 nm in mixture of 20% HCl and 20%  $\text{H}_2\text{SO}_4$ , at 80 °C (30 min).

# Appendix C

## Supporting Information: Chapter 4

### C.1. Custom-made reaction vessel for preparation of polymer brushes with varied thickness

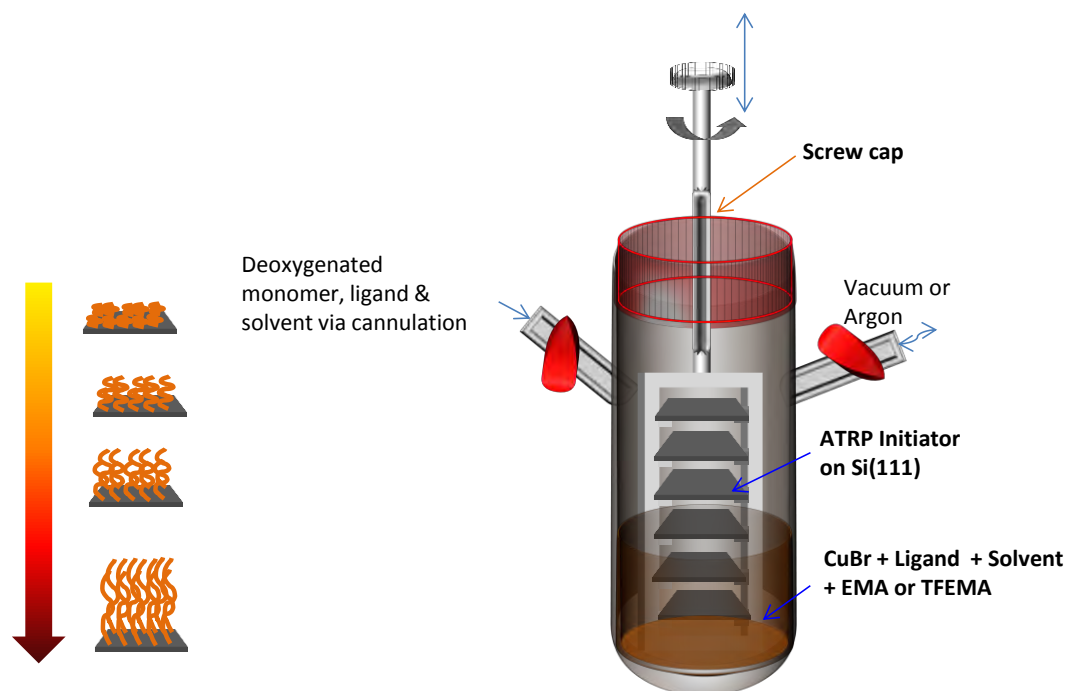


**Figure SI-1.** Schematic representation of custom-made reaction vessel used for preparation of polymer brushes with varied thickness.



## C.2. XPS spectra of modified Si(111)

### C.2.1 XPS spectra of (S2) hydroxyl-terminated monolayer on Si(111)

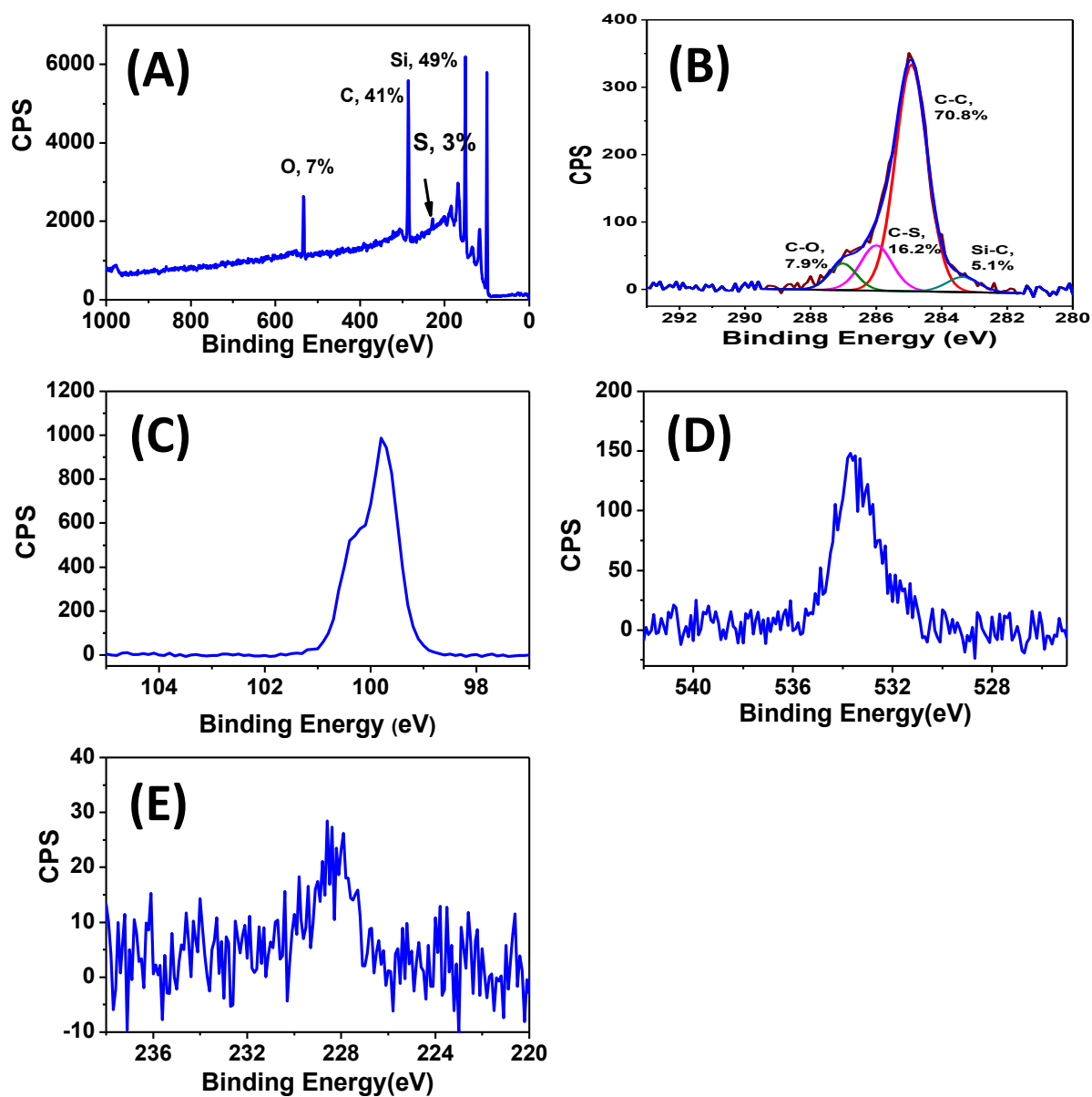


**Figure SI-2.** XPS spectra of Si(111) functionalized with mercaptoethanol (A) survey scan, (B) C1s, (C) Si2p, (D) O1s and (E) S2s.

## C.2.2 XPS spectra of (S3) initiator-terminated Si(111)

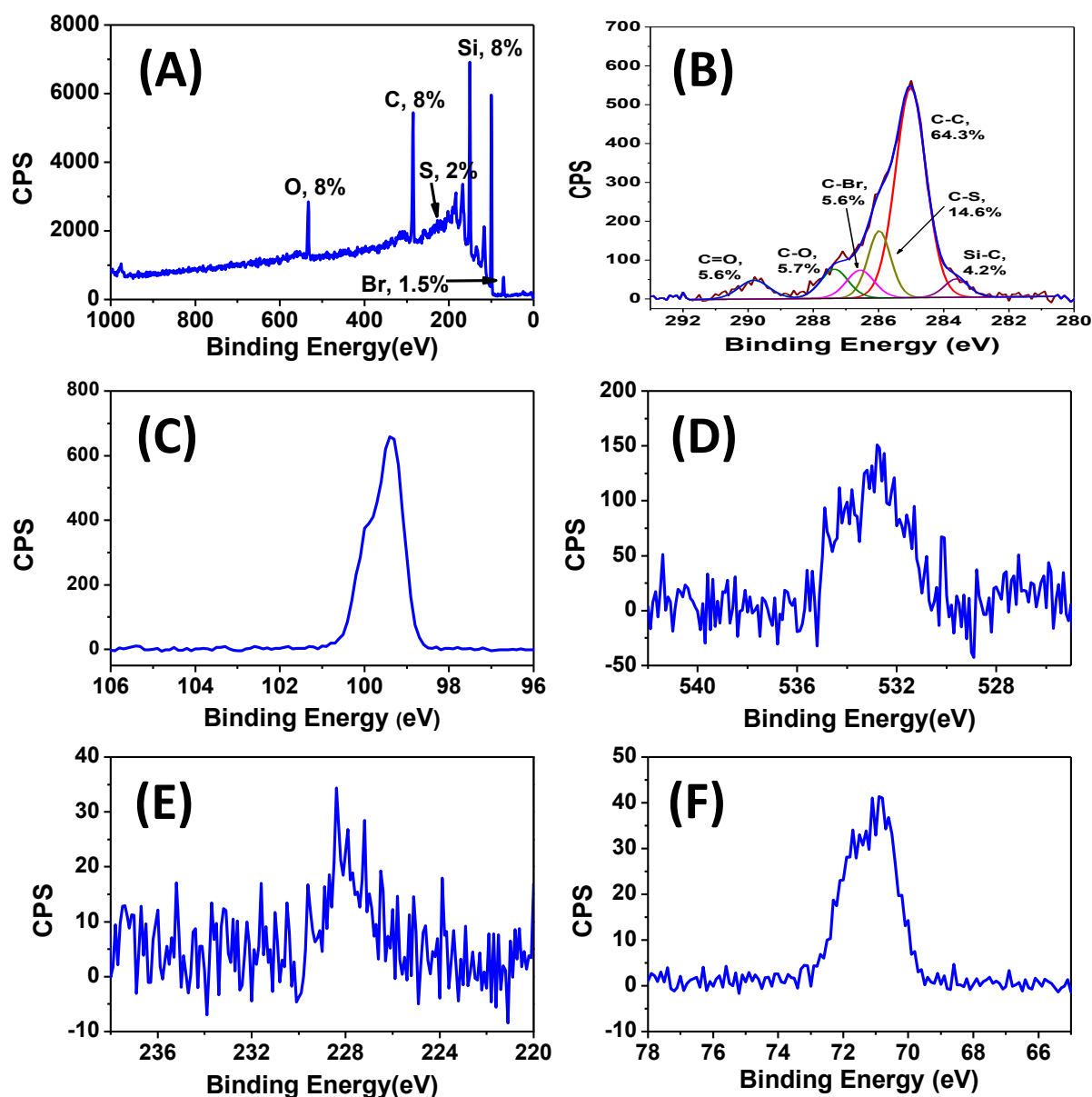


**Figure SI-3.** XPS spectra of ATRP initiator ( $\alpha$ -bromoisobutryl bromide) immobilized on Si(111) surface (S3) (A) survey scan, (B) C1s, (C) Si2p, (D) O1s, (E) S2s and (F) Br3d.

### C.2.3 XPS spectra of (SPF3) poly(2,2,2-trifluoroethyl methacrylate) on Si(111)

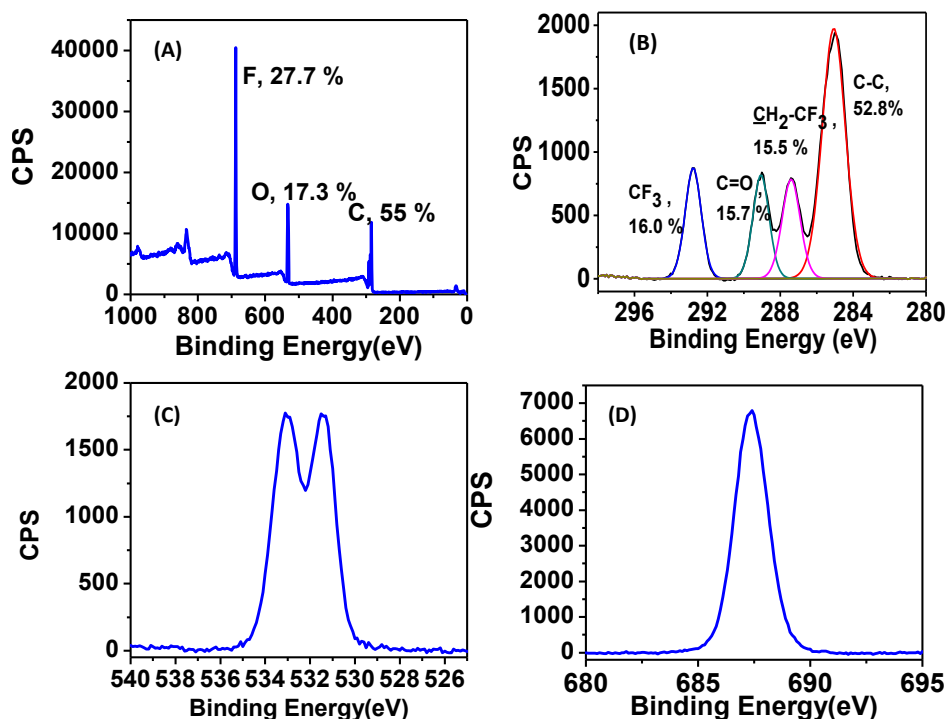


Figure SI-4. XPS spectra of (2,2,2-trifluoroethyl methacrylate) brushes (SPF3) on Si(111) surface (A) survey scan, (B) C1s, (C) O1s, and (D) F1s.

### C.2.4 XPS spectra of (SPF0) poly(ethyl methacrylate) brushes

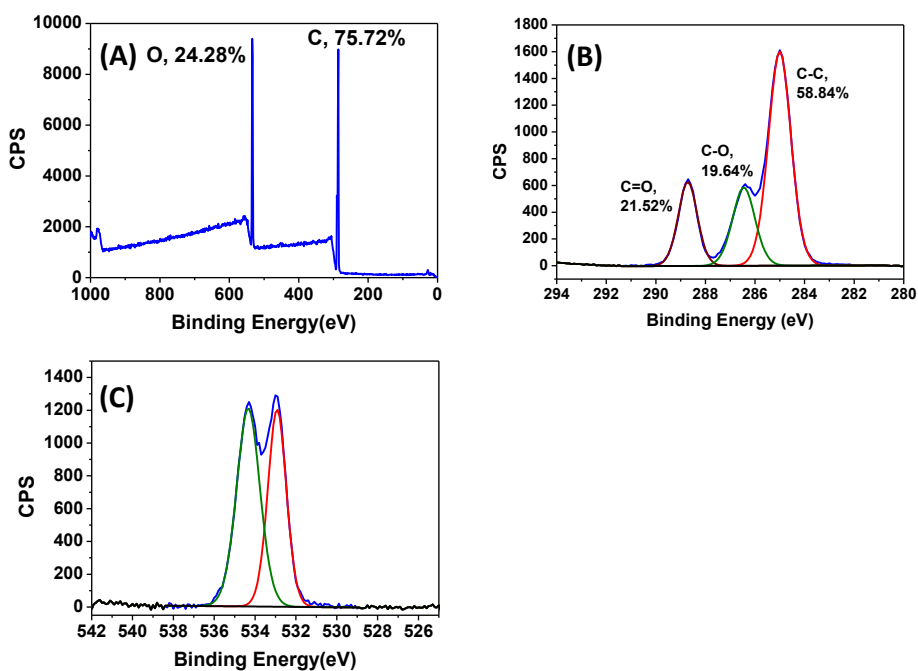


Figure SI-5. XPS spectra of poly(ethyl methacrylate) (SPF0) brushes on Si(111) surface (A) survey scan, (B) C1s and (C) O1s.

### C.3 IRRAS of (SPF3) ) poly(2,2,2-trifluoroethyl methacrylate on Si(111)

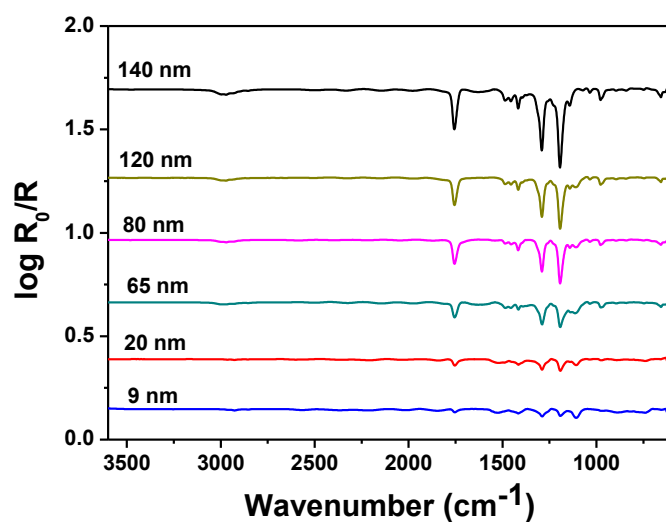


Figure SI-6. IRRAS of polymer brushes (SPF3) with varied thicknesses.

### C.4 Electronic core level calculations

#### C.4.1 Mercaptoethanol-terminated monolayer

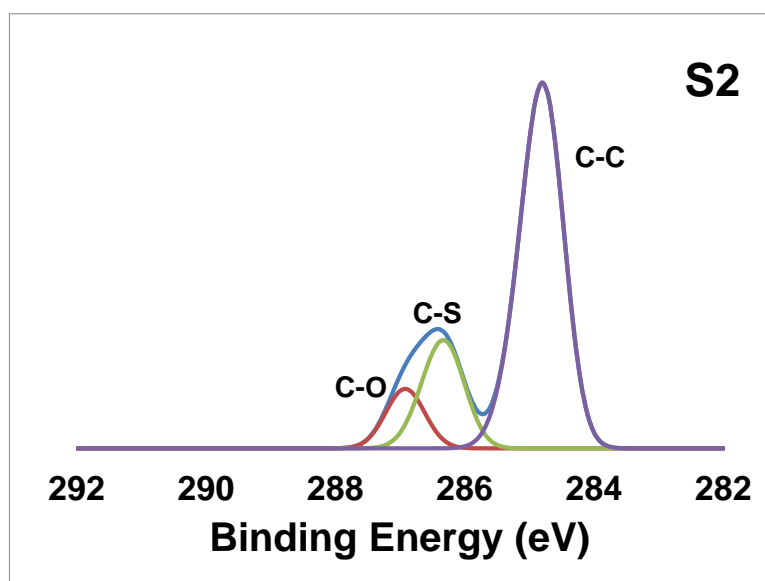


Figure SI-7. DFT-simulated core level C1s XPS-spectra for mercaptoethanol-functionalized (S2) Si(111). The carbon-capped Si surface was represented in this simulation as (SiCH<sub>3</sub>)<sub>3</sub>Si- group.

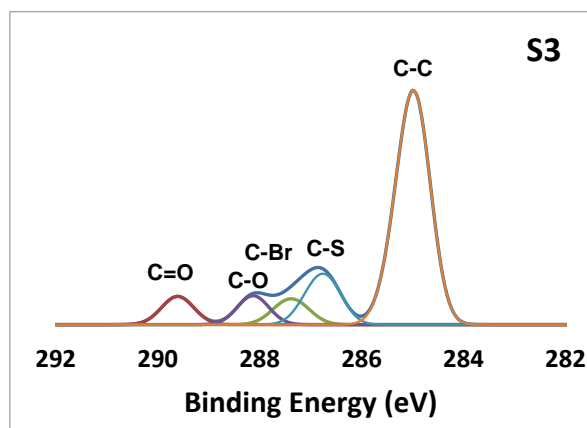
**Table SI-1.** Calculated  $\Delta$ BE of carbon atoms in mercaptoethanol-functionalized Si(111).

Carbon type	Atom number	$\Delta$ BE (eV)	Structure
C-C	1	-0.3	
C-C	2	0.3	
C-C	3	0.1	
C-C	4	0.0	
C-C	5	-0.1	
C-C	6	-0.2	
C-C	7	-0.2	
C-C	8	-0.3	
C-C	9	-0.3	
C-C	10	-0.3	
C-C	11	-0.3	
C-C	12	-0.3	
C-C	13	-0.3	
C-C	14	-0.1	
C-S	15	1.6	
C-S	18	1.2	
C-S	20	1.3	
C-S	21	1.3	
C-O	22	1.9	
C-O	24	1.9	

**Table SI-2.** Analysis of the simulated C1s spectra and comparison with experimental data (relative to 285 eV) for mercaptoethanol-functionalized Si(111).

XPS peak	C-O	C-S	C-C
Assigned carbons	22,24	15-21	1-14
Calculated (average) $\Delta$ BE(eV)	1.9	1.3	-0.2
Experimental BE(eV)	287.0	286.0	285.0
Experimental $\Delta$ BE(eV)	1.0	1.0	0.0

#### C.4.2 Initiator-terminated monolayer ( $\alpha$ -bromoisobutyryl bromide, S3)

**Figure SI-8.** DFT-simulated core level C1s XPS-spectra for initiator-immobilized ( $\alpha$ -bromoisobutyryl bromide, S3) Si(111). The carbon-capped Si surface was represented in this simulation as  $(\text{SiCH}_3)_3\text{Si-}$  group.

**Table SI-3.** Calculated  $\Delta$ BE of carbon atoms on initiator-immobilized ( $\alpha$ -bromoisobutyryl bromide, **S3**) Si(111).

Carbon type	Atom number	$\Delta$ BE (eV)	Structure
C-C	1	-0.2	
C-C	2	0.3	
C-C	3	0.2	
C-C	4	0.1	
C-C	5	-0.0	
C-C	6	-0.1	
C-C	7	-0.1	
C-C	8	-0.1	
C-C	9	-0.1	
C-C	10	-0.1	
C-C	11	-0.1	
C-C	12	-0.0	
C-C	13	0.0	
C-C	14	0.4	
C-S	15	2.0	
C-S	17	1.6	
C-S	19	1.6	
C-S	20	1.8	
C-O	21	2.2	
C-O	23	2.5	
C=O	25	4.7	
C-C	26	3.2	
C-C	27	0.1	
C-C	29	-0.0	
C=O	31	4.5	
C-C	32	3.1	
C-C	34	-0.1	
C-C	35	0.0	

**Table SI-4.** Analysis of the simulated C1s spectra and comparison with experimental data ( relative to 285 eV) for initiator-immobilized ( $\alpha$ -bromoisobutyryl bromide, **S3**) Si(111).

XPS peak	C=O	C-O	C-S	C-C
Assigned carbons	25,31	21,23	15-20	1-14, 26, 27,32-35
Calculated (average) $\Delta$ BE(eV)	4.6	2.4	1.8	0.0
Experimental BE(eV)	289.8	287.3	286.0	285.0
Experimental $\Delta$ BE(eV)	4.8	2.3	0.8	0.0

## C.4.3 SPF0 polymer brushes

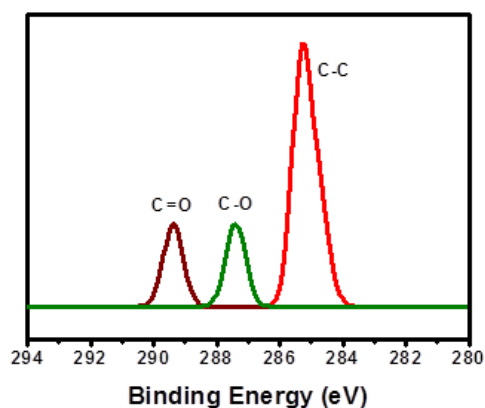


Figure SI-9. Simulated core level C1s XPS-spectrum for SPF0 brushes.

Table SI-5. Calculated  $\Delta$ BE of carbon atoms in SPF0 brushes.

Carbon Type	Atom No.	$\Delta$ BE(eV)
CH <sub>2</sub>	59	0.2
C=O	60	4.4
C-O	62	2.4
CH <sub>3</sub>	63	0.3
CH <sub>2</sub>	64	0.3
CH <sub>3</sub>	68	-0.3

Table SI-6. Analysis of the simulated C1s spectra and comparison with experimental data (relative to 285 eV) for SPF0 brushes.

XPS peak	C=O	C-O	C-C
Assigned carbons	60	62	59,63,64,68
Calculated (average) $\Delta$ BE(eV)	4.4	2.4	0.3
Experimental BE(eV)	288.7	286.4	285.00
Experimental $\Delta$ BE(eV)	4.7	1.4	0.0

## C.4.4 XPS C1s spectrum for SPF3 simulated using electronic core level calculations

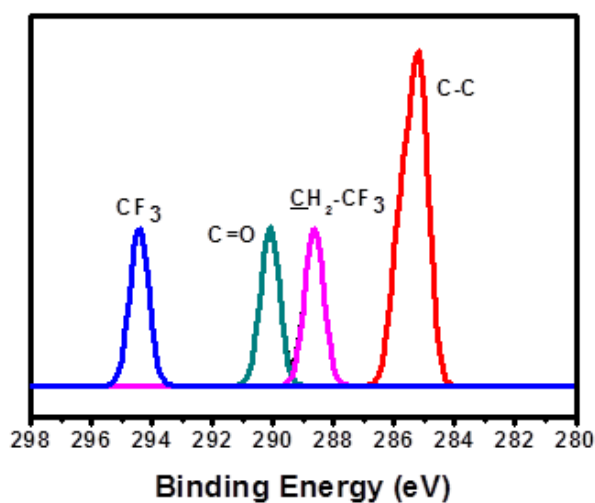


Figure SI-10. Simulated core level C1s XPS-spectrum for SPF3 brushes.

Table SI-7. Calculated  $\Delta BE$  of carbon atoms in SPF3 brushes.

Carbon Type	Atom No.	$\Delta BE(eV)$
CH <sub>2</sub>	59	0.2
C=O	60	5.1
CH <sub>2</sub> -CF <sub>3</sub>	62	3.6
CF <sub>3</sub>	63	9.4
CH <sub>2</sub>	64	0.8
CH <sub>3</sub>	68	-0.1



**Table SI-8.** Analysis of the simulated C1s spectra and comparison with experimental data ( relative to 285 eV) for **SPF3** brushes.

XPS peak	CF <sub>3</sub>	C=O	<u>CH</u> <sub>2</sub> -CF <sub>3</sub>	C-C
Assigned carbons	63	60	62	59,64,68
Calculated (average) ΔBE(eV)	9.4	5.1	3.6	0.3
Experimental BE(eV)	292.7	289.0	287.4	285.00
Experimental ΔBE(eV)	7.7	4.0	2.4	

**Table SI-9.** Surface coverage calculated from XPS C1s percentage area for **S2** and **S3**.

S2 (OH-terminated)					S3 (Initiator-terminated)			
	C-S,C-C, Si-C	C-O	Ratio	Number of Thiols/alkyne	C-O, C-Br, C- S, C-C Si-C	C=O	Ratio	Number of initiators/S2
Theor.	18	2	0.111	2.0	26	2	0.077	2
Expt.	92.1	7.9	0.086	1.5	94.4	5.6	0.059	1.5

\*number of initiator per OH-terminated monolayer (S2) e.g. 2 hydroxyl groups per alkyne terminated monolayer as expected from TYC reaction

# Appendix D

## Supporting Information: Chapter 5

### D.1 Experimental and calculated XPS binding energy of polymer brushes.

**Table SI-1.** The expected and experimental elemental composition of **SPF0**, **SPF3**, **SPF7** and **SPF17** polymer brushes derived from XPS survey scan Figure 3.

Polymer Brush		Elements (Atomic %)					C1s ratio			
		C1s	F1s	O1s	$\underline{\text{C}}\text{F}_3$	$\underline{\text{C}}\text{F}_2$	$-\underline{\text{C}}\text{F}_2\underline{\text{C}}\text{F}_2-\underline{\text{C}}\text{H}_2\underline{\text{C}}\text{H}_2-$	$\underline{\text{C}}\text{H}_2\underline{\text{O}}/\underline{\text{C}}\text{F}_2\underline{\text{C}}\text{H}_2$	$\underline{\text{C}}=\underline{\text{O}}$	$\underline{\text{C}}\text{H}-\underline{\text{C}}\text{H}_3$
SPF17	Theor.	42.42	51.51	6.06	1	6	1	2	1	3
	Expt.	43.91	49.93	6.16	1.0 (293.3)	6.1 (291.1)	0.9 289.6	2.0 (285.8/ 286.9)	0.9 (288.5)	3.0 (285.0)
SPF7	Theor.	47.04	41.16	11.76	1	2	-	1	1	3
	Expt.	47.77	40.71	11.52	0.9 (293.4)	1.9 (290.9)		0.9 (287.2)	1.0 (288.9)	3.3 (284.9)
SPF3	Theor.	54.54	27.27	18.18	1	-		1	1	3
	Expt.	55.1	26.7	18.2	0.9 (291.9)	-		0.9 (286.4)	1.0 (288.2)	3.2 (285.0)
SPF0	Theor.	75	25	-	-	-		1 (286.3)	1 (288.7)	4 (285.0)
	Expt.	75.2	24.8	-	-	-		1.1	1.0	3.9

The values in parenthesis are XPS binding energy of corresponding elements.

## D.2 AFM topographic images of polymer brushes

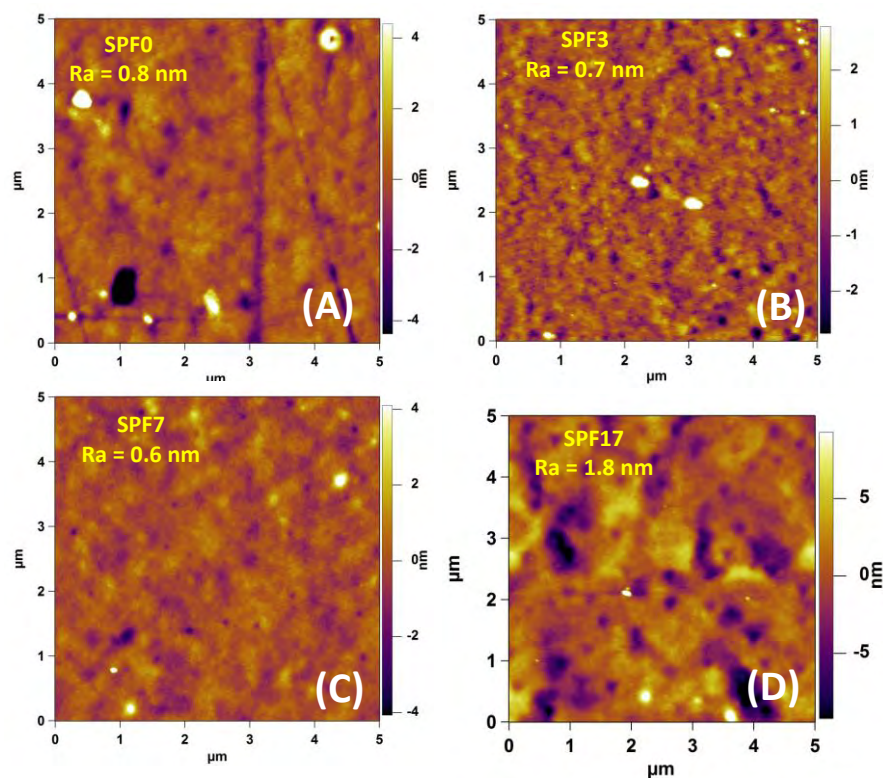


Figure SI-1. AFM topographic images of (A) SPF0, (B) SPF3, (C) SPF7, and (D) SPF17 obtained in dry state.

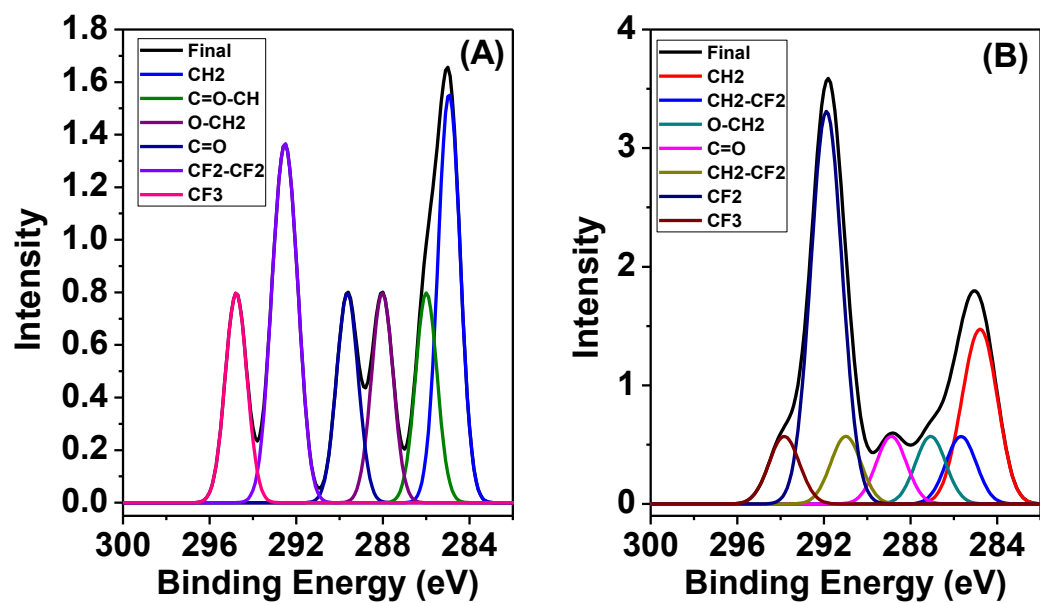


Figure SI-2. DFT-simulated core level C1s XPS-spectra of SPF7 (A) and SPF17 (B) on Si(111).

# Summary

A major concern in the ever-growing field of nanotechnology is associated with the miniaturization of specific critical device components in micro- and nano-electromechanical systems (MEMS/NEMS). Because of the reduction in size, the surface-area to volume ratio increases and in situations where two surfaces with areas below the micrometer range come into close proximity (as in an accelerometer), they may adhere together. At this scale, electrostatic and/or Van der Waals and hydrogen bonding forces become significant and issues like unwanted sticking of surfaces (also known as stiction), due to high adhesion and high friction forces should be avoided. Mostly, MEMS/NEMS devices are fabricated from silicon and silicon-based materials, and their main function is mechanically and mechatronically defined movements. Under ambient conditions, silicon-based materials form a nanometer thick hydrophilic silicon oxide layer (native oxide). In many cases this native oxide layer is beneficial to the required MEMS function because of its electrical insulating property. Its hydrophilic character, however, may introduce an enhanced stiction between moving parts (due to hydrogen bonding) and will negatively affect the device performance and ultimately failure. In order to overcome these issues, fluoropolymer coatings are generally applied. However, such coatings are not strongly adhered to the substrate surfaces and this may lead to premature wear. Alternatively, fluorinated self-assembled monolayers (SAMs) have proven to be strongly binding to specific substrate surfaces. The stability of binding between surface and monolayers depends on their chemistry (e.g. thiol or silane based monolayers) under specific device operating conditions. The adhesion and friction generally decrease with increasing density and chain length of monolayers forming molecules, as both of them are dependent on each other. Furthermore it is well known that fluorination can lower the surface energy thereby lowering adhesion and friction. However, the stability of monolayers in different environments determines how long this kind of coating will maintain low adhesion and friction properties. In this thesis we systematically addressed all these issues and here we summarize those achievements in short.

Firstly, we evaluated the surface functionalization on Si(111) surfaces, as silicon is the predominantly used substrate in MEMS/NEMS. The alkyne-terminated covalently bound monolayers were prepared on oxide-free Si(111) surfaces using 1,15-hexadecadyne under thermal condition (**Chapter 2**). Thiol-yne click (TYC) chemistry was utilized for further functionalization of alkyne-terminated monolayers (Figure 1A). In TYC each alkyne-terminal group predominantly reacts with two thiol groups leading to a higher surface coverage than thiol-ene (TEC) (Figure 1B) or copper-catalyzed azide-alkyne cycloaddition (CuAAC) reactions. An ultimate goal of this approach is to prepare densely

grafted polymer brushes and it can be achieved by immobilizing initiator via TYC approach. The efficiency of TYC reaction on surface bound alkyne-terminated monolayer using various functional thiols is compared to TEC reaction. The results showed that up to ~1.5 thiols can be attached per alkyne moiety via the TYC reaction.

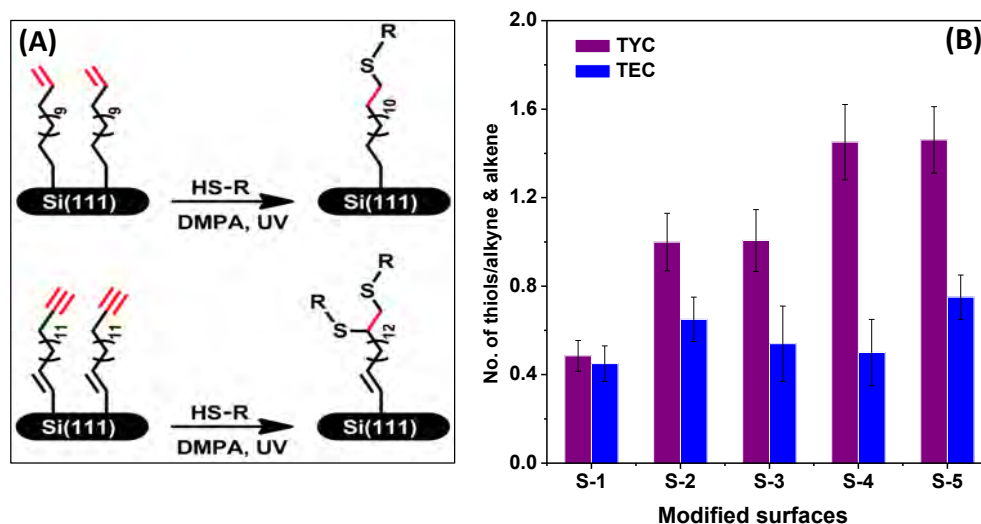


**Figure 1.** (A) Functionalization of alkene- and alkyne-terminated monolayers on Si(111) surfaces using TEC and TYC reactions, (B) surfaces coverage of TYC versus TEC reaction.

Further, for finding good combinations of monolayer and substrates, we studied the hydrolytic and thermal stability of surface bound monolayers on various inorganic surfaces such as Si(111), Si(100), SiC, SiN, SiO<sub>2</sub>, CrN, ITO, PAO, Au and stainless steel (**Chapter 3**) (Figure 2).

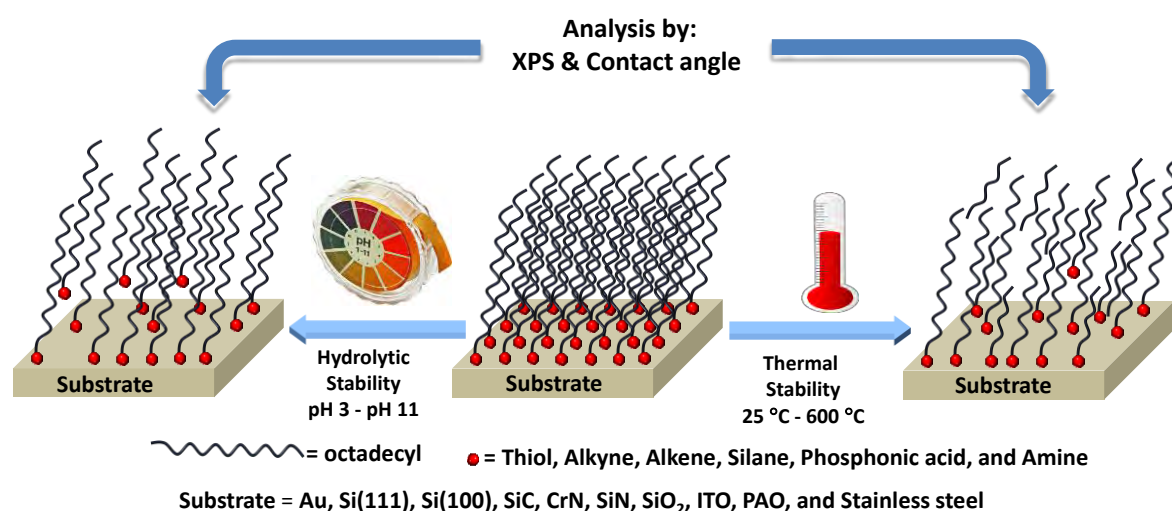


**Figure 2.** Hydrolytic and thermal stability of organic monolayers on various inorganic substrates.

The hydrolytic stability study was conducted in acidic, neutral, basic and physiological aqueous solutions for a period from 1 to 30 days for 24 different monolayer-substrate combinations. The stability of the monolayers was followed by static contact angle and X-ray photoelectron spectroscopy (XPS) measurements at regular intervals. The hydrolytic

stability studies revealed that monolayers derived from alkynes on H-Si(111), H-Si(100), and SiC were most stable under extreme pH conditions compared to monolayers on other substrates. On other hand, the thiol and silane-derived monolayers were hydrolyzed quickly even under neutral conditions. Furthermore, the alkyne-derived monolayers were comparatively stable at elevated temperature ( $> 300\text{ }^{\circ}\text{C}$ ) under vacuum. Under thermal conditions, the phosphonic acid-derived monolayers appeared to be most stable. No significant carbon decay was observed for phosphonic acid derived monolayer on porous aluminium oxide (PAO) surfaces even heating up to  $600\text{ }^{\circ}\text{C}$ . This was the first report of a comprehensive comparative study including a dataset of  $> 1400$  measurements and it disclosed both hydrolytic and thermal stability over a wide range of conditions. These results show that selection of monolayer-substrate combination is strongly dependent on final application of interest.

The combination of stable alkyne-terminated monolayers and TYC reaction was used to immobilize the ATRP-initiator with a high surface coverage ( $\sim 1.5$  initiator/alkyne group), and allowed us to obtain densely grafted polymer brushes. We examined the adhesion and friction properties of polymer brushes using colloidal probe atomic force microscopy (CP-AFM) under ambient condition (Figure 3). The adhesion and friction of polymer brushes was studied with respect to a varying thickness of the polymer. We also studied the adhesion and friction properties of polymer brushes by keeping thickness constant but varying fluorine content in polymer brushes (**Chapter 4**). In the first case, fluoro and non-fluoropolymer brushes were prepared with different thickness and high graft density ( $\sim 0.1$  to  $0.8$  chains/ $\text{nm}^2$ ) using SI-ATRP method on Si(111) surfaces. As explained above, a high graft density of polymer brushes was achieved by densely grafted initiators, which were immobilized via TYC reaction. The non-fluoro polymer brushes (**SPF0**) showed a high adhesion under ambient conditions ( $\text{RH} = 44 \pm 2\%$ ) for all types of thicknesses (6 nm to 206 nm), whereas no significant effect of humidity was observed for fluoropolymer brushes. Under ambient conditions, the  $\text{CF}_3$ -terminated fluoropolymer (**SPF3**) with 140 nm thickness showed a 9.75 nN adhesion force at 10 nN applied load by the colloidal probe. Under similar condition a friction coefficient of 0.0057 was found on fluoropolymer brushes (**SPF3**). To eliminate the humidity effect, we carried out adhesion and friction measurements under controlled environments ( $\text{RH} < 5\%$ ). Under controlled conditions, non-fluoropolymer brushes (**SPF0**) were appeared to have high adhesion and friction properties in comparison with fluoropolymer brushes (**SPF3**). However, under both conditions ( $\text{RH} = 44 \pm 2\%$  and  $\text{RH} < 5\%$ ) a low adhesion and friction forces were observed on increasing the thickness of polymer brushes. The results showed the influence of humidity, grafting density, thickness and fluorine content of polymer brushes on their adhesion and friction properties.

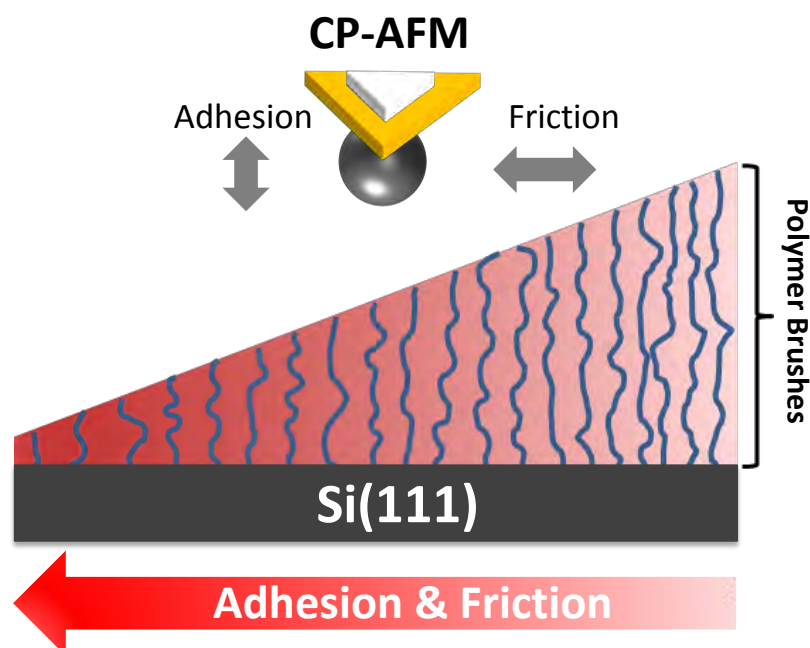


**Figure 3.** Adhesion and friction measurement on polymer brushes with varied thickness using CP-AFM.

Secondly, the adhesion and friction properties of polymer brushes were further evaluated by varying fluorine (SPF<sub>x</sub> were  $x = 0, 3, 7$ , and  $17$ ) content and keeping thickness constant ( $\sim 80$  nm) (**Chapter 5**). We obtained highly grafted polymer brushes by the combination of TYC and SI-ATRP approaches. The adhesion and friction properties were measured using CP-AFM under ambient conditions ( $RH = 44 \pm 2\%$ ) (Figure 4).

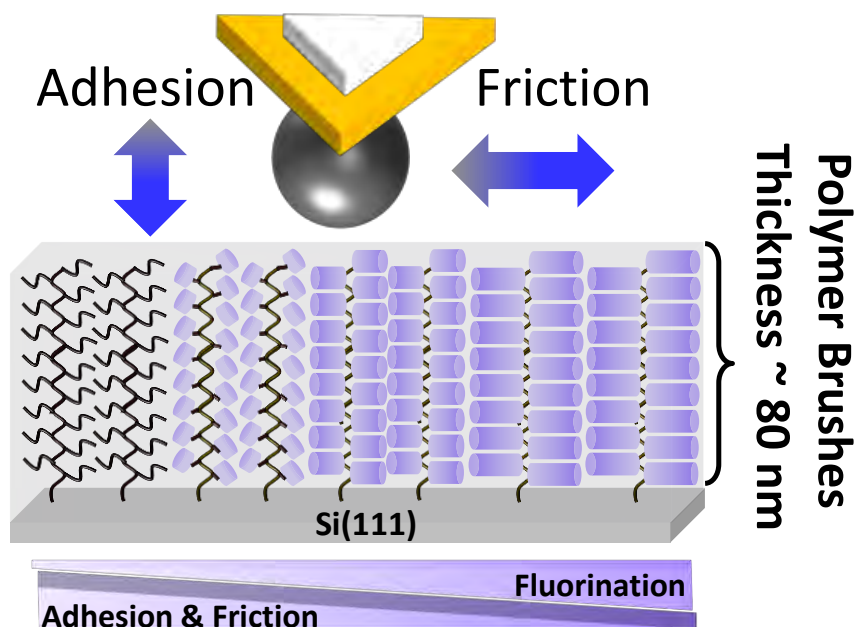


**Figure 4.** Adhesion and friction measurement on polymer brushes with varied fluorine content and at constant thickness using CP-AFM.

The adhesion and friction forces decreased with increasing the fluorine content in the polymer brushes. The lowest friction coefficient (0.005) was observed for polymer brushes with highest fluorine (**SPF17**). With such a low friction coefficient (in absences of external lubricants) under ambient conditions, these polymer brushes can be used as dry-lubricants. Moreover, the adhesion and frictions properties were also measured for two different lubricating fluids (hexadecane and Fluorinert<sup>®</sup> FC-40). A lowest adhesion force of 0.003 nN at 10 nN applied load on colloidal probe was found for **SPF17** using FC-40 as a lubricating fluid. Almost equal friction coefficient of 0.002 in FC-14 and 0.003 in hexadecane was observed for **SPF17**. Fluoropolymer brushes with such low adhesion and friction properties under ambient conditions display the potential of covalently bound polymer brushes as dry-lubricants for MEMS/NEMS and high-performance, heavy-duty industrial applications in bearings, etc.

Finally, in **Chapter 6** we presented some of the outstanding outcomes of this thesis, including covalently bound surface functionalization approaches and formation of dense fluoropolymer brushes with low adhesion and low friction properties. Furthermore, insightful ideas for future applications in nanotechnology are presented along with unsolved issues and recommendation for further research.



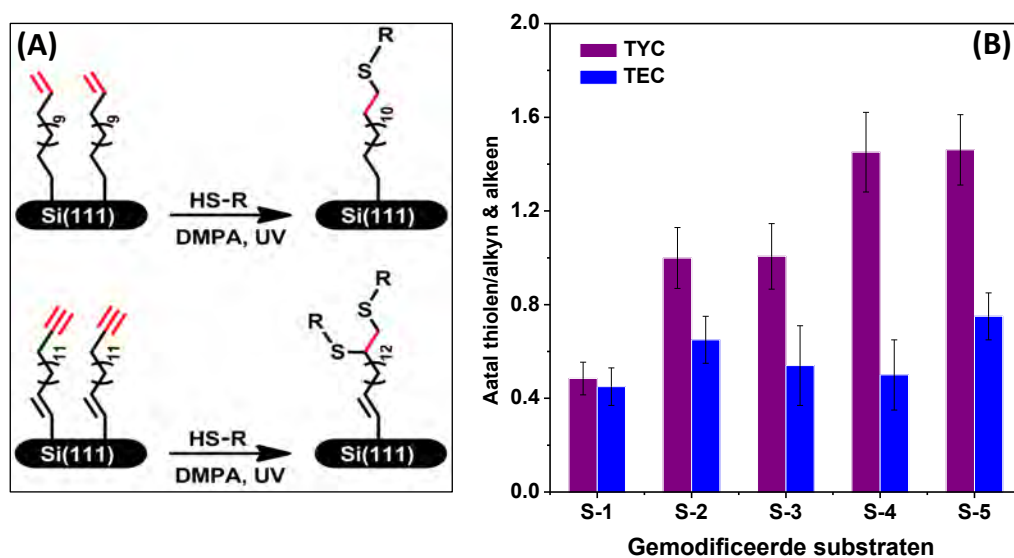


# Samenvatting

In het almaar groeiende veld van nanotechnologie is er steeds meer oog voor de toenemende miniaturisatie van specifieke kritieke onderdelen van micro- en nano-electromechanische systemen (MEMS/NEMS). Vanwege de afname in grootte neemt de verhouding tussen oppervlak en volume toe. In situaties waar twee oppervlakken met sub-micron afmetingen dichtbij elkaar komen (zoals in een versnellingsmeter) kan het gebeuren dat de oppervlakken samenplakken. Op deze lengteschaal spelen elektrostatische krachten, Van der Waals krachten en waterstofbruggen een significante rol. Problemen zoals het ongewenst samenplakken van oppervlakken (zogenaamde stictie) door grote adhesie- en frictiekrachten moeten vermeden worden. MEM/NEM systemen worden voornamelijk van silicium en silicium-derivaten gemaakt. Hun voornaamste functie ligt in het maken van goed gedefinieerde mechanische bewegingen. Onder normale omstandigheden zal zich een hydrofiele oxide-laag van enkele nanometers vormen op het silicium. Vaak is deze oxide-laag gunstig voor de werking van MEM/NEM systemen omdat deze laag isolerend is. Het hydrofiele karakter van deze oxide-laag zorgt echter voor extra stictie tussen bewegende delen (door waterstofbruggen) en zal de werking van het MEM/NEM systeem negatief beïnvloeden, en zelfs leiden tot falen van het systeem. Om deze problemen te verhelpen worden vaak coatings aangebracht van fluorhoudende polymeren. Dit soort coatings zit niet sterk aan het oppervlak gebonden, wat leidt tot vroegtijdige slijtage. Aan de andere kant heeft men aangetoond dat gefluoreerde monolagen sterk aan het oppervlak hechten. De stabiliteit van de binding tussen oppervlak en monolaag is afhankelijk van hun chemie (bijvoorbeeld thiol- of silaan-monolagen) en de omstandigheden waaronder de MEM/NEM systemen gebruikt worden. Adhesie en frictie nemen doorgaans af met toenemende dichtheid en ketenlengte van monolaag-vormende moleculen, omdat deze twee eigenschappen van elkaar afhangen. Verder is het bekend dat het introduceren van fluor de oppervlakte-energie kan verlagen en daarmee ook adhesie en frictie. Echter, de stabiliteit van monolagen onder verschillende condities bepaalt hoe lang deze coating de lage adhesie- en frictie-eigenschappen behoudt. In dit proefschrift onderzoeken we al deze facetten systematisch en hieronder vatten we de belangrijkste bevindingen samen.

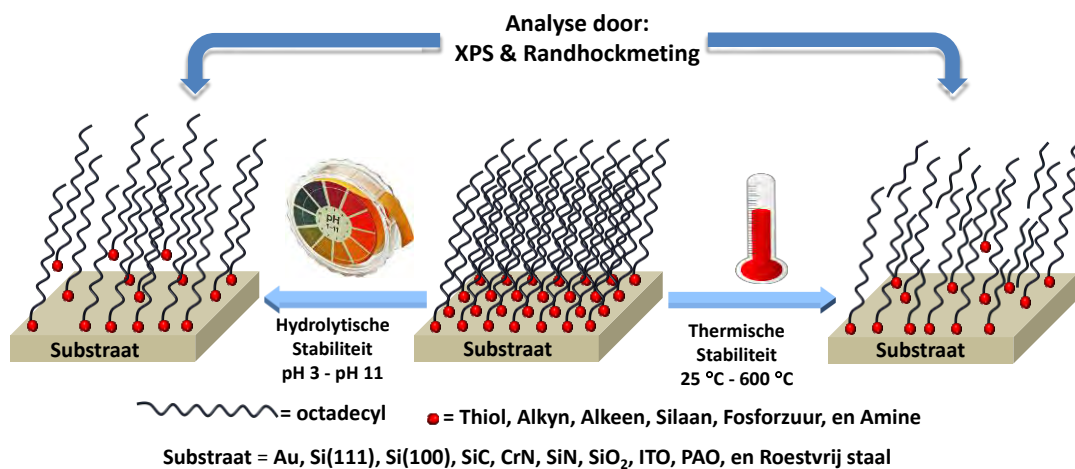
Ten eerste hebben we de modificatie van het oppervlak van Si(111) substraten bekeken, omdat silicium het meeste gebruikte materiaal is in MEM/NEM systemen. Alkyn-getermineerde, covalent gebonden monolagen zijn gesynthesiseerd op oxide-vrije Si(111) substraten door reactie met 1,15-hexadecadiyne onder thermische condities (**Hoofdstuk 2**). Thiol-yne click chemie is gebruikt om alkyn-getermineerde monolagen verder te functionaliseren (Figuur 1A). Omdat onder thiol-yne click reacties het terminale alkyn

voornamelijk twee keer reageert met thiolen, leidt deze chemie tot een hogere conversie van functionele groepen aan het oppervlak dan onder thiol-ene click (TEC) (Figuur 1B) of koper-gekatalyseerde azide-alkyn cyclo-additie (CuAAC) reacties. Een van de uiteindelijke doelen van deze aanpak is om dichtgepakte polymeerborstels op het oppervlak te groeien. Dit kan door een initiator te immobiliseren via TYC. De efficiëntie van de TYC reactie versus de TEC reactie op covalent gebonden, alkyn-getermineerde oppervlakken is onderzocht met verschillende functionele thiolen. De resultaten laten zien dat ongeveer 1.5 thiol per alkyn reageert met behulp van thiol-yne click.



**Figuur 1.** (A) Functionalisering van alkeen- en alkyn-getermineerde monolagen op Si(111) substraten met behulp van TEC en TYC reacties, (B) bezettingsgraad op het substraat na TYC versus TEC reacties.

Verder hebben we de hydrolytische en thermische stabiliteit van covalent gebonden monolagen bekeken op verscheidenen substraten, waaronder Si(111), Si(100), SiC, SiN, SiO<sub>2</sub>, CrN, ITO, PAO, goud en roestvrij staal, teneinde de beste combinaties tussen monolaag in substraat te vinden (**Hoofdstuk 3**) (Figuur 2).

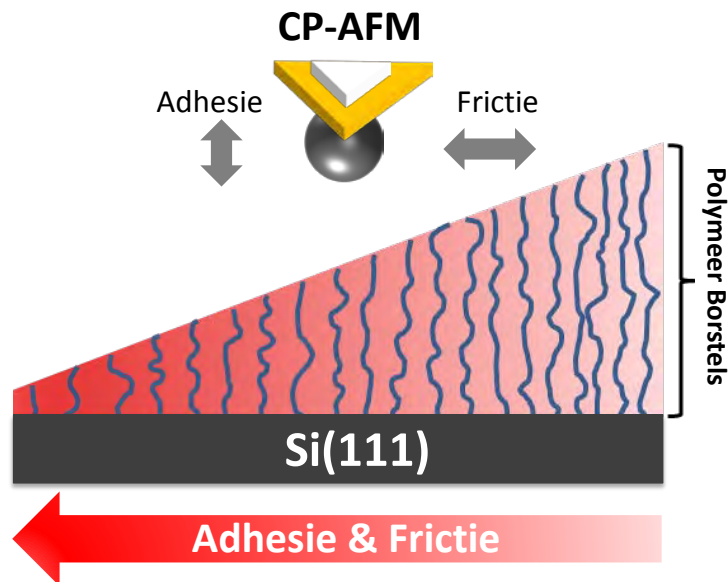


**Figuur 2.** Hydrolytische en thermische stabiliteit van organische monolagen op verschillende anorganische substraten.

De hydrolytische stabiliteit is onderzocht in neutrale, zure, basische en fysiologische omstandigheden in water, gedurende een periode van dertig dagen, voor 24 monolaag-substraat koppels. De stabiliteit van de monolagen is gevolgd met behulp van randhoek- en XPS-metingen op gezette tijden. De hydrolytische stabiliteit van monolagen afgeleid van alkynen op H-Si(111), H-Si(100) en SiC bleken het stabielst van alle geteste combinaties, zelfs onder extreme pH. Monolagen afgeleid van thiolen en silanen werden daarentegen zelfs onder neutrale condities snel gehydrolyseerd. Verder bleken de alkyn-monolagen relatief stabiel bij hoge temperatuur ( $>300\text{ }^{\circ}\text{C}$ ) onder vacuüm. De monolagen, afgeleid van fosforzuren, bleken het stabielst onder thermische condities. Er is geen significante afname in het koolstofgehalte waar te nemen voor deze monolagen op poreus aluminium oxide (PAO), zelfs wanneer ze tot  $600\text{ }^{\circ}\text{C}$  verhit worden. Met ruim 1400 metingen is dit het eerste uitgebreide vergelijkingsonderzoek en het laat zowel hydrolytische als thermische stabiliteit zien over een groot bereik. Het selecteren van de juiste monolaag-substraat combinatie is volgens onze resultaten sterk afhankelijk van de uiteindelijke toepassing.

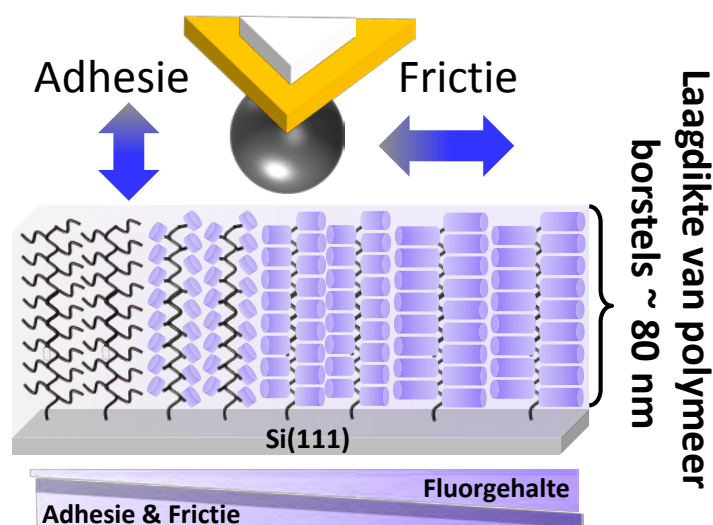
De combinatie van stabiele, alkyn-getermineerde monolagen en de TYC reactie is gebruikt om een ATRP-initiator op het oppervlak te verankeren met een hoge bezettingsgraad ( $\sim 1.5$  initiator moleculen per alkyn). Dit stelde ons in staat om dicht-bepakte polymeerborstels te synthetiseren. We onderzochten de adhesie en frictie eigenschappen van deze polymeerborstels met behulp van colloidal probe atomic force microscopy (CP-AFM) onder normale omstandigheden (Figuur 3). De adhesie en frictie van polymeerborstels is bestudeerd als functie van de laagdikte van de polymeerborstels. Verder zijn de adhesie en frictie van polymeerborstels bestudeerd waarbij laagdikte constant werd gehouden en de hoeveelheid fluor in de polymeren werd gevarieerd (**Hoofdstuk 4**). In het eerste geval zijn fluorhoudende en niet-fluorhoudende polymeren gesynthetiseerd met verschillende laagdiktes en hoge oppervlakedichtheid ( $\sim 0.1$  tot  $0.8$  ketens per  $\text{nm}^2$ ) met behulp van oppervlakte-geïnitieerde ATRP op Si(111) substraten. Zoals eerder vermeldt werd een hoge oppervlakedichtheid van polymeerborstels bereikt door een hoge dichtheid van initiators, welke veranderd zijn middels de TYC reactie. De niet-fluorhoudende polymeerborstels (**SPF0**) lieten een hoge adhesiekracht zien onder normale omstandigheden (relatieve luchtvochtigheid  $44 \pm 2\%$ ) voor alle bestudeerde laagdiktes (6 tot 206 nm), terwijl er geen significant effect van luchtvochtigheid op fluorhoudende polymeerborstels is waargenomen. Onder normale omstandigheden liet het CF<sub>3</sub>-getermineerde fluoropolymeer (**SPF3**) met 140 nm laagdikte een adhesiekracht zien van 9.75 nN bij een belasting door de colloidal probe van 10 nN. Onder vergelijkbare omstandigheden is een frictie-coëfficiënt van 0.0057 gevonden voor fluorhoudende polymeerborstels (**SPF3**). Om de invloed van luchtvochtigheid uit te sluiten, hebben we de adhesie- en frictiemetingen uitgevoerd onder beheerste omstandigheden (relatieve luchtvochtigheid  $<5\%$ ). Onder deze omstandigheden bleken niet-fluorhoudende

polymeerborstels (**SPF0**) hogere adhesie en frictie te vertonen, vergeleken met fluorhoudende polymeerborstels (**SPF3**). Echter, onder beide omstandigheden (relatieve luchtvochtigheid  $44 \pm 2\%$  en  $<5\%$ ) werden lage adhesie- en frictiekrachten gemeten wanneer de laagdikte van de polymeerborstels toenam. Deze resultaten laten zien dat luchtvochtigheid, oppervlaktedichtheid, laagdikte en fluorgehalte allen invloed hebben op de adhesie- en frictie-eigenschappen van polymeerborstels.



**Figuur 3.** Adhesie- en frictiemeting op polymeerborstels met verschillende laagdiktes met behulp van CP-AFM.

Ten tweede zijn de adhesie- en frictie-eigenschappen van polymeerborstels verder onderzocht door de laagdikte constant te houden ( $\sim 80$  nm) en het fluorgehalte te variëren (**SPF<sub>x</sub>**,  $x=0, 3, 7$  en  $17$ ) (**Hoofdstuk 5**).



**Figuur 4.** Adhesie- en frictiemetingen op polymeerborstels met constante laagdikte en verschillend fluorgehalte met behulp van CP-AFM.

We verkregen dichtgepakte polymeerborstels met behulp van TYC en SI-ATRP technieken. De adhesie- en frictie-eigenschappen zijn gemeten met CP-AFM onder normale omstandigheden (relatieve luchtvochtigheid  $44 \pm 2\%$ ) (Figuur 4). De adhesie- en frictiekrachten namen af met toenemend fluorgehalte in de polymeerborstels. De laagste frictiecoëfficiënt (0.005) werd gemeten voor polymeerborstels met het hoogste fluorgehalte (**SPF17**). Met zulke lage frictiecoëfficiënten (zonder toevoeging van smeermiddelen) onder normale omstandigheden, kunnen deze polymeerborstels gebruikt worden als zogenaamde “droge smeermiddelen”. Verder zijn de adhesie- en frictie-eigenschappen bekeken voor twee verschillende smeermiddelen (hexadecaan en Fluorinert® FC-40). De laagste adhesiekracht, 0.003 nN bij 10 nN belasting door de colloidal probe, werd gevonden voor **SPF17** met FC-40 als smeermiddel. Nagenoeg gelijke frictiecoëfficiënten werden gemeten met FC-14 (0.002) en hexadecaan (0.003) voor **SPF17**. Fluorhoudende polymeerborstels, met zulke lage adhesie- en frictie-eigenschappen onder normale omstandigheden, bieden perspectief voor covalent gebonden polymeerborstels als “droge smeermiddelen” voor MEM/NEM systemen en industriële toepassingen in bijvoorbeeld lagers onder zware belasting hoge prestaties moeten leveren.

Ten slotte presenteren we in **Hoofdstuk 6** enkele van de opmerkelijkste resultaten van dit proefschrift, waaronder covalent gebonden oppervlakte-modificatie technieken en synthese van dichtgepakte fluorhoudende polymeerborstels met lage adhesie en frictie. Verder worden verhelderende ideeën voor toekomstige toepassingen in nanotechnologie evenals onopgeloste vraagstukken en aanbevelingen voor toekomstig onderzoek gepresenteerd.



## Overview of Completed Training Activities

### Discipline specific activities

NWO Lunteren meeting Netherlands (Poster)	Lunteren, Netherlands	2013
AVS 59 <sup>th</sup> International Symposium and Exhibition (Oral)	Tampa, FL, USA	2012
SANAM 2011 Würzburg Germany (Poster)	Würzburg Germany	2011
S.P.A.M. project review by the European Commission (Poster) (Oral)	Eindhoven, Netherlands	2011
Winter School on Lithography, complementary competences and advance training by SRT 1 and TEP A	Delft, Netherlands	2011
NWO Lunteren meeting Netherlands (Poster)	Lunteren, Netherlands	2010
Basic training surface conditioning and preparation by SRT 2 and TEP C, BESSY	Berlin, Germany	2010
Ultra Clean Processing of Semiconductor Surfaces UCPSS 2010 conference	Oostende, Belgium	2010
Advanced organic chemistry 1&2	ORC, Wageningen	2010-2013

### General courses

Career Perspectives	WSG	2013
Philosophy and Ethics of Food Science & Technology	WSG	2013
Mobilising your scientific network	WSG	2013
Techniques for Writing and Presenting a Scientific paper	WSG	2012
PhD competence assessment	WGS	2012
Voice matters	WGS	2012
Information literacy	WGS	2011
PhD week	VLAG	2011

### Optionals

Preparing PhD research proposal	ORC/VLAG, Wageningen	2010
Colloquia	ORC, Wageningen	2010-2014
Group meetings	ORC, Wageningen	2010-2014
PhD study trip organization	Switzerland and Germany	2013
PhD study trip	Scotland and England	2011





# Acknowledgment

I met many people during my PhD who contributed both directly and indirectly to accomplish this thesis. Without their valuable supports and encouragements, this thesis would not have been achieved. I would like to take this opportunity to thank them all.

I am deeply indebted to my promoter **Prof. Dr. Han Zuilhof**, whose advice, motivation and support were invaluable to me. I feel privileged for having been able to work with a very understanding and encouraging professor like him. He always encouraged me to take initiatives, not only in research-related tasks but also in general, like his continuous motivation to take part in PhD trip committee. Because of his continuous encouragements, I successfully managed the financial segment of the ORC PhD Trip 2013 to the Germany and Switzerland.

I would also like to thank **Prof. Dr. Cees van Rijn** for his guidance and stimulating discussions. His comment on the influence of the humidity effect in controlling adhesion has resulted in further scientific study and understanding of the work presented in this thesis. I would also like to thank him for handling industry-oriented issues. His presence in meetings at ASML always gave me confidence to speak in front of industrial project partners.

I am grateful to **Dr. Jos Paulusse** for his guidance, assistance and expertise that were required at initial stages of my PhD. He always gave me freedom along with valuable advice and great encouragements that helped me to shape my research interests. Thanks for those rides from ORC to ASML and to Marie Curie network meetings. I also would like to thank **Dr. Mabel A. Caipa Campos** for introducing me to surface modification techniques. It really had a great impact in rest of my doctoral research.

I gratefully acknowledge **Prof. Dr. Martien A. Cohen Stuart** and **Prof. Dr. Frans A. M. Leermakers** for several insightful discussions, particularly for their timely help with polymer physics-related difficulties. Particularly, I thank Soumi Banerjee for giving me silica particles for my last few experiments. Also thanks to Evan Spruijt for many helpful discussions on tribology.

I am very thankful to my project partners at ASML, **Dr. Ninna Dziomkina** and **Dr. Jeanette Sontag** for their motivating help with the monolayer stability study under EUV in ASML's clean room environments. I also would like to extend my gratitude to all the people involved in the Marie Curie European Union FP7 network "*Surface Physics for Advanced Materials (SPAM)*" for several insightful discussions during progress and mid-term review meetings.

I would like to thank to **Prof. Yahia A. Alhamed**, **Prof. Ahmed A. Khamis** and Florencio Gerardo Trovela (Omar) from King Abdulaziz University, Jeddah, Saudi Arabia

for fruitful collaboration, which lead to a joint publication on stability study of monolayers. A special thanks to Omar for measuring enormous number of XPS samples.

I extend my sincere thanks to the members of my PhD committee for their valuable time and feedback on the preliminary version of my thesis.

I would like to thank all ORC staff members for their support during my PhD. Thanks to Teris, Ton, Maurice, Michel, Tom, Maarten for some extra organic chemistry essence in AOC courses. I am thankful to the supporting staff: Barend, Marcel, Pepijn and Remco Fokkiink for their technical support with various instruments. Also thanks to Elbert, Frank, Ronald for timely ordering the chemicals required for my research. Without their support I would not have had accomplished my project in time. Furthermore, I also thank the education staff: Erik, Cees, Carel, Anne-Marie for their help during practical assistance. A special thank to Elly, Aleida and Anita for assistance with official and financial matters.

I would like to thank my students: Jan Bart ten Hove and Remco Steijsiger, who did their bachelors thesis under my supervision. Thank you guys for all the hard work which boosted my research. I am thankful to Raoul Frijns who spent his summer holidays with an unexpectedly long synthesis in the lab.

I thank all my PhD colleagues from the beginning: Kim, Loes, Ai, Willem, Nagesh, Sourav, Jaime, Wouter, Tin, Anke, Alexandre, Sidhu, Radostina, Umesh, Saurabh, Satesh, Florine, Yao, Bas, Aline, Wilco, Sweccha, Jorin, Tjerk, Rick, Christie, Sjoerd, Medea, Esther and Digvijay for all the great times that we have shared during my stay at ORC. A special thanks to Radostina, Sidhu, Satesh, Umesh, Saurabh, Nagesh and Sachin for helping me while transferring all my home appliances and furniture and arranging them nicely at my new home in Wageningen and then Bennekom. I am particularly thankful to “Doc” (Sourav) for providing me contacts of sponsors for PhD trip that helped me to raise sufficient funds for PhD trip 2013. Thanks also to Saurabh, Wilco and Jorin for their cooperation during PhD trip organization. Together with the whole group of ORC PhD students, Han and Tom, we had a fantastic trip to the Germany and Switzerland.

Special thanks to Sidhu! Hey buddy, you are a great friend and surface scientist. Sidhu’s contributions and helps with tribological experiments helped me a lot to accomplish my project. Also Thanks to Satesh for his help with computational chemistry. Thanks to the “Surfix-crew”: Luc, Anke, Esther, Julian and Jelmer for several scientific and non-scientific discussions. Thanks to Frank and Bram for sharing your experience and tips on wrapping up thesis.

I would particularly like to acknowledge Bas for translation of my thesis summary in Dutch. Bas, you did a very critical job. Thanks also to Aline, Medea, Christie, Satesh, Esther, Txema and Wang for correcting my thesis chapters. Particularly thanks to Txema, Sweccha and Fatima for helping me in lab and being nice labmates. I would like to thank Hamilton for helping me with basics of the ATRP technique. Thanks to Steven and

Remco for their helps in stability project. I would extend my thanks to Jacob, Ai, Alexandre and Dani for Christmas dinner arrangements every year. Alex, thanks for your help during practical courses. I will miss your companionship whenever I teach practicals in future. I would like extend my sincere gratitude to Enid Tomkinson for her contribution to improve my English communication.

I cannot imagine how difficult it would have been to be abroad alone without my Indian friends: Nagesh, Ankush, Umesh, Sidhu, Satesh, Sourav, Saurabh and Kuldeep who made my stay in lab as well as in Netherlands as home feel. Thank you guys for a great time we shared together playing cricket, cooking during weekends and travelling together. I also would like to thank Indian community in Wageningen, notably Priyanka, Jueeli, Rashmi, Sachin, Soumi, Surender, Liyakat, Uttara and Urmila for arranging all those social events and gatherings which resisted me missing all the Indian festivals here in the Netherlands.

I owe a great debt of gratitude to my previous supervisor, **Dr. Prakash P. Wadgaonkar**, for his guidance and motivation that boosted my scientific career at NCL, Pune. I would like to thank all my friends and colleagues at NCL: Anjana Madam, Sony, Snehalata, Arvind, Arun, Nana (Dnyaneshwar), Vijay, Pandurang, Prakash, Neelakshi, Savita, Mahadeo, Mahesh, Sharadrao, Kishorji, Anil, Vidya, Mugdha, Parimal, Bhausahab, Shraddha, Indravadan and Deepshika. You all made my stay at NCL enjoyable and cherished. I would like to express my gratitude to **Dr. N. N. Maldar** and all teaching staff for their guidance and encouragement during my Master study at Solapur University, Solapur.

I am deeply thankful to all my friends and relatives from India whose names are not mentioned here. You were always with me and made finest years of my life. Immense thanks for your love, care and inspirations during my study and stay in the Netherlands.

I am truly grateful to my parents (Pappa and Mammi) for their support, continuous encouragements, sacrifices and immeasurable love and care. I precisely express my deep gratitude to my sisters, Ningu and Sangita, brother Doddu, nephews Sachin and Samarth for their praises, enforcements and love which assisted me to accomplish my study abroad. Many thank to my parents-in-laws for their role in encouraging me to finish my doctoral study.

Above all, I would like to thank my lovely wife Rajashri for her everlasting encouragement, continuous support and patience over the last three years of my PhD. Also thanks for keeping me sane, being my proofreader and editor while I was writing this thesis. But most of all, I owe you everything for your love, care and being my best friend. Love you, sweetheart!



Nagendra Somaling Bhairamadgi



# List of Publications

1. *Synthesis and characterization of new aromatic polyesters containing cardo decahydronaphthalene groups.* Honkhambe, P. N.; Bhairamadgi, N. S.; Biyani, M. V.; Wadgaonkar, P. P.; Salunkhe, M. M. *Eur. Polym. J.* **2010**, 46 (4), 709-718.
2. *Synthesis and characterization of new aromatic polyesters containing pendent naphthyl units.* Honkhambe, P. N.; Biyani, M. V.; Bhairamadgi, N. S.; Wadgaonkar, P. P.; Salunkhe, M. M. *J. Appl. Polym. Sci.* **2010**, 117 (5), 2545-2552.
3. *Synthesis and characterization of polyesters from 2,3-bis (4'-hydroxy phenyl) quinoxaline and 2,3-bis (2'-hydroxynaphthalene-6'-yl) quinoxaline.* Patil, V. B.; Medhi, M.; Bhairamadgi, N. S.; Wadgaonkar, P. P.; Maldar, N. N. *Mater. Sci. Eng., B* **2010**, 168 (1), 186-192.
4. *Poly(ether ether ketone)s and poly(ether ether ketone ketone)s containing cardo decahydronaphthalene groups: Synthesis and characterization.* Honkhambe, P. N.; Pasale, S. K.; Bhairamadgi, N. S.; Kumbhar, K. P.; Salunkhe, M. M.; Wadgaonkar, P. P. *J. Appl. Polym. Sci.* **2011**, 122 (3), 1607-1613.
5. *Synthesis and characterization of soluble polyamides from bis-[(4'-aminobenzyl)-4-benzamide] ether and various diacids.* Patil, A. S.; Sayyed, M. M.; Bhairamadgi, N. S.; Han, S. H.; Maldar, N. N. *Polym. Bull.* **2011**, 66 (9), 1207-1218.
6. *Efficient functionalization of oxide-free silicon(111) surfaces: Thiol-yne versus thiol-ene click chemistry.* Bhairamadgi, N. S.; Gangarapu, S.; Caipa Campos, M. A.; Paulusse, J. M. J.; Van Rijn, C. J. M.; Zuilhof, H. *Langmuir* **2013**, 29 (14), 4535-4542.
7. *Adhesion and friction properties of polymer brushes: Fluoro versus nonfluoro polymer brushes at varying thickness.* Bhairamadgi, N. S.; Pujari, S. P.; Leermakers, F. A. M.; Van Rijn, C. J. M.; Zuilhof, H. *Langmuir* **2014**, 30 (8), 2068-2076.
8. *Ambient surface analysis of organic monolayers using direct analysis in real time orbitrap mass spectrometry.* Manova, R. K.; Joshi, S.; Debrassi, A.; Bhairamadgi, N. S.; Roeven, E.; Gagnon, J.; Tahir, M. N.; Claassen, F. W.; Scheres, L. M. W.; Wennekes, T.; Schroën, K.; Van Beek, T. A.; Zuilhof, H.; Nielen, M. W. F. *Anal. Chem.* **2014**, 86 (5), 2403-2411.
9. *Hydrolytic and thermal stability of organic monolayers on various inorganic substrates.* Bhairamadgi, N. S.; Pujari, S. P.; Trovela, F. G.; Debrassi, A.; Khamis, A. A.; Alonso, J. M.; Al Zahrani, A. A.; Wennekes, T.; Al-Turaif, H. A.; van Rijn, C. J. M.; Alhamed, Y. A.; Zuilhof, H. *Langmuir* **2014**, DOI: 10.1021/la500533f.
10. *Adhesion and friction properties of fluoropolymer brushes: On the tribological inertness of fluorine.* Bhairamadgi, N. S.; Pujari, S. P.; van Rijn, C. J. M.; Zuilhof, H. *Langmuir* **2014**, submitted.
11. *Hydrolytic stability and polymer antifouling studies of fluoro-hydro monolayers on Si(111).* Wang, Z. Bhairamadgi, N. S.; Zuilhof, H. *manuscript in preperation.*



## About the Author



Nagendra was born on 6<sup>th</sup> June, 1983 in Tolnur, (MH) India. He obtained his bachelor's degree in Chemistry from Akkalkot College, affiliated to Shivaji University, Kolhapur, India from 2002-2005. Then, he started his master's degree in Organic Chemistry, Solapur University, Solapur, India during 2005-2007. After finishing his master's degree, he worked as a project assistant for two and half years under the guidance of Dr. Prakash P. Wadgaonkar on synthesis of melt-extrudable polymers at Polymer Science and Engineering Division, National Chemical Laboratory (NCL), Pune between 2007-2010. From June 2010 onwards, he became a Ph.D. student under the supervision of Prof. Han Zuilhof, Laboratory of Organic Chemistry, Wageningen University, Wageningen, The Netherlands. His research was focused on surface modification of inorganic substrates to obtain stable, low adhesion and low friction coatings for MEMS/NEMS applications. The most important findings of his research are described in this thesis.



The research described in this thesis was financially supported by the Marie Curie European Union FP7 project “*Surface Physics for Advanced Materials (SPAM)*.”

Design & Layout: Nagendra S. Bhairamadgi & Sidharam P. Pujari  
Printed By: GVO drukkers & vormgevers B.V. / Ponsen & Looijen, Ede, NL



